

Micromechanical Properties of the Extracellular and Pericellular Matrices
of Articular Cartilage

by

Rebecca Elizabeth Wilusz

Department of Biomedical Engineering
Duke University

Date: _____

Approved:

Farshid Guilak, Supervisor

Mansoor Haider

Roger Nightingale

Lori Setton

Stefan Zauscher

Dissertation submitted in partial fulfillment of
the requirements for the degree of Doctor of Philosophy in the Department of
Biomedical Engineering in the Graduate School
of Duke University

2013

ABSTRACT

Micromechanical Properties of the Extracellular and Pericellular Matrices
of Articular Cartilage

by

Rebecca Elizabeth Wilusz

Department of Biomedical Engineering
Duke University

Date: _____

Approved:

Farshid Guilak, Supervisor

Mansoor Haider

Roger Nightingale

Lori Setton

Stefan Zauscher

An abstract of a dissertation submitted in partial
fulfillment of the requirements for the degree
of Doctor of Philosophy in the Department of
Biomedical Engineering in the Graduate School
of Duke University

2013

Copyright by
Rebecca Elizabeth Wilusz
2013

Abstract

The role of articular cartilage in diarthrodial joints is primarily mechanical as the tissue provides a nearly frictionless, load-bearing surface that supports and distributes forces generated during joint loading. Embedded within the extensive cartilage extracellular matrix (ECM), chondrocytes are surrounded by a narrow, distinct pericellular matrix (PCM) that is thought to regulate the biomechanical microenvironment of the cell and influence chondrocyte metabolism, cartilage homeostasis, and overall joint health. While previous studies of PCM mechanical properties required physical extraction of the cell and PCM from the tissue, atomic force microscopy (AFM) provides a means for high resolution microindentation testing that can be used to measure local mechanical properties *in situ*. This dissertation develops and applies AFM microindentation techniques to 1) evaluate the microscale elastic properties of the cartilage PCM and ECM *in situ* and 2) correlate site-specific biochemical composition with biomechanical properties of the PCM and ECM.

An AFM-based stiffness mapping technique was experimentally validated and applied to cartilage sections to evaluate ECM and PCM properties *in situ* with minimal disruption of native matrix integration. As expected, PCM elastic moduli were significantly less than ECM moduli, uniform with depth, and mechanically isotropic. ECM moduli exhibited distinct depth-dependent anisotropy and unexpectedly, were

found to decrease with depth from the articular surface. Both the PCM and ECM exhibited alterations in microscale moduli and their spatial distributions when evaluated in cartilage presenting early degenerative changes associated with osteoarthritis (OA) as compared to healthy tissue.

The ability to correlate site-specific biochemical composition with local biomechanical properties provides a more complete characterization of the chondrocyte microenvironment. To this end, we developed novel immunofluorescence (IF)-guided AFM stiffness mapping and demonstrated that PCM mechanical properties correlate with the presence of type VI collagen. Extending this technique by using dual IF, we presented new evidence for a defining role of perlecan in the PCM, showing that interior regions of the PCM rich in perlecan and type VI collagen exhibit lower elastic moduli than peripheral PCM and ECM regions lacking perlecan. Furthermore, lower moduli at the PCM interior were significantly influenced by the presence of heparan sulfate. IF-guided AFM stiffness mapping was combined with enzymatic digestion to demonstrate that the micromechanical properties of the PCM exhibit high resistance to specific enzymatic digestion of aggrecan and aggrecan-associated glycosaminoglycans but are vulnerable to proteolytic degradation by leukocyte elastase.

Overall, this research generates new insights into the complex structural, compositional, and functional relationships between the cartilage ECM and PCM and

provides the tools and framework for further studies to continue to investigate their importance in regulating chondrocyte physiology in health and disease.

Dedication

In loving memory of my grandparents, Charles and Elizabeth Miller.

Contents

Abstract	iv
List of Tables.....	xv
List of Figures	xvi
List of Abbreviations	xix
List of Variables.....	xxii
Acknowledgments	xxiv
1. Background and Significance	1
1.1 Articular Cartilage Matrix Organization.....	1
1.1.1 Extracellular Matrix	1
1.1.2 Pericellular Matrix.....	3
1.1.3 Territorial Matrix	5
1.2 Biomechanical Role of the Pericellular Matrix	6
1.3 Glycosaminoglycans and Proteoglycans of Articular Cartilage.....	7
1.3.1 Glycosaminoglycans	8
1.3.2 Hyaluronan	9
1.3.3 Aggrecan.....	11
1.3.4 Decorin and Biglycan.....	13
1.3.5 Perlecan.....	14
1.4 Osteoarthritis.....	15
1.5 Atomic Force Microscopy.....	18

1.5.1 Principles of Operation.....	19
1.5.2 Evaluation of Elastic Indentation using Modified Hertz Model	21
1.5.3 Influence of Probe Geometry on AFM-based Indentation	25
1.6 Research Goals and Significance	28
1.7 Hypotheses and Aims.....	29
2. Spatial Mapping of the Biomechanical Properties of the Pericellular Matrix of Articular Cartilage Measured <i>in situ</i> via Atomic Force Microscopy	32
2.1 Introduction.....	32
2.2 Materials and Methods	34
2.2.1 Mechanical characterization via AFM.....	34
2.2.2 Elastomeric ECM/PCM model system	35
2.2.3 Tissue sample preparation	37
2.2.4 Data evaluation.....	38
2.2.5 Scanning electron microscopy	39
2.2.6 Histological staining and immunofluorescence.....	40
2.2.7 Statistical analysis.....	41
2.3 Results	41
2.3.1 Stiffness mapping of ECM/PCM model system.....	41
2.3.2 Stiffness mapping of articular cartilage.....	44
2.4 Discussion.....	47
2.5 Summary.....	53
3. Depth-Dependent Anisotropy of the Micromechanical Properties of Porcine Articular Cartilage Measured via Atomic Force Microscopy	55

3.1 Introduction.....	55
3.2 Materials and Methods.....	58
3.2.1 Tissue sample preparation.....	58
3.2.2 Mechanical characterization via AFM-based stiffness mapping.....	60
3.2.3 Data evaluation.....	62
3.2.4 Histological staining.....	62
3.2.5 Statistical analyses.....	63
3.3 Results.....	64
3.3.1 Picrosirius red staining of porcine articular cartilage.....	64
3.3.2 Depth- and directional-dependence of ECM elastic moduli.....	65
3.3.3 Depth- and directional-dependence of PCM elastic moduli.....	65
3.4 Discussion.....	68
3.5 Summary.....	72
4. Stiffness Mapping of Early Osteoarthritic Changes in the Micromechanical Properties of the Pericellular Matrix in Human Articular Cartilage.....	74
4.1 Introduction.....	74
4.2 Materials and Methods.....	77
4.2.1 Tissue sample preparation.....	77
4.2.2 Mechanical characterization via AFM-based stiffness mapping.....	78
4.2.3 Data evaluation.....	79
4.2.4 Histological staining and immunofluorescence.....	80
4.2.5 Statistical analyses.....	80

4.3 Results	81
4.3.1 Histological staining and immunofluorescence-labeling of human articular cartilage.....	81
4.3.2 AFM stiffness mapping of human articular cartilage	83
4.4 Discussion.....	87
4.5 Summary.....	90
5. Immunofluorescence-Guided Atomic Force Microscopy to Measure the Micromechanical Properties of the Pericellular Matrix of Porcine Articular Cartilage	91
5.1 Introduction.....	91
5.2 Materials and Methods	95
5.2.1 Tissue sample preparation	95
5.2.2 Immunofluorescence for type VI collagen.....	96
5.2.3 Mechanical characterization via AFM stiffness mapping	96
5.2.4 Data evaluation.....	99
5.2.5 Statistical analyses.....	103
5.3 Results	103
5.3.1 Immunofluorescence for type VI collagen.....	103
5.3.2 Influence of immunofluorescence-labeling on articular cartilage micromechanical properties.....	104
5.3.3 AFM stiffness mapping of immunofluorescence-labeled articular cartilage PCM and ECM.....	105
5.3.4 Zonal variation of PCM elastic moduli	108
5.4 Discussion.....	111

5.5 Summary.....	117
6. A Biomechanical Role for Perlecan in the Articular Cartilage Pericellular Matrix	118
6.1 Introduction.....	118
6.2 Materials and Methods.....	121
6.2.1 Tissue sample preparation.....	121
6.2.2 Dual Immunofluorescence for type VI collagen and perlecan	121
6.2.3 Enzymatic digestion of heparan sulfate with heparinase III.....	122
6.2.4 Mechanical characterization via AFM stiffness mapping	123
6.2.5 Data evaluation.....	124
6.3.6 Statistical analyses.....	126
6.3 Results.....	127
6.3.1 Immunofluorescence for type VI collagen and perlecan.....	127
6.3.2 AFM stiffness mapping of type VI collagen and perlecan dual-labeled articular cartilage PCM and ECM.....	128
6.3.3 Immunofluorescence for 3G10, perlecan, and type VI collagen and histological staining analyses of heparinase III-digested articular cartilage.....	131
6.3.4 Effect of heparinase III digestion on PCM and ECM mechanical properties .	133
6.4 Discussion.....	138
6.5 Summary.....	143
7. The Mechanical Properties of the Chondrocyte Pericellular Matrix Exhibit High Resistance to Enzymatic Digestion.....	144
7.1 Introduction.....	144
7.2 Materials and Methods.....	149

7.2.1 Tissue sample preparation	149
7.2.2 Specific enzymatic digestion of aggrecan with ADAMTS-4	149
7.2.3 Specific enzymatic digestion of chondroitin/dermatan sulfate with chondroitinase ABC	150
7.2.4 Specific enzymatic digestion of hyaluronan with bacterial hyaluronidase	150
7.2.5 Broad spectrum enzymatic digestion with elastase	151
7.2.6 Histological staining	151
7.2.7 Immunofluorescence for type VI collagen.....	151
7.2.8 Mechanical characterization via AFM stiffness mapping	152
7.2.9 Data analysis	153
7.2.10 Statistical analysis.....	154
7.3 Results	154
7.3.1 Histological staining of porcine articular cartilage following enzymatic digestion	154
7.3.2 Effect of ADAMTS-4 digestion on PCM and ECM micromechanical properties	155
7.3.3 Effect of chondroitinase ABC digestion on PCM and ECM micromechanical properties.....	157
7.3.4 Effect of hyaluronidase digestion on PCM and ECM micromechanical properties.....	158
7.3.5 Effect of elastase digestion on PCM and ECM micromechanical properties..	159
7.4 Discussion.....	160
7.5 Summary.....	165
8. Summary and Conclusions.....	167

Appendix A. Finite Thickness Correction for Hertz Model.....	173
Appendix B. Low Force Stiffness Mapping of Articular Cartilage.....	175
Appendix C. Effect of Indentation Velocity on the Microscale Properties of Articular Cartilage	179
Appendix D. Spatial Mapping of Proteoglycan and Glycosaminoglycan Depleted Porcine Articular Cartilage.....	182
References	187
Biography	221

List of Tables

Table 2-1: Elastic moduli of ECM and PCM regions from human, porcine, and murine articular cartilage.	46
Table B-1: Elastic moduli of ECM and PCM regions from human, porcine, and murine articular cartilage using low force stiffness mapping.....	177

List of Figures

Figure 1-1: Schematic of AFM operation.	20
Figure 1-2: AFM-based elastic indentation.....	23
Figure 1-3: Comparison of nanoscale and microscale contact areas during AFM indentation of articular cartilage.....	27
Figure 2-1: Selection of PCM and ECM scan regions.....	38
Figure 2-2: Elastomeric ECM/PCM model system.	43
Figure 2-3: Identification of PCM regions in porcine articular cartilage.....	44
Figure 2-4: Stiffness mapping of human, porcine, and murine articular cartilage.....	45
Figure 3-1: Split-line identification and sample preparation for porcine articular cartilage.	60
Figure 3-2: AFM scan regions in articular cartilage zones.	61
Figure 3-3: Picrosirius red staining of porcine articular cartilage.	64
Figure 3-4: Evaluation of ECM microscale anisotropy.	66
Figure 3-5: Evaluation of PCM microscale anisotropy.	67
Figure 4-1: Macroscopic grading of human articular cartilage.	77
Figure 4-2: Histological staining of human articular cartilage.	82
Figure 4-3: Immunofluorescence-labeling of type VI collagen in human articular cartilage.	82
Figure 4-4: Stiffness mapping of human articular cartilage.....	84
Figure 4-5: Stiffness progression of elastic moduli of human articular cartilage from the medial condyle.	85

Figure 4-6: Stiffness progression of elastic moduli of human articular cartilage from the lateral condyle.	86
Figure 5-1: Selection of PCM and ECM scan regions using immunofluorescence.	98
Figure 5-2: Data analysis of immunofluorescence-labeled PCM scan regions.....	102
Figure 5-3: Stiffness mapping of immunofluorescence-labeled PCM.	104
Figure 5-4: Effect of immunofluorescence-labeling on articular cartilage microscale moduli.....	105
Figure 5-5: Elastic modulus vs. fluorescence intensity in PCM scan regions.....	106
Figure 5-6: Linear regression analysis of elastic modulus vs. fluorescence intensity in PCM scan regions.....	107
Figure 5-7: Zonal uniformity in PCM elastic moduli.....	109
Figure 5-8 Stiffness progression of elastic moduli.....	110
Figure 6-1: Dual immunofluorescence-labeling of type VI collagen and perlecan in porcine articular cartilage.	127
Figure 6-2: Stiffness mapping of dual immunofluorescence-labeled PCM.	129
Figure 6-3: Spatial distribution of PCM biochemical composition and biomechanical properties.	130
Figure 6-4: Dual immunofluorescence-labeling of heparinase III-digested porcine articular cartilage.	132
Figure 6-5: Effect of heparinase III digestion on ECM composition and micromechanical properties.	135
Figure 6-6: Effect of heparinase III digestion on PCM micromechanical properties.....	136
Figure 6-7: Effect of heparinase III digestion on the spatial distribution of PCM biochemical composition and biomechanical properties.	137
Figure 7-1: Histological staining of porcine articular cartilage following enzymatic digestion.....	155

Figure 7-2: Stiffness mapping of ADAMTS-4 digested porcine articular cartilage.	156
Figure 7-3: Stiffness mapping of chondroitinase ABC digested porcine articular cartilage.	157
Figure 7-4: Stiffness mapping of hyaluronidase digested porcine articular cartilage.....	158
Figure 7-5: Stiffness mapping of elastase digested porcine articular cartilage.	159
Figure A-1: Effect of finite sample thickness on calculated micromechanical properties of articular cartilage.	174
Figure B-1: Effect of indentation force on measured micromechanical properties of articular cartilage.	178
Figure C-1: Effect of indentation velocity on ECM micromechanical properties.	180
Figure D-1: Stiffness progression of elastic moduli in aggrecanase digested porcine articular cartilage.	183
Figure D-2: Stiffness progression of elastic moduli in chondroitinase ABC digested porcine articular cartilage.	184
Figure D-3: Stiffness progression of elastic moduli in hyaluronidase digested porcine articular cartilage.	185
Figure D-4: Stiffness progression of elastic moduli in elastase digested porcine articular cartilage.	186

List of Abbreviations

Note: Abbreviations defined upon first usage in each chapter

ADAMTS	a disintegrin and metalloproteinase with thrombospondin motifs
AFM	atomic force microscopy
ANOVA	analysis of variance
BSA	bovine serum albumin (bovine albumin solution)
Col6a1	mouse type VI collagen gene alpha-1 subunit
CS	chondroitin sulfate
C-4-S	chondroitin-4-sulfate (chondroitin sulfate A)
C-6-S	chondroitin-6-sulfate (chondroitin sulfate C)
C-ABC	chondroitinase ABC
DS	dermatan sulfate (chondroitin sulfate B)
ECM	extracellular matrix
ERK	extracellular regulated kinase
FCD	fixed charge density
FGF	fibroblast growth factor
FITC	fluorescein isothiocyanate
G1, G2, G3	globular domains of aggrecan
GAG	glycosaminoglycan

HtrA1	high temperature requirement A1
IGD	interglobular domain of aggrecan
KS	keratan sulfate
HA	hyaluronan (hyaluronic acid)
HA-ase	hyaluronidase
HS	heparan sulfate
IF	immunofluorescence
IU	international units
LSD	least significant difference
MMP	matrix metalloproteinase
OA	osteoarthritis
PA	polyacrylamide
PBS	phosphate-buffered saline
PCM	pericellular matrix
PDMS	polydimethylsiloxane
PG	proteoglycan
SEM	scanning electron microscopy
SLRP	small leucine-rich repeat proteoglycan
TBS	tris-buffered saline
TEMED	N,N,N,N-tetramethylethylene diamine

TM	territorial matrix
U	enzyme units
1-dir	direction parallel to split-line orientation
2-dir	direction perpendicular to split-line orientation
3-dir	direction normal to the articular surface

List of Variables

Note: Variables defined upon description of relevant equations in the Introduction.

a	contact radius
α_0, β_0	coefficients in finite thickness correction for Hertz model
C	indentation constant related to z-piezo position and deflection at contact point
C^*	indentation constant in linearized Hertz model related to selected contact point
d	cantilever deflection
d_0	cantilever deflection at contact point
δ	indentation depth
Δ	tip-sample separation
E	elastic modulus
F	force
h	sample thickness
k	cantilever spring constant
ν	Poisson's ratio
r	spherical probe radius
R^2	coefficient of determination

χ	correction factor in finite thickness correction for Hertz model
z	z-piezo position
z_0	z-piezo position at contact point

Acknowledgments

A Ph.D. is a marathon, not a sprint. There are countless ways to measure the distance – 743 GB of data, 8.3 lab notebooks, or 5 years, 6 months, and 8 days. However, the most meaningful measure is the number of people who have been with me every step of the way and helped me reach the finish line.

First and foremost is my advisor, Dr. Farshid Guilak. There are not enough words to express my gratitude for everything that Farsh has done for me over the last 7+ years through his never-ending support, guidance, flexibility, and understanding. I could not have asked for a better person to have as a lifelong mentor and friend. I also extend the sincerest of thanks to the members of my committee – Dr. Mansoor Haider, Dr. Roger Nightingale, Dr. Lori Setton, and Dr. Stefan Zauscher – for their time, insightful discussions, ideas, and collaborations.

There are a number of individuals who deserve recognition for their contributions to the work presented in this dissertation. Dr. Eric Darling introduced me to AFM and his collaboration on the initial stiffness mapping study was invaluable. Dr. Lou DeFrate and his expertise in image analysis in Mathematica were central to the data analysis of IF-guided stiffness mapping. I had the pleasure of working with an incredible Pratt Fellow in Morgan McLeod, who spent countless hours evaluating depth-dependent cartilage microscale anisotropy. The osteoarthritis studies were made

possible by the generosity of the Anatomical Gifts Program of Duke University Medical Center and the surgeons of the Department of Orthopaedic Surgery, specifically Dr. Michael Bolognesi. Lastly, thank you to my funding sources – the NSF Graduate Research Fellowship Program, the Duke University James B. Duke and Pratt-Gardner Fellowships, and grants from the NIH.

The members of the Orthopaedic Research Laboratories have given me so many wonderful memories that I will cherish forever and I have a few scars to ensure that I will never forget. Dr. Amy McNulty, my Pratt Fellows mentor, I cannot thank enough for teaching me to be a scientist and mentor. Every day in lab, I applied a lesson that I learned from her. Thank you to Dr. Holly Leddy for never being too busy for a laugh or a pep talk. I am forever indebted to Bridgette Furman, Dr. Dianne Little, Dr. Brian Diekman, Dr. Chris Gilchrist, Chris Rowland, Jonathan Brunger, and Chia-Lung Wu for their helpful advice about research, classes, and otherwise. Nothing in lab would have been possible without Bob Nielsen, Steve Johnson, and especially Elaine Campbell, without whom we could not have purchased our AFM system.

While the Pratt School of Engineering and MSRB I have been my classrooms, Duke Athletics has been my playground. Over my 10 years at Duke, I attended 185 men's basketball games and was on the quad for the 2010 National Championship bonfire. I will never forget the sleepless Campouts and games in Cameron shared with the GPSC Basketball Committee and Graduate Ushers. I witnessed the reinvention of

Duke Football, rang the Victory Bell, and attended the 2012 Belk Bowl. Beyond all that, I have been truly blessed to interact with amazing athletes, coaches, trainers, and staff. Thank you to Bob Weiseman and Mitch Moser for welcoming me into the Athletics family. To everyone in Facilities and Game Operations, it's been my pleasure to work with you from long before sunrise to long after sunset.

Thanks to everyone who made graduate school unforgettable. To Aubrey Francisco, for all the caffeine breaks, field trips, and hallway laps through every high and low. To Matt Novak, Jon McDaniel, Alex Kent, Chris Grigsby, Meghan Petrie, Stephanie Eyerly, Sarah & Tom Hogan, Adrienne Blount, Sarah Dettenwanger, Michael & Jill Sinclair, Kelly Kimmerling, and my fellow BMEs for all the laughs. To Pam Hanson, Kim Davis, Jennifer Crumpler, and Dr. Michael Gustafson for the dinners, Pratt gear, and memories over 10 Phonathons. To Tracy Wester, Emily Schmidt, Aaron Baxter, and Cameron Harrison for always making time despite the distance. To Mike Sobb, the most positive person I've ever met, for pointing out the 1000 reasons I had to smile over the 100 reasons I saw to cry.

Last but not least, my family. Your unconditional love and support has meant everything to me. To my mom for all that she has given me so that I have had the opportunity to chase every dream. To my dad for introducing me to science and for making me the Duke fan, Phillies fan, runner, and athlete that I am today. Jeremy for being the best big brother a little sister could ask for and for setting the bar so high that I

always had something to reach for. To Fred and Carol for always being in my corner. To my little siblings, Evan and Gwen, for understanding beyond their years and making the most of every visit. I love all you guys more than I can say.

I spent my entire childhood dreaming of coming to Duke. After 10 years and 3 degrees, this place has been more and given me more than I could have ever imagined.

1. Background and Significance

1.1 Articular Cartilage Matrix Organization

1.1.1 Extracellular Matrix

Articular cartilage is the connective tissue that lines the articulating surfaces of diarthrodial joints. The role of cartilage in the joint is primarily mechanical; the tissue provides a nearly frictionless, lubricating, load-bearing surface that supports and distributes forces generated during joint motion. The functional mechanical properties of cartilage are conferred by the tissue's extensive extracellular matrix (ECM) that is composed primarily of water (65 – 80%), type II collagen (15 – 22% wet weight), and proteoglycans (PGs) (4 – 7% wet weight) (McDevitt 1973; Mow et al. 1992; Martel-Pelletier et al. 2008). The ECM is produced and maintained by a single population of cells known as chondrocytes that are found sparsely embedded within the tissue, generally occupying less than 10% of the total tissue volume in adult cartilage (Stockwell 1971; Hunziker et al. 2002).

The cartilage ECM is subdivided into three zones (superficial, middle, and deep) based on distance from the articular surface that are characterized by differences in ECM composition and ultrastructure (Muir et al. 1970; Venn and Maroudas 1977; Jeffery et al. 1991; Hwang et al. 1992; Hunziker et al. 1997; Hughes et al. 2005; Vanden Berg-Foels et al. 2012) and chondrocyte morphology and arrangement (Hwang et al. 1992; Hunziker et al. 2002; Hughes et al. 2005; Quinn et al. 2005). In terms of composition, ECM collagen

content is highest in the superficial zone and decreases with depth through the middle and deep zones. PG content follows an inverse trend, being lowest in the superficial zone and highest in the deep zone (Stockwell and Scott 1967; Muir et al. 1970; Venn and Maroudas 1977; Maroudas et al. 1980). Type II collagen fibers are arranged in an arcade-like architecture through the tissue depth (Jeffery et al. 1991; Hwang et al. 1992). In the superficial zone, closely packed thin fibers (25 – 50 nm diameter) lie parallel to the articular surface with split-lines indicating the preferred fiber orientation relative to the joint surface (Meachim et al. 1974; Below et al. 2002). In the middle zone, fibers are thicker (60 – 140 nm diameter) and are oriented at angles oblique to the articular surface following the split-line direction (Jeffery et al. 1991). In the deep zone, thick fibers (up to 160 nm diameter) are oriented perpendicular to the articular surface and comprise the base of the arcades. Chondrocyte morphology and arrangement reflect the local type II collagen fiber orientation in the ECM. Chondrocytes are ellipsoidal and elongated along split-lines in the superficial zone, more spherical in the middle zone, and are found in a columnar arrangement in the deep zone (Quinn et al. 2005).

Variations in matrix composition and ultrastructure contribute to depth- (Kempson et al. 1973; Jurvelin et al. 1997; Schinagl et al. 1997; Chen et al. 2001; Wu and Herzog 2002; Wong and Sah 2010) and directional-dependent (Mizrahi et al. 1986; Jurvelin et al. 2003; Wang et al. 2003; Chahine et al. 2004; Huang et al. 2005) macroscale mechanical properties of the ECM. In tension, ECM stiffness decreases with depth from

the superficial to the deep zone, reflecting differences in collagen and PG content (Akizuki et al. 1986) and fiber orientation (Chahine et al. 2004). In compression, the aggregate modulus of the ECM increases through the depth of the tissue (Schinagl et al. 1997; Chen et al. 2001), with a difference of up to two orders of magnitude observed between the superficial and deep zones in bovine cartilage (Schinagl et al. 1997).

1.1.2 Pericellular Matrix

Each chondrocyte is surrounded by a narrow region called the pericellular matrix (PCM) that together with the enclosed cell(s) is termed the “chondron” (Benninghoff 1925; Poole et al. 1987). The PCM is biochemically (Poole et al. 1988; Poole et al. 1997; Hunziker et al. 2002) and structurally (Poole et al. 1984; Poole et al. 1987; Hunziker et al. 1997) distinct from the bulk ECM. In normal cartilage, the PCM is often defined by the exclusive presence and localization of type VI collagen around the chondrocyte (Poole et al. 1988; Poole et al. 1992; Hagiwara et al. 1993; Youn et al. 2006) but also contains thin type II collagen fibers (15 – 20 nm diameter) (Poole et al. 1982) as well as type IX and XI collagen (Poole 1997; Poole et al. 1997). The PCM is also characterized by an elevated concentration of PGs (Hunziker et al. 2002), including aggrecan (Poole et al. 1982; Poole et al. 1991a), hyaluronan (HA) (Poole et al. 1991a; Knudson 1993; Cohen et al. 2003), biglycan (Kavanagh and Ashhurst 1999), and perlecan (SundarRaj et al. 1995; Melrose et al. 2006), and glycoproteins, including link protein (Poole et al. 1982), fibronectin (Chang et al. 1997), and laminin (Durr et al. 1996). Unlike

the large, distinct triple helical fibers formed by type II collagen, type VI collagen monomers assemble into characteristic thin (3 – 10 nm diameter) beaded filaments (Bruns et al. 1986). These microfilaments interact with PGs and small diameter type II collagen fibers to form extended hexagonal networks (Kielty et al. 1992; Wiberg et al. 2001; Wiberg et al. 2002; Wiberg et al. 2003) that constitute the mesh-like capsule of the PCM (Poole et al. 1984; Poole et al. 1987). PCM thickness varies locally around single chondrocytes (Poole et al. 1987; Hunziker et al. 1997) and increases with depth through the cartilage zones, ranging from 2 μm thick in the superficial zone to 4 μm thick in the deep zone of porcine cartilage (Youn et al. 2006). PCM morphology, like that of its enclosed chondrocytes, reflects the type II collagen orientation of the local ECM (Youn et al. 2006; Vanden Berg-Foels et al. 2012).

Quantification of the biomechanical properties of the PCM is a challenge due to its micrometer length scale. Previous studies that have directly quantified the elastic and biphasic properties of the PCM required enzymatic (Guilak et al. 1999; Nguyen et al. 2010) and mechanical (Alexopoulos et al. 2003; Alexopoulos et al. 2005b; Guilak et al. 2005; Alexopoulos et al. 2009) isolation of chondrons from the tissue. In micropipette aspiration studies, the Young's modulus of the PCM of mechanically isolated chondrons from human cartilage was reported to be 40 – 70 kPa, an order of magnitude less than the macroscale properties of the surrounding ECM (Alexopoulos et al. 2003; Alexopoulos et al. 2005b). Micropipette aspiration of canine (Guilak et al. 2005) and

human (Alexopoulos et al. 2003; Alexopoulos et al. 2005b) chondrons mechanically isolated from the superficial and middle/deep zones revealed zonal uniformity in the mechanical properties of the PCM, despite the significant zonal differences in ECM properties. One more recent study evaluated the biomechanical properties of the PCM *in situ* indirectly using an inverse boundary element analysis coupled with three-dimensional confocal microscopy of porcine chondrons (Kim et al. 2010). In this study, the Young's modulus of middle zone PCM was estimated to be 25 – 59 kPa. The results from all methods agree that the mechanical properties of the PCM are significantly less than those of the surrounding ECM. However, these methods fail to provide a means for full evaluation of the chondrocyte micromechanical environment *in situ*.

1.1.3 Territorial Matrix

The territorial matrix (TM) is a structural transition region between the fine type VI collagen microfilaments of the PCM and the thick type II collagen fibers of the ECM (Poole et al. 1984). Since no distinct structural boundaries exist among these three matrix regions, the TM has been identified based on qualitative differences in PG staining and type II collagen fibril architecture (Poole et al. 1982; Poole et al. 1984; Poole et al. 1987; Hunziker et al. 1997). While some studies report an abrupt loss in type VI collagen staining at the PCM periphery to mark the PCM-TM transition (Poole et al. 1992; Pullig et al. 1999), others have reported a gradient of increasing type II collagen fiber diameter outward from the PCM, with the TM comprising the regions of thinner, widely-spaced

type II collagen fibers that are directly interwoven with type VI collagen (Soder et al. 2002). Since previous studies of the chondrocyte micromechanical environment have been limited by the need for physical extraction of the chondron and the lack of a precise biochemical definition of the TM, the mechanical properties of the TM region have not been evaluated.

1.2 Biomechanical Role of the Pericellular Matrix

During joint activity, chondrocytes are subjected to a complex mechanical environment consisting of temporal and spatial variations in stress and strain, hydrostatic pressure, streaming potentials, and osmotic pressure (Mow et al. 1994; Bachrach et al. 1998; Lai et al. 2002; Mow and Guo 2002; Wang et al. 2002b). While the exact functional role of the PCM in cartilage is unknown, any signal perceived by the chondrocyte, either biochemical or biomechanical, is likely influenced by the presence of the PCM (Guilak et al. 2006). Since this mechanical environment has been shown to significantly impact the balance of chondrocyte anabolic and catabolic activities and influence the overall health of the joint (Guilak et al. 1997; Grodzinsky et al. 2000; Williams et al. 2010; Guilak 2011), there has been considerable speculation regarding the biomechanical role of the PCM.

It has been hypothesized that each chondrocyte tailors its PCM based on the unique set of dynamic mechanical forces at its position within the matrix (Poole et al. 1988), suggesting that the PCM serves to regulate the biomechanical microenvironment

of the chondrocyte, protecting the cell during compressive loading (Poole et al. 1987), and serving as a transducer of mechanical signals during joint loading (Guilak et al. 2006). Previous theoretical models (Guilak and Mow 2000; Wu and Herzog 2002; Alexopoulos et al. 2005a; Korhonen et al. 2006; Michalek and Iatridis 2007; Korhonen and Herzog 2008; Julkunen et al. 2009) and experimental studies (Knight et al. 1998; Knight et al. 2001; Hing et al. 2002; Choi et al. 2007; Villanueva et al. 2009) have demonstrated that stress and strain in the vicinity of the chondrocyte is significantly influenced by the relative mechanical properties of the cell, PCM, and ECM. In particular, the ratio of PCM to ECM mechanical properties significantly alters stress and strain in the chondrocyte microenvironment (Guilak and Mow 2000), allowing the PCM to facilitate the amplification or shielding of forces depending on a cell's position within the tissue (Choi et al. 2007).

1.3 Glycosaminoglycans and Proteoglycans of Articular Cartilage

Articular cartilage is characterized by a high concentration of PGs and glycosaminoglycans (GAGs). GAGs are long, linear polysaccharides that are most commonly found covalently attached to the core protein of PGs. GAGs are characterized by their high concentration of negatively-charged carboxylate and sulfate groups. The five GAG species found in cartilage are chondroitin sulfate (CS), dermatan sulfate (DS), keratan sulfate (KS), heparan sulfate (HS), and hyaluronan (HA). The specific functional

properties of PGs and their interactions with other matrix proteins are conferred by their unique combination of GAG chains and protein domain structures.

1.3.1 Glycosaminoglycans

Chondroitin sulfate (CS) and dermatan sulfate (DS) are derived from the same unsulfated precursor, chondroitin, which consists of galactosamine and glucuronic acid disaccharide units. The most common chondroitin derivatives, chondroitin-4-sulfate (chondroitin sulfate A, C-4-S), DS (chondroitin sulfate B), and chondroitin-6-sulfate (chondroitin sulfate C, C-6-S), are differentiated by their chemical modifications. C-4-S and C-6-S are sulfated at the 4-position and 6-position of the galactosamine, respectively, whereas DS undergoes conversion of glucuronic acid to iduronic acid and is sulfated at the 4-position of the galactosamine (Ernst et al. 1995; Gandhi and Mancera 2008). CS is the most prominent GAG in articular cartilage (Knudson and Knudson 2001), consisting of at least 80% of the total GAG in the tissue (McDevitt 1973). The proportions of C-4-S and C-6-S vary with age, anatomical location, and depth from the articular surface (Mourao 1988; Caterson et al. 1990; Bayliss et al. 1999). In human cartilage, the proportions of C-4-S and C-6-S in young cartilage (9 years) are approximately 40% and 60%, respectively, as compared to approximately 15% and 85% in old cartilage (60 years) (Bayliss et al. 1999). Overall, CS content and chain length decrease with age (Rosenberg et al. 1965; Buckwalter et al. 1994). On the other hand, DS accounts for less than 1% of the total GAG in cartilage (Burkhardt et al. 1995; Hall et al. 2009).

Keratan sulfate (KS) consists of repeating disaccharide units of glucosamine and galactose with sulfate groups found at the 6-position on almost all glucosamine units and some galactose units (Ernst et al. 1995; Funderburgh 2000). There are two major species of KS (KSI and KSII) that differ in their linkage to the PG core protein. Both are found in articular cartilage. In contrast to CS, KS content and chain length in cartilage increase with age (Bayliss and Ali 1978; Venn 1978; Brown et al. 1998). In porcine cartilage, the ratio of KS to CS increases from approximately 1:30 in fetal tissue to 1:4 in adults (McDevitt 1973).

Heparan sulfate (HS) is structurally related to heparin, containing repeating disaccharide units of glucosamine and either glucuronic acid or iduronic acid (Scott 1988; Ernst et al. 1995; Gandhi and Mancera 2008). While HS has a lower charge density than heparin (Ernst et al. 1995; Gandhi and Mancera 2008), it is still one of the most highly negatively charged extracellular molecules in the body (Kirn-Safran et al. 2009). HS is a minor GAG species in articular cartilage, found on cell-surface PGs and in the chondrocyte microenvironment (Heinegard 2009). In adult rabbit articular cartilage, the ratio of HS to CS was reported to be 1:40 (Price et al. 1996).

1.3.2 Hyaluronan

Hyaluronan (HA) has a homogeneous structure of repeating disaccharide units of glucosamine and glucuronic acid. HA is unique among GAGs in that it is unsulfated, has a very high molecular weight (100 – 10⁴ kDa), and is synthesized as a free

polysaccharide at the plasma membrane that is released directly into the ECM (Ernst et al. 1995; Fraser et al. 1997; Roughley 2006).

Unlike other GAGs, HA is not covalently linked to a PG core protein. Instead, it is recognized by and interacts with several glycoproteins and PGs to form and stabilize large PG aggregates, most notably link protein and aggrecan in the cartilage ECM. While HA demonstrates no electrostatic binding with type II collagen (Scott 1988; Vogel 1994), HA affects type II collagen fiber spacing and sliding and contributes to the very low permeability of cartilage through its role as the backbone of PG aggregates (Vogel 1994; Fraser et al. 1997; Bastow et al. 2008). Specific enzymatic digestion of HA from cartilage explants results in an increase in macroscale tensile properties (Asanbaeva et al. 2008) and a loss of macroscale compressive properties (Broom and Poole 1983) due to the disruption of PG aggregates.

In the cell microenvironment, HA provides a direct link between the chondrocyte and its surrounding matrix via interactions with CD44 (Knudson 2003) and its roles in PCM organization. *In vitro*, chondrocytes synthesize an expansive HA-rich PCM that is dependent on CD44-HA interactions for assembly and retention (Knudson 1993; Lee et al. 1993; Knudson et al. 1996; Maleski and Knudson 1996; Cohen et al. 2003; Rilla et al. 2008). Several studies have demonstrated that HA interacts with type VI collagen microfilaments (McDevitt et al. 1991; Kielty et al. 1992; Specks et al. 1992) and that the presence of HA facilitates spontaneous reassembly of depolymerized type VI collagen

microfilaments (Kielty et al. 1992). Extensive enzymatic digestion of HA significantly alters PCM ultrastructure and morphology *in situ* (Poole et al. 1985). These results suggest that interactions between HA and type VI collagen are essential for microfilament assembly and network stabilization in the PCM.

1.3.3 Aggrecan

Aggrecan is the most prominent PG in articular cartilage. The aggrecan core protein has a modular structure of three globular domains (G1, G2, G3), an inter-globular domain (IGD) between the G1 and G2 domains, and an extended GAG attachment domain between the G2 and G3 domains (Paulsson et al. 1987). The GAG attachment region consists of one KS domain, containing approximately 30 KS chains (Doege et al. 1991; Funderburgh 2000), and two CS domains, containing a total of approximately 100 CS chains (Doege et al. 1991). Aggrecan monomers assemble into large PG aggregates through G1 domain interactions with HA and link protein (Morgelin et al. 1988). The functional properties of aggregates depend upon the number of monomers (10 – 100 per aggregate), the degree of proteolytic processing of the monomers, and the proportion of link protein stabilizing the aggrecan-HA interactions (Roughley et al. 2003; Roughley 2006).

In the ECM, aggrecan fills the spaces within the type II collagen network to generate a fiber-reinforced composite solid matrix (Poole et al. 1982; Mow et al. 1992). Aggrecan interacts with type II collagen through the GAG domains of its core protein

(Hedlund et al. 1999) and strong electrostatic interactions with its CS chains (Obrink et al. 1975; Oegema et al. 1975; Junqueira and Montes 1983; Scott 1988). Through these interactions, aggrecan is thought to mediate type II collagen fiber sliding and retard deformation in response to tensile loading of the tissue (Schmidt et al. 1990; Scott and Stockwell 2006; Asanbaeva et al. 2008).

Aggrecan is the main contributor to cartilage macroscale compressive properties due to its high abundance and highly negative charge (Lai et al. 1991). In total, CS chains contribute 8,000 – 10,000 negatively charged sulfate groups to each aggrecan monomer (Dudhia 2005). These closely spaced, immobilized groups give rise to a high charge density within the tissue referred to as the fixed charge density (FCD). In order to maintain electroneutrality, each fixed negative charge requires a nearby positive ion in the interstitial fluid. As a result, the total ion concentration inside the tissue is greater than in its environment. This imbalance in mobile ions generates the Donnan osmotic pressure and is the main force behind cartilage swelling behavior (Lai et al. 1991). The Donnan osmotic pressure contributes 30 – 50% of the compressive aggregate modulus of articular cartilage (Eisenberg and Grodzinsky 1985; Mow et al. 1998) and approximately 20% of the equilibrium Young's modulus at physiological ionic strength (Sun et al. 2004). Loss of FCD, either through experimental enzymatic digestion (DiSilvestro and Suh 2002; Korhonen et al. 2003; Basalo et al. 2004) or disease (Maroudas and Venn 1977;

Flahiff et al. 2004; Le and Fleming 2008), significantly reduces cartilage macroscale compressive properties.

1.3.4 Decorin and Biglycan

Decorin, a small leucine-rich repeat PG (SLRP), carries a single DS/CS chain on the N-terminal region of its core protein (Krishnan et al. 1999) and non-PG forms are present in adult cartilage (Witsch-Prehm et al. 1992). Decorin is found predominantly in the cartilage ECM, preferentially localized to the superficial and middle zones (Archer et al. 1996; Poole et al. 1996; Kavanagh and Ashhurst 1999). While decorin is designated as a minor component of cartilage, it has been speculated to play a major role in organizing the type II collagen network (Scott 1988; Roughley 2006). Decorin interacts with type II collagen via its core protein (Hedbom and Heinegard 1989; Hedbom and Heinegard 1993) and DS chains (Scott 1988; Vogel 1994) and has been implicated in regulating fiber spacing and inter-fiber interactions (Hedbom and Heinegard 1993; Scott and Stockwell 2006). Specific digestion of DS had no effect on cartilage macroscale tensile or compressive properties, suggesting that DS is not a load-bearing element in the ECM (Hall et al. 2009).

Biglycan is the predominant SLRP in the cartilage PCM (Vogel 1994; Archer et al. 1996; Kavanagh and Ashhurst 1999). Biglycan is biochemically similar to decorin but carries two DS/CS chains on its core protein (Krishnan et al. 1999) and non-PG forms are present in adult cartilage (Witsch-Prehm et al. 1992; Roughley et al. 1993). Biglycan

strongly interacts with type VI collagen via its core protein (Wiberg et al. 2001) and shows no affinity for type II collagen (Roughley 2006). *In vitro*, biglycan efficiently assembles type VI collagen microfilaments into extensive hexagonal networks in a manner that is dependent on intact DS/CS chains (Wiberg et al. 2002). Complexes of biglycan and matrilin-1 mediate interactions between type VI collagen microfilaments and type II collagen and aggrecan in a GAG-independent manner (Wiberg et al. 2003). These results suggest that biglycan is necessary for PCM assembly and structural connection to the adjacent ECM.

1.3.5 Perlecan

Though more commonly associated with basement membranes, perlecan is a prominent PG in the cartilage PCM (SundarRaj et al. 1995; Melrose et al. 2005; Melrose et al. 2006; Kvist et al. 2008). Perlecan is a large, modular HS PG with five distinct domains that contains up to three HS chains in domain I and an additional HS substitution in domain V (SundarRaj et al. 1995; Melrose et al. 2005; Melrose et al. 2006; Kvist et al. 2008), though all can also be alternatively substituted with CS (Kvist et al. 2006; Smith et al. 2007). Perlecan is essential for normal cartilage development and likely plays an important role in cartilage matrix organization. Functional null mutations of perlecan in humans and mice result in potentially lethal skeletal dysplasias (Arikawa-Hirasawa et al. 1999; Costell et al. 1999; French et al. 1999; Arikawa-Hirasawa et al. 2001a; Arikawa-Hirasawa et al. 2001b; Arikawa-Hirasawa et al. 2002) and perlecan-null mice exhibit

similar skeletal abnormalities as type II collagen-null mice (Gustafsson et al. 2003). Perlecan promotes chondrocyte attachment and its prevalence in the chondrocyte microenvironment suggests a functional role in cell-matrix interactions (SundarRaj et al. 1995; Kirn-Safran et al. 2009). Though perlecan domain I HS-deficient mice develop phenotypically normal cartilage (Rossi et al. 2003), the HS chains of perlecan have been implicated in biochemical signaling and matrix organization. Perlecan interacts with and modulates the signaling of multiple growth factors through its HS chains, most notably the fibroblast growth factors (FGFs) (Aviezer et al. 1994; Whitelock et al. 1996; Knox et al. 2002; Smith et al. 2007; Whitelock et al. 2008; Chuang et al. 2010). HS demonstrates strong electrostatic binding affinity for many PCM matrix components, including type VI collagen (Tillet et al. 1994), type II collagen (Scott 1988), fibronectin and laminin (Battaglia et al. 1992). Through these interactions, perlecan may have an important role in structural organization and stabilization of the chondrocyte PCM.

1.4 Osteoarthritis

Osteoarthritis (OA) is a joint disease characterized by the progressive degeneration and loss of articular cartilage, causing severe pain and disability. In the United States, over 20 million people suffer from OA, resulting in a total economic burden of over \$80 billion annually (Buckwalter and Martin 2006; Bitton 2009). While initially thought to be a disease of “normal wear and tear” associated with advanced age, it is now recognized that OA is caused by a complex interplay among biochemical

factors, joint structure, and joint biomechanics (Aigner et al. 2006; Poole et al. 2007; Goldring 2008) that result in an imbalance in anabolic and catabolic signaling pathways in joint tissues (Sandell and Aigner 2001; Sandell 2007).

In the cartilage ECM, degeneration begins at the articular surface and progresses through the depth of the tissue. Early degeneration is marked by physical disruption of the articular surface. Over time, surface fibrillation leads to erosion of the superficial zone and the formation of vertical fissures that eventually reach the subchondral bone (Pritzker et al. 2006). The degradation front is marked by extensive proteolysis of the type II collagen network (Dodge and Poole 1989; Hwang et al. 1992; Hollander et al. 1995; Poole et al. 1997) and PGs (Plaas et al. 2007). During the early stages of OA, chondrocytes increase synthesis of matrix components in an attempt to replace the lost tissue. However, there is evidence of phenotypic change in OA chondrocytes marked by altered expression patterns of types I, II, III, and X collagen (Aigner et al. 1999; Fukui et al. 2008) and altered patterns of PG synthesis (Cs-Szabo et al. 1997; Tesche and Miosge 2004), sulfation (Caterson et al. 1990; Rizkalla et al. 1992; Roughley 2001), glycosylation (Witsch-Prehm et al. 1992; Roughley et al. 1993), distribution (Venn and Maroudas 1977; Poole et al. 1996; Bock et al. 2001; Tesche and Miosge 2004), and aggregate assembly (McDevitt and Muir 1976). This limited repair response cannot overcome the catabolic signaling cascades initiated by the inflammatory and abnormal mechanical environments in the joint (Poole et al. 2007). The net result is an overall loss of ECM

components and a progressive loss of cartilage thickness until the underlying bone is exposed.

Relationships between structural and histological changes and altered cartilage mechanical properties have been observed in all stages of OA degeneration (Armstrong and Mow 1982; Kleemann et al. 2005; Hennerbichler et al. 2008). Disruption of the type II collagen network dramatically decreases the cartilage tensile modulus (Kempson et al. 1973; Akizuki et al. 1986; Setton et al. 1999). Damage to the collagen network, coupled with an increase in water content and loss of PGs, leads to abnormal swelling of the tissue (McDevitt and Muir 1976; Venn and Maroudas 1977) and increased hydraulic permeability (Armstrong and Mow 1982; Setton et al. 1999; Hennerbichler et al. 2008). Combined, these changes contribute to the loss of cartilage compressive properties associated with OA (Armstrong and Mow 1982; Setton et al. 1999; Kleemann et al. 2005; Hennerbichler et al. 2008).

Since chondrocytes produce many of the catabolic enzymes implicated in OA (Cawston and Young 2010), it is not surprising that the PCM undergoes extensive structural and mechanical changes as well. Away from the articular surface, type II collagen and aggrecan degradation products are first observed in the PCM/TM region and later appear in the bulk ECM (Dodge and Poole 1989; Hollander et al. 1995; Gibson et al. 2001; Plaas et al. 2007), supporting the hypothesis that degradative enzymes involved in OA slowly digest their way into and through the tissue to gain access to

remote regions (Bonassar et al. 1995). Despite local enzymatic degradation of the matrix, enlarged chondrons are prevalent OA cartilage (Poole et al. 1991b; Lee et al. 2000). This increase in chondron volume is due to a net increase in PCM matrix component production and deposition (Poole et al. 1991b; Lee et al. 2000; Horikawa et al. 2004), most notably type VI collagen (Hambach et al. 1998; Pullig et al. 1999; Lee et al. 2000), and a loosely organized ultrastructure (Poole et al. 1991b; Lee et al. 2000; Murray et al. 2010), which may be influenced by an altered type VI collagen microfilament structure (Soder et al. 2002) and abnormal swelling (Poole 1997). These structural changes are coupled to a loss of PCM mechanical function. Micropipette aspiration of isolated chondrons from OA cartilage demonstrated a 50% drop in Young's modulus and increased permeability as compared to chondrons from healthy tissue (Alexopoulos et al. 2003; Alexopoulos et al. 2005b).

1.5 Atomic Force Microscopy

The atomic force microscope (AFM) was developed in 1986 by Binnig and colleagues (Binnig et al. 1986) as a means for high resolution topographical imaging of non-conductive surfaces. Over the last 25 years, the applications of AFM have reached beyond topographical imaging and into the realm of biomechanics with its unique combination of piconewton force sensitivity, nanometer spatial resolution, and its ability to perform real-time measurements in aqueous environments (Costa 2003).

1.5.1 Principles of Operation

The principal component of an AFM is a microscopic cantilever and its associated tip (Figure 1-1). The cantilever acts as a mechanical transducer as forces generated during interaction between the tip and the substrate cause the cantilever to deflect. Cantilever deflection is measured using a laser that is reflected off the end of the cantilever onto a photodiode. The distance between the cantilever and the photodiode amplifies the reflected laser motion such that sub-nanometer changes in cantilever deflection can be detected. By calibrating the spring constant (k) of the cantilever from its thermal oscillations (Hutter and Bechhoefer 1993), the force (F) generated during tip-sample interactions is calculated from cantilever deflection (d) using Hooke's Law

$$F = kd \quad (1.1)$$

As a result, the AFM is capable of applying a wide range of loads based on the spring constant of the cantilever.

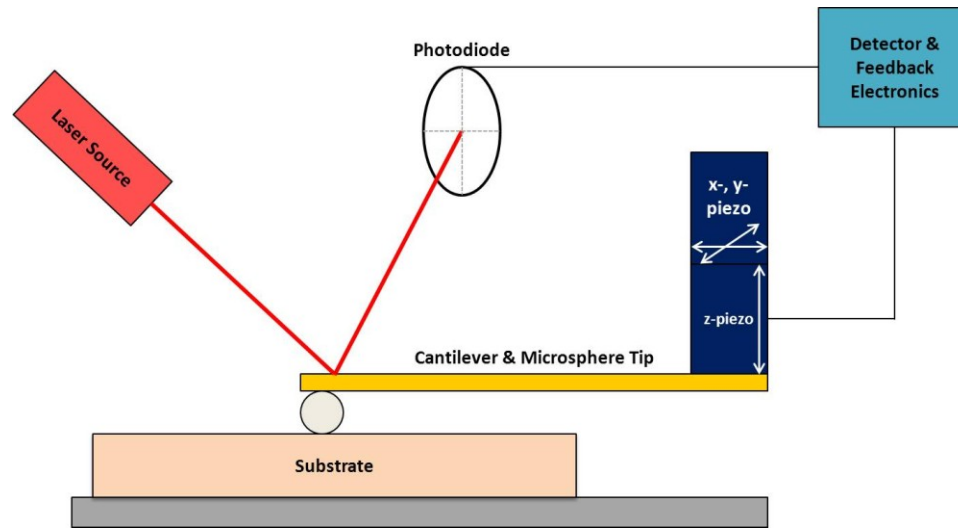


Figure 1-1: Schematic of AFM operation. Interaction between the tip and the substrate causes the cantilever to deflect. This deflection is measured using a laser reflected off the end of the cantilever onto a photodiode. By calibrating the spring constant of the cantilever, the applied force can be calculated. Three piezoelectric actuators control the movement of the cantilever in the x-, y-, and z- directions.

The vertical position of the cantilever is controlled with sub-nanometer precision by a piezoelectric actuator (z-piezo). Two additional piezoelectric actuators control the position of the cantilever in the plane of the substrate (x- and y-piezo), allowing the tip to be raster scanned over a defined region to generate a topographical image.

By taking advantage of the movement capabilities of all three piezos, the AFM can be used to combine topographical imaging with precisely controlled indentation. By collecting indentation arrays, spatial maps of mechanical properties can be overlaid on topographical images for the direct correlation of local mechanical properties with underlying structural features (Radmacher et al. 1992). This technique known as stiffness

or force-volume mapping has been used to investigate the mechanical properties of a number of biological substrates including cells (Hofmann et al. 1997; Rotsch et al. 1997; A-Hassan et al. 1998; Haga et al. 2000; Sato et al. 2007) and local features in soft tissues, including hippocampus (Elkin et al. 2007), cornea (Last et al. 2009), atherosclerotic plaques (Tracqui et al. 2011), and cartilaginous tissues like intervertebral disc (Lewis et al. 2008), fibrocartilage (Hu et al. 2001), growth plate (Allen and Mao 2004; Radhakrishnan et al. 2004), and articular cartilage (Stolz et al. 2004; Tomkoria et al. 2004; Park et al. 2009; Stolz et al. 2009; Desrochers et al. 2010; Loparic et al. 2010).

1.5.2 Evaluation of Elastic Indentation using Modified Hertz Model

For AFM-based elastic indentation, voltage is applied to the z-piezo to displace the cantilever at a specified velocity. Probe contact with the substrate is marked by a sharp increase in cantilever deflection. Once in contact with the substrate, the cantilever continues to descend until a specified trigger force is reached. At this point, the downward motion of the cantilever is stopped and the cantilever is retracted from the surface (Figure 1-2A, B).

Raw data for cantilever deflection and z-piezo position from the indentation portion of the approach curve is subsequently modeled using the Hertz equation for indentation of an isotropic elastic half space with a hard spherical indenter

$$F = \frac{4}{3} \frac{Er^{1/2}}{1-\nu^2} \delta^{3/2} \quad (1.2)$$

where F is the applied force, E is the elastic modulus, r is the radius of the spherical indenter, ν is the Poisson's ratio, and δ is the applied indentation (Harding and Sneddon 1945). The applied force (F) is derived from cantilever deflection using Hooke's Law (Equation 1.1). Indentation (δ) is related to the z -piezo position and cantilever deflection through

$$\delta = (z - z_0) - (d - d_0) \quad (1.3)$$

where z is the z -piezo position at the trigger point, z_0 is the z -piezo position at the contact point, d is the cantilever deflection at the trigger point, and d_0 is the cantilever deflection at the contact point (Dimitriadis et al. 2002) (Figure 1-2c).

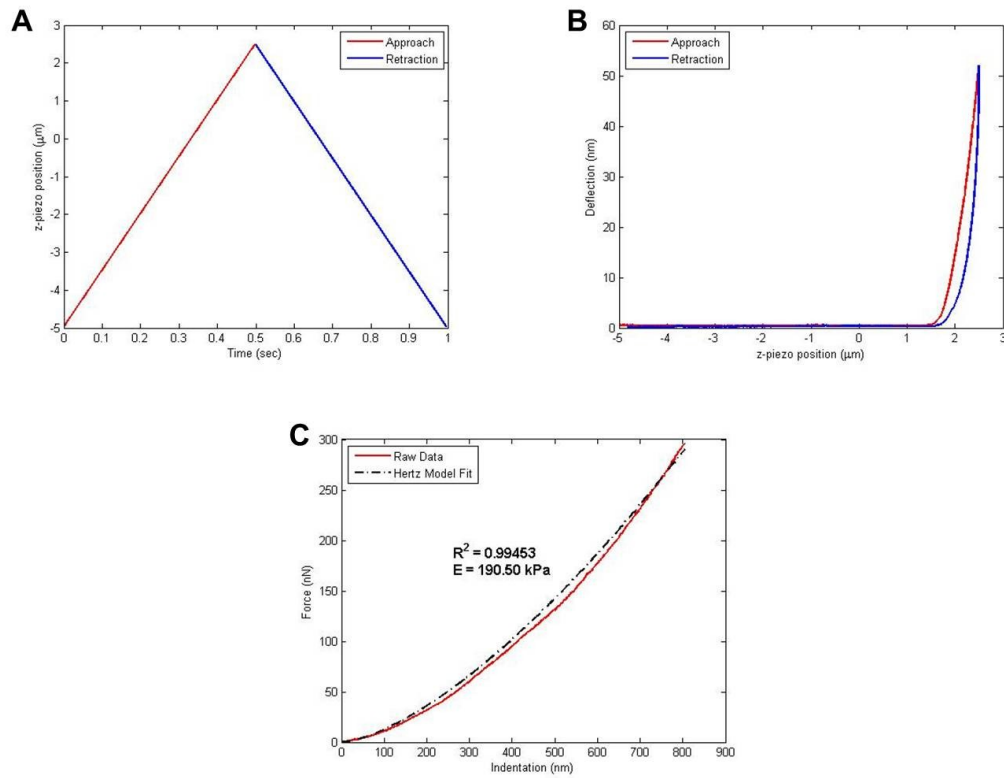


Figure 1-2: AFM-based elastic indentation. (A) Z-piezo movement during a single indentation consists of two ramp displacements at a specified velocity comprising the approach (red) and retraction (blue) of the cantilever. (B) Raw data for cantilever deflection and z-piezo position is recorded during indentation. Contact with the substrate is marked by a sharp increase in cantilever deflection. (C) Force-indentation data from the indentation portion of the approach curve (red) is curve-fit with a modified Hertz model (black) to calculate the elastic modulus of the substrate.

When the Hertz model is used in the form presented in Equation 1.2, it is essential to determine the exact contact point between the probe and the substrate to achieve an accurate calculation of the indentation. Precise definition of the contact point is difficult when performing indentation on low modulus materials and even small errors in contact point selection can result in significant errors in the calculated elastic

modulus (Dimitriadis et al. 2002; Guo and Akhremitchev 2006). To address this problem, Guo and Akhremitchev introduced a contact point extrapolation method that applies a linearized Hertz model to calculate the elastic modulus (Guo and Akhremitchev 2006). Briefly, indentation can be rewritten as

$$\delta = C - \Delta \quad (1.4)$$

where $C = d_0 - z_0$ represents a constant related to the unknown contact point and $\Delta = z - d$ represents the tip-sample separation. The linearized Hertz model uses the slope of the $F^{2/3}$ vs. Δ curve to calculate the elastic modulus

$$F^{2/3} = C^* - \left[\frac{4}{3} \frac{Er^{1/2}}{1-\nu^2} \right]^{2/3} \Delta \quad (1.5)$$

where C^* is a constant that depends on the selection of tip-sample contact point. The Poisson's ratio (ν) is selected based on previously published values for the substrate of interest. Following calculation of the elastic modulus, the contact point can be extrapolated from the x- and y-intercepts of the linearized Hertz model.

Application of the Hertz model to thin soft samples can lead to significant errors in calculated moduli under finite deformations due to contributions from the underlying substrate. However, few theoretical models are tractable for routine analysis of the large number of force-indentation curves required for AFM-based stiffness mapping. To this end, a polynomial-based correction factor for the Hertz model was developed by Dimitriadis and colleagues (Dimitriadis et al. 2002) that depends on probe radius,

indentation depth, sample thickness, and sample Poisson's ratio (Appendix A). In cases of finite deformation, the calculated elastic modulus from the linearized Hertz model can be multiplied by the polynomial to correct for apparent stiffening related to finite sample thickness. In the current work, applied forces and indentation depths were selected to minimize these effects.

1.5.3 Influence of Probe Geometry on AFM-based Indentation

Previous studies have shown that experimental parameters chosen for AFM-based indentation, including applied force (Appendix B)(Park et al. 2009), indentation velocity (Appendix C)(Han et al. 2011), probe shape and size (Costa and Yin 1999; Dimitriadis et al. 2002; Stolz et al. 2004; Stolz et al. 2009; Loparic et al. 2010), and accurate representation of tip geometry in model fitting (Costa and Yin 1999), can impact the measured mechanical properties (Stolz et al. 2004; Park et al. 2009). Probe geometry in particular has been shown to significantly affect the material properties drawn from AFM indentation of soft samples (Costa and Yin 1999; Dimitriadis et al. 2002), including articular cartilage (Stolz et al. 2004; Stolz et al. 2009; Loparic et al. 2010).

Nanometer-sized pyramidal tips (20 nm diameter) generate local stress concentrations and large strains at the point of contact that often fall outside the linear, small strain regime. In addition to potentially damaging soft biological samples, these finite deformations generate significant errors when using models that are derived from linear elasticity, including the Hertz model (Equation 1.2). On the other hand, microscale

spherical probes cause minimal stress and strain concentrations for the same applied force (Costa and Yin 1999; Dimitriadis et al. 2002).

Furthermore, there are inherent physical differences in load support when performing indentation with a nanometer-sized tip as compared to a microscale spherical probe. Since nanometer-sized tips are smaller than the diameter of individual collagen fibers (20 – 160 nm diameter (Hwang et al. 1992)), moduli obtained using nanoindentation methods reflect those of individual matrix components (Loparic et al. 2010) (Figure 1-3). On the other hand, micrometer-sized spherical tips are large enough that structural elements act in concert to support the applied load in a manner that is more similar to macroscale indentation (Stolz et al. 2004; Loparic et al. 2010). As a result, a difference of two-orders of magnitude was observed in articular cartilage ECM elastic moduli measured using a nanometer-scale pyramidal tip as compared to a micrometer-scale spherical tip (Stolz et al. 2004) with microscale elastic moduli being more comparable to macroscale measurements.

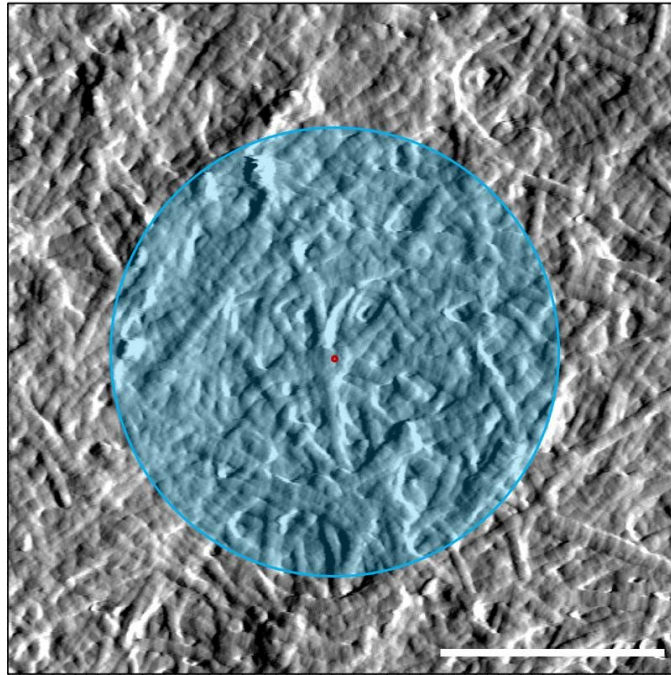


Figure 1-3: Comparison of nanoscale and microscale contact areas during AFM indentation of articular cartilage. A representative AFM image of the porcine articular cartilage ECM is shown. Nanometer-sized pyramidal tips generate contact footprints (10 nm contact radius; red) that are smaller than the diameter of individual collagen fibers, resulting in moduli that reflect individual matrix components. Micrometer-sized spherical tips generate contact footprints (1 μm contact radius; blue) that are large enough that matrix components act in concert to support the applied load in a manner more similar to macroscale indentation. Scale bar = 1 μm.

While microscale spherical probes reduce stress concentration and yield moduli comparable to macroscale properties, use of large probes limits lateral resolution. Any topographical image obtained with AFM is the convolution of the true surface topography and the probe geometry. As a result, information is lost when features have smaller or similar radii as compared to the probe. When performing indentation, the

contact radius, a , scales with both probe radius (r) and indentation depth (δ) (Dimitriadis et al. 2002) as described by

$$a = \sqrt{r\delta} \quad (1.6)$$

For a given indentation depth, larger radius probes generate a larger contact footprint than smaller probes and calculated mechanical properties reflect those of the entire contact footprint, not just the specific point of interest. As a result, the mechanical properties of features smaller than the contact radius cannot be independently resolved.

1.6 Research Goals and Significance

The overall goals of this research are to develop techniques that seek to:

1) evaluate the microscale elastic properties of the cartilage PCM and ECM *in situ* and

2) correlate site-specific biochemical composition with biomechanical properties of the PCM and ECM.

Previous studies of PCM mechanical properties have been limited by the need for physical extraction of chondrons from the tissue. The first research goal seeks to validate and apply an AFM-based microindentation technique to directly evaluate the biomechanical properties of the PCM and ECM *in situ* with minimal disruption of native matrix integration.

The relationship between the molecular constituents of the cartilage matrix and its mechanical properties are not fully understood. The second research goal seeks to

develop a novel immunofluorescence-guided AFM microindentation technique to correlate site-specific biochemical composition with biomechanical properties within the cartilage PCM and ECM, allowing for a more complete characterization the chondrocyte micromechanical environment *in situ*.

1.7 Hypotheses and Aims

These two research goals were addressed through a total of six hypotheses and specific aims. Aim 1 involved the validation of AFM-based stiffness mapping for determining site-specific mechanical properties at the microscale in control surfaces and human, porcine, and murine articular cartilage. Aim 2 was accomplished through the application of AFM stiffness mapping to evaluate microscale anisotropy of porcine articular cartilage ECM and PCM. Aim 3 was accomplished by evaluating PCM and ECM biomechanical properties in human articular cartilage from macroscopically normal and early OA knee joints. Aims 4 and 5 were accomplished by developing a novel immunofluorescence (IF)-guided AFM microindentation technique. Using IF-labeling for PCM-specific matrix components in porcine articular cartilage, biochemical composition of the PCM was correlated with its biomechanical properties. Aim 6 was accomplished by combining IF-guided AFM stiffness mapping with enzymatic digestion of GAGs and PGs in porcine articular cartilage.

Hypothesis 1: *The microscale elastic modulus of the cartilage ECM is greater than that of the PCM.*

Specific Aim 1: The microscale mechanical properties of the articular cartilage ECM and PCM will be evaluated *in situ* using an experimentally-validated AFM stiffness mapping technique.

Hypothesis 2: *The cartilage ECM exhibits depth- and directional-dependent microscale mechanical properties whereas PCM moduli are uniform with depth and isotropic.*

Specific Aim 2: Microscale elastic moduli of porcine articular cartilage ECM and PCM will be evaluated within each zone in three mutually-perpendicular directions relative to the split-line orientation.

Hypothesis 3: *The cartilage ECM and PCM exhibit alterations in microscale elastic moduli and their spatial distribution with the onset of OA.*

Specific Aim 3: ECM and PCM microscale mechanical properties will be mapped quantitatively in normal and early OA human articular cartilage.

Hypothesis 4: *PCM biomechanical properties correlate with the presence of type VI collagen in the chondrocyte microenvironment.*

Specific Aim 4: Immunofluorescence will be combined with AFM-based stiffness mapping to evaluate the influence of the presence of type VI collagen on site-specific mechanical properties of cartilage *in situ*.

Hypothesis 5: *Perlecan is a defining factor in the boundaries of the PCM and contributes to site-specific mechanical properties within PCM regions. The enzymatic removal of*

heparan sulfate reduces the microelastic properties of the PCM while having no effect on ECM properties.

Specific Aim 5: Dual immunofluorescence for type VI collagen and perlecan will be used to guide AFM-based stiffness mapping and characterize the role of perlecan in the PCM.

Hypothesis 6: Loss of mechanical integrity in the cartilage PCM and ECM is observed following enzymatic digestion of aggrecan and aggrecan-associated GAGs.

Specific Aim 6: Specific and broad spectrum enzymatic digestion will be performed in conjunction with immunofluorescence-guided AFM stiffness mapping to characterize the region-specific contributions of aggrecan, CS/DS, and HA to cartilage micromechanical properties.

2. Spatial Mapping of the Biomechanical Properties of the Pericellular Matrix of Articular Cartilage Measured *in situ* via Atomic Force Microscopy

A version of this chapter was published as the following:

Darling, E.M.*, Wilusz, R.E.*, Bolognesi, M.P., Zauscher, S., Guilak, F. Spatial Mapping of the Biomechanical Properties of the Pericellular Matrix of Articular Cartilage Measured *in situ* via Atomic Force Microscopy. *Biophysical Journal*, 98(12):2848-56, 2010. (*E.M. Darling and R.E. Wilusz contributed equally to this work)

2.1 Introduction

Chondrocytes are embedded within an extensive extracellular matrix (ECM) that gives articular cartilage its functional mechanical properties. Each chondrocyte is surrounded by a distinct narrow region called the pericellular matrix (PCM) that together with the enclosed cell is termed the “chondron” (Benninghoff 1925; Poole et al. 1987). The mechanical properties of chondrocytes (Lee and Bader 1995; Trickey et al. 2000; Trickey et al. 2004; Leipzig and Athanasiou 2005; Darling et al. 2006; Shieh and Athanasiou 2006; Trickey et al. 2006; Darling et al. 2008) and the cartilage ECM (Mow et al. 1980; Armstrong and Mow 1982; Athanasiou et al. 1991; Schinagl et al. 1997; Stolz et al. 2004; Tomkoria et al. 2004; Kleemann et al. 2005; Stolz et al. 2009) have been characterized extensively using multiple techniques. For the PCM, previous studies have evaluated the elastic and biphasic properties of enzymatically and mechanically isolated chondrons using micropipette aspiration (Guilak et al. 1999; Alexopoulos et al. 2003; Alexopoulos et al. 2005b; Guilak et al. 2005; Alexopoulos et al. 2009). The Young’s

modulus of the PCM was reported to be 40 – 70 kPa, an order of magnitude less than that of the macroscale modulus of the surrounding ECM (Alexopoulos et al. 2003). While enzymatic isolation has been shown to significantly reduce PCM mechanical properties as compared to mechanical isolation (Knight et al. 2001; Guilak et al. 2005), the influence of mechanical isolation on PCM properties is unknown. Few studies have measured the biomechanical properties of cartilage PCM and its associated ECM *in situ*. In one recent study (Kim et al. 2010), the mechanical properties of the PCM were determined *in situ* using an inverse boundary element analysis coupled with three-dimensional confocal microscopy of chondron shape during compressive loading. In that study, the Young's modulus of the PCM in intact porcine cartilage was estimated to be 24 – 59 kPa.

Atomic force microscopy (AFM) provides a method for precise control of indentation testing that can be used to characterize samples down to the nanometer length scale (Ludwig et al. 2008). In addition to allowing for microscale measurements, a major advantage of AFM is its ability to simultaneously obtain height and elasticity data for a region of interest (Radmacher et al. 1992). This stiffness mapping technique, sometimes referred to as force-volume mapping (Gad et al. 1997), can be used to measure the elastic modulus of a sample at distinct points as the probe raster scans across a specified region. Stiffness mapping via AFM has been used to investigate the mechanical properties of cells (Hofmann et al. 1997; Rotsch et al. 1997; A-Hassan et al. 1998) and local features in soft tissues, including the hippocampus (Elkin et al. 2007),

cornea (Last et al. 2009), and cartilaginous tissues (Hu et al. 2001; Allen and Mao 2004; Stolz et al. 2004; Tomkoria et al. 2004; Lewis et al. 2008; Park et al. 2009; Stolz et al. 2009). For example, using a nanoscale approach, Allen and Mao (Allen and Mao 2004) showed significant differences between the elastic moduli of the pericellular and interterritorial matrices of rat growth plate cartilage. Previous studies have shown that experimental parameters chosen for mechanical testing, including probe shape and size, indentation velocity, indentation depth, and accurate representation of tip geometry in model fitting (Costa and Yin 1999), impact the measured mechanical properties derived from AFM indentation (Stolz et al. 2004; Park et al. 2009).

The objective of this study was to use AFM to quantify the microscale biomechanical properties of matched ECM and PCM regions of articular cartilage *in situ*. First, we validated the microscale stiffness mapping technique and its ability to measure the spatial distribution and mechanical properties of two materials using an elastomeric ECM/PCM model system. This indentation technique was subsequently used to measure the elastic properties of ECM and PCM in the middle/deep zones of human, porcine, and murine articular cartilage *in situ*.

2.2 Materials and Methods

2.2.1 Mechanical characterization via AFM

Elastic moduli were mapped quantitatively with the use of a stand-alone atomic force microscope (MFP-3D; Asylum Research, Santa Barbara, CA). Borosilicate glass

spheres (5 μm diameter) were attached to the end of AFM cantilevers ($k = 7.5 \text{ N/m}$; Novascan Technologies, Ames, IA) to facilitate microscale testing. Indentation curves were sampled at 5 kHz, with a force trigger of 750 nN prescribing the point at which the cantilever approach was stopped and retracted. An additional set of experiments was performed using a force trigger of 50 nN, but results indicated that larger indentations were necessary to evaluate macroscale-equivalent cartilage properties (Appendix B). For evaluation of PCM elastic properties, indentations (900 – 1600 sites per region, 15 $\mu\text{m/s}$ indentation velocity) were sequentially applied over a region of interest as defined by microscopic examination (Figure 2-1, 2-2). ECM elastic properties were evaluated using the same technique over regions visually devoid of PCM (16 sites per region, 15 $\mu\text{m/s}$ indentation velocity).

2.2.2 Elastomeric ECM/PCM model system

We validated the stiffness mapping technique by probing an elastomeric model of a soft inclusion within a stiff medium. Polyacrylamide (PA) hydrogels were chosen as our model materials because they have been used previously to create cell culture substrates with ECM-like stiffness (Engler et al. 2006), have mechanical properties that are tunable over three orders of magnitude by adjusting the relative amounts of acrylamide and bis-acrylamide in solution to vary the gel cross-link density (Pelham and Wang 1997; Peyton and Putnam 2005; Engelmayr and Sacks 2008), and can be patterned using soft lithography (Di Benedetto et al. 2005; Snyder et al. 2007).

For our model system, soft lithography was used form a higher-modulus PA mold (final acrylamide concentration of 15%, final bis-acrylamide concentration of 1.2%) with a regular pattern of holes (20 μm diameter, 12 μm depth, 50 μm center-to-center distance). Holes were filled with a lower-modulus PA (final acrylamide concentration of 8%, final bis-acrylamide concentration of 0.6%) supplemented with tissue marking dye to distinguish the two materials (Figure 2-2). To lower surface tension and improve filling of the mold, 0.1% v/v Tween20 (Sigma-Aldrich, St. Louis, MO) was added to the lower-modulus PA solution. All solutions were prepared using pre-mixed solutions of 40% acrylamide and 2% bis-acrylamide (Bio-Rad Laboratories, Hercules, CA) with 1% v/v 1.0 M HEPES (pH 8.5; Gibco, Carlsbad, CA) and purified water (Sigma-Aldrich). Polymerization was initiated with ammonium persulfate (10% w/v solution in water; Bio-Rad) (1:200 v/v) and N,N,N,N-tetramethylethylene diamine (1:2000 v/v; TEMED; Bio-Rad).

A similar model was made using polydimethylsiloxane (PDMS) to validate testing on higher-modulus materials. The higher-modulus mold was comprised of 10:1 elastomer/curing agent mixture of PDMS (Sylgard 184 Silicone Elastomer Kit; Dow Corning Corporation, Midland, MI). Holes were filled with a 30:1 elastomer/curing agent mixture of PDMS supplemented with tissue marking dye.

PA models were tested in water, and PDMS models were tested in air by AFM using the previously described protocol. Bulk gels from the same PA mixtures were

tested in unconfined compression on a materials testing system (ElectroForce 3200; Bose-EnduraTec, Eden Prairie, MN) to obtain macroscale properties.

2.2.3 Tissue sample preparation

Articular cartilage was obtained from three different species (human, porcine, and murine) to illustrate the versatility of the microscale stiffness mapping technique. Human samples were taken from macroscopically normal regions of femoral condyles removed during total knee replacement surgery or from normal knee joints at autopsy. Porcine samples were collected from central regions of the medial condyle of skeletally mature knee joints with no visible signs of joint degeneration. For murine samples, entire knee joints from 3-week-old C57BL/6 mice were harvested for evaluation purposes. All cartilage samples were wrapped in phosphate-buffered saline (PBS)-soaked gauze and frozen at -20°C for intermediate storage.

To evaluate *in situ* matrix properties, samples were sectioned perpendicular to the cartilage surface in 3 – 5 µm thick slices using a cryostat microtome (Leica CM1850; Leica Microsystems, Inc., Buffalo Grove, IL). Human and porcine samples were composed completely of articular cartilage. Due to size limitations, murine samples were sectioned through the entire joint to obtain a cross-section of the cartilage tissue. Samples were sectioned onto glass slides, and the water-soluble embedding medium (Tissue-Tek O.C.T. Compound; Sakura Finetek USA, Inc., Torrance, CA) was washed

thoroughly from all samples before AFM indentation was performed. Cartilage slices remained in PBS at room temperature for the duration of mechanical testing.

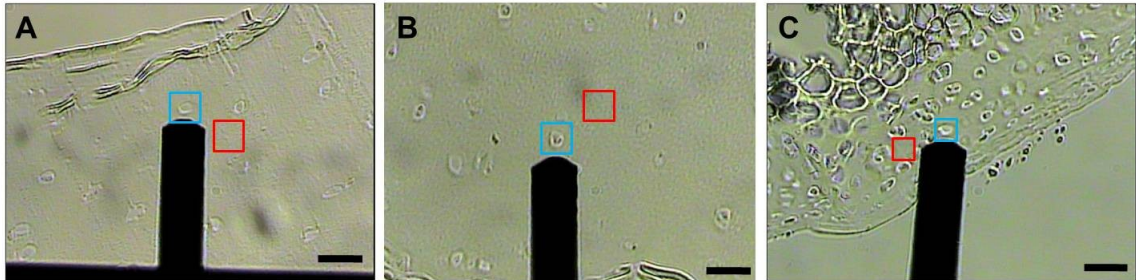


Figure 2-1: Selection of PCM and ECM scan regions. PCM (blue) and ECM (red) scan regions in (A) human, (B) porcine, and (C) murine articular cartilage were selected based on microscopic examination of cell-sized voids in the tissue section. The AFM cantilever is also shown. Scale bar = 30 μm .

2.2.4 Data evaluation

Raw data for cantilever deflection and z-piezo movement were collected and subsequently analyzed using a custom MATLAB script (The MathWorks, Natick, MA). Elastic moduli, E , were determined by fitting a modified Hertz model to force-indentation curves as described previously (Darling et al. 2006). For the elastomeric ECM/PCM model systems, the Poisson's ratio, ν , was assumed to be 0.5 for PDMS (Carrillo et al. 2005) and 0.45 for PA (Engler et al. 2004). For articular cartilage, past studies have reported a wide range of Poisson's ratios, and a definitive value describing the ECM and PCM at the microscale is uncertain. In this study, the local Poisson's ratio was assumed to be 0.04 for both the ECM (Chen et al. 2001; Choi et al. 2007) and PCM (Alexopoulos et al. 2005b) based on previous experimental reports. Nonetheless, from

the Hertz model, the presented modulus values can be converted from $\nu = 0.04$ to a different assumed value of ν by multiplying by the conversion factor $(1 - \nu^2)/(1 - 0.04^2)$. Probe surface contact was identified using contact point extrapolation, a method that focuses on the indentation portion of the approach curve to determine where indentation begins based on a mathematical model (Guo and Akhremitchev 2006). With the contact point determined, relative surface heights were calculated within each scan region. Height maps were generated and overlaid with a graded color map representative of material modulus (Figure 2-2C, Figure 2-4A, D, G).

PCM regions were identified using spatial indicators present in each stiffness map. Thinly sliced cartilage sections provided a relatively flat, uniform surface interspersed with cell-sized holes (Figure 2-1). Voids were chosen that had no apparent cell debris and exhibited sharp contact with the underlying glass substrate in their centers. Contact with the glass was readily apparent from the indentation curves and used to define the edge of each cell void. For evaluation purposes, PCM data were included for a region extending 1 μm outward from this edge (Figure 2-4B, E, H), although it is possible that the PCM extends further depending on its position within the tissue depth (Youn et al. 2006).

2.2.5 Scanning electron microscopy

Cartilage sections were examined via scanning electron microscopy (SEM) to visualize tissue ultrastructure present during mechanical testing. Sectioned samples of

healthy porcine cartilage were prepared using the standard protocols of Duke University's Shared Materials Instrumentation Facility. Briefly, samples were fixed in 3.7% formaldehyde, washed with PBS, and treated with 1% OsO₄ (Electron Microscopy Sciences, Hatfield, PA) for 1 hour, followed by dehydration in serial gradations of ethanol. Samples were then incubated in tetramethylsilane (Electron Microscopy Sciences) and allowed to dry before being sputter-coated with gold by means of a Desk IV sputter coater (Denton Vacuum, Moorestown, NJ). Cartilage sections were imaged using an FEI XL30 scanning electron microscope (FEI, Hillsboro, OR).

2.2.6 Histological staining and immunofluorescence

For histological staining, porcine cartilage sections were fixed in 10% formaldehyde for 10 minutes at room temperature immediately after mechanical testing. Fixed sections were rinsed with PBS and dehydrated in ethanol. Sections were stained with 0.02% aqueous fast green (Sigma-Aldrich) and Accustain Safranin-O solution (Sigma-Aldrich).

Unfixed porcine sections were labeled using immunofluorescence (IF) for type VI collagen to illustrate the presence of the PCM around cell-shaped holes using a previously described protocol (Youn et al. 2006). Specimens were labeled using a primary anti-type VI collagen antibody (RDI-6000401108; Fitzgerald Industries International, Acton, MA) followed by a fluorescein isothiocyanate (FITC)-conjugated anti-rabbit secondary antibody (RDO-7111095152; Fitzgerald). IF-labeled sections were

visualized on a confocal laser scanning microscope (LSM 510; Carl Zeiss, Inc., Thornwood, NY).

2.2.7 Statistical analysis

Differences between the two regions for PA (n = 6) or PDMS (n = 4) model systems were evaluated using a two-way ANOVA (region, length scale; $\alpha = 0.05$) with Fisher's least significant difference (LSD) *post-hoc* analysis to determine the level of significance. A two-way ANOVA (region, species; $\alpha = 0.05$) and Fisher's LSD *post-hoc* test were used to analyze ECM/PCM comparisons in the middle/deep zones of human (N = 6 joints, n = 19 total regions), porcine (N = 6 pigs, n \geq 15 total regions), and murine (N = 6 mice, n \geq 16 total regions) cartilage samples. All data are presented as mean \pm standard deviation.

2.3 Results

2.3.1 Stiffness mapping of ECM/PCM model system

Stiffness mapping successfully depicted the spatial arrangement of moduli in elastomeric model systems (Figure 2-2). Artificial PA ECM/PCM structures exhibited moduli of 309 ± 16 kPa and 55 ± 12 kPa for the ECM and PCM materials, respectively ($p < 0.0001$; Figure 2-2D). For the PCM material, there was no statistical difference between microscale moduli and the macroscale value of 55 ± 5 kPa ($p = 0.39$). The microscale modulus of the ECM material was significantly greater than that observed at the microscale (259 ± 27 kPa; $p < 0.001$), a difference likely attributed to local variations in

acrylamide cross-link density (Matsuo et al. 1994). Microscale elastic moduli showed excellent agreement with previously published macroscale values for the chosen acrylamide and bis-acrylamide concentrations (Peyton and Putnam 2005).

The elastomeric model system was also validated for higher modulus materials using a combination of high- and low-modulus PDMS. These ECM/PCM samples possessed moduli of 2.8 ± 0.5 MPa and 0.8 ± 0.3 MPa for the ECM and PCM materials, respectively ($p < 0.0001$). Microscale moduli measured for PDMS agreed with the macroscale values previously reported in the literature ($E = 2.8$ MPa for 10:1 PDMS, $E = 0.88$ MPa for 30:1 PDMS; (Carrillo et al. 2005)).

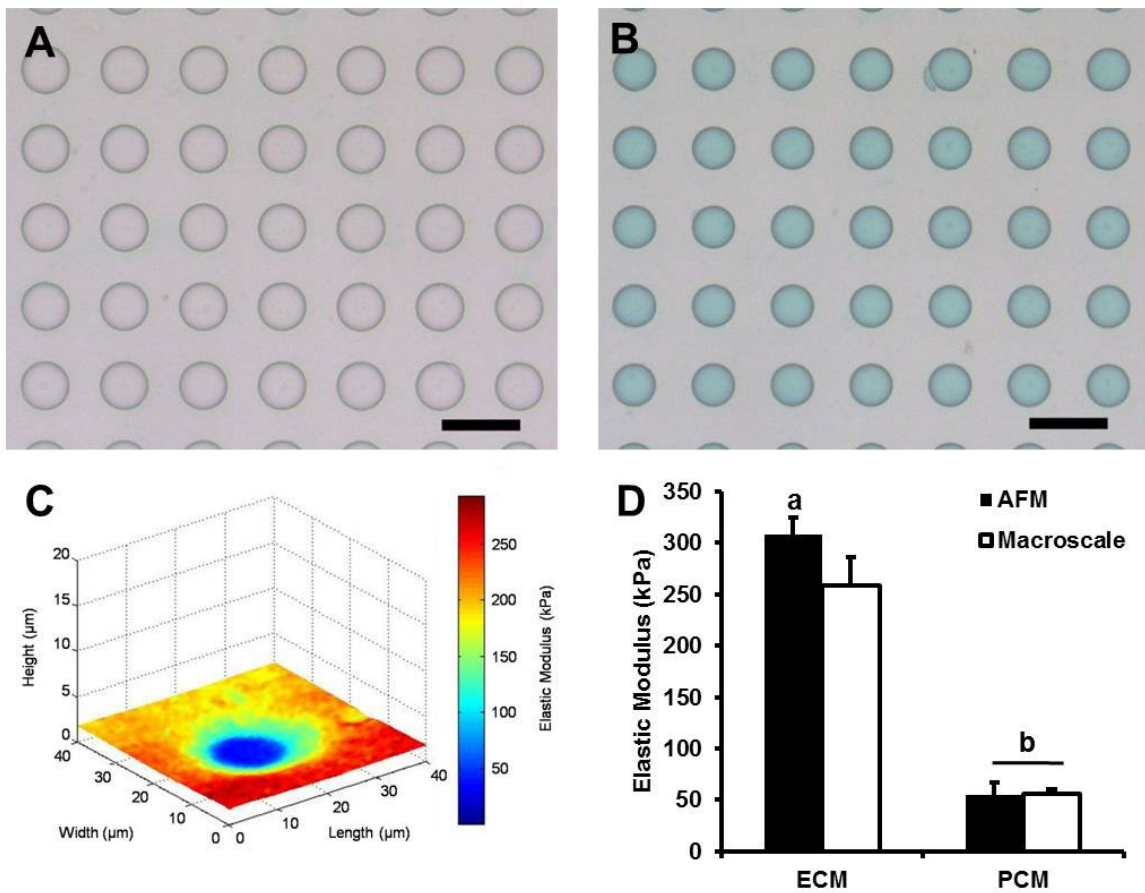


Figure 2-2: Elastomeric ECM/PCM model system. (A) Higher modulus PA gel mold of regularly spaced holes representing the ECM. (B) Holes filled with lower modulus PA gel (green) complete the ECM/PCM model system. Scale bar = 50 μm . (C) Stiffness map of model PCM region showing relative height and calculated elastic moduli. (D) Elastic moduli of the model ECM and PCM PA gels observed at the microscale (black) and macroscale (white). a: $p < 0.0001$ for microscale ECM PA gel moduli as compared to macroscale moduli. b: $p < 0.001$ for PCM PA gel moduli as compared to respective ECM PA gel moduli. Moduli presented as mean + standard deviation ($n = 6$ regions).

2.3.2 Stiffness mapping of articular cartilage

Thinly sectioned articular cartilage samples exhibited microscopic features that were consistent with the location of PCM within the tissue. Tissue within 1 μm of cell-sized voids was considered PCM, an assumption validated by SEM images of tissue sections, a higher concentration of PGs in Safranin-O stained samples, and localization of type VI collagen around chondrocytes (Figure 2-3).

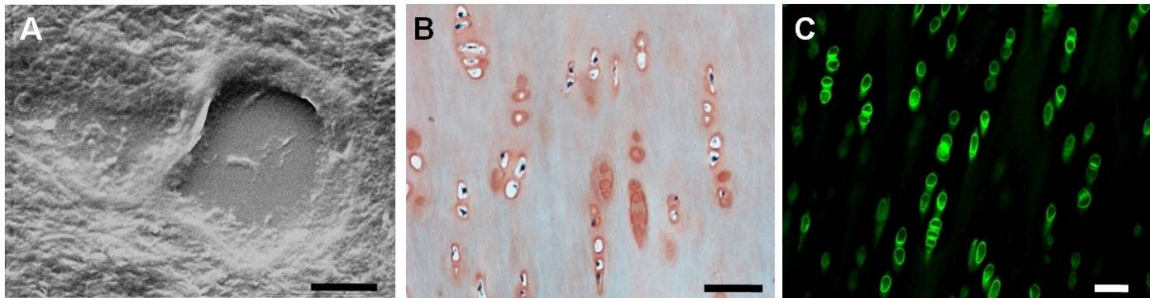


Figure 2-3: Identification of PCM regions in porcine articular cartilage. (A) In a SEM image of a cell-sized void in the middle/deep zone of a tissue section, the capsule-like PCM is structurally distinct from the surrounding ECM. Scale bar = 5 μm . (B) In sections stained with Safranin-O (red, PG) and fast green (blue, collagen), Safranin-O staining is more intense in regions surrounding cell-sized voids. Scale bar = 50 μm . (C) IF illustrates the localization of type VI collagen to the pericellular region. Scale bar = 50 μm .

Topographical maps corresponded to the images created from collected force-indentation data, allowing for co-localization of height and elasticity measurements throughout the tested regions (Figure 2-4A, D, G). Hertzian contact mechanics provided excellent fits to the experimental data for all force-indentation curves ($R^2 > 0.90$). Histograms of calculated elastic moduli (Figure 2-4C, F, I) exhibited a bimodal

distribution with a lower modulus peak corresponding to points within the pre-defined 1 μm PCM region and a higher modulus peak corresponding to the local ECM within each scan region.

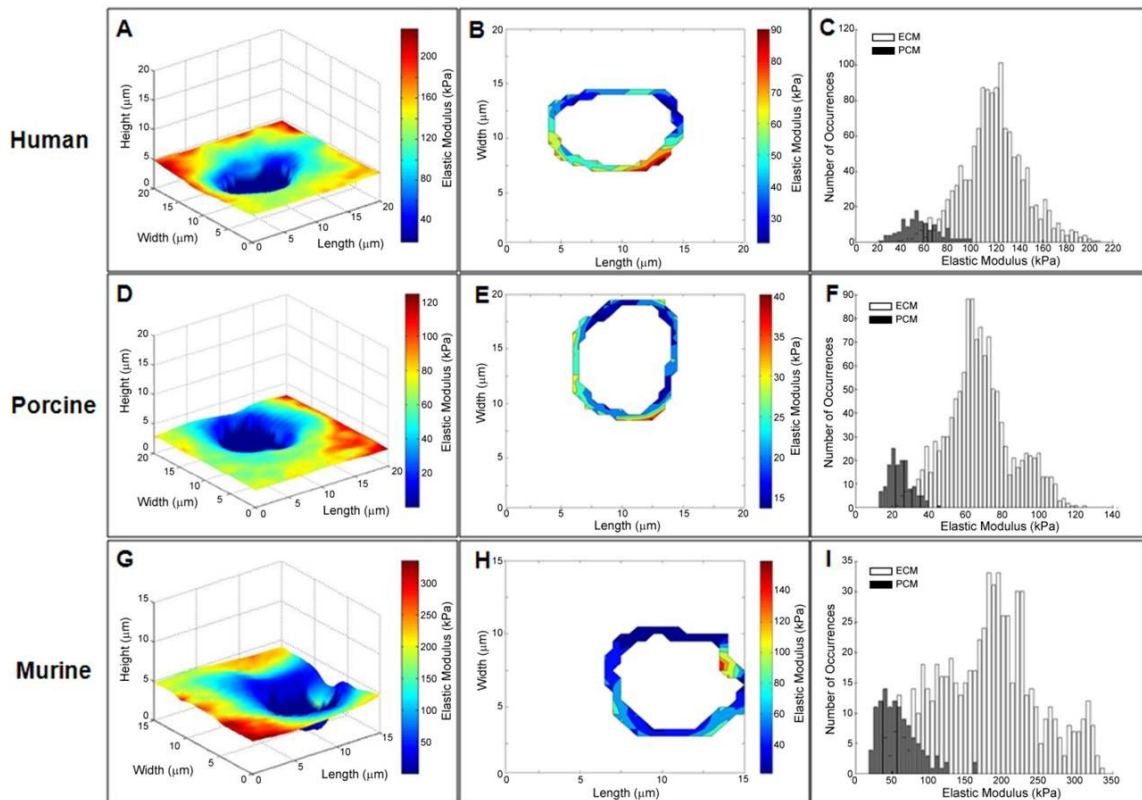


Figure 2-4: Stiffness mapping of human, porcine, and murine articular cartilage. (A, D, G) Stiffness maps of the PCM showing height and calculated elastic moduli. (B, E, H) Contour maps of the pre-defined 1 μm PCM region. Cell-sized voids and local ECM regions are depicted in white. (C, F, I) Histograms of calculated elastic moduli in PCM (black) and local ECM (white) regions within each scan.

As shown in Table 2-1, the elastic modulus of the ECM was significantly greater than that of the PCM ($p < 0.005$) for human, porcine, and murine articular cartilage.

Among the three species investigated, the elastic moduli for both the ECM and PCM

were the highest in human cartilage, the lowest in porcine articular cartilage, and the 3-week-old murine samples fell in between. Human cartilage showed similar properties whether it was obtained from macroscopically normal regions of femoral condyles removed during total joint replacement surgery (ECM = 306 ± 133 kPa; PCM = 104 ± 51 kPa) or from normal femoral cartilage from cadaver knee joints (ECM = 359 ± 39 kPa; PCM = 162 ± 22 kPa). ECM regions were consistently comprised of 15 – 16 indentations/site whereas PCM regions had 80 – 110 indentations/site. This variability in PCM measurements was associated with cell void size, which was typically larger in human and porcine samples than in murine samples.

Table 2-1: Elastic moduli of ECM and PCM regions from human, porcine, and murine articular cartilage. Stiffness mapping of sectioned cartilage samples showed clear differences between ECM and PCM regions for each species ($p < 0.002$). Moduli shown as mean \pm standard deviation.

Sample	ECM E (kPa)	ECM E range (kPa)	PCM E (kPa)	PCM E range (kPa)
Human (N = 6) n = 19, ECM n = 19, PCM	306 ± 133	103 – 573 (301 total sites)	104 ± 51	27 – 205 (2062 total sites)
Porcine (N = 6) n = 16, ECM n = 15, PCM	81 ± 19	46 – 114 (254 total sites)	30 ± 19	13 – 75 (1540 total sites)
Murine (N = 6) n = 17, ECM n = 16, PCM	197 ± 92	78 – 391 (272 total sites)	69 ± 22	34 – 110 (1290 total sites)

2.4 Discussion

Our results demonstrate that microscale stiffness mapping using AFM is a viable means of determining site-specific mechanical properties of soft biological samples *in situ*. Validation of this technique in an elastomeric model system clearly illustrated the spatial arrangement of two different materials based on local micromechanical properties. For control surfaces, microscale elastic properties showed excellent agreement with macroscale properties for all materials. Stiffness mapping of articular cartilage from human, porcine, and murine knee joints illustrated local elastic moduli for cell-sized regions and verified that ECM elastic moduli are significantly greater than PCM moduli in human, porcine, and murine tissues when measured *in situ*.

Previous studies of the mechanical properties of the PCM of articular chondrocytes focused on extracting chondrons from the tissue (Guilak et al. 1999; Alexopoulos et al. 2003; Alexopoulos et al. 2005b; Guilak et al. 2005; Alexopoulos et al. 2009) or extrapolating material parameters using inverse mathematical analyses (Michalek and Iatridis 2007; Kim et al. 2010). By allowing matrix integration between the PCM and ECM to remain relatively intact, the method presented here provides an additional direct measure of the mechanical properties of the PCM *in situ*. Of particular importance, PCM and ECM moduli were measured in the same sample using the same technique, providing a means of directly comparing ECM and PCM properties. Results from all methods agree that the modulus of the PCM is greater than that of chondrocytes

but significantly lower than that of the ECM. Human PCM values measured in this study correspond to those found using micropipette aspiration on extracted chondrons ($E = 40 - 70$ kPa (Alexopoulos et al. 2003; Alexopoulos et al. 2005b)). PCM moduli for 3-week-old mice were lower than those previously reported for extracted chondrons for 1-month-old CD1 mice ($E = \sim 280$ kPa (Alexopoulos et al. 2009)), a difference that may be related to the maturity of the cartilage or differences in the strains of mice used.

Although earlier studies have reported the relationship between ECM and PCM deformation in porcine cartilage (Choi et al. 2007), to our knowledge, this is the first study to directly measure the mechanical properties of the porcine PCM. The results for the PCM modulus in this study ($E = \sim 30$ kPa) are in direct agreement with a recent study that used an inverse method to match the predictions of a boundary element model of the chondron with three-dimensional confocal imaging of cell, PCM, and ECM deformation (Kim et al. 2010). Overall, the *in situ* mechanical properties of the PCM as measured by AFM are comparable to those measured previously for mechanically isolated chondrons, suggesting that mechanical extraction does not dramatically affect the elastic properties of the PCM.

It is hypothesized that the local mechanical environment of the chondrocyte is one of many factors that regulate chondrocyte physiology. The presence of the PCM has been shown to significantly influence the mechanical and physiochemical environment of the chondrocyte (for review, see (Alexopoulos et al. 2005a)). The mismatch between

mechanical properties of the PCM and ECM in the middle/deep zones has been shown to result in significant strain amplification in the vicinity of the chondrocyte (Guilak and Mow 2000; Alexopoulos et al. 2005a). This strain amplification may be an important factor in mechanotransduction in these regions since local ECM strains are low during bulk tissue deformation (Choi et al. 2007). In this study, the ratio of PCM to ECM properties was similar for all species, with values of 0.34 ± 0.16 , 0.37 ± 0.20 , and 0.45 ± 0.23 for human, porcine, and murine cartilage, respectively. This consistency across species suggests that the mismatch in PCM and ECM properties is an intrinsic characteristic of articular cartilage and may reflect the role of the PCM as a transducer of mechanical signals from the ECM to the chondrocyte during joint loading (Poole 1997; Guilak et al. 2006).

In general, ECM modulus values were lower than previously reported results for cartilage macroscale properties, a finding consistent with previous AFM studies (Coles et al. 2008; Park et al. 2009). Modulus values were found to depend on the force threshold used during indentation. At a force threshold of ~ 50 nN, the measured elastic moduli were approximately two- to fivefold lower than those measured at ~ 750 nN (see Appendix B). These findings are consistent with the indentation-dependent macroscale properties of bovine cartilage observed by Park *et al.* (Park et al. 2009). This apparently non-linear behavior may be related to depth- and strain-dependent behavior of articular cartilage observed at the macroscale (Schinagl et al. 1997; Chen et al. 2001; Wang et al.

2003). This behavior is unlikely to be due to fluid pressurization effects during loading at the microscale. The time constant for interstitial fluid pressurization in cartilage during AFM-based indentation has been estimated to be less than a millisecond (Park et al. 2009), two orders of magnitude smaller than the duration of indentation from first contact to maximum load. This suggests that fluid load support is minimal and that our technique measures the intrinsic equilibrium mechanical properties of the solid matrix. Apparent softening at the microscale may also be due to indentation of exposed proteoglycans on the cut surface of the tissue. Previous work by Dean and colleagues (Dean et al. 2006) on the compressive nanomechanics of aggrecan illustrated that the mechanical stiffness of aggrecan increases dramatically when compressed at strains greater than 40%. Given that the length of aggrecan macromolecules is on order of a micrometer (Mow et al. 1992), this strain-stiffening behavior could be observed with indentations greater than ~400 nm and may contribute to the indentation-dependent behavior observed in this study. Overall, our findings suggest that large indentations are required to obtain AFM-based mechanical properties representative of macroscale measurements for articular cartilage.

For this study, cartilage slices were tested in the transverse direction relative to the articular surface. In the middle/deep zones, collagen fibers transition from a more random orientation in the middle zone to a highly aligned orientation perpendicular to the articular surface in the deep zone (Mow et al. 1992). Thus, measurements in this

direction may yield different mechanical properties as compared to the direction normal to the articular surface. Additionally, cartilage mechanical properties have been shown to depend on the orientation of loading relative to the split-line direction (Chahine et al. 2004). The split-line direction was not taken into account during sample preparation for this study.

Measured ECM elastic moduli were likely influenced by joint degeneration, maturity, and/or tissue structure in the cartilage samples. Human samples were collected from femoral condyles removed during joint replacement surgery. Other studies have shown a decrease in the compressive stiffness of articular cartilage with age (Armstrong and Mow 1982), as well as increasing severity of degeneration at the macro- (Armstrong and Mow 1982; Kleemann et al. 2005), micro- and nanoscales (Stolz et al. 2009). Kleeman *et al.* (Kleemann et al. 2005) recently reported that the macroscale modulus of degenerated cartilage ranges from 280 – 500 kPa, which is comparable to ECM moduli measured in the current study.

In this work, porcine tissue was harvested from healthy, skeletally mature animals. Consistent with our results, previous reports have indicated a lower compressive modulus for porcine articular cartilage (Fermor et al. 2007; Hennerbichler et al. 2008) as compared to human (Athanasίου et al. 1991; Magnussen et al. 2005) or murine (Cao et al. 2006; Alexopoulos et al. 2009) tissue. Although ECM moduli in this study are comparable to those reported for AFM indentation of the superficial zone of

porcine patellar cartilage (Coles et al. 2008), they are inconsistent with macroscale values.

Murine knee joints from 3-week-old, skeletally immature mice were collected to allow for tissue sectioning without chemical treatments, such as decalcification. It is likely that skeletally immature mice do not exhibit the same mechanical properties that are characteristic of more mature animals. The average elastic modulus measured in the current study was ~55% lower than that reported for AFM indentation of hip joint cartilage from 20-week-old mice (Coles et al. 2008). Murine cartilage also has a much greater cell density than that of larger animals (Stockwell 1971). This high cellularity made it difficult to isolate testing regions that were solely ECM, resulting in lower than expected values (Figure 2-1).

This study aimed to characterize the mechanical properties of articular cartilage PCM at the microscale. A recent AFM study by Stolz and colleagues (Stolz et al. 2004) demonstrated that micrometer-sized indenters obtain elastic modulus values that better reflect macroscale measurements as compared to nanometer-sized tips. However, there are limitations to using micrometer-sized indenters for the stiffness mapping approach presented in this study. Larger tips have a larger contact area, which decreases the lateral resolution of the stiffness maps, particularly for soft materials (Radmacher et al. 1995). For spherical indenters, the contact radius scales with tip radius and indentation depth. Since measurements were conducted using a force threshold (750 nN),

indentations were smaller in stiffer materials like the ECM but larger in softer materials like the PCM. For the softest cases, this could result in contact radii of greater than 2.5 μm . In these cases, indenter contact with the adjacent ECM might contribute to artificial stiffening of measured PCM moduli. To minimize this effect, the PCM was defined as the region within 1 μm of cell-shaped voids. Since previous studies have indicated that PCM thickness varies locally around single chondrocytes (Poole et al. 1987; Hunziker et al. 1997) and that the PCM in the middle/deep zones of porcine cartilage is 3 – 4 μm thick (Youn et al. 2006), this 1 μm region may under- or over-represent the true extent of the PCM for any given site.

2.5 Summary

The results of this study suggest that stiffness mapping via AFM is a viable method for determining site-specific mechanical properties at the microscale. AFM-based stiffness mapping accurately obtained site-specific mechanical properties of soft substrates and captured the spatial arrangement of different materials based on their elastic moduli. Furthermore, elastic moduli obtained using AFM microindentation are comparable to other micro- and macroscale techniques. This study supports previous work demonstrating that PCM mechanical properties are significantly lower than those of the local ECM. The scale level accessible with AFM-based measurements facilitates more detailed investigation of the spatial distribution of PCM properties and the

chondrocyte micromechanical environment as a whole than that afforded by other techniques.

3. Depth-Dependent Anisotropy of the Micromechanical Properties of Porcine Articular Cartilage Measured via Atomic Force Microscopy

A version of this chapter was published as the following:

McLeod, M.A., Wilusz, R.E., Guilak, F. Depth-Dependent Anisotropy of the Micromechanical Properties of the Extracellular and Pericellular Matrices of Articular Cartilage Evaluated via Atomic Force Microscopy, *Journal of Biomechanics*, 46(3):586-592, 2013.

3.1 Introduction

Articular cartilage is the connective tissue that lines the articulating ends of diarthrodial joints, providing a nearly frictionless surface for joint articulation and functioning to support and distribute mechanical loads. Since the tissue is structurally and mechanically inhomogeneous and anisotropic (as reviewed in (Mow and Guo 2002)), joint activity generates a complex mechanical environment that varies with depth from the articular surface. Locally, chondrocytes experience stress and strain in directions both parallel and perpendicular to the direction of the applied external load as well as osmotic stress, fluid pressurization, and streaming potentials (Mow et al. 1994; Bachrach et al. 1998; Lai et al. 2002; Mow and Guo 2002; Wang et al. 2002b; Wong and Sah 2010). This mechanical environment has been shown to significantly affect chondrocyte metabolic activity, regulating the balance of catabolic and anabolic processes and influencing overall tissue and joint health (as reviewed in (Williams et al. 2010; Guilak 2011)).

Cartilage derives its bulk mechanical properties from the structure and composition of its extensive extracellular matrix (ECM), which is rich in type II collagen and proteoglycans (PGs). Based on distance from the articular surface, the ECM is divided into three zones (superficial, middle, and deep) that vary in molecular composition (Muir et al. 1970; Venn and Maroudas 1977) and matrix architecture (Jeffery et al. 1991; Hwang et al. 1992; Yin et al. 2011; Vanden Berg-Foels et al. 2012). Split-lines are indicative of the preferred collagen fiber orientation parallel to the articular surface (Meachim et al. 1974; Below et al. 2002) and provide an additional component of structural anisotropy. Variations in composition and ultrastructure contribute to depth-dependent (Kempson et al. 1973; Jurvelin et al. 1997; Schinagl et al. 1997; Chen et al. 2001; Wang et al. 2002a; Wang et al. 2002b; Wu and Herzog 2002) and directional-dependent (Mizrahi et al. 1986; Jurvelin et al. 2003; Wang et al. 2003; Chahine et al. 2004; Huang et al. 2005) macroscale mechanical properties of the cartilage ECM. While recent studies have evaluated variations in cartilage biomechanical properties with depth at the nanoscale (Tomkoria et al. 2004), depth-dependent anisotropy relative to the split-line orientation at the microscale has not been examined.

Each chondrocyte is surrounded by a distinct pericellular matrix (PCM) that together with the enclosed cell makes up a chondron (Poole et al. 1987). The PCM differs from the ECM in its composition (Poole et al. 1992; Poole 1997; Hunziker et al. 2002; Wang et al. 2008), structure (Poole et al. 1987; Hunziker et al. 1997; Vanden Berg-Foels et

al. 2012), and mechanical properties (Alexopoulos et al. 2003; Alexopoulos et al. 2005b; Guilak et al. 2005; Kim et al. 2010). In normal cartilage, the PCM is generally defined by the presence of type VI collagen (Poole et al. 1988) and has a higher concentration of PGs than the ECM (Poole et al. 1984; Hunziker et al. 2002). Type VI collagen microfilaments interact with PGs (Wiberg et al. 2001; Wiberg et al. 2002; Wiberg et al. 2003) and small diameter type II collagen fibers (Wiberg et al. 2003) to constitute the mesh-like capsule of the PCM (Poole et al. 1987) and contribute significantly to the mechanical properties of the PCM (Alexopoulos et al. 2009).

The local mechanical environment of the chondrocyte depends heavily on the relative mechanical properties of the PCM and local ECM at the cell's position within the tissue (Guilak and Mow 2000; Wu and Herzog 2002; Korhonen et al. 2006; Choi et al. 2007; Korhonen and Herzog 2008; Julkunen et al. 2009). Unlike ECM properties that vary significantly with depth, PCM mechanical properties have been shown to exhibit zonal uniformity (Alexopoulos et al. 2003; Alexopoulos et al. 2005b; Guilak et al. 2005). While previous studies have shown that PCM morphology reflects the local collagen fiber orientation of the ECM within each zone (Youn et al. 2006), PCM mechanical anisotropy has yet to be characterized. Confocal microscopy studies of chondrocyte deformation *in situ* have shown that the relationship between cell and ECM deformation is anisotropic in the surface zone and dependent on the split-line direction (Guilak et al. 1995). Finite element studies have demonstrated that ECM anisotropy may have a significant effect

on cell deformation under load (Wu and Herzog 2002; Korhonen and Herzog 2008), suggesting that the existence of PCM anisotropy could also affect the local mechanical environment of the chondrocyte.

The goal of this study was to characterize the depth and directional dependence of microscale mechanical properties of porcine articular cartilage ECM and PCM *in situ* using atomic force microscopy (AFM). We hypothesized that microscale elastic moduli in the cartilage ECM exhibit depth-dependent anisotropy reflecting the local structure and composition in each zone and that PCM microscale moduli are uniform with depth and isotropic. To test these hypotheses, AFM-based stiffness mapping (Chapter 2; (Darling et al. 2010)) was used to measure the elastic properties of ECM and PCM regions in three mutually-perpendicular directions relative to the split-line orientation.

3.2 Materials and Methods

3.2.1 Tissue sample preparation

Full thickness cartilage samples were collected from the medial condyle of 2 – 3 year old, skeletally mature, female pigs with no macroscopic signs of cartilage degeneration (N = 12 pigs). Local split-line direction was visualized by inserting a surgical needle dipped in India ink (Below et al. 2002) into the cartilage surface immediately adjacent to each 6 mm diameter explant (Figure 3-1A). Each explant was cut in half either parallel or perpendicular to the local split-line direction, removed from

the condyle, and wrapped in gauze soaked in phosphate-buffered saline (PBS) for intermediate storage at -20°C.

Samples were embedded in water-soluble embedding medium (Tissue-Tek O.C.T. Compound; Sakura Finetek USA) and sectioned in 5 µm-thick slices using a cryostat microtome (Leica CM1850; Leica). Cartilage samples were cut in the transverse plane to generate full thickness samples oriented for indentation parallel (1-dir) and perpendicular (2-dir) to the split-line orientation. Additional zone-specific slices were cut parallel to the articular surface to generate sections oriented for indentation normal to the articular surface (3-dir) (Figure 3-1B). The cartilage zones were defined such that the superficial zone consisted of the region 0 – 150 µm from the articular surface, the middle zone from 200 – 300 µm from the articular surface, and the deep zone as the bottom half of the explant (Figure 3-1C). These designations were made based on cell morphology and tissue architecture described previously in the literature (Hwang et al. 1992; Hunziker et al. 1997; Youn et al. 2006). Samples were collected on glass slides and rinsed with PBS to remove the water-soluble embedding medium. Samples remained in PBS at room temperature for AFM testing.

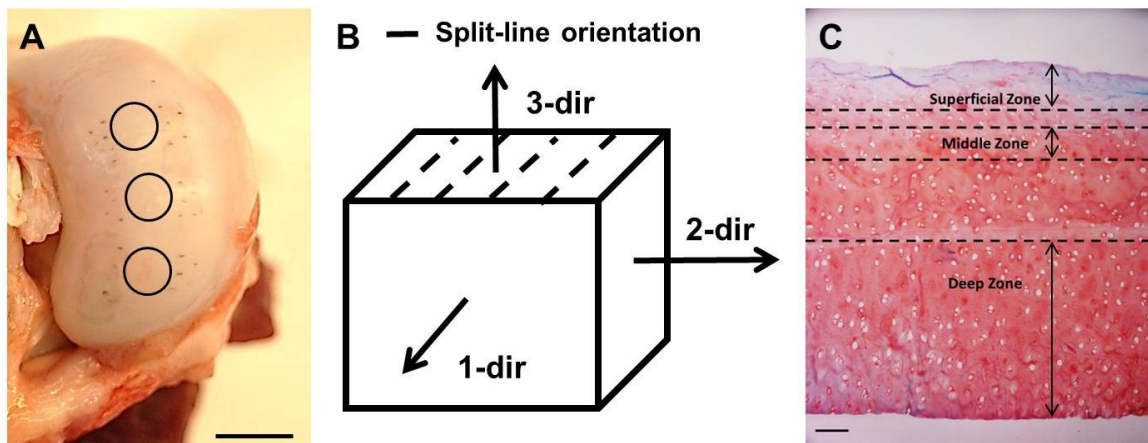


Figure 3-1: Split-line identification and sample preparation for porcine articular cartilage. (A) Local split-line orientation near collected explants (circles) visualized using India Ink on the medial femoral condyle. Scale bar = 10 mm. (B) Direction of applied loads relative to the split-line orientation. (C) For AFM testing, cartilage zones were defined as superficial (0 – 150 μm from the articular surface), middle (200 – 300 μm), and deep (bottom 50% of sample thickness). Sample stained with Safranin-O (red, PG) and fast green (blue, collagen). Scale bar = 100 μm .

3.2.2 Mechanical characterization via AFM-based stiffness mapping

Elastic moduli were mapped quantitatively using an AFM system (MFP-3DBio; Asylum Research) integrated with an optical microscope (AxioObserver A1; Zeiss) to allow for phase contrast imaging of cartilage samples. Borosilicate glass spheres (5 μm diameter) were attached to AFM cantilevers ($k = 4.5 \text{ N/m}$, Novascan) for microscale mechanical measurements. Indentations were applied with a force trigger of 200 nN and an indentation velocity of 15 $\mu\text{m/s}$. Curves were sampled at 7.5 kHz.

Scan regions were selected based on microscopic examination of cartilage sections. ECM testing sites were located in areas visually devoid of cells (Figure 3-2A, B,

C) and ECM properties were evaluated by performing 16 indentations applied over each $20\ \mu\text{m} \times 20\ \mu\text{m}$ region ($n \geq$ total 91 regions per zone, per direction). PCM scan regions were placed along the edge of cell-sized voids in the tissue section (Figure 3-2D) and 400 indentations were applied over each $10\ \mu\text{m} \times 10\ \mu\text{m}$ region ($n \geq$ 28 total regions per zone, per direction).

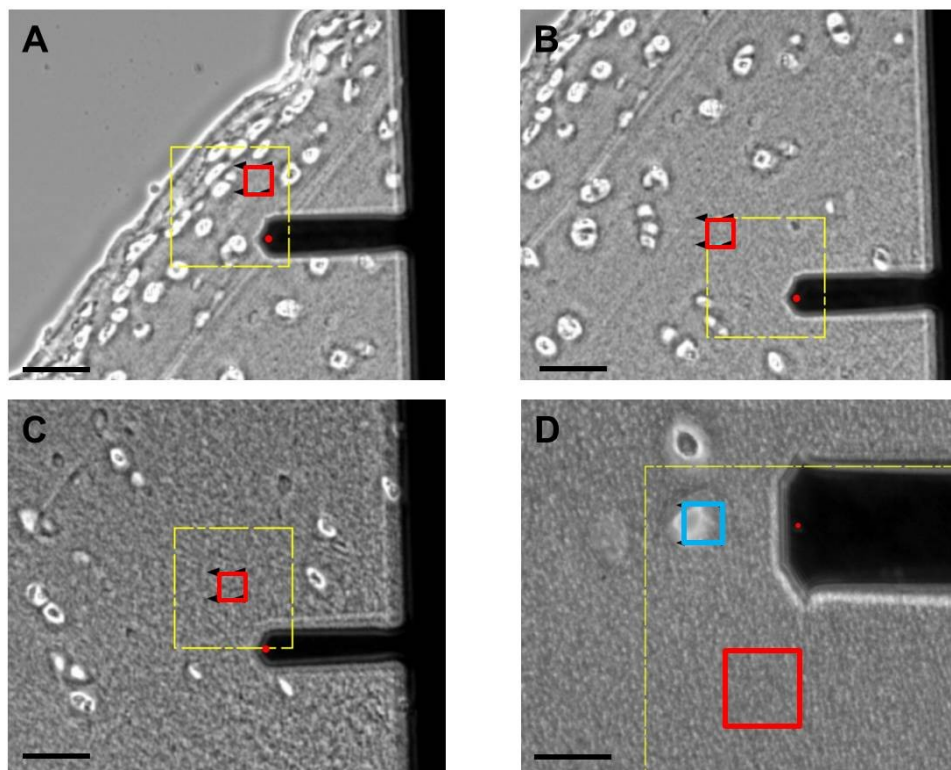


Figure 3-2: AFM scan regions in articular cartilage zones. Phase contrast images show ECM scan regions (red) in the (A) superficial, (B) middle, and (C) deep zones. Cartilage section shown is oriented for loading parallel to the split-line orientation (1-dir). AFM cantilever is also shown. Scale bar = $50\ \mu\text{m}$. (D) PCM scan regions (blue) were placed along the edge of cell-sized voids. An adjacent ECM scan region (red) and AFM cantilever are also shown. Scale bar = $20\ \mu\text{m}$.

3.2.3 Data evaluation

Raw data for cantilever deflection and z-piezo movement were analyzed using a custom MATLAB script (The MathWorks). A Hertzian contact model was used to calculate tissue elastic moduli, E , (Darling et al. 2006) from force-indentation curves and provided excellent fits to the experimental data ($R^2 > 0.90$). For ECM regions, the Poisson's ratio, ν , was assumed to be $\nu = 0.03$ in the superficial zone and $\nu = 0.12$ in the middle and deep zones based on published values for porcine cartilage (Choi et al. 2007). For PCM regions, the Poisson's ratio was assumed to be $\nu = 0.04$ in all zones (Alexopoulos et al. 2005b). Probe-surface contact was identified using a contact point extrapolation method described previously (Guo and Akhremitchev 2006). Two-dimensional contour maps of calculated elastic moduli were generated for each ECM and PCM scan region.

Elastic moduli for PCM regions were extracted using the distance-based definition of the PCM outlined in Chapter 2 (Darling et al. 2010). Briefly, the inner edge of the PCM was identified using spatial indicators of contact with the underlying glass substrate within each cell-sized void. PCM data were included for a region extending 1 μm radially from this edge to provide a consistent definition across all samples.

3.2.4 Histological staining

For histological staining of collagen and PGs, unfixed cartilage sections were rinsed with PBS to remove the water-soluble embedding medium. Sections were stained

with 0.02% aqueous fast green (Sigma-Aldrich) and Accustain Safranin-O solution (Sigma-Aldrich).

Picrosirius red staining (Junqueira et al. 1979) was utilized to visualize collagen fiber alignment in unfixed cartilage sections. Cartilage samples were sectioned in the transverse plane to generate full thickness samples oriented parallel to the split-line orientation (1-dir). Sections were rinsed with PBS to remove the water-soluble embedding medium and digested in 50 μ L of 0.25 U/mL chondroitinase-ABC solution (Sigma-Aldrich) in 50 mM Tris buffer containing 60 mM sodium acetate (Sigma-Aldrich) and 0.02% bovine serum albumin (BSA; Invitrogen, Carlsbad, CA), pH 8.0 at 37°C for 30 minutes to remove glycosaminoglycans. Sections were stained with picrosirius red solution (ScyTek Laboratories, Inc., Logan, UT) for 1 hour at room temperature, rinsed twice with 0.5% acetic acid, and dehydrated in ethanol. Stained sections were visualized using polarized light microscopy. A green bandpass filter ($\lambda = 546$ nm) was used to provide monochromatic illumination so that differences in light intensity, rather than hue variation, could be visualized (Thomopoulos et al. 2003). To determine the direction of maximum birefringence, images were taken at 10° increments as the analyzer and polarizer were rotated from 0° to 90° (data not shown).

3.2.5 Statistical analyses

ECM and PCM data were evaluated separately for differences among cartilage zones and loading direction using a two-way ANOVA (zone, direction; $\alpha = 0.05$) and

Fisher's least significant difference *post-hoc* test. All data are presented as mean \pm standard error.

3.3 Results

3.3.1 Picrosirius red staining of porcine articular cartilage

Picrosirius red staining viewed with polarized light revealed distinct ECM collagen alignment through the tissue depth (Figure 3-3A). High collagen birefringence was observed in a region extending 100 – 125 μm from the articular surface and in the bottom 50% of the cartilage section. PCM birefringence varied considerably from site-to-site and was complicated by edge effects associated with the circular cell-sized voids in the tissue section (Figure 3-3B).

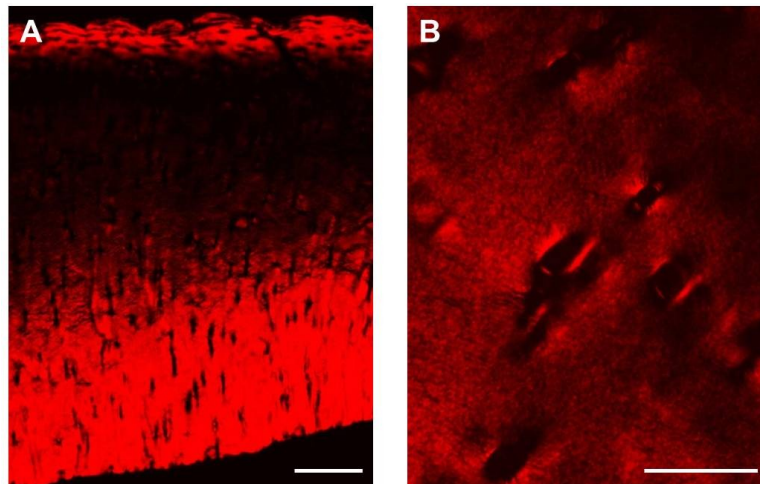


Figure 3-3: Picrosirius red staining of porcine articular cartilage. Representative polarized light images of picrosirius red-stained sections cut parallel to the local split-line orientation (1-dir). Images shown were captured at the orientation of maximum birefringence. (A) Distinct ECM collagen alignment was observed through the tissue depth. Scale bar = 200 μm . (B) Collagen alignment in the PCM was highly variable site-to-site and complicated by edge effects associated with circular cell-sized voids. Scale bar = 50 μm .

3.3.2 Depth- and directional-dependence of ECM elastic moduli

Stiffness mapping revealed that ECM elastic moduli within each zone exhibit distinct directional dependence relative to the split-line orientation (Figure 3-4). In the superficial zone, 1-dir moduli were 20% greater than 2- and 3-dir moduli ($p < 0.0005$; Figure 3-4A). In the middle zone, 1-dir moduli were 14% greater than 2-dir moduli and no significant differences were observed between 1- or 2-dir moduli with 3-dir moduli ($p > 0.05$). In the deep zone, 3-dir moduli were 24% greater than moduli in the both the 1- and 2-directions ($p < 0.0005$). A decrease in elastic moduli with depth was present in all three tested directions. In both the 1- and 2-directions, superficial zone moduli were significantly greater than those measured in the middle and deep zones ($p < 0.000005$) and middle zone moduli were greater than deep zone moduli ($p < 0.05$). In the 3-direction, the only significant difference observed was between the superficial and deep zones ($p < 0.05$).

3.3.3 Depth- and directional-dependence of PCM elastic moduli

In PCM scan regions, stiffness mapping revealed lower modulus regions immediately surrounding cell-sized voids (Figure 3-5). There was no significant interactive effect between cartilage zone and loading direction for PCM elastic moduli ($p = 0.27$) and PCM properties exhibited zonal uniformity through the tissue depth ($p = 0.38$; Figure 3-5B). When pooled across zones, 1-dir PCM moduli were 16% greater than 2- and 3-dir moduli ($p < 0.05$).

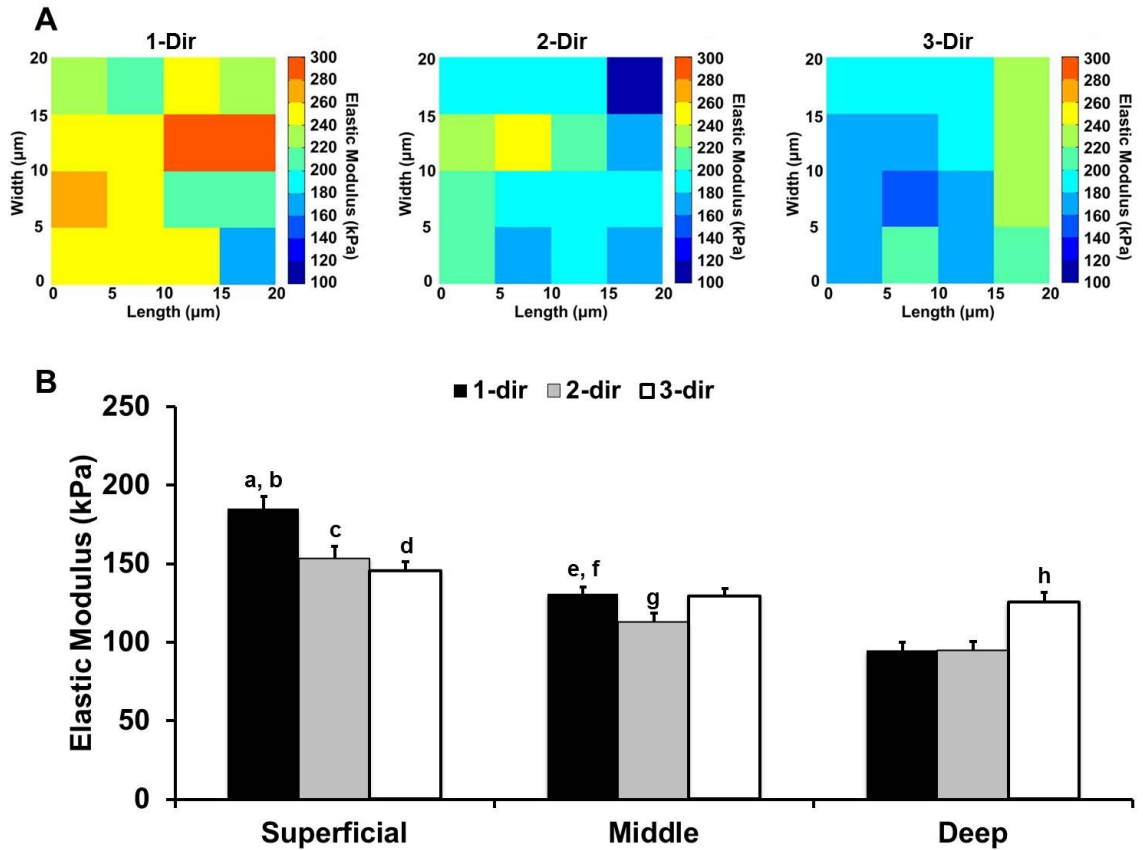


Figure 3-4: Evaluation of ECM microscale anisotropy. (A) Representative elastic maps of superficial zone ECM scan regions evaluated in the 1-, 2-, and 3-directions. (B) Elastic moduli for ECM regions in the superficial, middle, and deep zones evaluated in the 1- (black), 2- (grey), and 3- (white) directions. a: $p < 0.0005$ for superficial zone 1-dir as compared to superficial zone 2- and 3-dir. b: $p < 0.000001$ for superficial zone 1-dir as compared to middle and deep zone 1-dir. c: $p < 0.000005$ for superficial zone 2-dir as compared to middle and deep zone 2-dir. d: $p < 0.05$ for superficial zone 3-dir as compared to deep zone 3-dir. e: $p < 0.05$ for middle zone 1-dir as compared to middle zone 2-dir. f: $p < 0.00005$ for middle zone 1-dir as compared to deep zone 1-dir. g: $p < 0.05$ for middle zone 2-dir as compared to deep zone 2-dir. h: $p < 0.0005$ for deep zone 3-dir as compared to deep zone 1- and 2-dir. Moduli presented as mean + standard error (N = 12 pigs, n \geq 91 regions per zone, per direction).

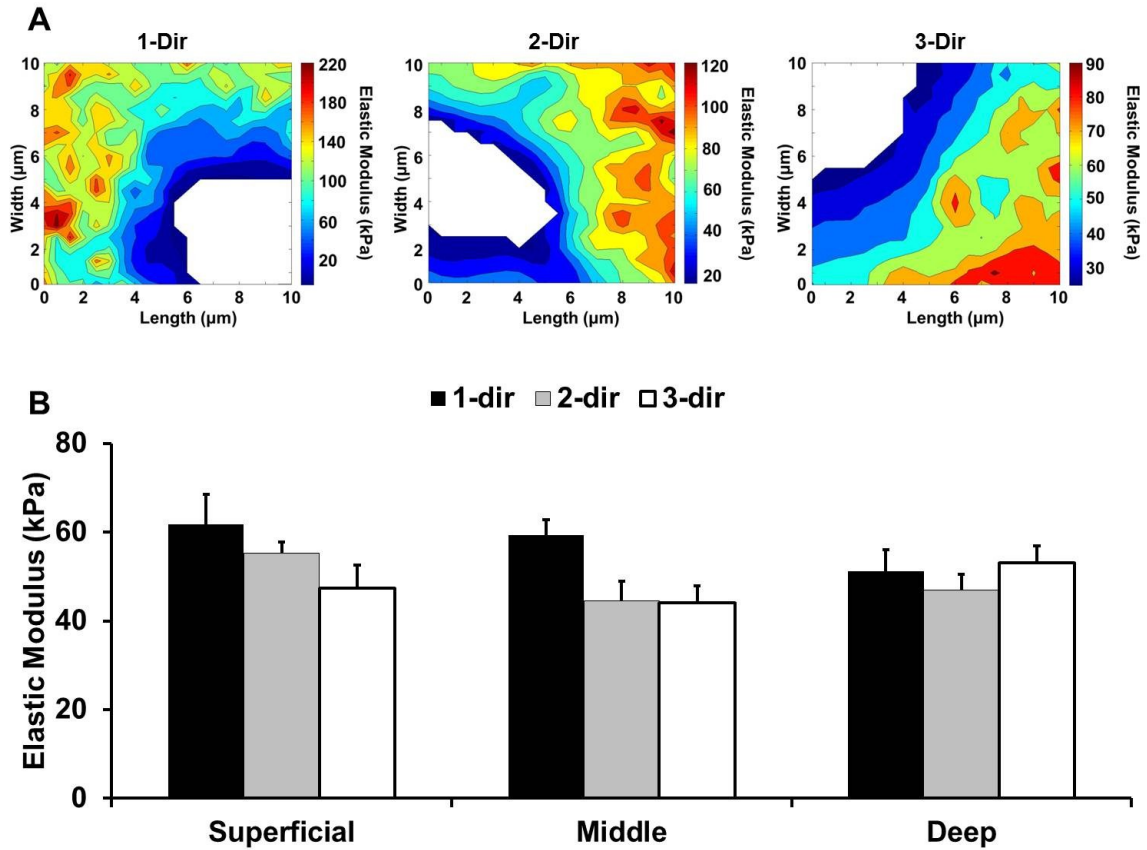


Figure 3-5: Evaluation of PCM microscale anisotropy. (A) Representative elastic maps of superficial zone PCM scan regions evaluated in the 1-, 2-, and 3-directions. (B) Elastic moduli for PCM regions in the superficial, middle, and deep zones evaluated in the 1- (black), 2- (grey), and 3- (white) directions. No significant zone*direction ($p = 0.27$) or zone effect ($p = 0.38$) was observed. When pooled across zones, 1-dir PCM moduli were greater than 2- and 3-dir moduli ($p < 0.05$). Moduli presented as mean + standard error (N = 10 pigs, $n \geq 28$ regions per zone, per direction).

3.4 Discussion

Our results present new evidence that articular cartilage mechanical properties exhibit inhomogeneity and anisotropy relative to the split-line orientation at the microscale. Distinct anisotropy in ECM elastic moduli was observed in the superficial and deep zones whereas the middle zone exhibited subtle anisotropy. Contrary to our initial hypothesis, ECM microscale moduli decreased with depth in all three tested directions. PCM elastic moduli exhibited zonal uniformity with depth and when pooled across zones, were greatest in the direction parallel to the split-line orientation.

Our study supports the hypothesis that collagen fiber orientation has a significant influence on the directional dependence of cartilage ECM mechanical properties. In agreement with our picrosirius red staining results and previous macroscale studies (Wang et al. 2003; Chahine et al. 2004; Huang et al. 2005), AFM-based stiffness mapping demonstrated that ECM microscale elastic moduli exhibit distinct anisotropy in the superficial and deep zones where the local collagen fibers are highly aligned (Jeffery et al. 1991; Hwang et al. 1992). In the superficial zone, collagen fibers run parallel to the articular surface along the split-line orientation. Following this fiber alignment, moduli measured parallel to split-lines (1-dir) were significantly greater than those measured perpendicular to the split-line orientation (2- and 3-dir). In the deep zone, collagen fibers are oriented perpendicular to the articular surface and elastic moduli measured normal to the articular surface (3-dir) were significantly greater than

moduli obtained in either transverse plane (1- and 2-dir). Furthermore, we observed subtle anisotropic behavior in the middle zone where moduli were greater parallel to the split-line orientation (1-dir) than perpendicular to it (2-dir). Following the cascade-like architecture of collagen fibers through the depth of the tissue, the middle zone serves as a structural transition between the mutually-perpendicular fiber orientations of the superficial and deep zones. Previous studies have shown that the collagen fiber alignment along split-lines in the superficial zone influences the angle at which middle zone fibers are oriented relative to the articular surface (Jeffery et al. 1991). This in-plane alignment of collagen fibers likely contributes to the observed anisotropy in the middle zone.

Unlike previous macroscale studies which show a depth-dependent increase in ECM elastic moduli (Schinagl et al. 1997; Chen et al. 2001; Wang et al. 2003; Chahine et al. 2004), the observed ECM microscale elastic properties in the current study decreased with depth in all three tested directions. These observations may be related to the fact that AFM measures highly localized mechanical properties that may be influenced by the molecular composition of the tissue. During AFM microindentation, the effects of interstitial fluid pressurization are minimal, with an estimated relaxation time constant of 30 – 60 milliseconds based on the moduli presented in our study (Park et al. 2009). As a result, fluid load support during localized indentation is minimal, approximately 10% based on the Peclet number (Bonnievie et al. 2012). This suggests that elastic moduli

measured in our study reflect the intrinsic properties of the solid matrix. The molecular composition of the cartilage ECM varies with depth from the articular surface; collagen content is highest in the superficial zone and decreases with depth while PG content follows an opposite trend, being lowest in the superficial zone and highest in the deep zone (Muir et al. 1970; Venn and Maroudas 1977). It has been shown previously that the *in situ* nanoscale elastic modulus of PGs is an order of magnitude softer than that of collagen fibers (Loparic et al. 2010). In the current work, the lowest moduli were observed in the deep zone where PG content is highest and collagen content is the lowest. The highest moduli were found in the superficial zone where PG content is lowest and collagen content is highest. This apparent softening of ECM properties with depth may be due in part to these depth-dependent variations in ECM composition.

AFM-based stiffness mapping allows for direct evaluation of PCM mechanical properties with minimal disruption of native matrix integration and a model framework for evaluating the depth and directional dependence of PCM properties. Consistent with previous micropipette aspiration studies (Alexopoulos et al. 2003; Alexopoulos et al. 2005b; Guilak et al. 2005), PCM microscale elastic moduli exhibited zonal uniformity with depth. Within each zone, PCM microscale elastic moduli exhibited no directional dependence, reflecting its mesh-like capsule architecture. However, when pooled across the three zones, PCM moduli were greater parallel to the split-line orientation (1-dir) as compared to the other two directions. This effect appears to be dominated by the

superficial and middle zones where 1-dir moduli tended to be greater than those measured in the 2- and 3- directions. Previous studies have shown that PCM morphology reflects the local collagen fiber orientation in the ECM (Youn et al. 2006). In regions closer to the articular surface where the PCM is thinner (Youn et al. 2006), it is possible that local ECM type II collagen fiber orientation in the plane of split-line orientation (Jeffery et al. 1991) contributes to subtle, but measurable, alignment of type VI collagen microfilaments or other molecular components in the PCM. While picrosirius red staining is useful for visualizing fibrillar collagen like types I, II, and III (Junqueira et al. 1979), there is little evidence suggesting that type VI collagen microfilaments are birefringent and can be visualized with this stain. In addition, an edge effect was found to be associated with the circular cell-sized voids in stained sections when viewed with polarized light. As a result, we were unable to confidently evaluate type II collagen alignment within the 1 μm PCM region using this method.

In the current study, the PCM was defined as the region extending 1 μm radially from the edge of each cell-sized void. PCM thickness is generally greater than 2 μm , but has been shown to vary locally around single chondrocytes (Hunziker et al. 1997) as well as with depth through the cartilage zones (Youn et al. 2006). As a result, this pre-defined 1 μm region may under-estimate the actual extent of the PCM. There are limitations in lateral resolution when using micrometer-sized indenters for AFM stiffness mapping of soft substrates due to the size of the contact area during indentation (Radmacher et al.

1995). The contact radius for a spherical indenter scales with tip radius and indentation depth. Using a single force trigger of 200 nN to evaluate both the PCM and ECM led to differences in contact radii between the two regions. PCM regions exhibit lower elastic moduli and therefore experience larger indentations than the adjacent ECM for the same applied force. As a result, contact radii in the PCM (1.8 – 2.0 μm) were larger than contact radii in the ECM (1.3 – 1.5 μm). Contact with adjacent ECM regions during indentation may have contributed to the observed anisotropy in PCM mechanical properties and to stiffening of PCM moduli. The pre-defined 1 μm region was selected in an attempt to minimize these effects. Use of smaller radius indenters would improve lateral resolution but may result in moduli that do not reflect macroscale measurements (Stolz et al. 2004). Alternatively, using a biochemical definition of the PCM, such as immunofluorescence for type VI collagen (Poole et al. 1988; Poole et al. 1992), would allow for more complete characterization of spatial variations in anisotropy within the chondrocyte microenvironment.

3.5 Summary

Our study provides new evidence for mechanical inhomogeneity and anisotropy at the microscale in articular cartilage. By demonstrating distinct depth-dependent anisotropy in ECM microscale elastic moduli, our results provide further support for local collagen fiber orientation and matrix composition as defining factors in cartilage mechanical behavior. In addition, our findings provide new insights into the

micromechanical environment of the chondrocyte, demonstrating zonal uniformity and mechanical isotropy of PCM elastic moduli. This detailed characterization of the cell microenvironment within each zone can be applied to theoretical models of cell-PCM-ECM interactions (Guilak and Mow 2000; Wu and Herzog 2002; Kim et al. 2008; Korhonen and Herzog 2008) to further our understanding of the specific mechanical stresses experienced by the chondrocyte in health and disease.

4. Stiffness Mapping of Early Osteoarthritic Changes in the Micromechanical Properties of the Pericellular Matrix in Human Articular Cartilage

4.1 Introduction

Osteoarthritis (OA) is a joint disease characterized by progressive degeneration and loss of articular cartilage, ultimately resulting in severe pain and disability. In the United States, over 20 million people suffer from OA, resulting in a total economic burden of over \$80 billion dollars annually (Buckwalter and Martin 2006; Bitton 2009). While initially thought to be a disease of “normal wear and tear” associated with advanced age, it is now recognized that OA is caused by a complex interplay among biochemical factors, joint structure, and joint biomechanics (Aigner et al. 2006; Poole et al. 2007; Goldring 2008) that alters the balance between anabolic and catabolic pathways in joint tissues (Sandell and Aigner 2001; Sandell 2007).

Articular cartilage derives its functional mechanical properties from its extensive extracellular matrix (ECM) of type II collagen and proteoglycans (PGs). As these molecular components undergo enzymatic degradation and are progressively lost in OA (McDevitt and Muir 1976; Cs-Szabo et al. 1995; Kleemann et al. 2005; Bay-Jensen et al. 2008; Hennerbichler et al. 2008; Stolz et al. 2009), cartilage loses its structural and mechanical integrity. Alterations in the mechanical properties of the cartilage ECM with OA have been characterized at the macroscale (Armstrong and Mow 1982; Setton et al. 1999; Kleemann et al. 2005; Hennerbichler et al. 2008), microscale (Stolz et al. 2009;

Desrochers et al. 2010; Desrochers et al. 2012), and nanoscale (Stolz et al. 2009) in both human tissue and experimental models. Results at all length scales agree that cartilage compressive properties decline with increasing disease severity. Interestingly, in knee joints with unicompartmental OA, the mechanical properties of the “unaffected” compartment are also compromised, though not to the same degree, despite the often normal macroscopic appearance of the tissue (Obeid et al. 1994).

While most investigations focus on the macroscale degradation of the cartilage ECM in OA, significant changes also occur in the chondrocyte microenvironment. Immediately surrounding each cell is a narrow region known as the pericellular matrix (PCM) that together with its enclosed cell forms the functional unit known as the chondron (Poole et al. 1987). The PCM is distinct from the bulk extracellular matrix in its biochemical composition, most notably the exclusive presence of type VI collagen (Poole et al. 1988; Poole et al. 1992; Hagiwara et al. 1993; Youn et al. 2006), ultrastructure (Poole et al. 1987; Hunziker et al. 1997; Vanden Berg-Foels et al. 2012), and biomechanical properties (Alexopoulos et al. 2003; Alexopoulos et al. 2005b; Guilak et al. 2005; Kim et al. 2010). Marked changes in the structural and biochemical profiles of the PCM in OA have been reported, including the presence of type II collagen and PG degradation products (Dodge and Poole 1989; Hollander et al. 1995; Gibson et al. 2001; Plaas et al. 2007), a loss of organization in PCM collagens and PG components (Poole et al. 1991b; Hambach et al. 1998; Horikawa et al. 2004; Murray et al. 2010), and the prevalence of

swollen and enlarged chondrons (Poole et al. 1991b; Lee et al. 2000). Micropipette aspiration studies revealed a significant loss of mechanical integrity in chondrons isolated from OA human cartilage as compared to normal tissue. OA chondrons exhibit Young's moduli 30 - 40% lower and permeability values 2 – 3 times greater than those of normal chondrons (Alexopoulos et al. 2003; Alexopoulos et al. 2005b). However, these studies were limited by the need for physical extraction of the chondron from the tissue and no studies, to our knowledge, have investigated degradative changes in the chondrocyte micromechanical environment *in situ*.

The objective of this study was to quantify osteoarthritic changes in the micromechanical properties of the ECM and PCM of human articular cartilage *in situ* using atomic force microscopy (AFM). To this end, AFM-based stiffness mapping (as described in Chapter 2 (Darling et al. 2010)) was used to evaluate the microscale elastic modulus of ECM and PCM regions of human articular cartilage collected from both femoral condyles of macroscopically normal and early OA knee joints. This approach was used to test the hypotheses that both ECM and PCM regions experience a loss of mechanical integrity with OA on both femoral condyles and that the mechanical footprint of the PCM is enlarged in OA cartilage as compared to normal tissue.

4.2 Materials and Methods

4.2.1 Tissue sample preparation

Full thickness articular cartilage samples were collected from matched sites on both femoral condyles from adult human knee joints at autopsy (6 female, 2 male; age = 65 ± 11 years; age range: 53 – 83 years). None of the patients had a history of knee surgery or clinical diagnosed OA. Joints were classified as macroscopically normal (Collins grade 0 – 1; N = 4) or arthritic (Collins grade 2 – 3; N = 4) based on the presence and extent of surface fibrillation, fissures, and/or focal defects on the condyles (Collins and McElligott 1960) (Figure 4-1). Degenerative changes were present on the medial condyle of all four OA joints, with one joint exhibiting arthritic changes on both condyles (Figure 4-1C).

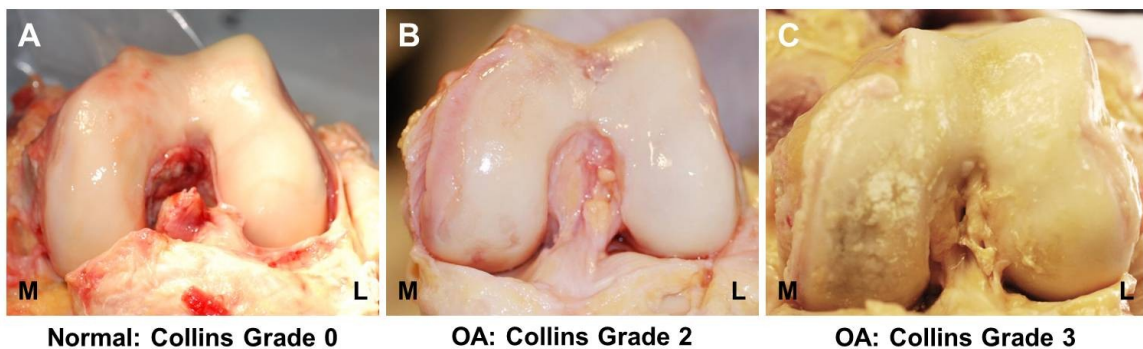


Figure 4-1: Macroscopic grading of human articular cartilage. Knee joints were classified as (A) macroscopically normal or (B, C) arthritic based on the presence of surface fibrillation, fissures, and/or focal defects on the medial (M) or lateral (L) condyle.

Cartilage samples were wrapped in phosphate-buffered saline (PBS)-soaked gauze and frozen at -20°C for intermediate storage. Samples were embedded in water-soluble embedding medium (Tissue-Tek O.C.T. Compound; Sakura Finetek USA) and sectioned perpendicular to the articular surface in 5 µm-thick slices using a cryostat microtome (Leica CM1850; Leica). Cartilage slices were collected on glass slides and washed thoroughly with PBS to remove the water-soluble embedding medium prior to AFM testing. Samples remained in PBS at room temperature for the duration of AFM testing.

4.2.2 Mechanical characterization via AFM-based stiffness mapping

Elastic moduli were mapped quantitatively with the use of a stand-alone atomic force microscope (MFP-3D; Asylum Research, Santa Barbara, CA). For microindentation, borosilicate glass spheres (5 µm diameter) were attached to the end of AFM cantilevers ($k = 7.5 \text{ N/m}$; Novascan Technologies, Ames, IA). Indentation curves were applied with a force trigger of 750 nN and sampled at 7.5 kHz.

For evaluation of PCM elastic properties, indentations (1600 sites per region, 15 µm/s indentation velocity; $n = 15 - 16$ regions per classification) were sequentially applied over each scan region as defined by microscopic examination of cell-sized voids in the cartilage section. ECM elastic properties were evaluated using the same technique over regions visually devoid of PCM (16 sites per region, 15 µm/s indentation velocity; $n = 15 - 16$ regions per classification).

4.2.3 Data evaluation

Raw data for cantilever deflection and z-piezo movement were analyzed using a custom MATLAB script (The MathWorks). A modified Hertzian contact model was used to calculate tissue elastic moduli, E , from force-indentation curves, as described previously (Darling et al. 2006). Probe-surface contact was identified using a contact point extrapolation method described previously (Guo and Akhremitchev 2006). The Poisson's ratio was assumed to be $\nu = 0.04$ in both ECM and PCM regions based on published values (Mow et al. 1980; Chen et al. 2001; Alexopoulos et al. 2005b; Choi et al. 2007). Hertzian contact mechanics provided excellent fits to the experimental data ($R^2 > 0.90$). Two-dimensional contour maps were generated of the spatial distribution of calculated elastic moduli in each scan region.

Elastic moduli for PCM regions were extracted using the distance-based definition of the PCM outlined in Chapter 2 (Darling et al. 2010). Glass contact was readily apparent from the force-indentation curves and was used to define the edge of each cell-sized void in PCM scan regions. PCM data were included for a region extending $1 \mu\text{m}$ radially from this edge to provide a consistent definition across all samples. To quantitatively evaluate the spatial distribution of moduli in the chondrocyte microenvironment, the stiffness progression from the PCM inner edge to the ECM was evaluated in radial increments of $0.5 \mu\text{m}$.

4.2.4 Histological staining and immunofluorescence

For histological staining, additional cartilage explants from both femoral condyles were cut in half to generate a transverse cross-section and fixed overnight in formalin. Fixed explants were dehydrated in ethanol, infiltrated with xylene, and embedded in paraffin. For histological staining of collagen and PGs, 10 μ m-thick sections were stained with 0.02% aqueous fast green (Sigma-Aldrich) and Accustain Safranin-O solution (Sigma-Aldrich).

Unfixed cryosections (5 μ m thick) of medial condyle cartilage were labeled using immunofluorescence (IF) for type VI collagen to visualize the PCM. Sections were blocked in 10% goat serum (Invitrogen) for 30 minutes at room temperature. Samples were incubated with primary antibody for type VI collagen (anti-collagen type VI raised in rabbit, sc-20649; Santa Cruz Biotechnology, Inc., Santa Cruz, CA) at a 1:200 dilution in 10% goat serum for 1 hour at room temperature. After three PBS washes of 5 minutes each, samples were incubated with secondary antibody (AlexaFluor 488 goat anti-rabbit IgG; Invitrogen) at a 1:200 dilution in 10% goat serum for one hour in the dark at room temperature. Sections were rinsed three times with PBS and visualized on a confocal laser scanning microscope (LSM 510; Zeiss).

4.2.5 Statistical analyses

Differences between ECM and PCM elastic moduli were evaluated separately on each condyle using a two-way ANOVA (region, disease state; $\alpha = 0.05$) and Fisher's least

significant difference (LSD) *post-hoc* test. Data were log-transformed for normality when required. Differences in ECM and PCM elastic moduli between the medial and lateral condyle were evaluated separately for each region using a repeated measures ANOVA ($\alpha = 0.05$). Stiffness progression data were evaluated separately for each disease state using a one-way ANOVA (distance; $\alpha = 0.05$) and Fisher's LSD *post-hoc* test. For analysis within the cell microenvironment, the pericellular/territorial matrix (PCM/TM) region was designated to include the region extending 3 μm radially from the PCM inner edge. All data are presented as mean \pm standard error.

4.3 Results

4.3.1 Histological staining and immunofluorescence-labeling of human articular cartilage

Histological staining qualitatively confirmed early degradative changes on the medial condyle of joints classified as arthritic. OA cartilage exhibited surface irregularities and a progressive loss of PG staining with depth as compared to macroscopically normal tissue (Figure 4-2).

IF-labeling for type VI collagen in medial condyle cartilage demonstrated distinct differences in the PCM between normal and OA cartilage (Figure 4-3). In normal cartilage, type VI collagen was tightly localized around cell-sized voids. In contrast in OA cartilage, expanded type VI collagen labeling was observed around cell-sized voids and faintly dispersed in ECM regions.

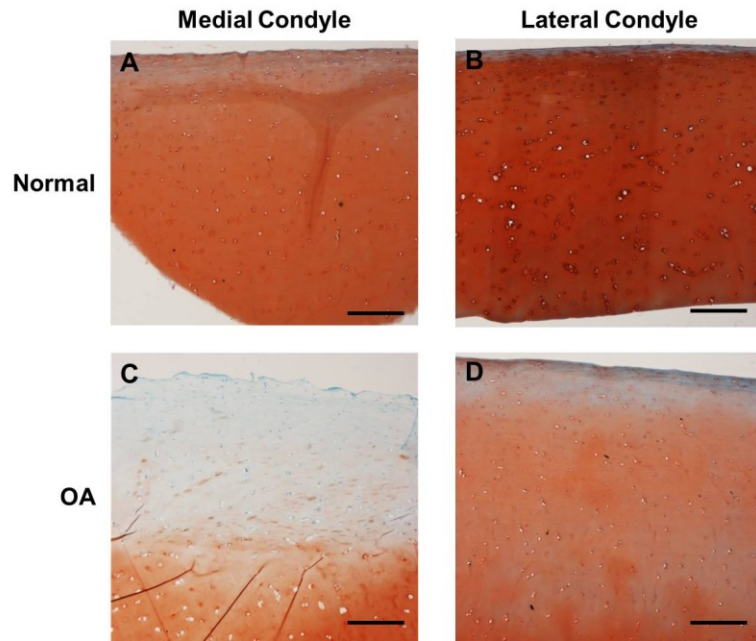


Figure 4-2: Histological staining of human articular cartilage. Safranin-O (red, PG) and fast green (blue, collagen) staining of cartilage sections from (A, B) macroscopically normal and (C, D) OA knee joints. Surface irregularities and loss of PG staining are present in OA cartilage sections from the medial condyle. Scale bar = 300 μm .

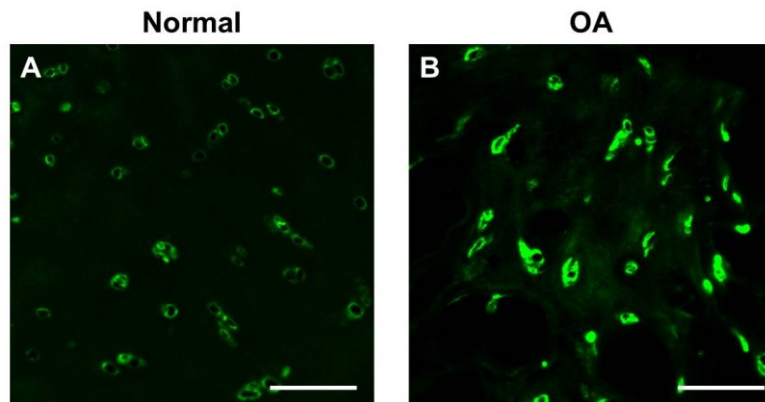


Figure 4-3: Immunofluorescence-labeling of type VI collagen in human articular cartilage. Representative images of IF-labeling of type VI collagen in medial condyle cartilage from (A) macroscopically normal and (B) OA knee joints. IF-labeling revealed expanded PCM regions in OA cartilage. Scale bar = 100 μm .

4.3.2 AFM stiffness mapping of human articular cartilage

Stiffness mapping of articular cartilage from the medial condyle revealed a significant loss of mechanical function in both the PCM and ECM of articular cartilage collected from the medial condyle. The elastic modulus of the PCM in OA cartilage was reduced by one-third (96 ± 8 kPa) as compared to normal cartilage (137 ± 10 kPa; $p < 0.05$, Figure 4-4A). The elastic modulus of the ECM was reduced by 45% (270 ± 36 kPa) in OA cartilage as compared to macroscopically normal joints (491 ± 52 kPa; $p < 0.0005$). On the lateral condyle, no change in either PCM or ECM elastic properties was observed with OA (Figure 4-4B; $p > 0.25$). On both condyles, ECM elastic moduli were significantly greater than PCM moduli in normal and OA cartilage ($p < 0.000001$).

Comparisons between the condyles demonstrated that ECM moduli on the medial condyle were significantly lower than those on the lateral condyle in OA joints ($p < 0.005$). No difference in ECM moduli was observed between the condyles in macroscopically normal joints ($p = 0.21$). PCM moduli were significantly greater on the medial condyle in healthy joints ($p < 0.05$). No difference was observed in PCM moduli between the condyles in OA joints ($p = 0.24$).

Spatial mapping of elastic moduli revealed distinct differences in the biomechanical footprint of the PCM in normal and OA cartilage on the medial condyle. Stiffness maps of PCM regions in OA cartilage illustrated expanded regions of lower moduli surrounding cell-sized voids as compared to normal cartilage (Figure 4-5A, B).

This radial expansion was reflected in a shallow stiffness gradient outward from the PCM inner edge (Figure 4-5C), in which elastic moduli failed to reach ECM-like values within a radial distance of 7 μm from the PCM inner edge. In contrast, ECM-like modulus values were observed at a radial distance of 6.0 μm from the PCM inner edge in normal cartilage. There were no differences in the biomechanical footprint of the PCM or the stiffness gradient between normal and OA cartilage on the lateral condyle (Figure 4-6).

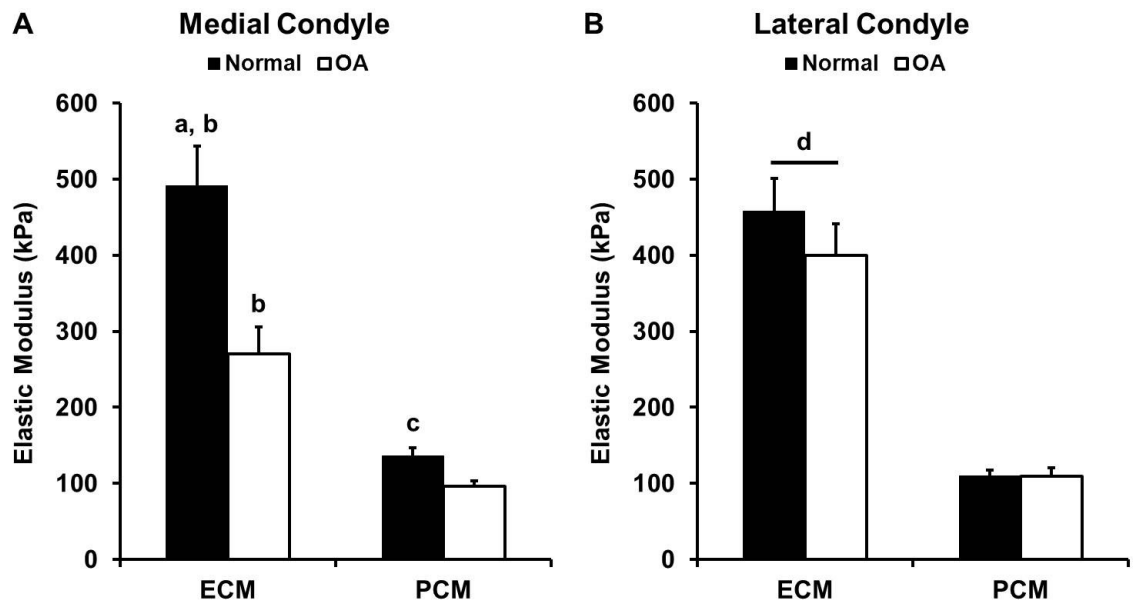


Figure 4-4: Stiffness mapping of human articular cartilage. Elastic moduli of cartilage ECM and PCM from the (A) medial and (B) lateral condyles of macroscopically normal (black) and OA (white) joints. a: $p < 0.0005$ for normal ECM moduli as compared to OA ECM moduli on the medial condyle. b: $p < 0.000005$ for ECM moduli as compared to their respective PCM moduli on the medial condyle. c: $p < 0.05$ for normal PCM moduli as compared to OA PCM moduli on the medial condyle. d: $p < 0.000001$ for ECM moduli as compared to their respective PCM moduli on the lateral condyle. Moduli presented as mean + standard error (N = 4 knees, n = 15 – 16 regions per classification).

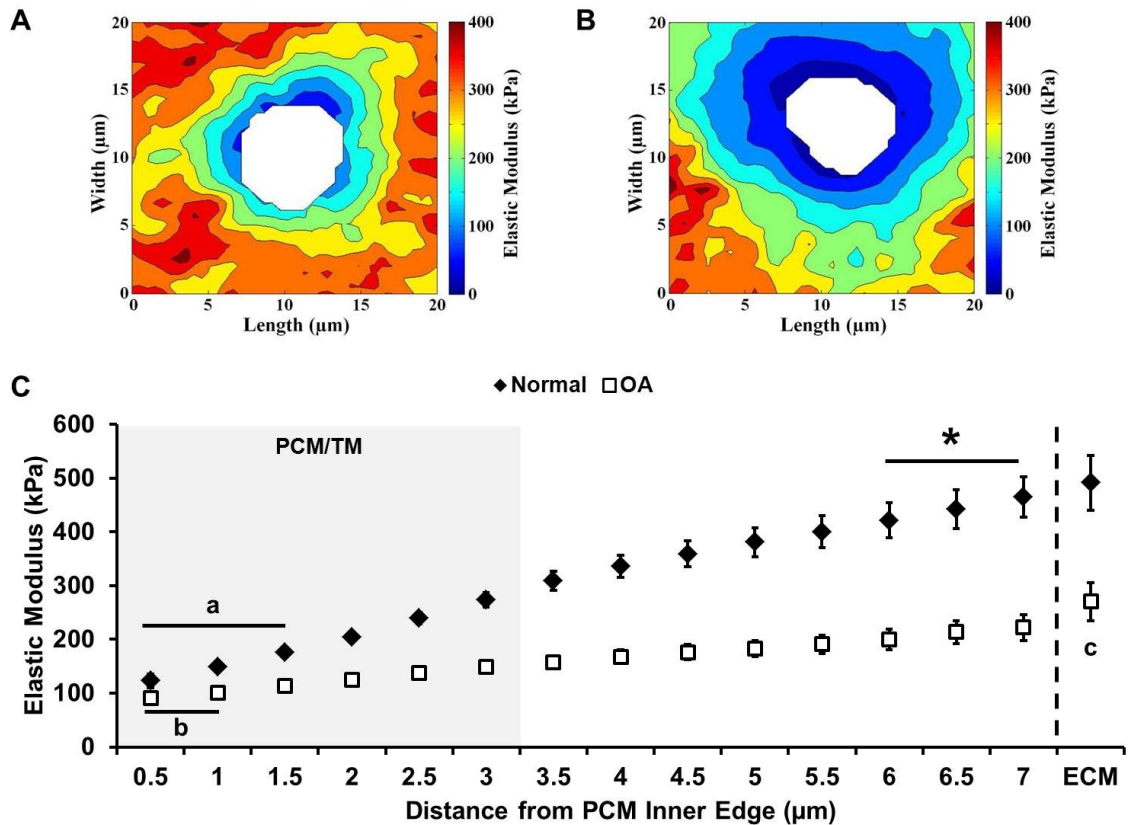


Figure 4-5: Stiffness progression of elastic moduli of human articular cartilage from the medial condyle. Representative contour maps of calculated elastic moduli for PCM scan regions of (A) macroscopically normal and (B) OA joints. (C) Outward stiffness progression of elastic moduli from the PCM inner edge to the ECM of macroscopically normal (black) and OA (white) cartilage. a: $p < 0.01$ for normal cartilage moduli within 1.5 μm of the PCM inner edge as compared to normal moduli at 3.0 μm . b: $p < 0.05$ for OA cartilage moduli within 1.0 μm of the PCM inner edge as compared to OA moduli at 3.0 μm . c: $p < 0.05$ for OA ECM moduli as compared to all distances in OA cartilage. *: Normal cartilage moduli reached normal ECM values 6.0 μm from the PCM inner edge. Moduli presented as mean \pm standard error (N = 4 knees, n = 15 – 16 regions per classification).

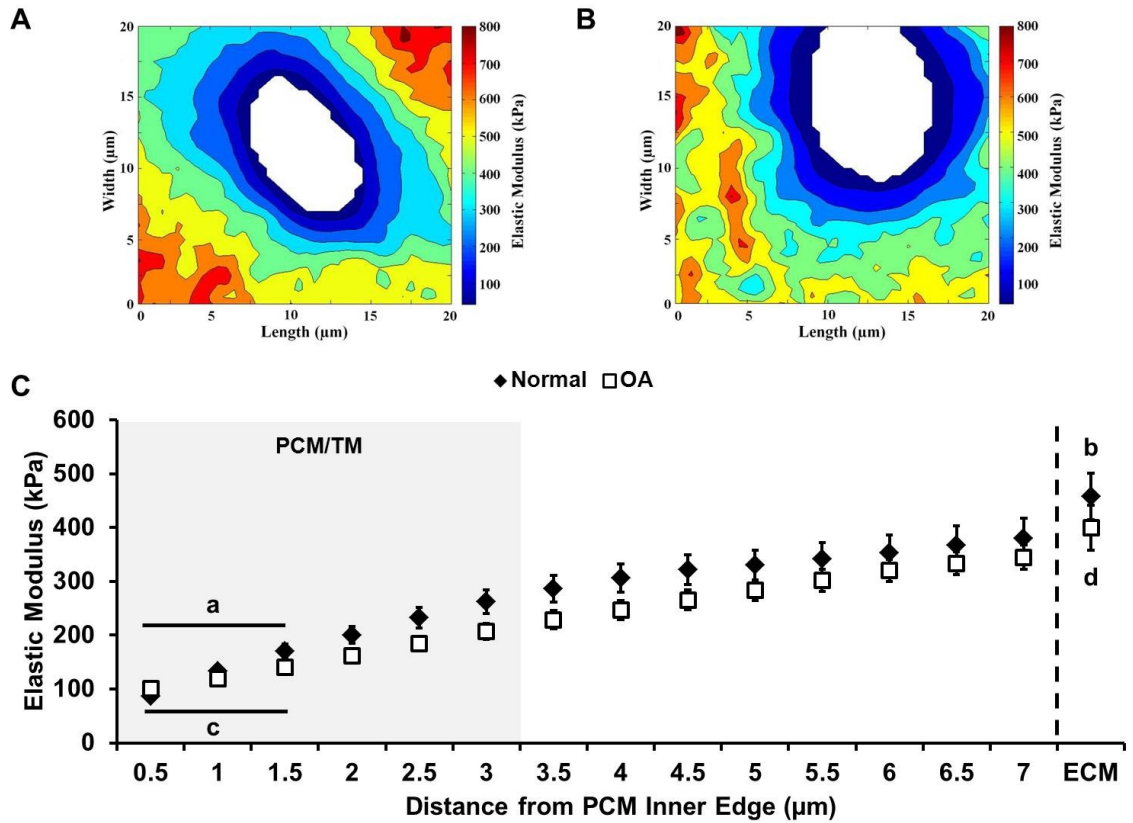


Figure 4-6: Stiffness progression of elastic moduli of human articular cartilage from the lateral condyle. Representative contour maps of calculated elastic moduli for PCM scan regions of (A) macroscopically normal and (B) OA joints. (C) Outward stiffness progression of elastic moduli from the PCM inner edge to the ECM of macroscopically normal (black) and OA (white) cartilage. a: $p < 0.05$ for normal cartilage moduli within 1.5 μm of the PCM inner edge as compared to normal moduli at 3.0 μm . b: $p < 0.05$ for normal ECM moduli as compared to all distances in normal cartilage. c: $p < 0.05$ for OA cartilage moduli within 1.5 μm of the PCM inner edge as compared to OA moduli at 3.0 μm . d: $p < 0.05$ for OA ECM moduli as compared to all distances in OA cartilage. Moduli presented as mean \pm standard error (N = 4 knees, n = 16 regions per classification).

4.4 Discussion

Our results demonstrate a significant loss in the mechanical function of the articular cartilage PCM and ECM *in situ* with OA at the microscale. AFM-based stiffness mapping of medial condyle cartilage revealed a significant decrease in both PCM and ECM elastic moduli in OA knee joints as compared to macroscopically normal tissue. In addition, radial expansion of the biomechanical footprint of the PCM was observed in medial condyle cartilage with OA. Contrary to our initial hypothesis, no changes in mechanical properties or their spatial distribution were observed in PCM or ECM regions of lateral condyle cartilage.

Our findings provide direct evidence for degenerative changes in the chondrocyte micromechanical environment with OA. Unlike previous micropipette aspiration studies of isolated OA chondrons (Alexopoulos et al. 2003; Alexopoulos et al. 2005b), the AFM-based method utilized in the current work allows for direct evaluation of PCM mechanical properties *in situ*. The observed ~30% decrease in PCM elastic moduli is comparable to that observed previously for mechanically isolated chondrons (Alexopoulos et al. 2003; Alexopoulos et al. 2005b) from normal and OA cartilage. The observed moduli fall within the range observed for human cartilage in our initial study presented in Chapter 2 (Darling et al. 2010) but are approximately two-fold higher than those reported for isolated chondrons (96 – 137 kPa vs. 41 – 66 kPa). This difference may be due to subject-to-subject variability in PCM properties. It is also possible that OA

PCM exhibits enhanced mechanical integrity *in situ* as compared to an isolated chondron due to its loosely organized ultrastructure (Poole et al. 1991b; Hambach et al. 1998; Horikawa et al. 2004; Murray et al. 2010).

In agreement with previous studies that demonstrate a significant decrease in cartilage compressive properties with the onset and progression of OA (Armstrong and Mow 1982; Setton et al. 1999; Kleemann et al. 2005; Hennerbichler et al. 2008), medial condyle ECM microscale elastic moduli decreased 45% in OA cartilage as compared to macroscopically normal tissue. Contrary to our initial hypothesis, no change was observed in either ECM or PCM elastic moduli on the lateral condyle. This lack of alteration is likely related to the relative health of the early-stage OA cartilage examined in this study as compared to end-stage OA cartilage (Obeid et al. 1994). Difficulties with sample preparation of severely degenerated tissue prevented end-stage OA cartilage collected at total knee arthroplasty from being included in this analysis. Overall, ECM moduli are in excellent agreement with previously reported macroscale values for normal and arthritic human cartilage (Armstrong and Mow 1982; Athanasiou et al. 1991; Kleemann et al. 2005) and results demonstrating similar moduli between the medial and lateral condyle (Athanasiou et al. 1991).

Stress and strain in the immediately vicinity of the chondrocyte depend heavily on the relative mechanical properties of the PCM and local ECM at the cell's position within the tissue (Guilak and Mow 2000; Wu and Herzog 2002; Korhonen et al. 2006;

Choi et al. 2007; Korhonen and Herzog 2008; Julkunen et al. 2009). In the current study, the ratio of PCM to ECM elastic moduli increased from 0.36 ± 0.06 in macroscopically normal medial condyle cartilage to 0.56 ± 0.13 in OA cartilage. This disruption of the normal ratio of PCM to ECM mechanical properties, coupled with the observed concurrent decrease in ECM moduli, may result in the chondrocyte experiencing significantly different biomechanical signals in OA (Guilak and Mow 2000; Alexopoulos et al. 2005a). This altered mechanical signaling, coupled with the inflammatory environment of the degenerative joint, would contribute to catabolic signaling cascades and further destruction of the cartilage (Sandell and Aigner 2001; Poole et al. 2007).

One noted advantage of our AFM-based approach is its ability to spatially map these mechanical changes in the chondrocyte microenvironment. In agreement with our qualitative IF-labeling results, the biomechanical footprint of the PCM was enlarged in OA medial condyle cartilage as compared to macroscopically normal samples. Quantitative analysis of collected stiffness maps revealed a shallow stiffness gradient outward from the PCM inner edge in OA cartilage as compared to normal tissue. This result suggests a direct relationship between the ultrastructural changes prevalent in OA chondrons (Poole et al. 1991b; Hambach et al. 1998; Lee et al. 2000; Horikawa et al. 2004; Murray et al. 2010) and their altered biomechanical properties.

While the distance-based definition of the PCM applied in this work provided a consistent region across all samples tested, the pre-defined $1 \mu\text{m}$ region likely

underestimates the true extent of the PCM (Youn et al. 2006). This is especially true in OA cartilage due to the prevalence of enlarged chondrons (Poole et al. 1991b; Lee et al. 2000). A biochemical definition of the PCM such as type VI collagen (Poole et al. 1988; Poole et al. 1992; Hagiwara et al. 1993; Youn et al. 2006), as opposed to the distance-based definition applied here, would allow for precise definition of PCM indentation points and full characterization of the PCM in OA cartilage.

4.5 Summary

Our study provides further evidence of significant degradative changes in articular cartilage at the microscale with OA. In addition, our findings provide new insight into the micromechanical environment of the chondrocyte in the early stages of disease progression, demonstrating radial expansion of the PCM biomechanical footprint in addition to a loss in mechanical integrity. A detailed mechanical characterization of PCM alterations throughout the progression of OA could be applied to theoretical models of the chondrocyte microenvironment (Guilak and Mow 2000; Alexopoulos et al. 2005a) to better understand alterations in cellular stress and strain which can, in turn, improve our understanding of the specific contributions of mechanical loading to cartilage degeneration in OA.

5. Immunofluorescence-Guided Atomic Force Microscopy to Measure the Micromechanical Properties of the Pericellular Matrix of Porcine Articular Cartilage

A version of this chapter was published as the following:

Wilusz, R.E., DeFrate, L.E. Guilak, F. Immunofluorescence-Guided Atomic Force Microscopy to Measure the Micromechanical Properties of the Pericellular Matrix of Porcine Articular Cartilage, *Journal of the Royal Society Interface*, 9(76):2997-3007, 2012.

5.1 Introduction

Articular cartilage is the connective tissue that lines the articulating surfaces of diarthrodial joints, providing a low-friction, load-bearing surface that supports and distributes the forces generated during joint motion. The functional mechanical properties of cartilage are conferred by the tissue's extensive extracellular matrix (ECM) that is produced and maintained by a single population of cells known as chondrocytes. During joint activity, chondrocytes are subjected to a complex mechanical environment consisting of temporal and spatial variations in stress and strain, hydrostatic pressure, streaming potentials, and osmotic pressure (Mow et al. 1994; Lai et al. 2002; Mow and Guo 2002). This mechanical environment has been shown to significantly impact the balance of chondrocyte anabolic and catabolic activities and, in turn, influence the overall health of the joint (reviewed in (Guilak et al. 1997; Grodzinsky et al. 2000; Williams et al. 2010)).

Within the ECM, chondrocytes are surrounded by a narrow region called the pericellular matrix (PCM) that together with the enclosed cell(s) is termed the chondron

(Poole et al. 1987). In normal cartilage, the PCM is often defined by the exclusive presence and localization of type VI collagen around the chondrocyte (Poole et al. 1988; Poole et al. 1992; Hagiwara et al. 1993; Youn et al. 2006) and is characterized by an elevated concentration of proteoglycans (PGs) and glycoproteins relative to the surrounding ECM (Poole et al. 1984; Poole 1997; Hunziker et al. 2002). While the exact function of the PCM in cartilage is not fully understood, it is thought to play an important biomechanical role in the tissue. It has been hypothesized that each chondrocyte tailors its PCM based on the unique set of dynamic mechanical forces at its position within the matrix (Poole et al. 1988), suggesting that the PCM serves to protect the chondrocyte during compressive loading (Poole et al. 1987) and act as a transducer of mechanical and biochemical signals in the cellular microenvironment (Guilak et al. 2006). Furthermore, the relationship between the molecular constituents of the PCM (e.g. type VI collagen) and its mechanical properties are not fully understood.

Previous theoretical models (Guilak and Mow 2000; Alexopoulos et al. 2005a; Michalek and Iatridis 2007; Korhonen and Herzog 2008) and experimental studies (Knight et al. 1998; Knight et al. 2001; Hing et al. 2002; Choi et al. 2007; Nicodemus and Bryant 2008) have demonstrated a functional biomechanical role for the PCM. In particular, the stress-strain environment of the chondrocyte depends heavily on the relative mechanical properties of the chondrocyte, its PCM, and the local ECM (Guilak and Mow 2000; Alexopoulos et al. 2005a; Choi et al. 2007). Cartilage is sub-divided into

three zones (superficial, middle, and deep) based on depth from the articular surface that are characterized by differences in ECM composition and ultrastructure (Venn and Maroudas 1977; Hwang et al. 1992; Hunziker et al. 1997; Hunziker et al. 2002) and chondrocyte morphology and arrangement (Poole et al. 1984; Quinn et al. 2005). Zonal variation in matrix composition and structure contribute to a depth-dependent increase in compressive properties of the cartilage ECM (Schinagl et al. 1997; Chen et al. 2001; Tomkoria et al. 2004). Isolated chondrocytes also demonstrate zonal differences in their mechanical properties with superficial zone cells exhibiting higher moduli than middle/deep zone cells (Darling et al. 2006; Shieh and Athanasiou 2006). While the three-dimensional morphology and thickness of the PCM varies among the cartilage zones (Hunziker et al. 2002; Youn et al. 2006), micropipette aspiration of mechanically isolated chondrons from canine (Guilak et al. 2005) and human (Alexopoulos et al. 2003; Alexopoulos et al. 2005b) cartilage revealed zonal uniformity in the mechanical properties of the PCM, despite significant zonal differences in ECM properties. While recent studies have evaluated the biomechanical properties of the cartilage PCM *in situ* indirectly using inverse boundary element analysis coupled with three-dimensional confocal microscopy (Kim et al. 2010) and directly via atomic force microscopy (AFM) (Chapter 2 (Darling et al. 2010); Chapter 3 (McLeod et al. 2013)), few studies have evaluated zonal variation in PCM properties *in situ*. In Chapter 3 (McLeod et al. 2013), the mechanical properties of a 1 μm region immediately adjacent to the chondrocyte

were shown to be uniform across the superficial, middle, and deep zones. However, this distance-based region does not represent the true extent of the PCM (Youn et al. 2006). A more precise definition based on the unique biochemical composition of the PCM would provide a means to fully evaluate the existence, or lack, of zonal variations in PCM properties *in situ*.

AFM has emerged as a powerful tool for biomechanics applications because it provides a means for precisely controlled nano- and microindentation in aqueous environments. Using a force spectroscopy technique known as stiffness or force-volume mapping, AFM can be used to collect arrays of indentation curves and map spatial variations in elastic modulus over a specified region (Radmacher et al. 1992; Gad et al. 1997; A-Hassan et al. 1998). In this regard, AFM indentation has been used to investigate the mechanical properties of local features in multiple cartilaginous tissues, including intervertebral disc (Lewis et al. 2008), fibrocartilage (Hu et al. 2001), growth plate (Allen and Mao 2004; Radhakrishnan et al. 2004), and articular cartilage (Chapter 2 (Darling et al. 2010), Chapter 3 (McLeod et al. 2013); (Stolz et al. 2004; Tomkoria et al. 2004; Park et al. 2009; Stolz et al. 2009; Desrochers et al. 2010; Loparic et al. 2010). More recently, AFM has been combined with a number of optical microscopy techniques, including phase contrast and fluorescence (Moreno Flores and Toca-Herrera 2009; Sen and Kumar 2009), allowing for simultaneous stiffness mapping and high resolution imaging, thereby

providing a means for direct correlation between structural features, biochemical composition, and biomechanical properties.

The objective of this study was to characterize the mechanical properties of the ECM and PCM in the microenvironment of the chondrocyte *in situ* using AFM and test the hypotheses that the biomechanical properties of the PCM correlate with the presence of type VI collagen and are uniform with depth from the articular surface. PCM regions in full thickness articular cartilage samples from porcine knee joints were identified using fluorescence immunolabeling for type VI collagen. Guided by this biochemical definition of the PCM, AFM stiffness mapping as described in Chapter 2 (Darling et al. 2010) was used to evaluate the elastic properties of matched PCM and ECM regions within the superficial, middle, and deep zones *in situ* and to correlate these properties to the presence of type VI collagen.

5.2 Materials and Methods

5.2.1 Tissue sample preparation

Full thickness articular cartilage samples were collected from central regions of the medial femoral condyle of 2 – 3 year old, skeletally mature, female pig knee joints with no macroscopic signs of joint degeneration. Cartilage samples were wrapped in phosphate-buffered saline (PBS)-soaked gauze and frozen at -20°C for intermediate storage. Samples were embedded in water-soluble embedding medium (Tissue-Tek O.C.T. Compound; Sakura Finetek USA) and sectioned perpendicular to the articular

surface in 5 μm -thick slices using a cryostat microtome (Leica CM1850; Leica). Cartilage slices were collected on glass slides and washed thoroughly with 0.1 M tris-buffered saline (TBS), pH 7.3, to remove the water-soluble embedding medium prior to immunofluorescence (IF) labeling and AFM testing.

5.2.2 Immunofluorescence for type VI collagen

Unfixed cartilage sections were labeled for type VI collagen using a modified IF protocol (Youn et al. 2006). Sections were blocked in 10% normal donkey serum (Lot #: S10011325; Fitzgerald) diluted in assay buffer (0.1% Bovine Albumin Solution (BSA; Invitrogen) in 0.1 M TBS, pH 7.3) for 20 minutes at room temperature. Samples were incubated with primary antibody for type VI collagen (anti-collagen type VI raised in rabbit, 70R-CR009X, Fitzgerald) at a 1:50 dilution in 10% donkey serum for 20 minutes at room temperature. After two TBS washes of 5 minutes each, samples were incubated with secondary antibody (FITC-conjugated donkey anti-rabbit IgG, 43R-ID061FT; Fitzgerald) at a 1:200 dilution in 10% donkey serum for 20 minutes in the dark at room temperature. Sections were rinsed twice with TBS for 5 minutes each and remained in TBS at room temperature during AFM testing.

5.2.3 Mechanical characterization via AFM stiffness mapping

Simultaneous force measurements and fluorescence imaging were performed using an AFM system (MFP-3DBio; Asylum Research) integrated with an inverted fluorescence microscope (AxioObserver A1; Zeiss). For microscale indentation,

borosilicate glass spheres (5 μm diameter) were attached to tip-less AFM cantilevers ($k = 4.5 \text{ N/m}$; Novascan). Indentations were applied with a force trigger of 300 nN and curves were sampled at 7.5 kHz. For evaluation of PCM elastic properties, indentations (1600 sites per region, 15 $\mu\text{m/s}$ indentation velocity) were sequentially applied over a 20 $\mu\text{m} \times 20 \mu\text{m}$ region of interest defined by microscopic examination with phase contrast imaging (Figure 5-1A) and positive IF-labeling for type VI collagen around cell-sized voids (Figure 5-1B). Topographical maps of relative height were collected simultaneously during stiffness mapping of each PCM scan region. Elastic properties of the adjacent ECM were evaluated using the same approach over 20 $\mu\text{m} \times 20 \mu\text{m}$ regions visually devoid of PCM and type VI collagen (16 indentations per region, 15 $\mu\text{m/s}$ indentation velocity).

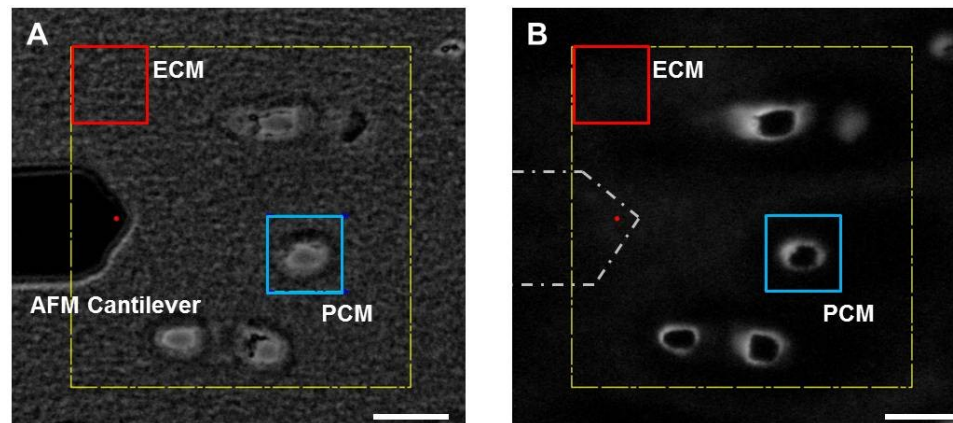


Figure 5-1: Selection of PCM and ECM scan regions using immunofluorescence. (A) Phase contrast and (B) fluorescence images of PCM (blue) and ECM (red) scan regions in the deep zone of porcine articular cartilage as seen during AFM testing. Localization of type VI collagen around cell-sized voids was used to identify the PCM in IF-labeled sections. The AFM cantilever is shown in (A) and outlined in (B) with the red circle indicating the approximate location of the spherical tip. Scale bar = 20 μm .

In order to investigate the potential influence of IF-labeling on measured microscale elastic properties, site-matched PCM/ECM regions were evaluated in the middle/deep zone (200 – 400 μm from the articular surface) of paired unlabeled and IF-labeled cartilage sections (N = 3 pigs, n = 17 total regions). Unlabeled sections underwent minimal washing to remove the water-soluble embedding medium and underwent AFM testing immediately. AFM testing was conducted in TBS at room temperature and was completed within 4 hours of initial sectioning. Preliminary studies showed no significant change in Safranin-O staining of PGs or mechanical properties in IF-labeled cartilage sections over the time course of AFM testing (113 ± 18 kPa vs. 94 ± 11 kPa, $p = 0.39$, Student's t -test).

To evaluate zonal variations in PCM elastic properties *in situ*, paired ECM/PCM regions (N = 5 pigs, n = 20 total regions per zone) were selected within each of the three cartilage zones. The superficial zone was defined to include the region 0 – 100 μm from the articular surface, the middle zone from 200 – 300 μm from the articular surface, and the deep zone as the bottom half of each cartilage section. These designations were selected based on variations in cell morphology and tissue architecture outlined previously in the literature (Hwang et al. 1992; Hunziker et al. 1997). The order of testing among the three zones was varied among cartilage the samples. All AFM testing was conducted in TBS at room temperature and completed within 4 hours of initial sectioning.

5.2.4 Data evaluation

Raw data for cantilever deflection and z-piezo movement were collected and analyzed using a custom MATLAB script (The MathWorks). The elastic modulus, E , was determined by fitting a modified Hertz model to force-indentation curves, as described previously (Darling et al. 2006). For articular cartilage, the local Poisson's ratio was assumed to be $\nu = 0.04$ for both the ECM (Mow et al. 1980; Chen et al. 2001; Choi et al. 2007) and PCM (Alexopoulos et al. 2005b) based on previous experimental reports in the literature. From the Hertz model, presented modulus values can be converted from $\nu = 0.04$ to a different assumed value of ν by multiplying by the conversion factor $(1 - \nu^2)/(1 - 0.04^2)$. Probe-surface contact was identified using contact point extrapolation,

a method that uses the indentation portion of the approach curve to determine the probe-surface contact point on soft substrates based on an applied mathematical model (Guo and Akhremitchev 2006). Hertzian contact mechanics provided excellent fits to the experimental data for all force-indentation curves ($R^2 > 0.90$). Two-dimensional contour maps were generated of the spatial distribution of calculated elastic moduli in each region.

To compare the elastic moduli of unlabeled and IF-labeled PCM, a distance-based definition of the PCM was used as described in Chapter 2 (Darling et al. 2010). Briefly, PCM regions were determined based on spatial indicators of contact with the underlying glass substrate within cell-sized voids. Glass contact was readily apparent from the force-indentation curves and was used to define the edge of each cell void. PCM data were included for a region extending 1 μm radially from this edge. This defined region may locally under- or over-represent the actual extent of the PCM for any given site but provided a consistent definition of the PCM among samples in the absence of IF-labeling.

For IF-labeled sections, the cartilage PCM was identified by positive type VI collagen labeling around cell-sized voids and data were included for all indentations that fell within labeled regions. For precise navigation using the AFM MFP-3D software (Asylum Research), the tip location on the AFM cantilever must be specified. Because the spherical tip was not visible in either captured light or fluorescence images, its

location was approximated to within 2 – 3 μm (Figure 5-1), and an image analysis algorithm was developed in Mathematica (Wolfram Research, Inc., Champaign, IL) to correct for any translational shift between captured IF images and stiffness maps. ImageJ (National Institutes of Health) was used to crop AFM navigation images (Figure 5-1B) and produce an IF image of each PCM scan region (Figure 5-2B, 256 x 256 pixels) that was imported into Mathematica. The corresponding topographical (Figure 5-2A) and elastic moduli contour maps (not shown) were resized from 40 x 40 pixels to 256 x 256 pixels using bilinear interpolation. The topographical map was used for alignment of stiffness maps due to its clear depiction of the cell-sized void associated with each PCM. Since indentation points on the topographical map perfectly align with points on the elastic moduli contour map, any translational shift in the topographical map could be directly applied to the contour map. Edge detection was used to define the inner edge of the cell-sized void in the topographical map and IF image (Figure 5-3C, D). Using an iterative closest-point technique (Abebe et al. 2009), the topographical map was translated in the x- and y-directions to minimize the distance between the cell void inner edge in the topographical map and IF image. With the magnitude of the translational shift between the two images determined, the IF image and elastic moduli contour maps were cropped as necessary to align the images (Figure 5-3E, F). Once aligned, IF images were converted to binary masks to indicate regions of positive IF-labeling using an optimal threshold value determined from a range of images (Figure 5-3G). IF-positive

masks and elastic moduli contour maps were analyzed in MATLAB to extract PCM data from each scan region (Figure 5-3H). To quantitatively evaluate the spatial distribution of moduli in the chondrocyte microenvironment, the stiffness progression from the PCM outer edge to the ECM was evaluated in radial increments of 0.5 μm .

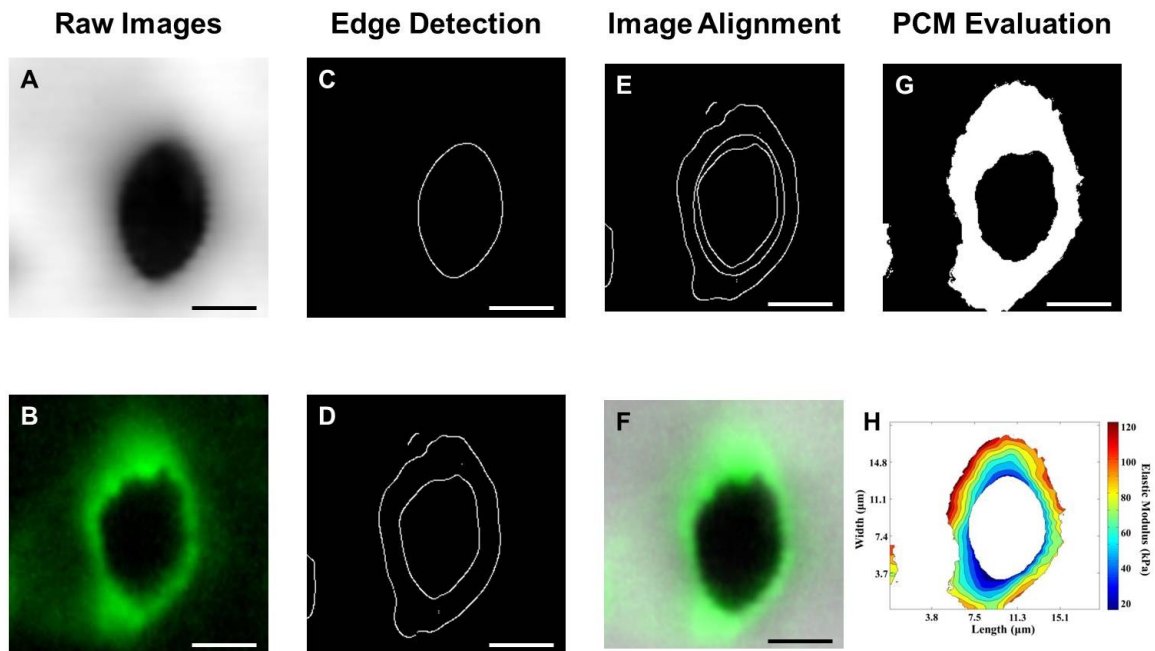


Figure 5-2: Data analysis of immunofluorescence-labeled PCM scan regions. The inner edge of cell-sized voids was detected in topographical maps (A) and IF images (B) using edge detection (C, D). The topographical map was translated in the x- and y-directions to minimize the distance between it and the IF image (E). Topographical maps and IF images were cropped for alignment as needed (shown overlaid in F). Aligned IF images were thresholded and converted to binary masks to determine regions of positive IF-labeling (G). IF-positive masks and elastic moduli contour maps were analyzed in MATLAB to extract PCM moduli from each scan region (H). Scale bar = 5 μm .

5.2.5 Statistical analyses

Differences in ECM and PCM elastic moduli between unlabeled and IF-labeled cartilage sections were evaluated using a two-way ANOVA (region, label; $\alpha = 0.05$) and Fisher's least significant difference (LSD) *post-hoc* test. In IF-labeled sections, differences between ECM and PCM elastic moduli among the three zones were evaluated using a two-way ANOVA (region, zone; $\alpha = 0.05$) and Fisher's LSD *post-hoc* test. Differences in PCM elastic moduli among the three zones were evaluated separately using a one-way ANOVA (zone; $\alpha = 0.05$). Stiffness progression data were evaluated separately within each zone using a one-way ANOVA (distance; $\alpha = 0.05$) and Fisher's LSD *post-hoc* test. The relationship between elastic modulus and fluorescence intensity for each PCM scan region was determined using linear regression.

5.3 Results

5.3.1 Immunofluorescence for type VI collagen

Immunolabeling of cartilage sections for type VI collagen showed clear localization of type VI collagen to the regions immediately surrounding cell-sized voids. In the superficial zone, cell-sized voids and their associated PCM were elongated parallel to the articular surface (Figure 5-3A). In the middle zone, the PCM and cell-sized voids exhibited a more rounded morphology (Figure 5-3B). In the deep zone, cell-sized voids and the PCM were elongated perpendicular to the articular surface (Figure 5-3C).

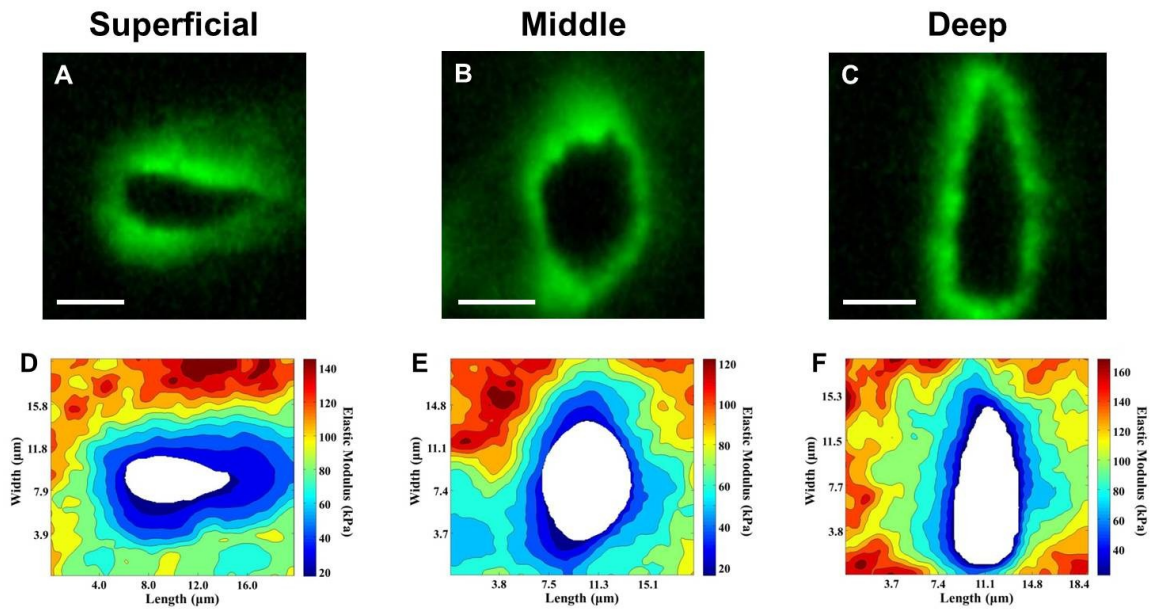


Figure 5-3: Stiffness mapping of immunofluorescence-labeled PCM. (A, B, C) Representative IF images showing the distribution of type VI collagen around cell-sized voids in the superficial, middle, and deep zones. (D, E, F) Representative contour maps of calculated elastic moduli of PCM scan regions in each zone. The spatial distribution of type VI collagen co-localized with softer modulus regions within each scan. Scale bar = 5 μm .

5.3.2 Influence of immunofluorescence-labeling on articular cartilage micromechanical properties

The influence of IF-labeling on the observed microscale mechanical properties was evaluated in the middle/deep zone of unlabeled and IF-labeled cartilage sections. No significant difference was observed in the measured elastic moduli in either the predefined 1 μm PCM region or the ECM with IF-labeling ($p = 0.97$ for PCM, $p = 0.39$ for ECM; Figure 5-4). ECM elastic moduli were significantly greater than PCM elastic moduli in both unlabeled and labeled sections ($p < 0.05$).

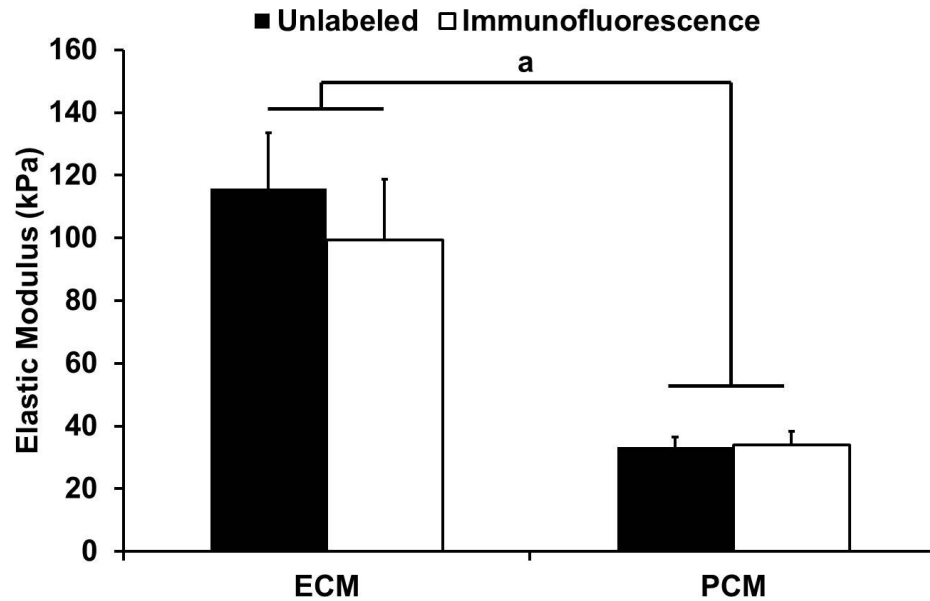


Figure 5-4: Effect of immunofluorescence-labeling on articular cartilage microscale moduli. Elastic moduli of ECM and PCM regions measured in the middle/deep zone of unlabeled (black) and IF-labeled (white) cartilage sections. No difference in moduli was observed with IF-labeling ($p = 0.39$ for ECM, $p = 0.97$ for PCM). a: $p < 0.001$ for ECM moduli as compared to PCM moduli. Moduli presented as mean + standard error (N = 3 pigs, n = 17 regions per treatment).

5.3.3 AFM stiffness mapping of immunofluorescence-labeled articular cartilage PCM and ECM

Stiffness mapping revealed that type VI collagen and lower elastic moduli co-localized in the pericellular space around cell-sized voids (Figure 5-3). Regions exhibiting higher fluorescence intensity had lower elastic moduli (Figure 5-5). There was a significant relationship between fluorescence intensity and elastic modulus within PCM scan regions ($p < 0.0001$). The strongest relationships, based on R^2 , existed between fluorescence intensity and elastic modulus when evaluated over the full scan region

(PCM + local ECM) as compared to PCM points or local ECM points alone (Figure 5-6).

Overall, the weakest relationships were observed in deep zone scan regions.

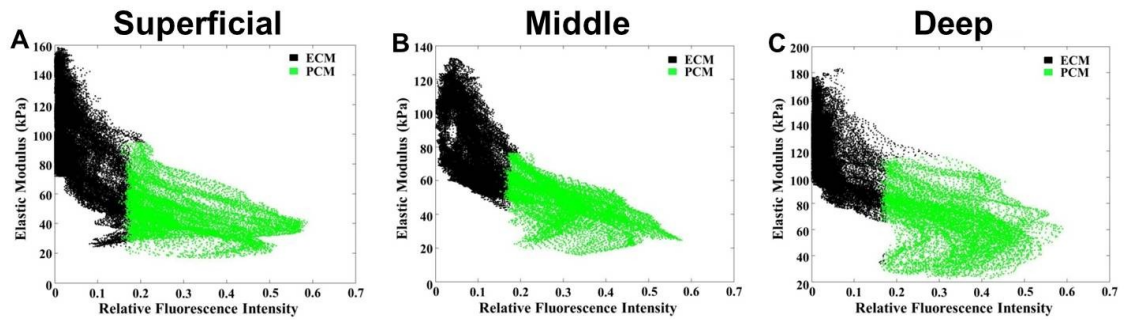


Figure 5-5: Elastic modulus vs. fluorescence intensity in PCM scan regions. Representative scatter plots of elastic modulus vs. relative fluorescence intensity in PCM scan regions in the (A) superficial, (B) middle, and (C) deep zones. PCM (green) and local ECM (black) areas are shown.

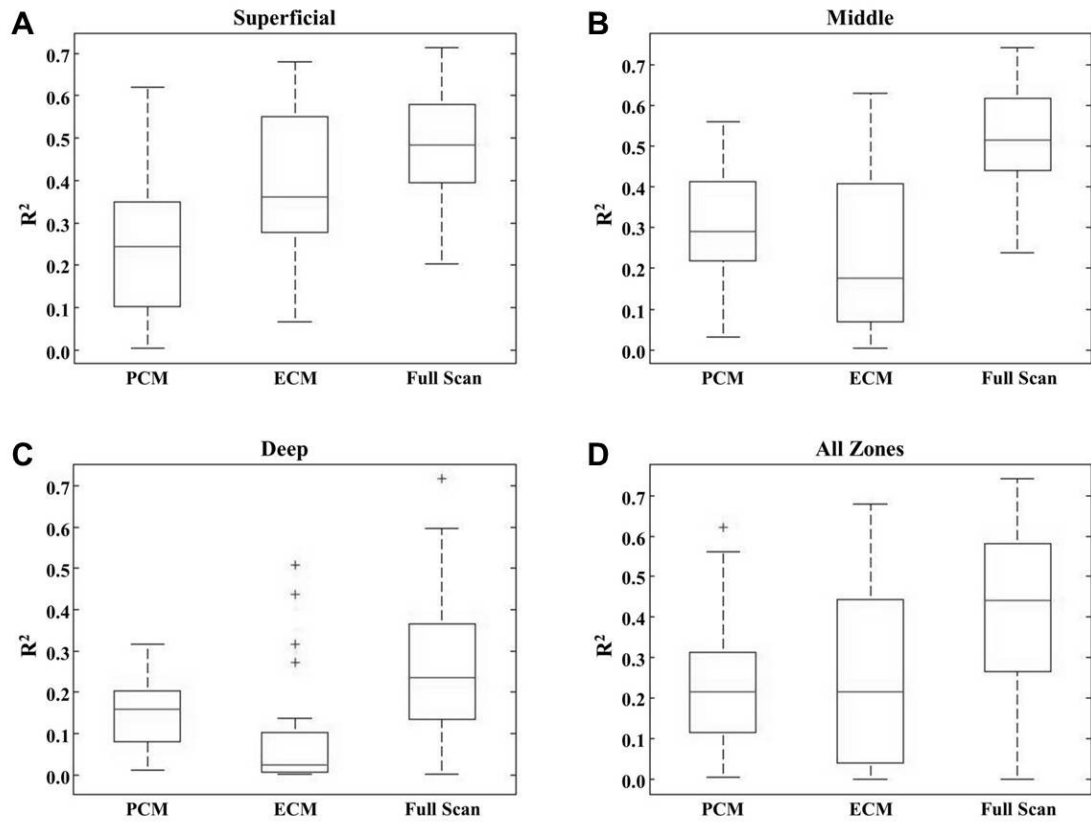


Figure 5-6: Linear regression analysis of elastic modulus vs. fluorescence intensity in PCM scan regions. Box plots of coefficient of determination (R^2) for each PCM scan region in the (A) superficial, (B) middle, and (C) deep zones and (D) across all zones. Separate regression analyses were performed on PCM regions alone, local ECM regions alone, and the full scan region (PCM + local ECM). Median R^2 value is designated by the horizontal line within each box (N = 5 pigs, n = 20 regions per zone).

5.3.4 Zonal variation of PCM elastic moduli

PCM elastic moduli exhibited no significant differences among the superficial (68 ± 5 kPa), middle (56 ± 4 kPa), and deep (58 ± 6 kPa) zones ($p = 0.21$, Figure 5-7). In the superficial zone, PCM regions exhibited lower elastic moduli than immediately adjacent regions lacking type VI collagen ($p < 0.05$, Figure 5-8). Elastic moduli reached values comparable to the ECM $2.5 \mu\text{m}$ from the PCM outer edge. In the middle zone, PCM elastic moduli were lower than those in regions greater than $1 \mu\text{m}$ from the PCM outer edge ($p < 0.05$). Middle zone elastic moduli reached ECM-like values $1.5 \mu\text{m}$ from the PCM outer edge. In the deep zone, PCM moduli exhibited lower values than regions greater than $1.5 \mu\text{m}$ from the PCM outer edge ($p < 0.05$) and ECM-like elastic moduli were observed immediately outside the PCM. In all three zones, ECM elastic moduli were greater than their respective PCM moduli ($p < 0.05$, Figure 5-7). The superficial zone exhibited higher ECM moduli as compared to the middle and deep zones ($p < 0.05$).

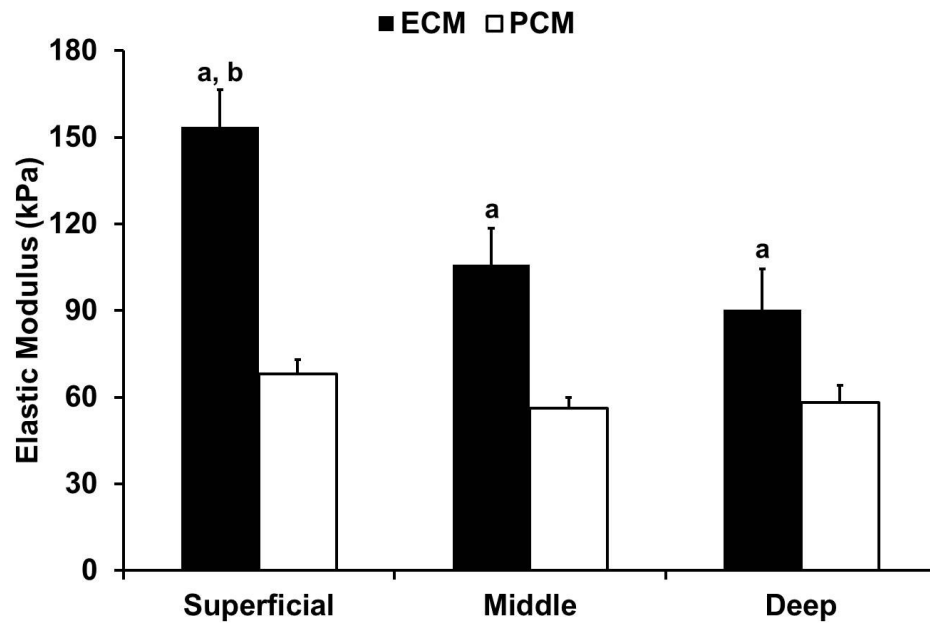


Figure 5-7: Zonal uniformity in PCM elastic moduli. Elastic moduli of ECM (black) and PCM (white) regions measured in the superficial, middle, and deep zones. PCM elastic moduli exhibited zonal uniformity ($p = 0.21$). a: $p < 0.05$ for ECM moduli as compared to their respective PCM moduli. b: $p < 0.05$ for superficial zone ECM moduli as compared to middle and deep zone ECM moduli. Moduli presented as mean + standard error (N = 5 pigs, n = 20 regions per zone).

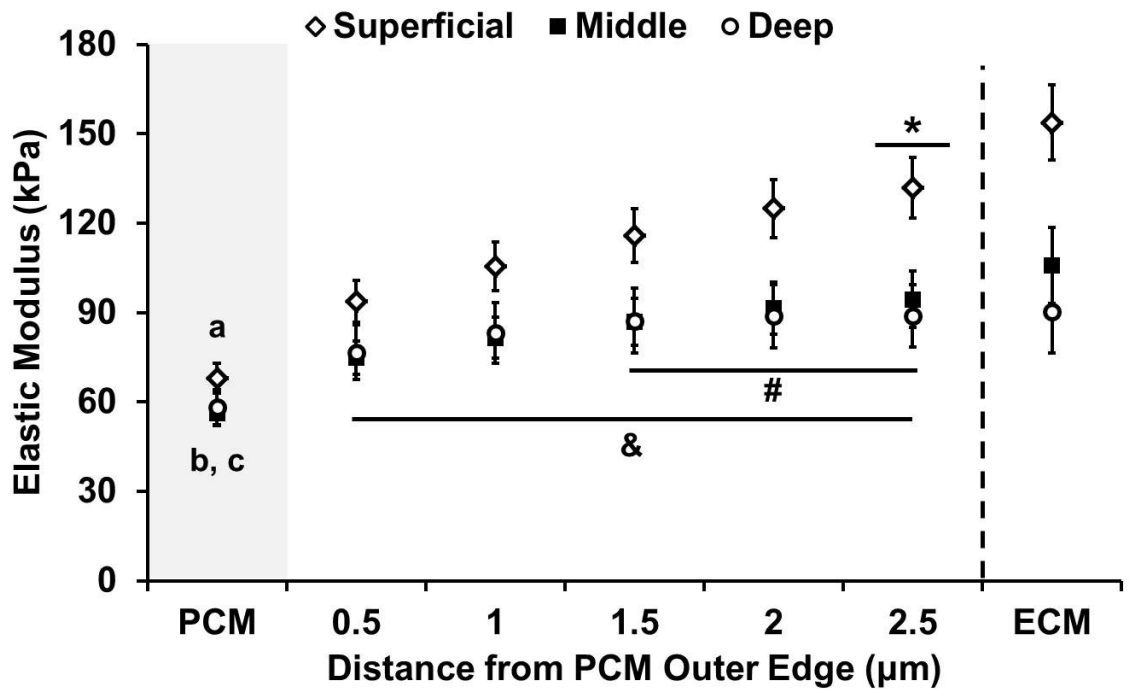


Figure 5-8 Stiffness progression of elastic moduli. Stiffness progression of moduli from the PCM outer edge to the ECM in the superficial (diamond), middle (square), and deep (circle) zones. a: $p < 0.05$ for superficial zone PCM moduli as compared to all superficial zone regions beyond the PCM outer edge. b: $p < 0.05$ for middle zone PCM moduli as compared to middle zone regions greater than 1.0 µm from the PCM outer edge. c: $p < 0.05$ for deep zone PCM moduli as compared to deep zone regions greater than 1.5 µm from the PCM outer edge. *: Superficial zone moduli reached ECM values 2.5 µm from PCM outer edge ($p > 0.05$). #: Middle zone moduli reached ECM values 1.5 µm from the PCM outer edge ($p > 0.05$). &: Deep zone moduli reached ECM values at the PCM outer edge ($p > 0.05$). Moduli presented as mean \pm standard error (N = 5 pigs, n = 20 regions per zone).

5.4 Discussion

Our results demonstrate that the biomechanical properties of the cartilage PCM correlate with the presence of type VI collagen in the chondrocyte microenvironment. Control experiments verified that immunolabeling had no effect on micromechanical properties of either the cartilage PCM or ECM. Immunolabeling in combination with AFM-based stiffness mapping revealed co-localization of type VI collagen and lower elastic moduli to the PCM. Matrix regions lacking type VI collagen immediately adjacent to the PCM exhibited higher elastic moduli than regions positive for type VI collagen. PCM elastic moduli measured *in situ* exhibited zonal uniformity across the superficial, middle, and deep zones of the cartilage.

By evaluating PCM mechanical properties within the context of the local ECM with minimal disruption of native matrix integration, the method presented here provides a direct means to fully evaluate the micromechanical environment of the chondrocyte *in situ*. Stiffness mapping demonstrated that type VI collagen is a defining factor for both the biochemical and biomechanical definitions of the PCM. PCM regions were softer than immediately adjacent regions lacking type VI collagen. In the superficial and middle zones, these regions exhibited intermediate elastic moduli between the PCM and ECM. This result suggests that the territorial matrix (TM), located between the PCM and ECM (Poole et al. 1984), may serve as a mechanical as well as structural transition region in articular cartilage. In addition, fluorescence intensity of

type VI collagen IF-labeling was found to be a significant predictor of elastic modulus. The strongest relationships, based on R^2 values, were observed when evaluated over the full scan region with fluorescence intensity contributing to 48%, 51%, and 23% of the observed variation in elastic modulus in the superficial, middle, and deep zones, respectively. Not surprisingly, the weakest relationships were observed in the deep zone where the difference between PCM and ECM elastic moduli was the smallest. This observation further supports the defining role of type VI collagen in the biomechanical properties of the PCM.

The results of this study provide evidence for site-specific variation of the elastic modulus within the PCM. For example, PCM elastic moduli in this study ($E = 56 - 68$ kPa) were approximately twice as stiff as those measured *in situ* via AFM for porcine cartilage ($E \approx 30$ kPa) in our initial study presented in Chapter 2 (Darling et al. 2010) and 10 – 15% greater than those presented in Chapter 3 (McLeod et al. 2013). This difference in moduli was not an effect of immunolabeling on microscale stiffness. Rather, it likely reflects a more accurate definition of the PCM boundary that is based on type VI collagen IF, rather than distance from the chondrocyte. When the same 1 μm thick, distance-based definition of the PCM was employed in the current work, measured PCM elastic moduli ($E = 33 - 34$ kPa) were in direct agreement with our previous results. The distribution of type VI collagen around cell-sized voids demonstrated that this distance-based definition underestimated the true local PCM thickness. It is also possible

that type VI collagen extends beyond the PCM and into the adjacent TM, where it has been reported to be interwoven with type II collagen fibers (Soder et al. 2002). Inclusion of higher modulus TM regions may have contributed to elevated PCM moduli. Furthermore, there are limitations in lateral resolution associated with using micrometer-sized indenters for AFM-based stiffness mapping of soft substrates (Radmacher et al. 1995). For spherical probes, the contact radius scales with tip radius and indentation depth. Since stiffness maps were collected using a single force trigger (300 nN), indentation depths were smaller in stiffer ECM regions (~800 nm) than in softer PCM regions (~1.5 μm). As a result, contact radii were larger in PCM regions (2.0 – 2.2 μm) as compared to ECM regions (1.5 – 1.8 μm). Indenter contact with adjacent TM and/or ECM regions might contribute to artificial stiffening of peripheral PCM regions.

PCM elastic moduli measured in the current study are in excellent agreement with those measured using other techniques such as micropipette aspiration of isolated chondrons (Alexopoulos et al. 2003; Alexopoulos et al. 2005b; Guilak et al. 2005). In particular, a recent study reported the mechanical properties of the PCM in intact cartilage by employing inverse boundary element analysis coupled with three-dimensional confocal microscopy of compressed porcine cartilage. This study estimated the Young's modulus of the PCM to be 24 – 59 kPa in the middle zone (Kim et al. 2010). The consistency in PCM properties among these different measurement techniques

suggests that the sample preparation methods in this study (i.e. frozen sectioning and immunolabeling) do not have significant effects on PCM properties.

Previous studies investigating zonal variation in PCM properties focused on mechanically extracting chondrons from the superficial and middle/deep zones of the tissue (Alexopoulos et al. 2003; Alexopoulos et al. 2005b; Guilak et al. 2005). Results from these micropipette aspiration studies and our *in situ* work agree that the PCM exhibits zonal uniformity in its mechanical properties. Zonal uniformity in PCM properties coupled with zonal differences in chondrocyte (Darling et al. 2006; Shieh and Athanasiou 2006) and ECM (Schinagl et al. 1997; Chen et al. 2001) properties generates depth-dependent variation in the ratio of chondrocyte to PCM to ECM properties which in turn influence the local mechanical and physiochemical environments of the cell (Guilak and Mow 2000; Alexopoulos et al. 2005a). This result supports the hypothesized role of the PCM as a mechanical transducer that provides a uniform cellular environment throughout the tissue depth despite large inhomogeneities in local strain during joint loading (Choi et al. 2007).

While type VI collagen is often used as the primary marker of the cartilage PCM, a recent study by Alexopoulos and colleagues (Alexopoulos et al. 2009) demonstrated that intact chondrons could be isolated from Col6a1 knockout mice that lack type VI collagen. A number of matrix molecules are found either exclusively or at higher concentrations in the PCM as compared to the surrounding ECM, including perlecan

(SundarRaj et al. 1995; Melrose et al. 2006), hyaluronan (Knudson 1993; Cohen et al. 2003), biglycan (Kavanagh and Ashhurst 1999), type IX collagen (Poole et al. 1997), fibronectin (Chang et al. 1997), and laminin (Durr et al. 1996). The fact that intact chondrons can be isolated from Col6a1 null mice (Alexopoulos et al. 2009) suggests that other molecular components likely contribute to the structural integrity and biomechanical properties of the PCM, potentially providing alternative composition-based definitions of the PCM.

Consistent with other AFM studies (Coles et al. 2008; Park et al. 2009), ECM modulus values observed in our study were lower than macroscale values for healthy porcine articular cartilage (Fermor et al. 2007; Hennerbichler et al. 2008). Measured ECM moduli were greater than those reported previously for the superficial zone ($E = 154$ kPa vs. 44 kPa) of porcine patellar cartilage (Coles et al. 2008) and the middle/deep zone ($E = 90 - 106$ kPa vs. 81 kPa) of porcine articular cartilage presented in Chapter 2 (Darling et al. 2010). Furthermore, the observed ECM microscale elastic properties decreased with depth from the articular surface, a finding in direct agreement with the results presented in Chapter 3 (McLeod et al. 2013) but inconsistent with the depth-dependent increase in ECM compressive properties observed in macroscale studies (Schinagl et al. 1997; Chen et al. 2001). These observations may be attributed to the fact that the AFM measures highly localized properties that may be dominated by the individual molecular components of the tissue. Previous work by Loparic and colleagues on the nanostiffness

of porcine articular cartilage (Loparic et al. 2010) demonstrated that PGs *in situ* are an order of magnitude softer than collagen fibers. In the cartilage ECM, PG content increases with depth from the articular surface (Venn and Maroudas 1977). Interstitial fluid pressurization in response to AFM microindentation is minimal (Park et al. 2009), with an estimated relaxation time constant of approximately 60 milliseconds based on moduli presented in our study. Consistent with previous AFM nano- and microindentation studies (Han et al. 2011), ECM elastic moduli increased slightly with increasing indentation velocity from 1 to 25 $\mu\text{m/s}$ (Appendix C). The observation that the effect of indentation rate was relatively small over a large range of rates indicates that the relaxation time of the tissue is significantly shorter than the characteristic loading time of these experiments. This suggests that the properties measured using this technique represent the intrinsic mechanical properties of the solid matrix independent of biphasic effects. As a result, the apparent softening of the ECM with depth observed in the present work may be due in part to the high concentration of PGs in the middle and deep zones.

Another important difference in these measurements as compared to most previous studies of depth-dependent cartilage properties is that in the current study, cartilage sections were tested in the transverse direction relative to the articular surface. While the mesh-like ultrastructure of the PCM (Poole et al. 1984; Poole et al. 1987; Hunziker et al. 1997) and our AFM results presented in Chapter 3 (McLeod et al. 2013)

suggest that the PCM is isotropic, distinct anisotropy is present in the ECM due to the arcade-like architecture of type II collagen fibers (Hwang et al. 1992). In addition, macroscale properties of cartilage ECM have been shown to depend on the direction of loading relative to the split-line orientation in the superficial zone (Chahine et al. 2004). Split-line direction was not taken into account in this study; however the effect of loading relative to the split-line direction was shown in Chapter 3 to significantly affect the micromechanical properties of the superficial and deep zones of the cartilage ECM (McLeod et al. 2013).

5.5 Summary

Our findings provide further support for type VI collagen as a defining factor in both the biochemical and biomechanical definitions of the PCM and the biomechanical role of the PCM in articular cartilage. In addition, our findings provide a more complete characterization of the matrix mechanical properties in the cellular microenvironment and suggest that the TM serves as a mechanical as well as structural transition between the cartilage PCM and ECM. The combined approach of IF-labeling and AFM stiffness mapping developed here provides a novel means for characterization of the relationship between tissue biochemical composition and biomechanical properties *in situ*.

6. A Biomechanical Role for Perlecan in the Articular Cartilage Pericellular Matrix

A version of this chapter was published as the following:

Wilusz, R.E., DeFrate, L.E., Guilak, F. A Biomechanical Role for Perlecan in the Articular Cartilage Pericellular Matrix. *Matrix Biology*, 31(6):320-7, 2012.

6.1 Introduction

Within the extensive extracellular matrix (ECM) of articular cartilage, chondrocytes are surrounded by a narrow pericellular matrix (PCM) that together with the enclosed cell is referred to as a “chondron” (Poole et al. 1987). The PCM is distinct from the surrounding ECM in its biochemical composition (reviewed in (Poole 1997)), ultrastructure (Poole et al. 1987; Hunziker et al. 1997), and biomechanical properties ((Alexopoulos et al. 2003; Alexopoulos et al. 2005b); Chapters 2 (Darling et al. 2010), 3 (McLeod et al. 2013), 4, and 5 (Wilusz et al. 2012)). While the exact function of the PCM in cartilage has yet to be determined, it is thought to play an important role in regulating the biomechanical environment of the chondrocyte, protecting the cell during compressive loading (Poole et al. 1987) and serving as a mechanical transducer during joint loading (Guilak et al. 2006). Previous theoretical models (Guilak and Mow 2000; Alexopoulos et al. 2005a; Michalek and Iatridis 2007; Korhonen and Herzog 2008) and experimental studies (Knight et al. 2001; Hing et al. 2002; Choi et al. 2007; Villanueva et al. 2009) have demonstrated that stress and strain in the vicinity of the chondrocyte is significantly influenced by the relative mechanical properties of the cell, PCM, and ECM.

In normal cartilage, the PCM is often defined by the exclusive presence and localization of type VI collagen around the chondrocyte (Poole et al. 1988; Poole et al. 1992). As such, previous studies investigating the biomechanical properties of the cartilage PCM have focused on type VI collagen and its role in PCM function. Using immunofluorescence (IF)-guided atomic force microscopy (AFM), we demonstrated in Chapter 5 that PCM biomechanical properties correlate with the presence of type VI collagen and that matrix regions lacking type VI collagen immediately adjacent to the PCM exhibit higher elastic moduli than PCM regions rich in type VI collagen (Wilusz et al. 2012). Alexopoulos and colleagues (Alexopoulos et al. 2009) demonstrated that intact chondrons can be isolated from Col6a1 knockout mice that lack type VI collagen and exhibit reduced mechanical properties as compared to wild-type controls. While these studies illustrate the important role of type VI collagen in the properties of the PCM, they also suggest that other PCM components likely contribute to its structural integrity and biomechanical properties.

A number of matrix molecules are found exclusively in the cartilage PCM as compared to the ECM including perlecan, a large heparan sulfate (HS) proteoglycan (PG) (SundarRaj et al. 1995; Melrose et al. 2005; Melrose et al. 2006; Kvist et al. 2008). Though its exact role in cartilage is unknown, perlecan is essential for normal cartilage development, and dysfunction of the perlecan gene results in potentially lethal skeletal dysplasias (Arikawa-Hirasawa et al. 1999; Costell et al. 1999; French et al. 1999;

Gustafsson et al. 2003). Perlecan modulates signaling of multiple growth factors through its HS chains including the fibroblast growth factors (FGFs) (Aviezer et al. 1994; Whitelock et al. 1996; Melrose et al. 2006; Smith et al. 2007; Vincent et al. 2007; Whitelock et al. 2008; Chuang et al. 2010) and has been implicated in cell-matrix interactions (SundarRaj et al. 1995; Kirn-Safran et al. 2009) and matrix organization (Melrose et al. 2008b). Importantly, perlecan demonstrates a strong electrostatic binding affinity for type VI collagen through its HS chains (Tillet et al. 1994) and interacts with fibronectin and laminin via its core protein (Hopf et al. 1999; Hopf et al. 2001) and HS chains (Battaglia et al. 1992). Through these interactions, perlecan may have an important role in the structural organization and stabilization of the cartilage PCM.

The objective of this study was to determine the biomechanical role of perlecan in the PCM of articular cartilage and its potential role as a defining factor of the PCM. Cryosections of porcine articular cartilage samples were labeled for type VI collagen and perlecan using dual IF. Guided by IF-labeling, AFM-based stiffness mapping as presented in Chapter 5 (Wilusz et al. 2012) was used to evaluate the elastic properties of matched PCM and ECM regions and correlate these properties with PCM biochemical composition. Enzymatic removal of HS chains from perlecan using heparinase III was performed to evaluate the functional role of HS in the biomechanical properties of cartilage. These methods were used to test the hypotheses that the presence of perlecan can be used to define the boundaries of the PCM, that PCM regions rich in perlecan

exhibit lower elastic moduli than regions lacking perlecan, and that enzymatic removal of HS significantly reduces the microscale elastic properties of the PCM while having no effect on ECM properties.

6.2 Materials and Methods

6.2.1 Tissue sample preparation

Full thickness articular cartilage samples were collected from central regions of the medial condyle of skeletally mature, macroscopically normal female pig knee joints. Cartilage samples were wrapped in phosphate-buffered saline (PBS)-soaked gauze and frozen at -20°C for intermediate storage. Samples were embedded in water-soluble embedding medium (Tissue-Tek O.C.T. Compound; Sakura Finetek USA) and sectioned perpendicular to the articular surface in 5 µm-thick slices using a cryostat microtome (Leica CM1850; Leica). Cartilage slices were collected on glass slides and washed thoroughly with PBS to remove the water-soluble embedding medium prior to IF-labeling and AFM testing.

6.2.2 Dual Immunofluorescence for type VI collagen and perlecan

Unfixed cartilage sections were simultaneously labeled for type VI collagen and perlecan. Sections were blocked in 10% normal goat serum (Invitrogen) for 20 minutes at room temperature. Samples were incubated with primary antibodies for type VI collagen (anti-collagen type VI raised in rabbit, 70R-CR009X; Fitzgerald) and perlecan (anti-perlecan raised in rat, sc-33707; Santa Cruz) at a 1:50 dilution in 10% goat serum for

20 minutes at room temperature. After three PBS washes of 5 minutes each, samples were incubated with secondary antibodies (AlexaFluor 568 goat anti-rabbit IgG and AlexaFluor 488 goat anti-rat IgG; Invitrogen) at a 1:200 dilution in 10% goat serum for 20 minutes in the dark at room temperature. Sections were rinsed twice in PBS for 5 minutes each and remained in PBS at room temperature during AFM testing.

6.2.3 Enzymatic digestion of heparan sulfate with heparinase III

Heparinase III (heparitinase I, EC 4.2.2.8; Sigma-Aldrich) is the most specific heparinase for HS, demonstrating no activity for heparin (Ernst et al. 1995). Cartilage sections were incubated in 50 μ L of 6 U/mL (0.01 IU/mL) heparinase III solution in 20 mM Tris-HCl (Sigma-Aldrich) containing 0.1 mg/mL bovine serum albumin (BSA; Invitrogen) and 4 mM calcium chloride (EM Science, Gibbstown, NJ), pH 7.0 at 37°C for 30 minutes. Undigested control sections were incubated at 37°C for 30 minutes in enzyme buffer.

Digestion was confirmed using IF for the heparinase III-specific HS epitope 3G10 (mouse monoclonal primary antibody H1890-75, US Biological, Swampscott, MA) (David et al. 1992) on undigested control and digested sections. Dual IF-labeling was used to evaluate localization of the HS epitope to the cartilage PCM using the protocol outlined in Section 6.2.2. Cartilage sections were simultaneously labeled with antibodies for 3G10 and type VI collagen to determine if digested HS was found exclusively in the PCM (secondary antibody AlexaFluor 488 goat anti-mouse IgG; Invitrogen). To confirm

that digested HS was associated with perlecan, sections were dual-labeled with antibodies for 3G10 and perlecan (secondary antibody AlexaFluor 568 goat anti-mouse IgG; Invitrogen). It is important to note that the monoclonal antibody used to label perlecan was raised against the core protein of perlecan and thus was not expected to be affected by heparinase III digestion. Control experiments were performed to confirm this result and no difference was observed between the IF-labeling of undigested perlecan and heparinase III-digested perlecan on adjacent sections from the same porcine cartilage specimens (data not shown). Histological staining with Accustain Safranin-O (Sigma-Aldrich) and 0.02% aqueous fast green (Sigma-Aldrich) was used to visualize global loss of PGs from sections with digestion.

For AFM testing, sample-matched undigested control and heparinase III-digested sections were dual-labeled for type VI collagen and perlecan as described in Section 6.2.2. Sections remained in PBS at room temperature during testing.

6.2.4 Mechanical characterization via AFM stiffness mapping

Simultaneous force measurements and fluorescence imaging were performed using an AFM system (MFP-3DBio; Asylum Research) integrated with an inverted fluorescence microscope (AxioObserver A1; Zeiss). For microscale indentation, borosilicate glass spheres (5 μm diameter) were attached to tip-less AFM cantilevers ($k = 4.5 \text{ N/m}$; Novascan). Indentations were applied with a force trigger of 300 nN and curves were sampled at 7.5 kHz. For evaluation of PCM elastic properties, indentations

(1600 sites per region, 15 $\mu\text{m/s}$ indentation velocity) were sequentially applied over a 20 $\mu\text{m} \times 20 \mu\text{m}$ region of interest defined by microscopic examination with phase contrast imaging and positive IF-labeling around cell-sized voids. Images of perlecan (green) and type VI collagen (red) labeling were captured for each PCM scan region. Elastic properties of the adjacent ECM were evaluated using the same approach over 20 $\mu\text{m} \times 20 \mu\text{m}$ regions visually devoid of PCM (16 indentations per region, 15 $\mu\text{m/s}$ indentation velocity). For all samples, AFM testing was completed within 4 hours of initial sectioning.

To evaluate the spatial relationship between biochemical composition and biomechanical properties within the PCM *in situ*, paired PCM/ECM regions were selected in the middle/deep zone (200 – 400 μm from the articular surface) of each cartilage sample (N = 4 pigs, n = 23 total regions). To evaluate the biomechanical role of HS in the cartilage PCM, site-matched PCM/ECM regions were evaluated in the middle/deep zone of paired undigested and heparinase III-digested cartilage sections (N = 6 pigs, n = 25 total regions per treatment).

6.2.5 Data evaluation

Raw data for cantilever deflection and z-piezo movement were collected and analyzed using a custom MATLAB script (The MathWorks). Elastic moduli, E , were determined by fitting a modified Hertz model to force-indentation curves as described previously (Darling et al. 2006). For articular cartilage, the local Poisson's ratio, ν , was

assumed to be 0.04 for both the ECM (Mow et al. 1980; Chen et al. 2001; Choi et al. 2007) and PCM (Alexopoulos et al. 2005b). Probe-surface contact was identified using contact point extrapolation, as described previously (Guo and Akhremitchev 2006). Hertzian contact mechanics provided excellent fits ($R^2 > 0.90$). Two-dimensional contour maps were generated of the spatial distribution of calculated elastic moduli in each region.

The cartilage PCM was defined based on positive IF-labeling around cell-sized voids and data were included for all indentations that fell within labeled regions. ImageJ (NIH) was used to crop collected images to produce single channel IF images of each PCM scan region (Figure 6-2A, B). For each PCM scan region, two IF images (green, red) and the corresponding topographical and elastic moduli contour maps were imported into Mathematica (Wolfram) for alignment, as described in Chapter 5 (Wilusz et al. 2012). Once aligned, IF images were converted to binary masks to indicate regions of positive labeling for each individual channel using an optimal threshold value determined from a range of IF images. IF-positive masks and elastic moduli contour maps were analyzed in MATLAB to extract PCM data for each scan region. Using single channel masks, overall PCM moduli were evaluated based on the presence of type VI collagen or perlecan. Relative staining areas for dual-labeled, type VI collagen alone, and perlecan alone regions within the PCM were determined by overlaying the single channel masks. Elastic properties were evaluated for each of these IF-defined regions.

To quantitatively evaluate the spatial distribution of moduli in the chondrocyte microenvironment, the stiffness progression of PCM moduli was evaluated in radial increments of 0.5 μm from the PCM inner edge. The same analysis was performed on overlaid IF masks to determine the relative composition of the PCM within each radial increment.

6.3.6 Statistical analyses

Differences between ECM and PCM elastic moduli were evaluated using a one-way ANOVA (region; $\alpha = 0.05$) and Fisher's least significant difference (LSD) *post-hoc* test. Differences among IF-defined regions within the PCM (dual-labeled, type VI collagen alone, perlecan alone) were evaluated using a one-way ANOVA (IF-labeling; $\alpha = 0.05$) and Fisher's LSD *post-hoc* test. Stiffness progression data were evaluated using a one-way ANOVA (distance; $\alpha = 0.05$) and Fisher's LSD *post-hoc* test. All data presented as mean \pm standard error.

The effect of HS-digestion with heparinase III on ECM elastic moduli was evaluated using a Student's *t*-test ($\alpha = 0.05$). Significant differences in overall PCM elastic moduli with digestion between type VI collagen- and perlecan-based definitions were evaluated using a two-way ANOVA (PCM definition, digestion; $\alpha = 0.05$) and Fisher's LSD *post-hoc* test. Significant differences in stained PCM areas and elastic moduli among IF-labeled regions within the PCM with heparinase III digestion were evaluated using a two-way ANOVA (IF-labeling, digestion; $\alpha = 0.05$) and Fisher's LSD *post-hoc* test.

Differences between control and digested elastic moduli were evaluated separately for each 0.5 μm increment in the outward stiffness progression using a Student's *t*-test ($\alpha = 0.05$). All data presented as mean \pm standard error.

6.3 Results

6.3.1 Immunofluorescence for type VI collagen and perlecan

IF-labeling of cartilage sections revealed a consistent presence of both type VI collagen and perlecan immediately surrounding cell-sized voids. PCM labeling for type VI collagen was uniform throughout the tissue depth (Figure 6-1A). Type VI collagen was also found to be faintly dispersed in the ECM in the deep zone. Perlecan labeling was exclusively pericellular and more pronounced in the middle and deep zones of the cartilage as compared to the superficial zone (Figure 6-1B).

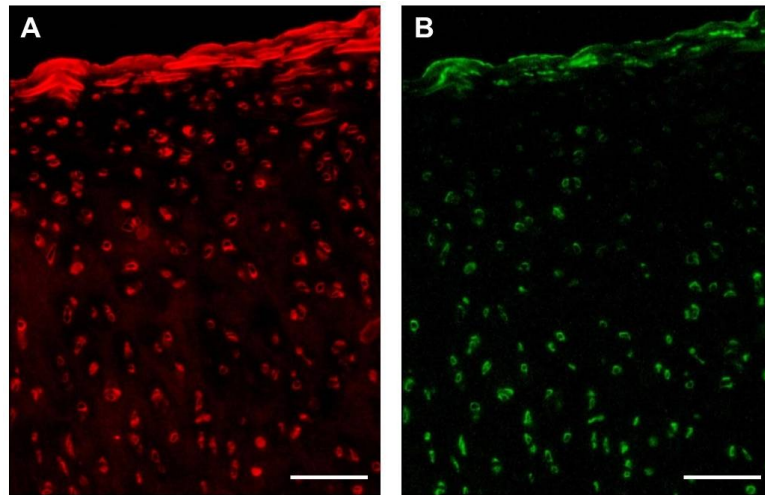


Figure 6-1: Dual immunofluorescence-labeling of type VI collagen and perlecan in porcine articular cartilage. (A) Labeling for type VI collagen was uniform throughout the cartilage thickness in pericellular regions and faintly dispersed in the ECM in deeper regions. (B) Perlecan labeling was localized to pericellular regions and more pronounced in the middle and deep zones. Scale bar = 100 μm .

6.3.2 AFM stiffness mapping of type VI collagen and perlecan dual-labeled articular cartilage PCM and ECM

Stiffness mapping revealed that type VI collagen, perlecan, and low elastic moduli localize in the pericellular space around cell-sized voids (Figure 6-2A, B, C, D). No difference in overall PCM elastic moduli was observed between type VI collagen-based (71 ± 3 kPa) and perlecan-based (68 ± 3 kPa) definitions of the PCM ($p = 0.70$; Figure 6-2E). Elastic moduli of the local ECM (93 ± 7 kPa) were significantly greater than PCM moduli using either biochemical definition ($p < 0.005$).

Type VI collagen and perlecan co-localized over $64 \pm 3\%$ of labeled PCM areas (positive for either type VI collagen or perlecan) and occupied inner regions of the PCM (Figure 6-3A, B). Regions positive for type VI collagen alone occupied $31 \pm 4\%$ of labeled PCM areas and were located in peripheral regions of the PCM. Within the PCM, elastic moduli in dual-labeled regions (68 ± 3 kPa) were significantly lower than moduli in regions positive for type VI collagen alone (81 ± 5 kPa; $p < 0.05$; Figure 6-2F). PCM regions positive for perlecan alone occupied $4 \pm 1\%$ of labeled PCM area, with only 9 of the 23 sites tested having regions consisting of sufficient area on the stiffness map for analysis. Of these perlecan alone regions, 6 spanned the width of small portions of the evaluated PCM, occupying up to 18% of the total labeled PCM area, and 3 were located on the PCM periphery. Perlecan alone regions exhibited greater elastic moduli (92 ± 7 kPa) than dual-labeled regions ($p < 0.01$). There was no difference in elastic moduli between PCM regions positive for type VI collagen alone and perlecan alone ($p = 0.19$).

Spatial mapping demonstrated that lower modulus regions were located within 1.0 μm of the PCM inner edge ($p < 0.05$) where 92 – 95% of the labeled area was dual labeled for perlecan and type VI collagen (Figure 6-3C, D).

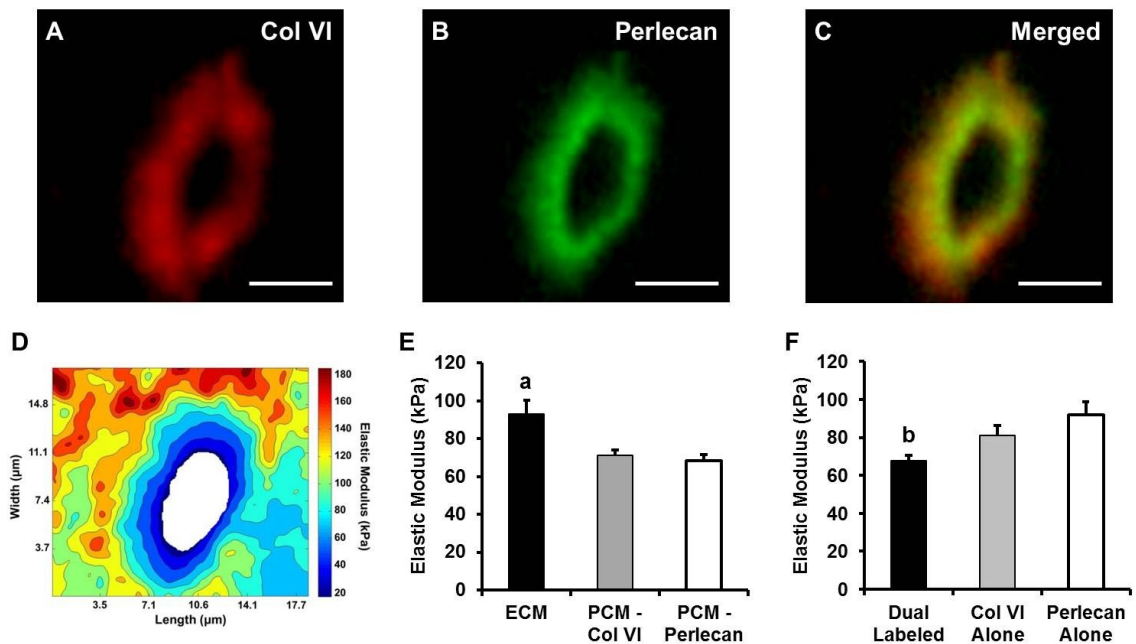


Figure 6-2: Stiffness mapping of dual immunofluorescence-labeled PCM. A representative PCM scan region in the middle/deep zone is shown. Dual IF-labeling for (A) type VI collagen and (B) perlecan demonstrated the (C) co-localization of these molecules in the pericellular space. Scale bar = 5 μm . (D) Contour map of calculated elastic moduli for the PCM scan region shown. (E) Elastic moduli of ECM (black) and PCM as defined by the presence of type VI collagen (grey) or perlecan (white). There was no difference between biochemical definitions of the PCM ($p = 0.70$). a: $p < 0.005$ for ECM moduli as compared to either PCM definition. (F) Elastic moduli of PCM regions dual-labeled for type VI collagen and perlecan (black), positive for type VI collagen alone (grey) and perlecan alone (white). b: $p < 0.05$ for dual-labeled regions as compared to single-labeled regions. Moduli presented as mean + standard error (N = 4 pigs, $n \geq 9$ regions).

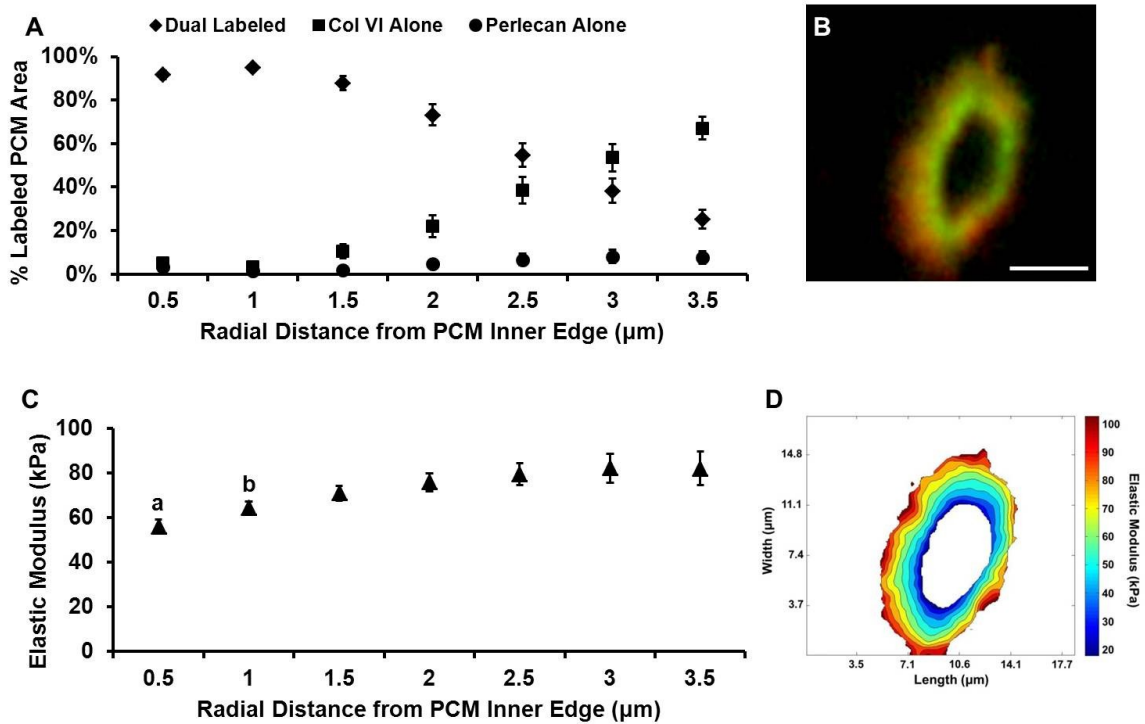


Figure 6-3: Spatial distribution of PCM biochemical composition and biomechanical properties. (A) Outward progression of PCM biochemical composition from the PCM inner edge. Within each radial increment, data represent the relative composition based on the percent of total IF-labeled area occupied by each antibody/antibody combination. (B) Representative IF-labeling demonstrating the colocalization of type VI collagen (red) and perlecan (green) within the PCM. Scale bar = 5 μm. (C) Outward stiffness progression of PCM elastic moduli from the PCM inner edge. a: $p < 0.05$ for moduli 0.5 μm from PCM outer edge as compared to distances greater than 1.5 μm. b: $p < 0.05$ for moduli 1 μm from PCM outer edge as compared to distances greater than 2.5 μm. (D) Contour map of calculated elastic moduli within the PCM for the scan region shown in (B). Data presented as mean ± standard error (N = 4 pigs, n = 23 regions).

6.3.3 Immunofluorescence for 3G10, perlecan, and type VI collagen and histological staining analyses of heparinase III-digested articular cartilage

Enzymatic digestion of HS with heparinase III was specific to PCM regions immediately surrounding cell-sized voids in cartilage sections. IF-labeling for 3G10 matched the pericellular distribution of perlecan (Figure 6-4A, B, C) and co-localized with type VI collagen (Figure 6-4D, E, F). There was no 3G10 labeling present in undigested controls (data not shown). Digestion had no effect on IF-labeling of either perlecan or type VI collagen (Figure 6-4G, H, I). Digestion with heparinase III did not induce a global loss of PGs in cartilage sections (Figure 6-5A, B).

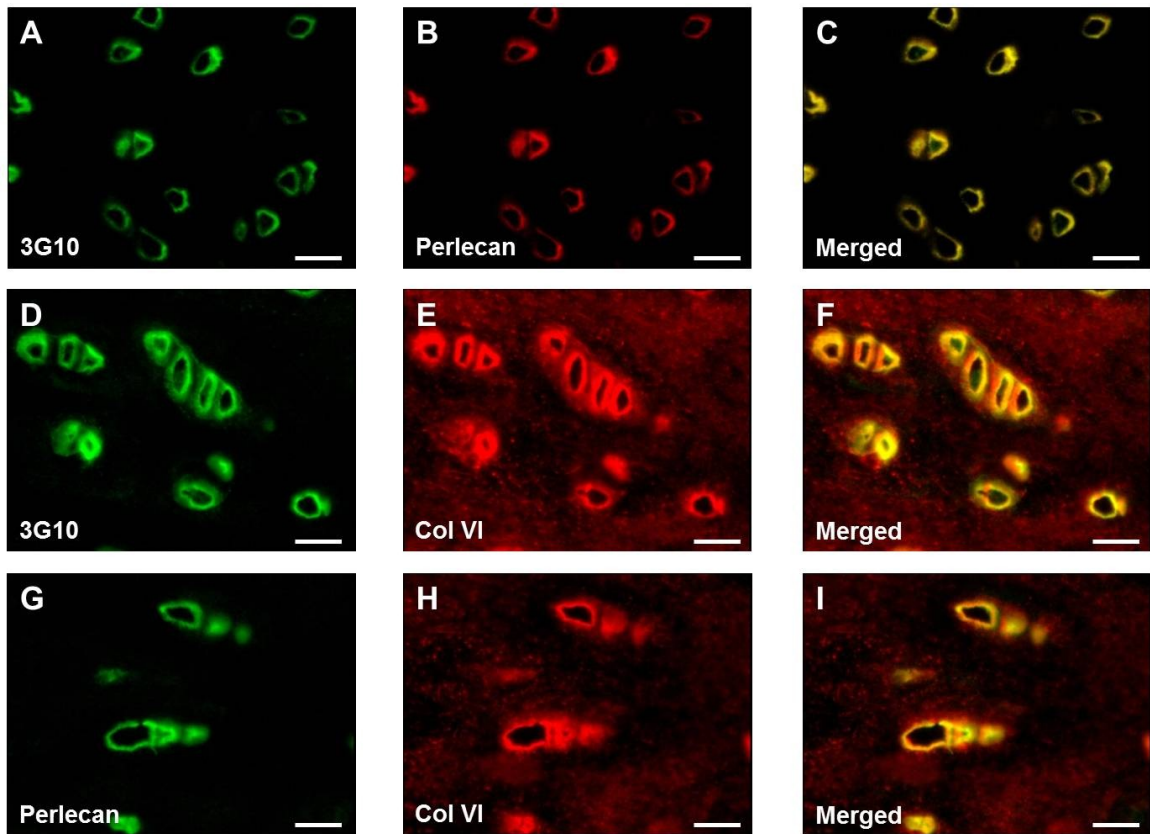


Figure 6-4: Dual immunofluorescence-labeling of heparinase III-digested porcine articular cartilage. Dual IF-labeling of (A) HS epitope 3G10 and (B) perlecan exhibited a nearly one-to-one overlay (C). (D) HS epitope 3G10 and (E) type VI collagen co-localized in the pericellular space (F). Heparinase III digestion had no effect on labeling of (G) perlecan or (H) type VI collagen and did not disrupt their co-localization in the PCM (I). Scale bar = 20 μ m.

6.3.4 Effect of heparinase III digestion on PCM and ECM mechanical properties

Digestion with heparinase III resulted in a significant increase in the overall elastic modulus of the PCM as defined by perlecan labeling (69 ± 5 kPa vs. 56 ± 3 kPa; $p < 0.05$; Figure 6-6A). There was a trend toward an increase in PCM properties as defined by the presence of type VI collagen with digestion (70 ± 4 kPa vs. 60 ± 3 kPa; $p = 0.05$). There were no differences in the relative composition of tested control and digested PCM regions, with dual-labeled, type VI collagen alone and perlecan alone regions consisting of $60 \pm 3\%$, $34 \pm 3\%$, and $5 \pm 1\%$ of labeled areas in control PCM regions as compared to $59 \pm 3\%$, $37 \pm 3\%$, and $3 \pm 1\%$ of labeled areas in digested PCM regions, respectively ($p > 0.39$). There was no significant change in ECM properties with heparinase III digestion as compared to undigested controls (103 ± 6 kPa vs. 93 ± 6 kPa; $p = 0.39$; Figure 6-5C).

Within the PCM, enzymatic removal of HS resulted in a significant increase in the elastic modulus of dual-labeled regions as compared to undigested controls (68 ± 5 kPa vs. 55 ± 2 kPa; $p < 0.05$; Figure 6-6B). There was no change in the properties of regions positive for type VI collagen alone (74 ± 4 kPa vs. 68 ± 4 kPa; $p = 0.31$). 15 of the 25 PCM regions tested in undigested controls and 13 of the 25 PCM regions tested in digested samples had perlecan alone regions consisting of sufficient area on the stiffness map for analysis. Of these perlecan alone regions, 16 spanned the width of small portions of the evaluated PCM, occupying up to 33% of the total labeled PCM area, and

13 were located on the PCM periphery. In these regions, there was a trend toward a significant increase in elastic moduli with digestion ($p = 0.09$). In heparinase III digested PCM, dual-labeled regions exhibited elastic moduli similar to those of regions occupied by type VI collagen alone ($p = 0.94$) but lower than perlecan alone areas ($p < 0.01$). In undigested controls, dual-labeled regions were significantly softer than regions positive for either type VI collagen or perlecan alone ($p < 0.05$) and there was no difference observed between type VI collagen and perlecan alone regions ($p = 0.34$).

Spatial mapping demonstrated significant increases in elastic moduli with digestion in regions within 1.0 μm of the PCM inner edge ($p < 0.05$; Figure 6-7A) where 80 – 85% of the labeled area was dual-labeled for perlecan and type VI collagen and 4 – 8% was positive for perlecan alone (Figure 6-7B).

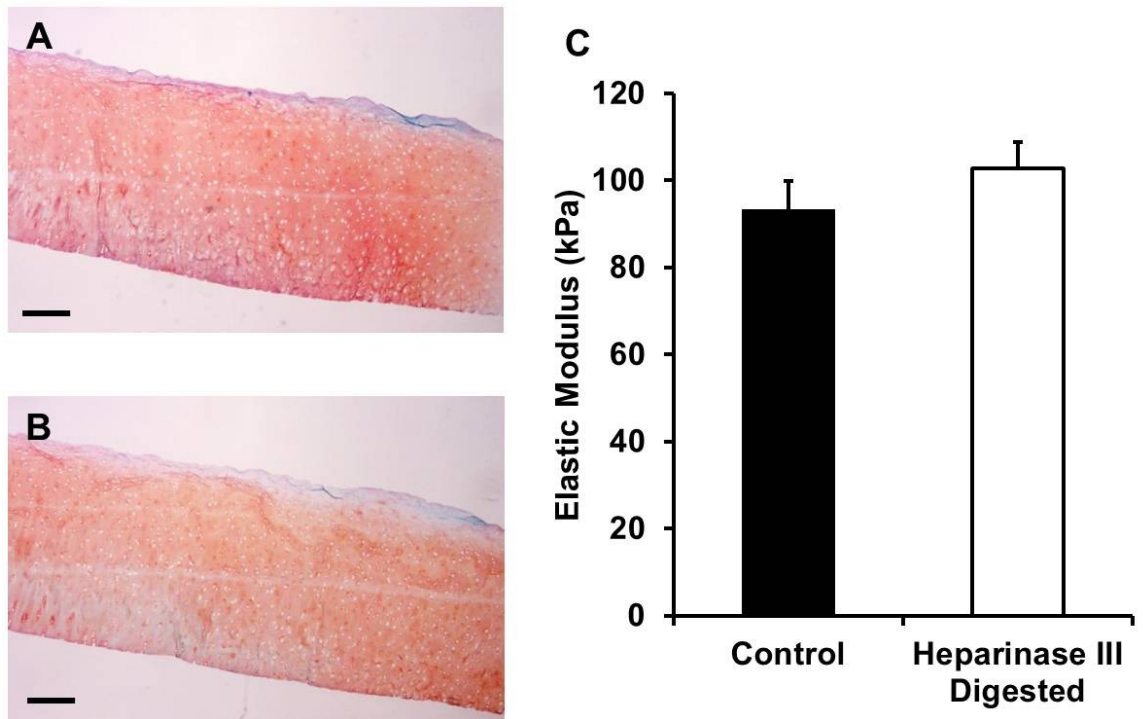


Figure 6-5: Effect of heparinase III digestion on ECM composition and micromechanical properties. (A) Histological staining with Safranin-O (red, PG) and fast green (blue, collagen) demonstrated that heparinase III digestion had a minimal effect on global PG content as compared to (B) undigested controls. Scale bar = 250 μm . (C) ECM elastic moduli in undigested control (black) and heparinase III digested (white) cartilage. Moduli were unaffected by heparinase III digestion ($p = 0.39$). Moduli presented as mean + standard error ($N = 6$ pigs, $n = 25$ regions per treatment).

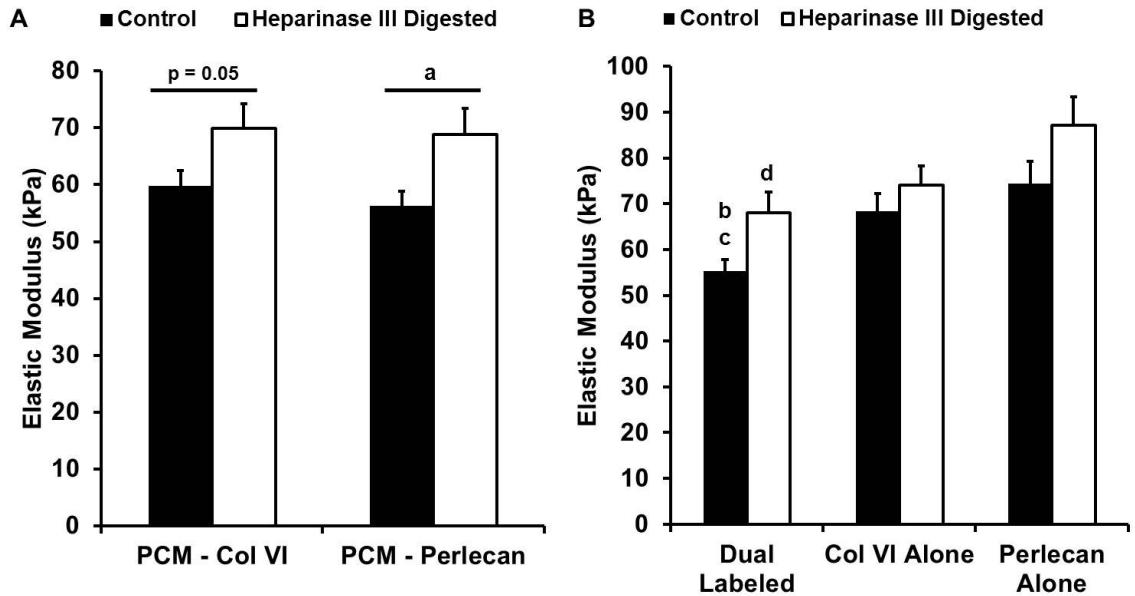


Figure 6-6: Effect of heparinase III digestion on PCM micromechanical properties. (A) PCM moduli as defined by type VI collagen and perlecan in undigested control (black) and heparinase III digested (white) samples. PCM moduli as defined by type VI collagen showed a trend toward higher moduli with heparinase III digestion ($p = 0.05$). a: $p < 0.05$ for PCM moduli as defined by perlecan in control as compared to digested samples. (B) Elastic moduli of PCM regions dual-labeled for type VI collagen and perlecan, positive for type VI collagen alone, and perlecan alone in undigested control (black) and heparinase III digested (white) samples. b: $p < 0.05$ for dual-labeled regions in controls as compared to digested samples. c: In controls, $p < 0.05$ for dual-labeled regions as compared to type VI collagen alone and perlecan alone regions. d: In digested samples, $p < 0.05$ for dual-labeled regions as compared to perlecan alone regions. Moduli presented as mean + standard error (N = 6 pigs, n \geq 13 regions per treatment).

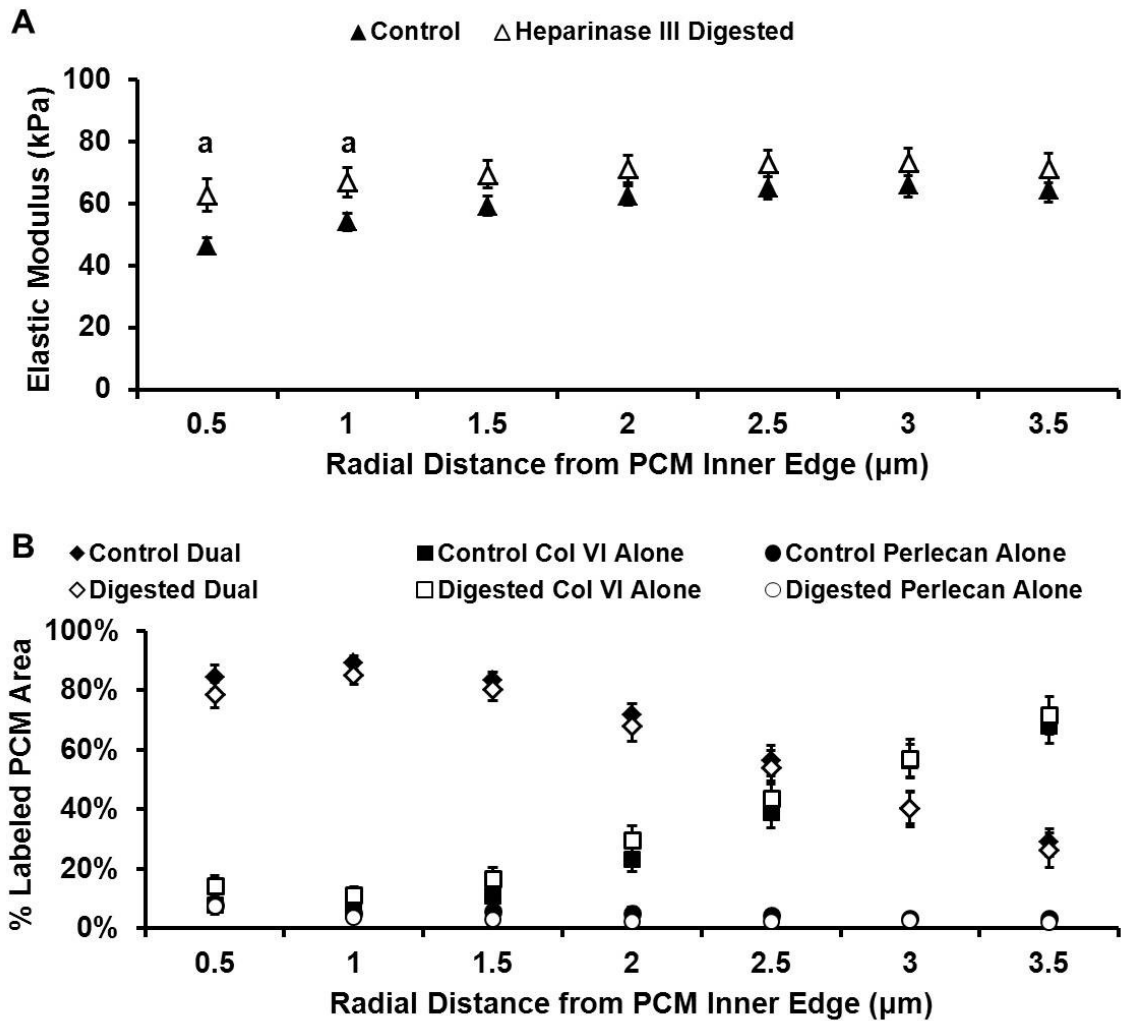


Figure 6-7: Effect of heparinase III digestion on the spatial distribution of PCM biochemical composition and biomechanical properties. (A) Outward stiffness progression of PCM elastic moduli from the PCM inner edge in undigested control (black) and heparinase III digested (white) samples. a: $p < 0.05$ for control as compared to digested moduli. (B) Outward progression of PCM biochemical composition from the PCM inner edge for undigested control (black) and heparinase III digested (white) samples. Within each radial increment, data represent the relative composition based on the percent of total IF-labeled area occupied by each antibody/antibody combination. Data presented as mean \pm standard error (N = 6 pigs, n = 25 regions per treatment).

6.4 Discussion

Our results provide new evidence for a biomechanical role for perlecan in the cartilage PCM. IF-guided AFM stiffness mapping revealed localization of perlecan, type VI collagen, and low elastic moduli to the pericellular region around cell-sized voids. While there was no difference in overall PCM mechanical properties between type VI collagen- and perlecan-based definitions of the PCM, interior regions within the PCM containing both type VI collagen and perlecan exhibited lower elastic moduli than more peripheral regions rich in type VI collagen alone. Contrary to our initial hypothesis, enzymatic removal of HS chains from perlecan with heparinase III resulted in increased elastic moduli in the PCM, specifically in the interior regions positive for both perlecan and type VI collagen. Heparinase III digestion had no effect on the micromechanical properties of the ECM.

AFM measures highly localized mechanical properties *in situ* that may be dominated by individual molecular components of the tissue. Therefore, our findings provide evidence for variations of elastic moduli within the PCM that are related to site-specific biochemical composition. PCM regions rich in perlecan and type VI collagen were located immediately adjacent to cell-sized voids and exhibited lower elastic moduli than more peripheral regions rich in type VI collagen alone. Previous work by Loparic and colleagues investigating the nanostiffness of porcine articular cartilage with AFM (Loparic et al. 2010) demonstrated that PGs *in situ* are an order of magnitude softer than

collagen fibers. The low elastic moduli observed in the PCM interior in the present work were likely due to the high concentration of HS in this region, further supported by the increase in elastic moduli in these regions following digestion of HS by heparinase III. In this regard, our results suggest heparinase III digestion could be utilized to selectively manipulate the biochemical and biomechanical properties of the PCM with minimal effect on the surrounding ECM.

The exact mechanism by which perlecan contributes to lower elastic moduli is not understood. PGs are known to have lower compressive moduli than collagen fibers, due in part to their glycosaminoglycan side chains (Loparic et al. 2010). The HS chains of perlecan may contribute to the lower elastic moduli in a manner analogous to a softer spring in series with a stiffer spring, where the effective spring constant of the system is lower than that of either component. In this respect, digestion of the HS chains exposes the underlying stiffer components of the solid matrix, thereby increasing the observed elastic moduli of these regions.

The localization of perlecan to low modulus, interior regions of the PCM provides support for a potential role for HS and perlecan in mechanotransduction in cartilage. Perlecan has been shown to regulate the bioactivity of FGFs through interaction with HS, serving as an extracellular store and mediating FGF binding to, and subsequent activation of, FGF receptor tyrosine kinases (Aviezer et al. 1994; Whitelock et al. 1996; Melrose et al. 2006; Smith et al. 2007; Chuang et al. 2010). Loading-induced

activation of extracellular regulated kinase (ERK) in cartilage (Vincent et al. 2002; Vincent et al. 2004) has been shown to depend on the presence and concentration of FGF-2 in the PCM (Vincent et al. 2007). Vincent and colleagues hypothesized that in unloaded cartilage, FGF-2 bound to HS chains of perlecan is sequestered away from the cell surface and that matrix deformation presents HS-bound FGF-2 to its receptor on the cell surface, activating downstream signaling pathways (Vincent et al. 2007). Since the cartilage PCM exhibits significantly lower compressive moduli than the ECM, it experiences significant strain amplification during mechanical loading and undergoes larger deformations than the surrounding ECM (Guilak and Mow 2000; Choi et al. 2007). Localization of perlecan to low modulus regions in the PCM interior, as observed in the current study, would facilitate HS-bound FGF signaling via this proposed mechanism. Furthermore, perlecan may transmit mechanical signals directly to the chondrocyte via core protein interactions with cell surface integrins (Hayashi et al. 1992; Brown et al. 1997; Melrose et al. 2008b).

The territorial matrix (TM) has been defined as a structural transition region between type VI collagen microfilaments in the PCM and type II collagen fibers in the ECM (Poole et al. 1984). Since there are no distinct structural boundaries among these three matrix regions, identification of the TM is difficult and often based on qualitative differences in PG content and collagen architecture (Poole et al. 1982; Poole et al. 1984; Poole et al. 1987; Hunziker et al. 1997; Poole et al. 1997). While type VI collagen is

considered the defining boundary of the PCM in articular cartilage (Poole et al. 1988), type VI collagen has been reported to be present in the TM where it is interwoven with type II collagen fibers (Soder et al. 2002). Given the exclusive localization of perlecan to the PCM observed here and in previous studies (SundarRaj et al. 1995; Melrose et al. 2005; Melrose et al. 2006; Kvist et al. 2008) and the distinct mechanical properties of regions positive for perlecan and type VI collagen in the immediate vicinity of the chondrocyte, our results suggest a defining role for perlecan as the boundary of the PCM with regions of type VI collagen alone representing the transition to the adjacent TM.

The fact that intact chondrons can be isolated from Col6a1 null mice (Alexopoulos et al. 2009) suggests that molecular components other than type VI collagen may provide alternative composition-based definitions of the PCM. In the present study, we focused on perlecan due to its exclusive presence to the PCM and documented roles in cartilage development and growth factor signaling. A number of other matrix molecules are found exclusively or at higher concentrations in the PCM as compared to the surrounding ECM, including hyaluronan (Knudson 1993; Cohen et al. 2003), biglycan (Kavanagh and Ashhurst 1999), type IX collagen (Poole et al. 1997), fibronectin (Chang et al. 1997; Martin et al. 2002), and laminin (Durr et al. 1996; Kvist et al. 2008), and are known to interact with type VI collagen (Kielty et al. 1992; Wiberg et al.

2002) and perlecan (Battaglia et al. 1992; Hopf et al. 1999; Hopf et al. 2001). These molecules also likely contribute to PCM structure and biomechanical function.

The aim of this study was to characterize the biomechanical properties of articular cartilage PCM at the microscale. When using micrometer-sized spherical indenters as presented here, there are limitations in the lateral resolution of AFM-based indentation of soft substrates (Radmacher et al. 1992; Dimitriadis et al. 2002). From Hertz contact mechanics, the contact radius of a spherical probe scales with tip radius and indentation depth. Since a force threshold (300 nN) was used for all stiffness mapping, indentation depths were not equivalent throughout a single scan region. Indentations were larger in the soft interior of the PCM and smaller in stiff peripheral PCM, TM, and ECM regions. As a result, contact radii were larger in PCM regions (~2.0 μm) as compared to ECM regions (~1.5 μm). This contact footprint would have masked the sharp transition in matrix stiffness between the PCM and ECM proposed in theoretical models (Guilak and Mow 2000; Alexopoulos et al. 2005a; Michalek and Iatridis 2007; Korhonen and Herzog 2008). In addition, contact with adjacent TM and/or ECM regions during indentation may have contributed to artificial stiffening of peripheral PCM regions. Nonetheless, PCM elastic moduli measured in this study are highly consistent with our previous studies of using AFM (Chapters 2 (Darling et al. 2010), 3 (McLeod et al. 2013), and 5 (Wilusz et al. 2012)) as well as other techniques such as micropipette

aspiration (Alexopoulos et al. 2003; Alexopoulos et al. 2005b; Guilak et al. 2005) and inverse computational methods (Kim et al. 2010).

6.5 Summary

This study provides new evidence for perlecan as a defining factor in both the biochemical and biomechanical boundaries of the PCM. The HS chains of perlecan soften the PCM in the immediate vicinity of the chondrocyte and presumably, generate an environment conducive for mechanotransduction via HS-bound growth factors or direct cell-matrix interactions. By determining site-specific differences in mechanical properties coincident with spatial variations in biochemical composition, our findings provide a more complete characterization of the chondrocyte microenvironment in articular cartilage.

7. The Mechanical Properties of the Chondrocyte Pericellular Matrix Exhibit High Resistance to Enzymatic Digestion

7.1 Introduction

In articular cartilage, the bulk extracellular matrix (ECM) and chondrocyte-associated pericellular matrix (PCM) are characterized by a high concentration of proteoglycans (PGs) and their associated glycosaminoglycan (GAG) chains. The specific functional properties of PGs are conferred by their unique combination of GAG chains and protein domain structures. In cartilage, PGs and their associated GAGs serve important structural, biochemical, and biomechanical roles (reviewed in (Iozzo 1998; Knudson and Knudson 2001; Roughley 2006)).

The most prominent PG in cartilage is aggrecan, consisting of three globular domains (G1, G2, G3), a short inter-globular domain (IGD) between the G1 and G2 domains, and an extensive GAG attachment region between the G2 and G3 domains containing over 100 GAG chains of chondroitin sulfate (CS) and keratan sulfate (KS) (Paulsson et al. 1987; Doege et al. 1991). The aggrecan G1 domain interacts with hyaluronan (HA) and link protein to form large PG aggregates (Morgelin et al. 1988). While the exact process of aggregate formation is unknown, initial assembly of smaller aggregates likely begins in the PCM, where concentrations of aggrecan monomer, HA, and link protein are high, followed by transport to the ECM for incorporation into larger aggregates and sequestration in the matrix (Sandy et al. 1989; Poole 1997; Winter et al.

1998; Bayliss et al. 2000; Dudhia 2005). In the ECM, sequestered aggregates fill the space between type II collagen fibers to generate a fiber-reinforced composite through physical entanglement and interaction with type II collagen via the aggrecan core protein (Hedlund et al. 1999) and CS chains (Obrink et al. 1975; Oegema et al. 1975; Junqueira and Montes 1983; Scott 1988). Due to its high abundance and fixed negative charge resulting from its numerous closely spaced GAG chains, aggrecan is the main contributor to the osmotic swelling behavior and low hydraulic permeability that confer the tissue's ability to support and distribute large compressive loads experienced during joint loading (Maroudas and Venn 1977; Eisenberg and Grodzinsky 1985; Lai et al. 1991; Mow et al. 1992; Mow et al. 1998; Sun et al. 2004).

Decorin and biglycan are low molecular weight, non-aggregating PGs that belong to the family of small leucine-rich repeat PGs (SLRPs). Decorin and biglycan are biochemically similar PGs; decorin is substituted with one dermatan sulfate (DS)/CS chain whereas biglycan is substituted with two DS/CS chains (Krishnan et al. 1999). Though considered minor components of cartilage, they are present in similar molar concentrations as aggrecan (Poole et al. 1996) and have been speculated to play major roles in organizing the larger structural components of the cartilage matrix (Scott 1988; Roughley 2006). Decorin is most prominent in the ECM (Archer et al. 1996; Poole et al. 1996; Kavanagh and Ashhurst 1999) where it interacts with type II collagen (Scott 1988; Hedbom and Heinegard 1989; Hedbom and Heinegard 1993; Vogel 1994). Its DS/CS

chain is thought to regulate type II collagen fibril spacing and fibril-fibril interactions (Hedbom and Heinegard 1993; Scott and Stockwell 2006). Biglycan is most prominent in the PCM (Vogel 1994; Archer et al. 1996; Kavanagh and Ashhurst 1999). *In vitro*, biglycan has been shown to strongly interact with and facilitate network assembly of type VI collagen (Wiberg et al. 2001; Wiberg et al. 2002), and mediate interactions between type VI collagen and aggrecan (Wiberg et al. 2003), suggesting a role for biglycan in PCM structural integrity and connection with the ECM.

HA is unique among GAGs in that it has a high molecular weight, is unsulfated, is synthesized at the plasma membrane and released directly into the matrix, and is not found covalently linked to a PG core protein (Ernst et al. 1995; Fraser et al. 1997; Roughley 2006). Beyond its role as the backbone of aggrecan macromolecular aggregates in the ECM, HA and its interactions with CD44 are important factors in cell-matrix interactions (Knudson 2003) and PCM matrix organization (Knudson 1993; Lee et al. 1993; Knudson et al. 1996; Maleski and Knudson 1996; Cohen et al. 2003; Rilla et al. 2008). HA interacts with type VI collagen (McDevitt et al. 1991; Kielty et al. 1992; Specks et al. 1992) and facilitates spontaneous assembly of depolymerized type VI collagen microfilaments (Kielty et al. 1992). Taken together, these results suggest that HA-type VI collagen interactions are essential for microfilament assembly and network stabilization in the PCM (Poole et al. 1985).

In healthy cartilage, matrix turnover is a slow, continuous process and maintenance of tissue structure and matrix architecture is achieved through a balance of anabolic and catabolic activities. Matrix turnover is predominantly related to PGs, due to their shorter half-lives *in situ*, 3 – 25 years for the aggrecan core protein (Maroudas et al. 1998), as compared to type II collagen, more than 100 years (Verzijl et al. 2000). Normal proteolytic processing of aggrecan occurs via cleavage within the GAG attachment domain and/or within the IGD by aggrecanases and matrix metalloproteinases (MMPs) (Lark et al. 1997; Plaas et al. 2007; Struglics and Hansson 2012). As a result, the prevalence of shortened aggrecan monomers exhibiting partial or complete loss of CS chains increases and residual G1 domains attached to HA accumulate in the ECM with age (Lark et al. 1997; Dudhia 2005).

In joint diseases characterized by cartilage degradation and inflammation, such as osteoarthritis (OA) and rheumatoid arthritis (RA), aggrecan and small PGs are the first matrix components to undergo measureable loss. Proteolytic enzymes secreted by chondrocytes, including aggrecanases and MMPs (reviewed in (Caterson et al. 2000)), and inflammatory cells, most notably the serine protease elastase (Janoff et al. 1976; Starkey et al. 1977; Barrett 1994; Momohara et al. 1997), are believed to play a prominent role in PG degradation. The loss of aggrecan has been primarily attributed to proteolytic cleavage within the IGD region where there are known, unique cleavage sites for aggrecanases (Glu³⁷³-Ala³⁷⁴) (Sandy et al. 1991), MMPs (Asn³⁴¹-Phe³⁴²) (Flannery et al.

1992), and elastase (Val³⁹⁷-Ile³⁹⁸) (Mok et al. 1992). Additional aggrecan cleavage sites are also known for all three enzyme classes within the GAG attachment domains (Mok et al. 1992; Tortorella et al. 2000; Little et al. 2002; Nagase and Kashiwagi 2003). Fragmentation of biglycan and decorin in OA and RA cartilage extracts (Witsch-Prehm et al. 1992) has been associated with aggrecanase (Melching et al. 2006; Gendron et al. 2007) and MMP (Monfort et al. 2006; Melrose et al. 2008a; Zhen et al. 2008) activity.

The objective of this study was to investigate the region-specific contributions of aggrecan, CS/DS, and HA to the micromechanical properties of the cartilage PCM and ECM. To this end, cryosections of porcine cartilage underwent specific enzymatic digestion with aggrecanase (ADAMTS-4), chondroitinase ABC (C-ABC), or bacterial hyaluronidase (HA-ase) or broad spectrum enzymatic digestion with human leukocyte elastase. Guided by immunofluorescence (IF) for type VI collagen as presented in Chapter 5 (Wilusz et al. 2012), AFM stiffness mapping was used to evaluate the elastic properties of matched PCM and ECM regions in paired control and digested cartilage sections. These methods were used to test the hypotheses that all enzymes would reduce both PCM and ECM elastic moduli and that elastase digestion would result in the greatest loss of mechanical integrity in both regions.

7.2 Materials and Methods

7.2.1 Tissue sample preparation

Full thickness articular cartilage samples were harvested from the medial condyle of 2 – 3 year old, skeletally mature, porcine knee joints exhibiting no signs of macroscopic degeneration. Cartilage samples were wrapped in phosphate-buffered saline (PBS)-soaked gauze and frozen at -20°C for intermediate storage. Samples were embedded in water-soluble embedding medium (Tissue-Tek O.C.T. Compound; Sakura Finetek USA) and sectioned perpendicular to the articular surface in 5 µm thick sections using a cryostat microtome (Leica CM1850; Leica). Cartilage slices were collected on glass slides and washed thoroughly with PBS to remove the embedding medium prior to further treatment.

7.2.2 Specific enzymatic digestion of aggrecan with ADAMTS-4

Cartilage sections were incubated in 50 µL of 0.04 mU/mL (100 nM) recombinant human ADAMTS-4 (aggrecanase-1; EC 3.4.24.82; Anaspec, Inc., San Jose, CA) in 50 mM Tris-HCl (Sigma-Aldrich) containing 150 mM sodium chloride (EM Science), 5 mM calcium chloride (EM Science), pH 7.5 at 37°C for 60 minutes. Undigested control sections from the same cartilage specimens were incubated at 37°C for 60 minutes in ADAMTS-4 enzyme buffer.

7.2.3 Specific enzymatic digestion of chondroitin/dermatan sulfate with chondroitinase ABC

Chondroitinase ABC (C-ABC) (from *Proteus vulgaris*, EC 4.2.2.4; Sigma-Aldrich) has demonstrated activity toward chondroitin-4-sulfate (C-4-S, chondroitin A), DS (chondroitin B), and chondroitin-6-sulfate (C-6-S, chondroitin C) (Yamagata et al. 1968). Cartilage sections were incubated in 50 μ L of 0.25 U/mL C-ABC solution in 50 mM Tris (Sigma-Aldrich) containing 60 mM sodium acetate (Sigma-Aldrich) and 0.02% bovine serum albumin (BSA; Invitrogen), pH 8.0 at 37°C for 30 minutes. At this higher pH, C-ABC demonstrates little activity toward HA (optimal pH 6.8) (Yamagata et al. 1968). Undigested control sections from the same cartilage specimens were incubated at 37°C for 30 minutes in C-ABC enzyme buffer.

7.2.4 Specific enzymatic digestion of hyaluronan with bacterial hyaluronidase

Hyaluronidase (HA-ase) (from *Streptomyces hyalurolyticus*; EC 4.2.2.1; Sigma-Aldrich) is specific for HA and is distinct from other hyaluronidases in that it is inactive toward unsulfated chondroitin and CS/DS (Ohya and Kaneko 1970). Cartilage sections were incubated in 50 μ L of 60 U/mL HA-ase solution in 20 mM phosphate buffer containing 77 mM sodium chloride (EM Science) and 0.01% BSA (Invitrogen), pH 6.0 at 37°C for 30 minutes. Undigested control sections from the same cartilage specimens were incubated at 37°C for 30 minutes in HA-ase enzyme buffer.

7.2.5 Broad spectrum enzymatic digestion with elastase

Cartilage sections were incubated in 50 μ L of 1 U/mL human leukocyte elastase (EC 3.4.21.37; Sigma-Aldrich) solution in 20 mM Tris (Sigma-Aldrich) containing 10 mM calcium chloride (EM Science), pH 8.0 at 37°C for 30 minutes. Undigested control sections from the same cartilage specimens were incubated at 37°C for 30 minutes in elastase enzyme buffer.

7.2.6 Histological staining

To visualize global loss of GAGs/PGs with each enzymatic digestion, histological staining was performed using Accustain Safranin-O solution (Sigma-Aldrich) and 0.02% aqueous fast green (Sigma-Aldrich). Control experiments confirmed that no significant loss of staining was observed between sections stained immediately after collection and undigested control sections incubated as described in each enzyme buffer (data not shown).

7.2.7 Immunofluorescence for type VI collagen

Following digestion, cartilage sections were labeled for type VI collagen using a modified IF protocol (Youn et al. 2006). Sections were blocked in 10% normal donkey serum (Lot #: S10011325; Fitzgerald) diluted in assay buffer (0.1% BSA (Invitrogen) in 0.1 M TBS, pH 7.3) for 20 minutes at room temperature. Samples were incubated with primary antibody for type VI collagen (anti-collagen type VI raised in rabbit, 70R-CR009X; Fitzgerald) at a 1:300 dilution in 10% donkey serum for 20 minutes at room

temperature. After two TBS washes of 5 minutes each, samples were incubated with secondary antibody (FITC-conjugated donkey anti-rabbit IgG, 43R-ID061FT; Fitzgerald) at a 1:200 dilution in 10% donkey serum for 20 minutes in the dark at room temperature. Sections were rinsed twice in TBS for 5 minutes each and remained in TBS at room temperature during AFM testing. No significant alteration in type VI collagen labeling was observed with any enzyme treatment (Figures 7-2, 3, 4, 5).

7.2.8 Mechanical characterization via AFM stiffness mapping

Simultaneous force measurements and fluorescence imaging were performed using an AFM system (MFP-3DBio; Asylum Research) integrated with an inverted fluorescence microscope (AxioObserver A1; Zeiss) as outlined in Chapter 5 (Wilusz et al. 2012). For microscale indentation, borosilicate glass spheres (5 μm diameter) were attached to tip-less AFM cantilevers ($k = 4.5 \text{ N/m}$; Novascan). Indentations were applied with a force trigger of 300 nN and curves were sampled at 7.5 kHz. For evaluation of PCM elastic properties, 1600 indentations (15 $\mu\text{m/s}$ indentation velocity) were sequentially applied over a 20 $\mu\text{m} \times 20 \mu\text{m}$ region of interest defined by microscopic examination with phase contrast imaging and positive IF-labeling for type VI collagen around cell-sized voids. Elastic properties of the adjacent ECM were evaluated using a similar approach over 20 $\mu\text{m} \times 20 \mu\text{m}$ visually devoid of PCM and type VI collagen (16 indentations per region, 15 $\mu\text{m/s}$ indentation velocity). For all samples, AFM testing was completed within 4 hours of initial sectioning.

PCM and ECM micromechanical properties were evaluated in paired PCM/ECM scan regions in the middle/deep zone (200 – 400 μm from the articular surface) of cartilage sections digested with ADAMTS-4 (N = 3 pigs, n = 9 total regions per treatment), C-ABC (N = 6 pigs, n = 24 total regions per treatment), HA-ase (N = 6 pigs, n = 24 total regions per treatment), or elastase (N = 3 pigs, n = 12 total regions per treatment).

7.2.9 Data analysis

Raw data for z-piezo movement and cantilever deflection were collected and analyzed using a custom Matlab script (The Mathworks). Elastic moduli, E , were determined by fitting a modified Hertz model to force-indentation curves as described previously (Darling et al. 2006; Guo and Akhremitchev 2006). For articular cartilage, the local Poisson's ratio, ν , was assumed to be 0.04 for both the ECM (Mow et al. 1980; Chen et al. 2001; Choi et al. 2007) and PCM (Alexopoulos et al. 2005b) in control and digested samples. Hertzian contact mechanics provided excellent fits to the experimental data for all force-indentation curves ($R^2 > 0.90$). Two dimensional contour maps were generated of the spatial distribution of calculated elastic moduli in each region. For clarity of comparisons, contour maps presented for each enzyme treatment are plotted on the same color scales.

The cartilage PCM was defined based on positive IF-labeling for type VI collagen around cell-sized voids and data were included for all indentations that fell within

labeled regions as described in Chapter 5 (Wilusz et al. 2012). To quantitatively evaluate the spatial distribution of moduli in the chondrocyte microenvironment, the stiffness progression of elastic moduli from the PCM outer edge to the ECM was evaluated in radial increments of 0.5 μm (Appendix D).

7.2.10 Statistical analysis

For each enzyme treatment, the effect of digestion on ECM and PCM elastic moduli was evaluated using a two-way ANOVA (region, digestion; $\alpha = 0.05$) and Fisher's least significant difference (LSD) *post-hoc* test. When required, data were log-transformed for normality. All data presented as mean \pm standard error.

7.3 Results

7.3.1 Histological staining of porcine articular cartilage following enzymatic digestion

Histological staining of porcine articular cartilage confirmed a loss of GAG/PG staining with all enzyme treatments (Figure 7-1). In the ECM, ADAMTS-4 digestion resulted in a more moderate loss of staining as compared to the complete loss observed following digestion with C-ABC, HA-ase, or elastase. In the PCM, GAG/PG staining remained in the chondrocyte microenvironment throughout the tissue depth following ADAMTS-4 and HA-ase digestion. In contrast, C-ABC and elastase digestion resulted in a complete loss of PCM GAG/PG staining.

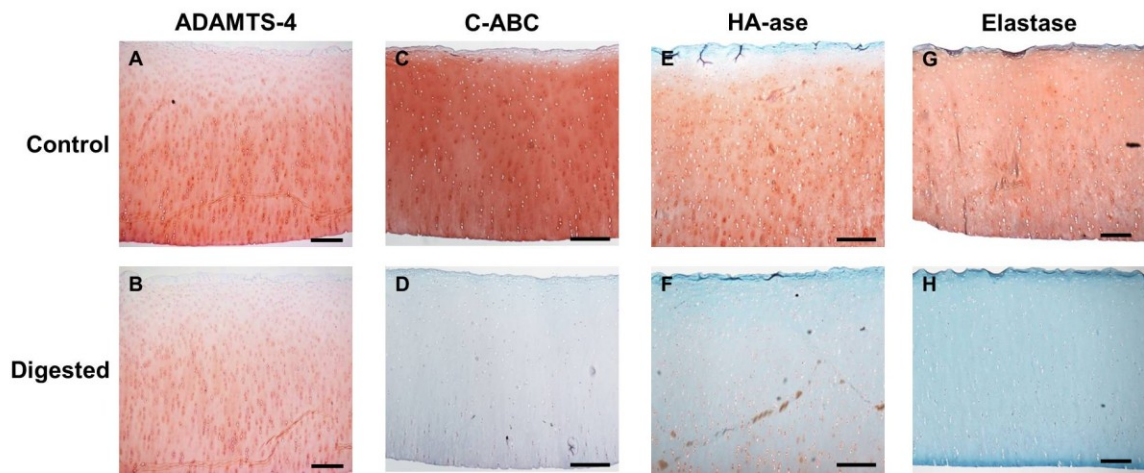


Figure 7-1: Histological staining of porcine articular cartilage following enzymatic digestion. Safranin-O (red, GAG/PG) and fast green (blue, collagen) staining of cartilage sections from paired undigested control (A, C, E, G) and digested (B, D, F, H) cartilage sections for ADAMTS-4, C-ABC, HA-ase, and elastase digestion. Loss of GAG/PG staining was observed with all digestions. Scale bar = 250 μ m.

7.3.2 Effect of ADAMTS-4 digestion on PCM and ECM micromechanical properties

In ADAMTS-4 samples, no difference was observed between PCM elastic moduli in undigested controls (44 ± 3 kPa) and digested samples (38 ± 3 kPa; $p = 0.30$; Figure 7-2). In contrast, ECM elastic moduli (77 ± 8 kPa) were reduced by 30% following ADAMTS-4 digestion (54 ± 7 kPa; $p < 0.01$). ECM moduli were significantly greater than PCM moduli in both control and digested samples ($p < 0.05$).

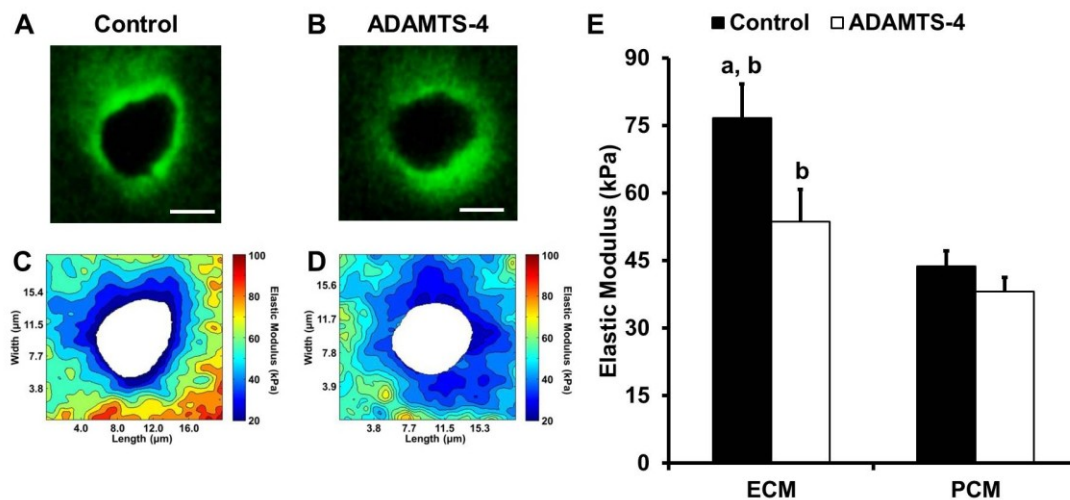


Figure 7-2: Stiffness mapping of ADAMTS-4 digested porcine articular cartilage. Representative PCM scan regions are shown for control and ADAMTS-4 digested sections. (A, B) IF-labeling for type VI collagen illustrated the distribution of type VI collagen around cell-sized voids. Scale bar = 5 μm . (C, D) Contour maps of calculated elastic moduli of the PCM scan regions shown. To highlight differences with digestion, contour maps are plotted on the same color scale. (E) Elastic moduli of ECM and PCM regions measured in undigested control (black) and ADMATS-4 digested (white) cartilage sections. a: $p < 0.01$ for control ECM moduli as compared to ADAMTS-4 digested ECM moduli. b: $p < 0.05$ for ECM moduli as compared to respective PCM moduli. PCM moduli were unaffected by ADAMTS-4 digestion ($p = 0.30$). Moduli presented as mean + standard error (N = 3 pigs, n = 9 regions per treatment).

7.3.3 Effect of chondroitinase ABC digestion on PCM and ECM micromechanical properties

In C-ABC samples, no difference was observed between PCM elastic moduli in undigested controls (58 ± 3 kPa) and digested samples (54 ± 4 kPa; $p = 0.68$; Figure 7-3). In contrast, ECM elastic moduli (95 ± 9 kPa) were reduced by 37% following C-ABC digestion (60 ± 7 kPa $p < 0.0005$). ECM elastic moduli were significantly greater than PCM moduli in undigested controls only ($p < 0.0001$).

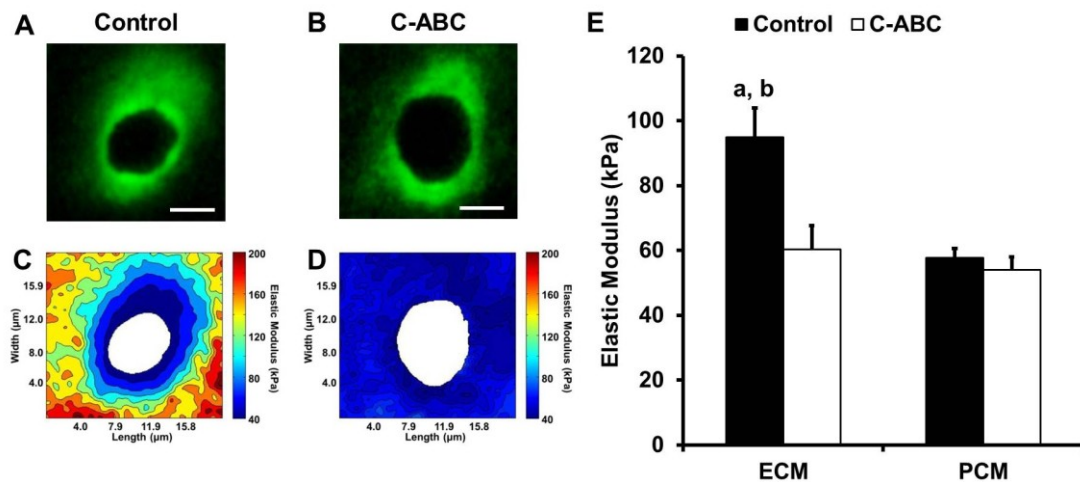


Figure 7-3: Stiffness mapping of chondroitinase ABC digested porcine articular cartilage. Representative PCM scan regions are shown for control and C-ABC digested sections. (A, B) IF-labeling for type VI collagen illustrated the distribution of type VI collagen around cell-sized voids. Scale bar = 5 μ m. (C, D) Contour maps of calculated elastic moduli of the PCM scan regions shown. To highlight differences with digestion, contour maps are plotted on the same color scale. (E) Elastic moduli of ECM and PCM regions measured in undigested control (black) and C-ABC digested (white) cartilage sections. a: $p < 0.0005$ for control ECM moduli as compared to C-ABC digested ECM moduli. b: $p < 0.0001$ for control ECM moduli as compared to control PCM moduli. PCM moduli were unaffected by C-ABC digestion ($p = 0.68$). Moduli presented as mean + standard error (N = 6 pigs, n = 24 regions per treatment).

7.3.4 Effect of hyaluronidase digestion on PCM and ECM micromechanical properties

In HA-ase samples, no difference in PCM elastic moduli was observed between undigested controls (52 ± 3 kPa) and digested samples (46 ± 2 kPa; $p = 0.43$; Figure 7-4). ECM elastic moduli (107 ± 9 kPa) were reduced by 32% following HA-ase digestion (73 ± 6 kPa; $p < 0.00005$). In contrast to C-ABC digestion, ECM elastic moduli were significantly greater than PCM moduli in both control and HA-ase digested samples ($p < 0.005$).

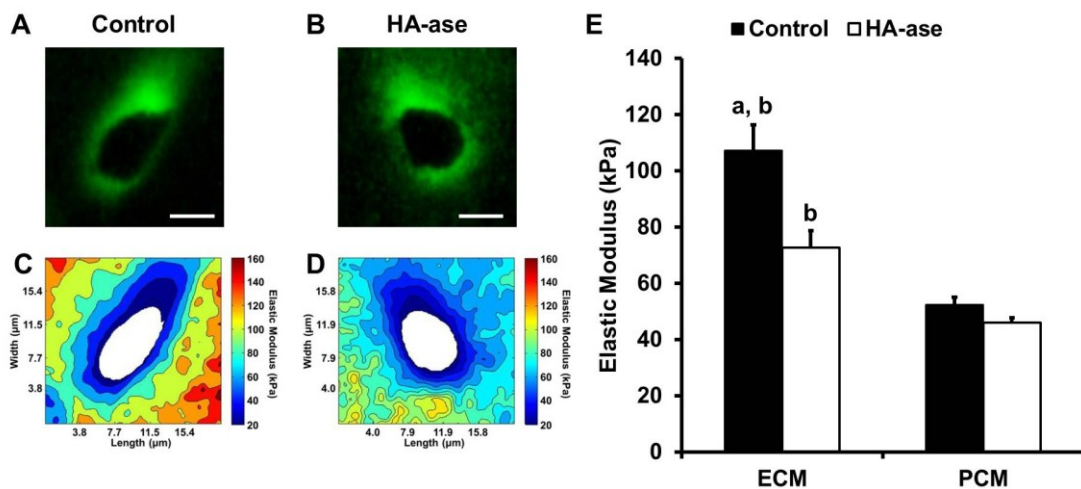


Figure 7-4: Stiffness mapping of hyaluronidase digested porcine articular cartilage. Representative PCM scan regions are shown for control and HA-ase digested sections. (A, B) IF-labeling for type VI collagen illustrated the distribution of type VI collagen around cell-sized voids. Scale bar = 5 μm . (C, D) Contour maps of calculated elastic moduli of the PCM scan regions shown. To highlight differences with digestion, contour maps are plotted on the same color scale. (E) Elastic moduli of ECM and PCM regions measured in undigested control (black) and HA-ase digested (white) cartilage sections. a: $p < 0.00005$ for control ECM moduli as compared to HA-ase digested ECM moduli. b: $p < 0.005$ for ECM moduli as compared respective PCM moduli. PCM moduli were unaffected by HA-ase digestion ($p = 0.43$). Moduli presented as mean + standard error (N = 6 pigs, n = 24 regions per treatment).

7.3.5 Effect of elastase digestion on PCM and ECM micromechanical properties

In elastase samples, PCM elastic moduli were reduced by 24% following digestion (39 ± 3 kPa) as compared to undigested controls (51 ± 3 kPa; $p < 0.05$; Figure 7-5). Similar results were observed in the ECM where elastase digestion resulted in a 57% reduction in elastic moduli (43 ± 3 kPa) as compared to controls (99 ± 13 kPa; $p < 0.000001$). ECM moduli were significantly greater than PCM moduli only in undigested controls ($p < 0.00005$).

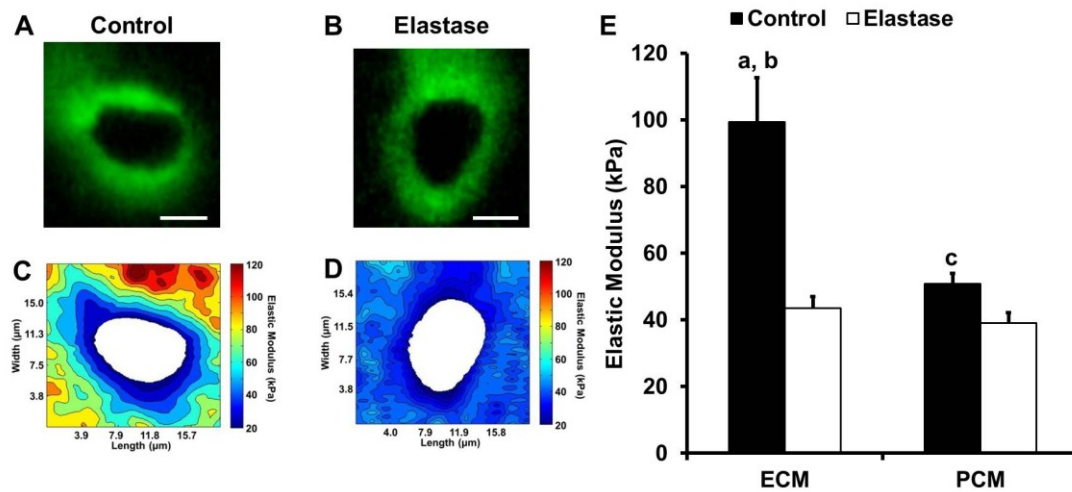


Figure 7-5: Stiffness mapping of elastase digested porcine articular cartilage. Representative PCM scan regions are shown for control and elastase digested sections. (A, B) IF-labeling for type VI collagen illustrated the distribution of type VI collagen around cell-sized voids. Scale bar = 5 μ m. (C, D) Contour maps of calculated elastic moduli of the PCM scan regions shown. To highlight differences with digestion, contour maps are plotted on the same color scale. (E) Elastic moduli of ECM and PCM regions measured in undigested control (black) and elastase digested (white) cartilage sections. a: $p < 0.000001$ for control ECM moduli as compared to elastase digested ECM moduli. b: $p < 0.00005$ for control ECM moduli as compared to control PCM moduli. c: $p < 0.05$ for control PCM moduli as compared to elastase digested PCM moduli. Moduli presented as mean + standard error (N = 3 pigs, n = 12 regions per treatment).

7.4 Discussion

Contrary to our initial hypothesis, our results demonstrate high resistance of the cartilage PCM to enzymatic degradation of aggrecan, CS/DS, and HA. Guided by IF-labeling of type VI collagen to mark the boundaries of the PCM, AFM stiffness mapping revealed no change in PCM elastic moduli following digestion with ADAMTS-4, C-ABC, or HA-ase despite significant reductions in ECM moduli. On the other hand, significant decreases in both PCM and ECM moduli were observed following broad spectrum digestion with leukocyte elastase.

Our results suggest that the micromechanical properties of the PCM exhibit high resistance to enzymatic degradation of aggrecan, CS/DS, and HA. The lack of alteration in PCM properties was not due to global inactivity of the enzyme preparations, as demonstrated by the concurrent decrease in ECM moduli and loss of Safranin-O staining in digested cartilage sections. In support of our findings, Lark and colleagues demonstrated a lack of aggrecanase-generated aggrecan G1 fragments in the PCM and territorial matrix regions in normal articular cartilage from central, weight-bearing regions of the femoral condyle despite abundant epitope staining in the ECM (Lark et al. 1997). Furthermore, Wiberg and colleagues demonstrated that while PG forms of biglycan facilitate assembly of type VI collagen networks *in vitro*, C-ABC digestion fails to disrupt networks formed in the presence of intact biglycan (Wiberg et al. 2002). If a similar mechanism governs PCM assembly *in situ*, removal of the CS/DS chains of

biglycan would have no effect on the structural integrity of the type VI collagen network and in turn, would not alter PCM mechanical integrity. With regard to HA, in agreement with our results, Poole and colleagues demonstrated no discernible change in PCM PG content or morphology following up to 10 hours of digestion with ovine testicular hyaluronidase (Poole et al. 1985). Overall, our study suggests that aggrecan, CS/DS, and HA have distinct mechanical roles in the PCM as compared to the ECM.

In agreement with previous studies that demonstrate a loss of cartilage macroscale properties following GAG depletion with C-ABC (Zhu et al. 1993; Lyyra et al. 1999; Korhonen et al. 2003; Laasanen et al. 2003) and various hyaluronidases (Broom and Poole 1983; Zhu et al. 1993), porcine cartilage in the current study exhibited a 30% - 37% reduction in ECM microscale elastic moduli following digestion with ADAMTS-4, C-ABC, and HA-ase. Since a recent study showed no effect of specific digestion of DS on cartilage GAG content or macroscale indentation properties (Hall et al. 2009), the observed effects of C-ABC digestion in the current study are likely dominated by the loss of CS chains from aggrecan rather than DS chains from decorin. Interestingly, all three enzymes exhibited similar effects on ECM mechanical properties despite their different mechanisms of aggrecan disruption. ADAMTS-4 cleavage of the aggrecan core protein has been mapped to six sites (Sandy et al. 1991; Tortorella et al. 2000; Nagase and Kashiwagi 2003), though the enzyme most efficiently cleaves within the CS GAG attachment domain near the C-terminal end of the core protein (Tortorella et al. 2000). C-

ABC acts directly on the CS GAG chains, reducing their length through cleavage of the bonds between adjacent disaccharide units (Ernst et al. 1995), leaving the PG core protein intact. HA-ase digestion disrupts aggrecan macromolecular aggregates via cleavage of the HA backbone releasing aggrecan monomers, link protein, and HA fragments from the tissue in the absence of aggrecan proteolysis (Durigova et al. 2011). Since interstitial fluid load support is minimal during AFM microindentation, approximately 10% based on the Peclet number (Bonnievie et al. 2012), the mechanical consequences of aggrecan disruption are not likely the result of biphasic and/or triphasic effects associated with the loss GAG-associated fixed charge density. Rather, our results suggest that disruption of aggrecan, regardless of the mechanism, significantly decreases the intrinsic properties of the solid matrix.

The loss of PCM and ECM mechanical integrity following digestion with leukocyte elastase provides additional support for elastase as an important contributor to cartilage degeneration. Elevated levels of elastase have been measured in synovial fluid from patients with RA (Momohara et al. 1997; Ishiguro et al. 2001; Elsaid et al. 2003), OA (Momohara et al. 1997; Elsaid et al. 2003), and joint injury (Elsaid et al. 2003; Elsaid et al. 2008). In addition to binding to the articular surface (Janoff et al. 1976; Kawabata et al. 1996), elastase is capable of diffusing through the cartilage matrix (Janoff et al. 1976) and binding to chondrocytes (Menninger et al. 1981; Bartholomew and Lowther 1987), providing a means and potential mechanism for enzyme localization to

the PCM. Elastase-based degradation of the PCM is likely driven by disruption of the type VI collagen network either through direct cleavage of type VI collagen microfilaments (Kielty et al. 1993) or disruption of biglycan-mediated interactions (Wiberg et al. 2001; Wiberg et al. 2002; Wiberg et al. 2003) through cleavage of the core protein (Owen and Campbell 1999). Beyond type VI collagen and biglycan, elastase is capable of degrading a wide range of substrates, including aggrecan (Mok et al. 1992), link protein (Mok et al. 1992), small PG core proteins (Owen and Campbell 1999), type IX and XI collagen (Gadher et al. 1988), and type II collagen cross-links (Starkey et al. 1977; Gadher et al. 1988; Barrett 1994), but not triple-helical type II collagen (Starkey et al. 1977; Gadher et al. 1988). This broad range of substrates likely contributed to the larger reduction in ECM moduli observed following elastase digestion (57%) as compared to ADAMTS-4 (-30%), C-ABC (-37%), or HA-ase (-32%). The observed 57% reduction in ECM microscale moduli is comparable to previous studies at the macro- (Menninger et al. 1981; Bader and Kempson 1994) and microscales (Stolz et al. 2004). Overall, our results suggest that treatment strategies targeting leukocyte elastase activity could be effective in reducing inflammation-mediated cartilage degeneration.

Digestion protocols used in this study were optimized on cryosections of porcine cartilage to achieve measureable changes in ECM biomechanical properties and a clear loss of Safranin-O staining, which has been shown previously to exhibit a linear relationship with GAG content as measured by DMMB for articular cartilage (Martin et

al. 1999; LeRoux et al. 2000; Flahiff et al. 2002). In our digestion protocols, incubation for 30 minutes to one hour was sufficient for significant and in some cases complete loss of Safranin-O staining in cartilage sections. The loss of GAG/PG staining was more moderate in ADAMTS-4 digested samples as compared to the other digestions.

ADAMTS-4 cleaves faster within the CS GAG attachment domains than within the IGD, with detectable CS domain epitopes present after as little as 5 minutes of digestion as compared to IGD epitopes which are detectable after 30 to 60 minutes (Tortorella et al. 2000). These site-to-site differences in efficiency likely contributed to the moderate loss of staining observed in the current work as aggrecan monomers may have lost only a fraction of their CS chains as opposed to their entire GAG attachment domain.

A number of proteolytic enzymes have been implicated in cartilage turnover and degeneration. In the present study, we focused on ADAMTS-4, C-ABC, *Streptomyces* HA-ase, and leukocyte elastase because of their prevalence in previously published work characterizing the macroscale mechanical properties of PG/GAG depleted cartilage and for the known roles of ADAMTS-4 and elastase in joint disease. ADAMTS-5 (aggrecanase-2) is another aggrecanase that has been implicated in cartilage degeneration (Song et al. 2007; Verma and Dalal 2011), has aggrecanase activity 1000-fold greater than ADAMTS-4 (Gendron et al. 2007), and has been shown to have a dominant role in aggrecan degradation in mice (Glasson et al. 2005). ADAMTS-5 is constitutively expressed by chondrocytes (Bau et al. 2002) and co-localizes with HA in

the PCM in normal and OA cartilage (Plaas et al. 2007). MMPs have a well-characterized role in cartilage degeneration and are known to cleave aggrecan (Flannery et al. 1992; Little et al. 2002) and small PGs (Monfort et al. 2006; Zhen et al. 2008) in addition to type II collagen (reviewed in (Bramono et al. 2004)). Other proteases associated with inflammation, including high temperature requirement A1 (HtrA1) and cathepsin B and L, are elevated in synovial fluid of patients with RA, OA, and following joint injury (Lang et al. 2000; Solau-Gervais et al. 2007; Polur et al. 2010). These enzymes provide interesting targets for future studies to ascertain which, if any, alter the mechanical integrity of the PCM.

7.5 Summary

This study provides new evidence for high resistance of PCM micromechanical properties to specific degradation of aggrecan and aggrecan-associated GAGs but vulnerability to leukocyte elastase digestion. This resistance may be an important intrinsic property of the chondrocyte microenvironment, allowing for enzyme transport from the chondrocyte to the ECM during normal matrix turnover without mechanical disruption of the PCM and suggesting that aggrecan and aggrecan-associated GAGs have distinct structural and mechanical roles in the PCM as compared to the ECM. In joint disease, our results suggest that the PCM is susceptible to proteolytic degradation by inflammatory cell-derived enzymes, like leukocyte elastase, that have wide substrate specificity. These inflammatory enzymes may be associated with degradative changes

observed in the chondrocyte micromechanical environment in OA (Chapter 4; (Alexopoulos et al. 2003; Alexopoulos et al. 2005b)).

8. Summary and Conclusions

This work developed and applied new techniques for evaluation of the mechanical properties of the extracellular (ECM) and pericellular matrices (PCM) of articular cartilage *in situ* and, by extension, correlation of site-specific mechanical properties with local biochemical composition. All techniques were applications of atomic force microscopy (AFM), taking advantage of its capabilities as a high resolution microindentation device and its ability to be directly integrated with traditional optical microscopy. Our first research goal, to evaluate the biomechanical properties of the cartilage PCM and ECM *in situ*, was accomplished through AFM-based stiffness mapping of articular cartilage from multiple species, in multiple loading directions, and in healthy and degenerative tissue. Our second research goal, to correlate site-specific mechanical properties with local biochemical composition, was accomplished by combining AFM stiffness mapping with immunofluorescence (IF) for type VI collagen, dual IF for type VI collagen and perlecan, and selective enzymatic digestion of proteoglycans (PGs) and glycosaminoglycans (GAGs).

In Chapter 2, we presented experimental validation of an AFM-based stiffness mapping technique and demonstrate its ability accurately obtain site-specific mechanical properties of soft substrates, capture the spatial arrangement of different materials based on their elastic moduli, and yield elastic moduli comparable to other micro- and macroscale techniques. Application of AFM stiffness mapping to cryosections of

articular cartilage from human, porcine, and murine knee joints demonstrated that PCM elastic moduli were significantly lower than local ECM elastic moduli in all species. This initial study demonstrates that AFM-based measurements are a viable means for direct, detailed investigation of the chondrocyte microenvironment *in situ*.

In Chapter 3, we provided new evidence for mechanical inhomogeneity and anisotropy at the microscale in articular cartilage by performing AFM stiffness mapping on cryosections of porcine articular cartilage generated in three mutually-perpendicular directions relative to the split-line orientation. PCM elastic moduli exhibited zonal uniformity and mechanical isotropy despite distinct, depth-dependent anisotropy in the ECM in the superficial and deep zones along the direction of local type II collagen fiber alignment. Unexpectedly, ECM microscale moduli decreased with depth in all three tested directions. Overall, our results provide further support for local collagen fiber orientation and matrix composition as defining factors in cartilage mechanical behavior.

In Chapter 4, we supported the hypothesis that significant degradative changes occur in articular cartilage at the microscale with the onset of osteoarthritis (OA). AFM stiffness mapping of human articular cartilage from the medial condyle of joints exhibiting early signs of OA revealed radial expansion of the biomechanical footprint of the PCM in addition to a loss of PCM and ECM mechanical integrity as compared to macroscopically normal joints. No significant changes were observed in either ECM or PCM mechanical properties in lateral condyle cartilage from the same joints. Our studies

provide a direct measure of and new insights into PCM degeneration within the context of local ECM degeneration in OA.

In Chapter 5, we developed a novel IF-guided AFM stiffness mapping technique for the direct correlation of type VI collagen localization and PCM biomechanical properties *in situ*. Control experiments confirmed that IF-labeling of cryosections of porcine articular cartilage did not alter the microscale elastic properties of the PCM or ECM. PCM elastic moduli correlated with the presence of type VI collagen. Matrix regions lacking type VI collagen immediately adjacent to the PCM exhibited higher elastic moduli than regions positive for type VI collagen, suggesting that the territorial matrix (TM) serves as a mechanical as well as structural transition region between the PCM and ECM. PCM properties were similar throughout the tissue depth. Our findings provide further support for type VI collagen as a defining factor of the chondrocyte PCM and an important contributor to its biomechanical properties.

In Chapter 6, we extended the applicability of our IF-guided AFM stiffness mapping technique by using dual IF to correlate site-specific differences in mechanical properties with spatial variations in composition within the PCM. Dual IF-labeling for type VI collagen and the heparan sulfate (HS) PG perlecan in cryosections of porcine articular cartilage demonstrated co-localization of these components to the PCM. While there was no difference in overall PCM moduli between type VI collagen- and perlecan-based definitions of the PCM, within the PCM, interior regions rich in both type VI

collagen and perlecan exhibited lower elastic moduli than more peripheral regions containing type VI collagen alone. Enzymatic removal of HS chains from perlecan with heparinase III resulted in increased elastic moduli in the PCM, specifically in interior regions positive for both perlecan and type VI collagen. As expected, heparinase III digestion had no effect on ECM elastic moduli. Our study supports a new role for perlecan as a defining factor in both the biochemical and biomechanical boundaries of the PCM and suggests that the HS chains generate an environment conducive for mechanotransduction by softening the PCM in the immediate vicinity of the chondrocyte.

In Chapter 7, we found that the micromechanical properties of the PCM exhibit high resistance to specific enzymatic degradation of aggrecan and aggrecan-associated GAGs but are vulnerable to degradation by leukocyte elastase. Unexpectedly, PCM elastic moduli were not altered following enzymatic digestion of cryosections of porcine articular cartilage with aggrecanase (ADAMTS-4), chondroitinase ABC (C-ABC), and bacterial hyaluronidase (HA-ase) despite significant decreases in ECM moduli with each enzyme. On the other hand, both PCM and ECM moduli were significantly decreased following enzymatic digestion with leukocyte elastase, presumably due to its wide substrate specificity. Overall, our findings suggest that resistance to enzymatic degradation is an intrinsic property of the chondrocyte PCM that would allow enzyme

transport from the PCM to the ECM during normal matrix turnover without disruption of the PCM and a role for elastase in cartilage degeneration.

Overall, our work demonstrates that the PCM is much more complex than the simple, uniform region with a sharp discontinuity in properties at its interface with the ECM presented in many theoretical models. Rather, the PCM exhibits spatial-variations in mechanical properties tied to local biochemical composition and, via the TM, exhibits a smooth mechanical transition to the local ECM. Unlike the depth-dependent moduli and anisotropy of the local ECM, PCM moduli demonstrate zonal uniformity and mechanical isotropy. This detailed zone-by-zone characterization of the cell microenvironment can be applied in computational modeling of cell-PCM-ECM interactions (Guilak and Mow 2000; Alexopoulos et al. 2005a; Korhonen and Herzog 2008; Julkunen et al. 2009) to further our understanding of the specific mechanical stresses experienced by the chondrocyte under normal loading conditions and advance our knowledge of mechanotransduction mechanisms in articular cartilage. Furthermore, this microscale approach can be readily adapted for mechanical assessment of neo-matrix deposition and evaluation of PCM and ECM development and maturation over time in tissue-engineered cartilage constructs (Fraser et al. 2006; Diekman et al. 2012).

In addition, our studies provide new insights into cartilage matrix turnover in healthy and diseased joints. Our novel finding of PCM-specific resistance to aggrecan-targeted digestion suggests that mechanical integrity of the PCM is maintained during

normal matrix turnover despite constitutive production of aggrecanases by chondrocytes. This surprising result provides many avenues for future work investigating the ability of specific PCM components to modulate local enzyme activity (Nakada and Wolfe 1961; Mio and Stern 2002) and the role of aggrecan in structural stability of the PCM. In OA cartilage, the PCM and ECM exhibit significant alterations in their microscale mechanical properties. Our demonstration of PCM and ECM susceptibility to leukocyte elastase digestion suggests treatment strategies targeting the activity of inflammatory cell-derived proteases could be effective in reducing cartilage degeneration in rheumatoid arthritis (RA), OA, and following joint injury (Momohara et al. 1997; Ishiguro et al. 2001; Elsaid et al. 2003). AFM stiffness mapping in combination with IF for specific enzymes and type II collagen or aggrecan epitopes would provide interesting insights into localized degradation patterns in cartilage throughout disease progression and distinguish between chondrocyte-mediated and inflammatory cell-mediated degradation.

Collectively, the work presented in this dissertation offers a more complete characterization of the chondrocyte micromechanical environment in articular cartilage. These studies provide the tools and framework for further studies to continue to elucidate the complicated structural, compositional, and functional relationships between the cartilage ECM and PCM and their importance in regulating chondrocyte physiology in health and disease.

Appendix A. Finite Thickness Correction for Hertz Model

Dimitriadis and colleagues developed an approximate, polynomial-based solution to the Hertz model for finite thickness samples (Dimitriadis et al. 2002). The final relation between the applied force, F , and indentation, δ , is given by

$$F = \frac{4}{3} \frac{Er^{1/2}}{1-\nu^2} \delta^{3/2} \left[1 - \frac{2\alpha_0}{\pi} \chi + \frac{4\alpha_0^2}{\pi^2} \chi^2 - \frac{8}{\pi^3} \left(\alpha_0^3 + \frac{4\pi^2}{15} \beta_0 \right) \chi^3 + \frac{16\alpha_0}{\pi^4} \left(\alpha_0^3 + \frac{3\pi^2}{5} \beta_0 \right) \chi^4 \right]$$

where the correction factor, χ , is given by

$$\chi = \frac{\sqrt{r\delta}}{h}$$

where r is the probe radius and h is the sample thickness. The coefficients, α_0 and β_0 , are given by

$$\alpha_0 = -\frac{1.2876 - 1.4678\nu + 1.3442\nu^2}{1-\nu}$$

$$\beta_0 = \frac{0.6387 - 1.0277\nu + 1.5164\nu^2}{1-\nu}$$

where ν is the sample Poisson's ratio.

To order to investigate the potential influence of finite sample thickness on our measurements of the microscale properties of porcine articular cartilage, ECM and PCM regions in porcine cartilage sections were mapped quantitatively using the protocol outlined in Chapter 2 with a force trigger of 300 nN at an indentation velocity of 15 $\mu\text{m/s}$.

As expected, when the finite thickness correction was applied, calculated moduli were reduced ($p < 0.05$; repeated measures ANOVA; Figure A-1) with equivalent effects on ECM and PCM moduli. Corrected moduli fell within the site-to-site variability both within a single testing region, variability among porcine cartilage specimens and within the expected error associated with contact point estimation in soft samples (Dimitriadis et al. 2002). Since force triggers for all experiments were carefully selected from a tested range in order to limit indentation depths for each group of samples, finite thickness effects were indistinguishable from the other errors associated with our testing modality.

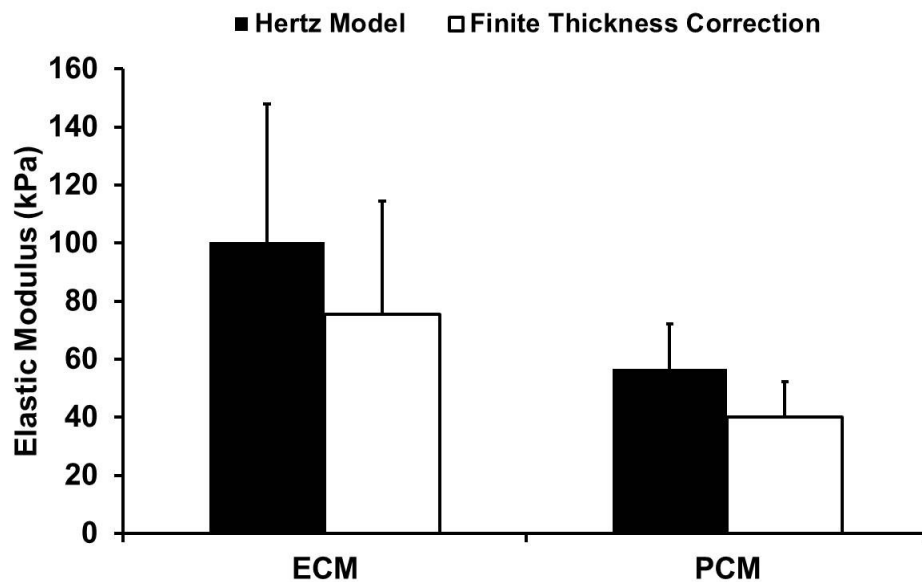


Figure A-1: Effect of finite sample thickness on calculated micromechanical properties of articular cartilage. Force-indentation curves collected in the ECM and PCM of porcine cartilage were evaluated using the Hertz model (black) and finite thickness correction (white). Calculated ECM and PCM elastic moduli decreased with finite thickness correction ($p < 0.05$). Moduli presented as mean + standard deviation (N = 4 pigs, n = 16 regions).

Appendix B. Low Force Stiffness Mapping of Articular Cartilage

A version of this appendix was published as supplemental material to the following:

Darling, E.M.*, Wilusz, R.E.*, Bolognesi, M.P., Zauscher, S., Guilak, F. Spatial Mapping of the Biomechanical Properties of the Pericellular Matrix of Articular Cartilage Measured *in situ* via Atomic Force Microscopy. *Biophysical Journal*, 98(12):2848-56, 2010.

Elastic moduli of articular cartilage PCM and ECM were mapped quantitatively using the protocol described in Chapter 2 with a force trigger of 50 nN (N = 6 cartilage samples, $n \geq 15$ total regions per species). This lower threshold resulted in smaller indentation depths and reduced contact radii. With this low threshold, measured elastic moduli were approximately two- to five-fold lower than those observed using a force trigger of 750 nN (Figure B-1, Table B-1). ECM elastic moduli were greater than PCM elastic moduli for human, porcine, and murine cartilage ($p < 0.001$). Murine cartilage exhibited the highest ECM and PCM moduli ($p < 0.001$), while porcine and human cartilage possessed similar values for both ECM and PCM properties ($p > 0.05$).

Depth-dependent (Schinagl et al. 1997; Chen et al. 2001) and strain-dependent (Wang et al. 2003) behavior of articular cartilage under compression has been observed previously at the macroscale. A similar phenomenon was recently reported in microscale indentation of bovine articular cartilage. Park and colleagues observed a non-linear increase in elastic moduli for indentation depths up to 600 nm (Park et al. 2009).

As in the current study, there was an order of magnitude difference between microscale and macroscale modulus values.

This strain-dependent behavior suggests that larger indentations are required to obtain microscale mechanical properties that are more representative of measurements recorded at the macroscale. Since cartilage is inhomogeneous, local variability in type II collagen content (Rieppo et al. 2009) and proteoglycan concentration (Samosky et al. 2005) likely affect the modulus measured via AFM indentation. Larger forces and indentation depths probe beyond microscale tissue swelling and allow for averaging of the mechanical contributions of the cartilage matrix components in a manner that is similar to that observed at the macroscale (Stolz et al. 2004). No consistent threshold indentation depth needed to achieve macroscale properties existed across tested samples. For example, some samples exhibited similar moduli for 500 nm and 1.5 μm indentations whereas other samples exhibited dramatically different moduli for the two depths. Prior to mapping, cartilage samples were probed with a range of indentations to determine a suitable depth for evaluating either the low-force or bulk mechanical properties of the tissue.

Table B-1: Elastic moduli of ECM and PCM regions from human, porcine, and murine articular cartilage using low force stiffness mapping. Stiffness mapping of sectioned cartilage samples showed clear differences between ECM and PCM regions for each species ($p < 0.0001$). Moduli shown as mean \pm standard deviation.

Sample	ECM E (kPa)	ECM E range (kPa)	PCM E (kPa)	PCM E range (kPa)
Human (N = 6) n = 35, ECM n = 34, PCM	58 \pm 20	23 – 114 (511 sites)	17 \pm 14	3 – 75 (4876 sites)
Porcine (N = 6) n = 20, ECM n = 20, PCM	53 \pm 25	15 – 101 (318 sites)	16 \pm 4	11 – 25 (2335 sites)
Murine (N = 6) n = 26, ECM n = 29, PCM	78 \pm 30	16 – 149 (474 sites)	40 \pm 20	4 – 89 (3907 sites)

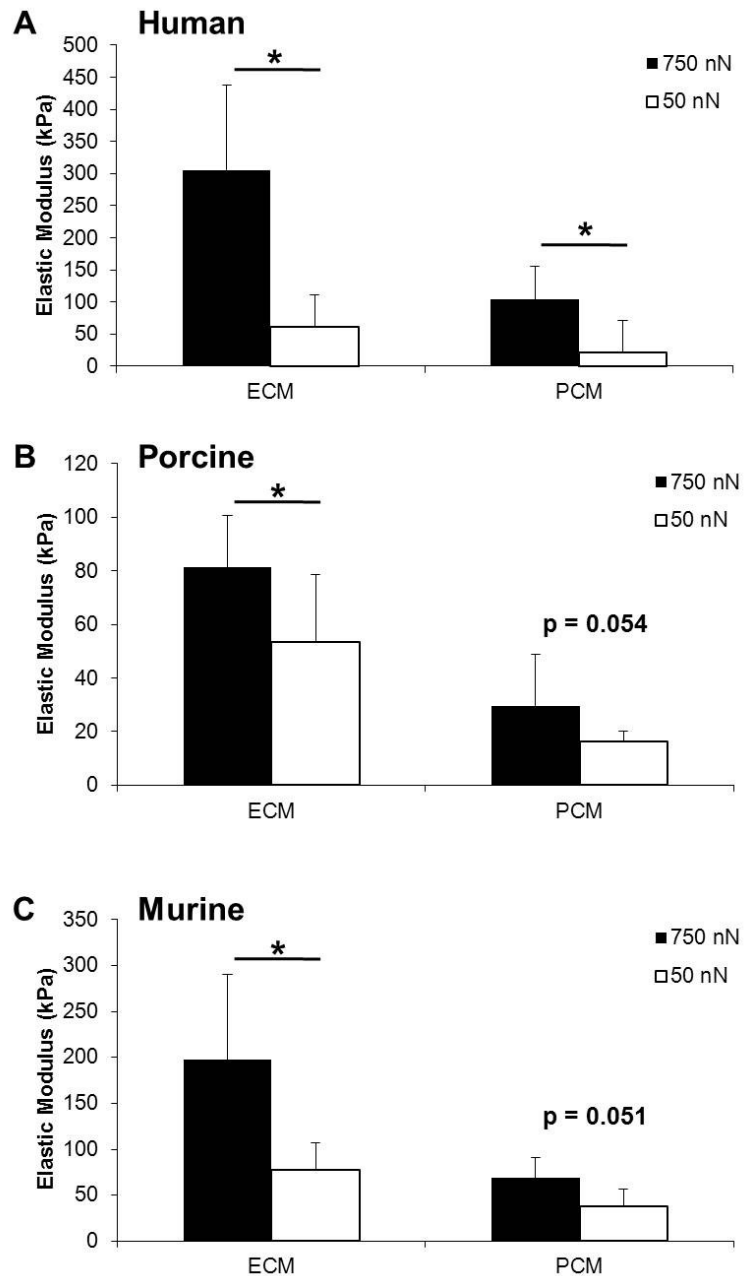


Figure B-1: Effect of indentation force on measured micromechanical properties of articular cartilage. ECM and PCM elastic moduli were measured using a force threshold of 750 nN (black) and 50 nN (white) for (A) human, (B) porcine, and (C) murine articular cartilage. *: $p < 0.005$ for 750 nN force threshold as compared to 50 nN force threshold. Moduli presented as mean + standard deviation (N = 6 knees, $n \geq 15$ regions).

Appendix C. Effect of Indentation Velocity on the Microscale Properties of Articular Cartilage

A version of this appendix was published as supplemental material to the following:

Wilusz, R.E., DeFrate, L.E. Guilak, F. Immunofluorescence-Guided Atomic Force Microscopy to Measure the Micromechanical Properties of the Pericellular Matrix of Porcine Articular Cartilage, *Journal of the Royal Society Interface*, 9(76):2997-3007, 2012.

In order to investigate the potential influence of indentation rate on the microscale properties of articular cartilage, ECM regions were evaluated in the middle/deep zone (200 – 400 μm from the articular surface) of unlabeled cartilage sections (N = 3 pigs, n = 15 total regions). Indentations were applied with a force trigger of 300 nN at indentation velocities of 1 $\mu\text{m/s}$, 5 $\mu\text{m/s}$, 10 $\mu\text{m/s}$, 15 $\mu\text{m/s}$, 20 $\mu\text{m/s}$, and 25 $\mu\text{m/s}$. The tissue was allowed to recover for 1 minute between successive scans.

ECM elastic moduli increased with indentation rate over the tested range ($p < 0.05$, repeated measures ANOVA; Figure C-1). Moduli observed at a 1 $\mu\text{m/s}$ indentation velocity were 24% lower than those measured at 15 $\mu\text{m/s}$ (used for data collection in all presented work). Moduli collected at velocities ranging from 5 – 25 $\mu\text{m/s}$ were within 3 – 12% of the values observed at 15 $\mu\text{m/s}$. The observed effect of indentation rate falls within the expected error associated with AFM indentation of soft substrates due to contact point estimation (Dimitriadis et al. 2002) and is small relative to the site-to-site variability observed both within and among ECM scan grids, where standard deviations were 15 – 30% of the mean.

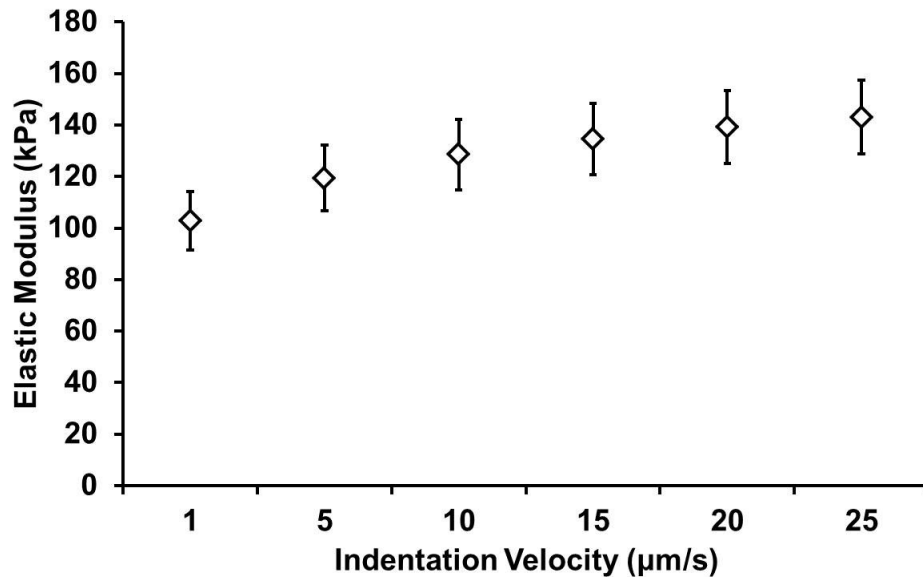


Figure C-1: Effect of indentation velocity on ECM micromechanical properties. ECM elastic moduli increased with indentation rate over the tested range ($p < 0.05$; repeated measures ANOVA). Moduli presented as mean \pm standard error (N = 3 pigs, n = 15 regions).

Loading rate-dependent behavior of articular cartilage under compressive loading has been observed previously at the macroscale (Li et al. 2003; Silver et al. 2004). A similar phenomenon was recently reported in microscale indentation of juvenile bovine cartilage (Han et al. 2011) where elastic moduli increased with z-piezo displacement rates of 0.1 – 10 $\mu\text{m/s}$. As observed in the current work, elastic moduli measured at 10 $\mu\text{m/s}$ indentation velocity were approximately 20% higher than moduli observed at 1 $\mu\text{m/s}$ (Han et al. 2011). Since interstitial fluid pressurization in response to AFM nano- and microindentation is minimal (Park et al. 2009; Bonnevie et al. 2012), the

observed rate dependence is likely due to intrinsic viscoelasticity of the solid matrix (Han et al. 2011), as opposed to a biphasic effect.

Appendix D. Spatial Mapping of Proteoglycan and Glycosaminoglycan Depleted Porcine Articular Cartilage

As described in Chapter 7, cryosections of porcine articular cartilage (5 μm thick) underwent control incubation or enzymatic digestion with ADAMTS-4, chondroitinase ABC (C-ABC), hyaluronidase (HA-ase), or leukocyte elastase and mapped quantitatively using immunofluorescence (IF)-guided atomic force microscopy (AFM)-based stiffness mapping. To quantitatively evaluate the spatial distribution of moduli in the chondrocyte microenvironment, the stiffness progression of elastic moduli from the PCM outer edge to the ECM was evaluated in radial increments of 0.5 μm . Stiffness progression data were evaluated separately for control and digested samples using a one-way ANOVA (distance; $\alpha = 0.05$) and Fisher's LSD *post-hoc* test. Differences between control and digested elastic moduli were evaluated separately at each 0.5 μm increment in the stiffness progression using a Student's *t*-test ($\alpha = 0.05$).

Overall, spatial mapping revealed distinct differences in the chondrocyte microenvironment following enzymatic digestion. In undigested control sections, spatial mapping revealed a trend or a significant effect of distance from the PCM outer edge in elastic moduli across all groups. In sections that underwent enzymatic digestion, a significant effect of distance from the PCM outer edge was observed only in moduli from HA-ase digested samples.

In ADAMTS-4 undigested controls, there was a trend toward a significant effect of distance from the PCM outer edge in elastic moduli ($p = 0.07$; Figure D-1). In digested samples, no variation in elastic moduli was observed with distance from the PCM outer edge ($p = 0.48$). Elastic moduli in ADAMTS-4 digested cartilage were less than undigested controls only in the ECM ($p < 0.05$).

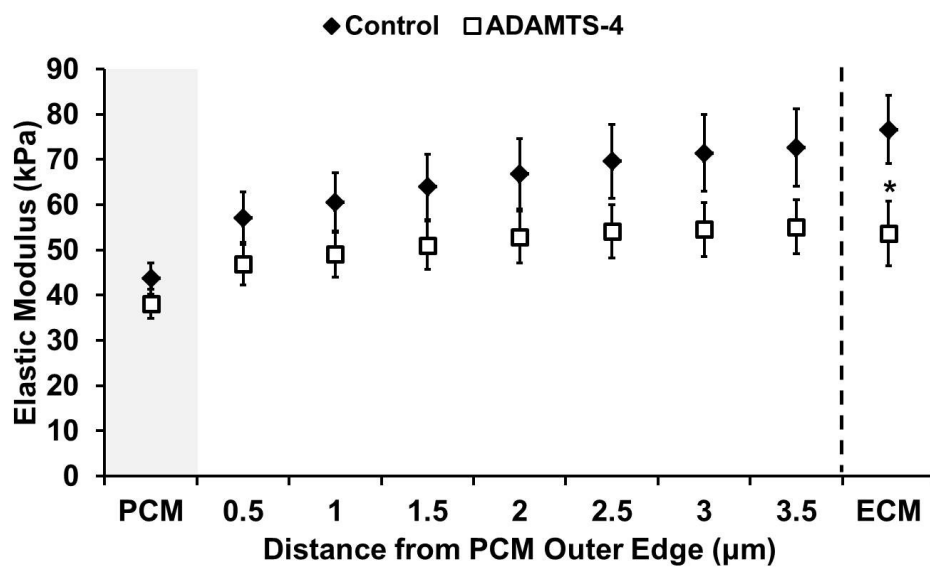


Figure D-1: Stiffness progression of elastic moduli in aggrecanase digested porcine articular cartilage. Stiffness progression of moduli from the PCM outer edge to the ECM in undigested control (black) and ADAMTS-4 digested (white) cartilage.

*: $p < 0.05$ for control ECM as compared to digested ECM. Undigested controls demonstrated a trend toward an effect of distance ($p = 0.07$). ADAMTS-4 digested moduli demonstrated no variation with distance ($p = 0.48$). Moduli presented as mean \pm standard error (N = 3 pigs, n = 9 regions per treatment).

In C-ABC undigested controls, PCM moduli were lower than those observed in regions greater than 1 μm from the PCM outer edge ($p < 0.05$). Elastic moduli comparable to ECM values were observed adjacent to the PCM outer edge (Figure D-2). Following C-ABC digestion, no variation in elastic moduli was observed with distance from the PCM outer edge ($p = 0.93$). Digested moduli were significantly lower than undigested controls at all distances beyond the PCM outer edge ($p < 0.05$).

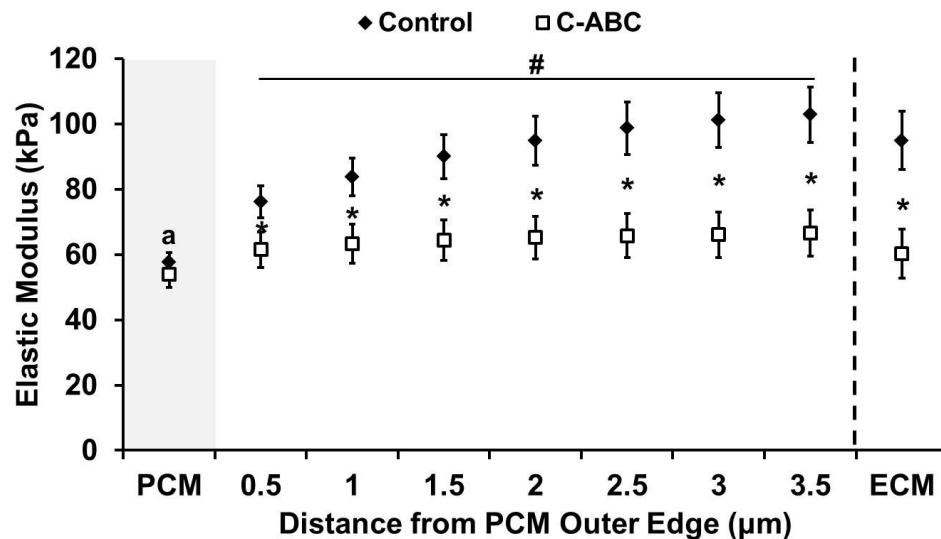


Figure D-2: Stiffness progression of elastic moduli in chondroitinase ABC digested porcine articular cartilage. Stiffness progression of moduli from the PCM outer edge to the ECM in undigested control (black) and C-ABC digested (white) cartilage. a: $p < 0.05$ for control PCM moduli as compared to control regions greater than 1.0 μm from the PCM outer edge. *: $p < 0.05$ for control moduli as compared to C-ABC digested moduli at each radial increment. #: Control moduli reached ECM values at the PCM outer edge. C-ABC digested moduli demonstrated no variation with distance ($p = 0.93$). Moduli presented as mean \pm standard error (N = 6 pigs, n = 24 regions per treatment).

In HA-ase undigested controls, PCM regions exhibited lower elastic moduli than immediately adjacent regions ($p < 0.05$) and ECM-like moduli were observed 2 μm from the PCM outer edge (Figure D-3). Following HA-ase digestion, PCM regions exhibited lower elastic moduli than immediately adjacent regions ($p < 0.05$) and ECM-like moduli were observed 1 μm from the PCM outer edge.

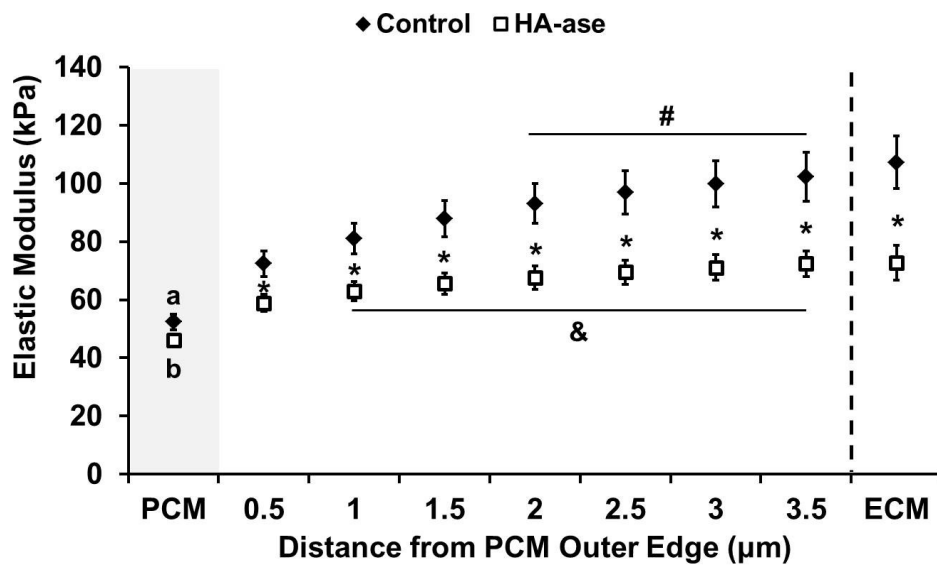


Figure D-3: Stiffness progression of elastic moduli in hyaluronidase digested porcine articular cartilage. Stiffness progression of moduli from the PCM outer edge to the ECM in undigested control (black) and HA-ase digested (white) cartilage. a: $p < 0.05$ for control PCM as compared to all control regions beyond the PCM. b: $p < 0.05$ for HA-ase digested PCM as compared to all digested regions beyond the PCM. *: $p < 0.05$ for control moduli as compared to HA-ase digested moduli at each radial increment. #: Control moduli reached ECM values 2.0 μm from the PCM outer edge. &: HA-ase digested moduli reached ECM values 1.0 μm from the PCM outer edge. Moduli presented as mean \pm standard error (N = 6 pigs, n = 24 regions per treatment).

In elastase undigested controls, PCM regions exhibited lower moduli than regions greater than 1 μm from the PCM outer edge ($p < 0.05$) and ECM-like moduli were observed 1.5 μm from the PCM outer edge (Figure D-4). Following elastase digestion, no variation in moduli was observed with distance from the PCM outer edge ($p = 0.32$). Digested moduli were significantly lower than undigested controls in PCM regions and at all distances beyond the PCM outer edge ($p < 0.05$).

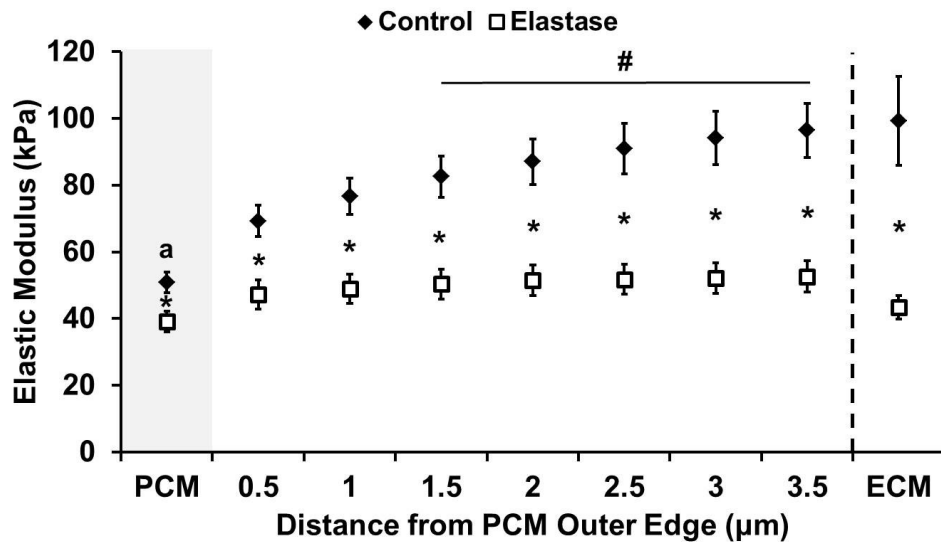


Figure D-4: Stiffness progression of elastic moduli in elastase digested porcine articular cartilage. Stiffness progression of moduli from the PCM outer edge to the ECM in undigested control (black) and elastase digested (white) cartilage. a: $p < 0.05$ for control PCM moduli as compared to control regions greater than 1.0 μm from the PCM outer edge. *: $p < 0.05$ for control moduli as compared to elastase digested moduli at each radial increment. #: Control moduli reached ECM values 1.5 μm from the PCM outer edge. Elastase digested moduli demonstrated no variation with distance ($p = 0.32$). Moduli presented as mean \pm standard error (N = 3 pigs, n = 12 regions per treatment).

References

- A-Hassan, E., Heinz, W. F., Antonik, M. D., D'Costa, N. P., Nageswaran, S., Schoenenberger, C. A. and Hoh, J. H., 1998. Relative microelastic mapping of living cells by atomic force microscopy. *Biophys J.* 74(3): 1564-1578.
- Abebe, E. S., Moorman, C. T., 3rd, Dziedzic, T. S., Spritzer, C. E., Cothran, R. L., Taylor, D. C., Garrett, W. E., Jr. and DeFrate, L. E., 2009. Femoral tunnel placement during anterior cruciate ligament reconstruction: an in vivo imaging analysis comparing transtibial and 2-incision tibial tunnel-independent techniques. *Am J Sports Med.* 37(10): 1904-1911.
- Aigner, T., Sachse, A., Gebhard, P. M. and Roach, H. I., 2006. Osteoarthritis: pathobiology-targets and ways for therapeutic intervention. *Adv Drug Deliv Rev.* 58(2): 128-149.
- Aigner, T., Zhu, Y., Chansky, H. H., Matsen, F. A., 3rd, Maloney, W. J. and Sandell, L. J., 1999. Reexpression of type IIA procollagen by adult articular chondrocytes in osteoarthritic cartilage. *Arthritis Rheum.* 42(7): 1443-1450.
- Akizuki, S., Mow, V. C., Muller, F., Pita, J. C., Howell, D. S. and Manicourt, D. H., 1986. Tensile properties of human knee joint cartilage: I. Influence of ionic conditions, weight bearing, and fibrillation on the tensile modulus. *J Orthop Res.* 4(4): 379-392.
- Alexopoulos, L. G., Haider, M. A., Vail, T. P. and Guilak, F., 2003. Alterations in the mechanical properties of the human chondrocyte pericellular matrix with osteoarthritis. *J Biomech Eng.* 125(3): 323-333.
- Alexopoulos, L. G., Setton, L. A. and Guilak, F., 2005a. The biomechanical role of the chondrocyte pericellular matrix in articular cartilage. *Acta Biomater.* 1(3): 317-325.
- Alexopoulos, L. G., Williams, G. M., Upton, M. L., Setton, L. A. and Guilak, F., 2005b. Osteoarthritic changes in the biphasic mechanical properties of the chondrocyte pericellular matrix in articular cartilage. *J Biomech.* 38(3): 509-517.
- Alexopoulos, L. G., Youn, I., Bonaldo, P. and Guilak, F., 2009. Developmental and osteoarthritic changes in Col6a1-knockout mice: biomechanics of type VI collagen in the cartilage pericellular matrix. *Arthritis Rheum.* 60(3): 771-779.

- Allen, D. M. and Mao, J. J., 2004. Heterogeneous nanostructural and nanoelastic properties of pericellular and interterritorial matrices of chondrocytes by atomic force microscopy. *J Struct Biol.* 145(3): 196-204.
- Archer, C. W., Morrison, E. H., Bayliss, M. T. and Ferguson, M. W., 1996. The development of articular cartilage: II. The spatial and temporal patterns of glycosaminoglycans and small leucine-rich proteoglycans. *J Anat.* 189 (Pt 1): 23-35.
- Arikawa-Hirasawa, E., Le, A. H., Nishino, I., Nonaka, I., Ho, N. C., Francomano, C. A., Govindraj, P., Hassell, J. R., Devaney, J. M., Spranger, J., Stevenson, R. E., Iannaccone, S., Dalakas, M. C. and Yamada, Y., 2002. Structural and functional mutations of the perlecan gene cause Schwartz-Jampel syndrome, with myotonic myopathy and chondrodysplasia. *Am J Hum Genet.* 70(5): 1368-1375.
- Arikawa-Hirasawa, E., Watanabe, H., Takami, H., Hassell, J. R. and Yamada, Y., 1999. Perlecan is essential for cartilage and cephalic development. *Nat Genet.* 23(3): 354-358.
- Arikawa-Hirasawa, E., Wilcox, W. R., Le, A. H., Silverman, N., Govindraj, P., Hassell, J. R. and Yamada, Y., 2001a. Dyssegmental dysplasia, Silverman-Handmaker type, is caused by functional null mutations of the perlecan gene. *Nat Genet.* 27(4): 431-434.
- Arikawa-Hirasawa, E., Wilcox, W. R. and Yamada, Y., 2001b. Dyssegmental dysplasia, Silverman-Handmaker type: unexpected role of perlecan in cartilage development. *Am J Med Genet.* 106(4): 254-257.
- Armstrong, C. G. and Mow, V. C., 1982. Variations in the intrinsic mechanical properties of human articular cartilage with age, degeneration, and water content. *Journal of Bone & Joint Surgery - American Volume.* 64(1): 88-94.
- Asanbaeva, A., Tam, J., Schumacher, B. L., Klisch, S. M., Masuda, K. and Sah, R. L., 2008. Articular cartilage tensile integrity: modulation by matrix depletion is maturation-dependent. *Arch Biochem Biophys.* 474(1): 175-182.
- Athanasiou, K. A., Rosenwasser, M. P., Buckwalter, J. A., Malinin, T. I. and Mow, V. C., 1991. Interspecies comparisons of in situ intrinsic mechanical properties of distal femoral cartilage. *J Orthop Res.* 9(3): 330-340.

- Aviezer, D., Hecht, D., Safran, M., Eisinger, M., David, G. and Yayon, A., 1994. Perlecan, basal lamina proteoglycan, promotes basic fibroblast growth factor-receptor binding, mitogenesis, and angiogenesis. *Cell*. 79(6): 1005-1013.
- Bachrach, N. M., Mow, V. C. and Guilak, F., 1998. Incompressibility of the solid matrix of articular cartilage under high hydrostatic pressures. *J Biomech*. 31(5): 445-451.
- Bader, D. L. and Kempson, G. E., 1994. The short-term compressive properties of adult human articular cartilage. *Biomed Mater Eng*. 4(3): 245-256.
- Barrett, A. J., 1994. The possible role of neutrophil proteinases in damage to articular cartilage. 1978. *Agents Actions*. 43(3-4): 194-200; discussion 200-191.
- Bartholomew, J. S. and Lowther, D. A., 1987. Receptor-mediated binding of leukocyte elastase by chondrocytes. *Arthritis Rheum*. 30(4): 431-438.
- Basalo, I. M., Mauck, R. L., Kelly, T. A., Nicoll, S. B., Chen, F. H., Hung, C. T. and Ateshian, G. A., 2004. Cartilage interstitial fluid load support in unconfined compression following enzymatic digestion. *J Biomech Eng*. 126(6): 779-786.
- Bastow, E. R., Byers, S., Golub, S. B., Clarkin, C. E., Pitsillides, A. A. and Fosang, A. J., 2008. Hyaluronan synthesis and degradation in cartilage and bone. *Cell Mol Life Sci*. 65(3): 395-413.
- Battaglia, C., Mayer, U., Aumailley, M. and Timpl, R., 1992. Basement-membrane heparan sulfate proteoglycan binds to laminin by its heparan sulfate chains and to nidogen by sites in the protein core. *Eur J Biochem*. 208(2): 359-366.
- Bau, B., Gebhard, P. M., Haag, J., Knorr, T., Bartnik, E. and Aigner, T., 2002. Relative messenger RNA expression profiling of collagenases and aggrecanases in human articular chondrocytes in vivo and in vitro. *Arthritis Rheum*. 46(10): 2648-2657.
- Bay-Jensen, A. C., Andersen, T. L., Charni-Ben Tabassi, N., Kristensen, P. W., Kjaersgaard-Andersen, P., Sandell, L., Garnero, P. and Delaisse, J. M., 2008. Biochemical markers of type II collagen breakdown and synthesis are positioned at specific sites in human osteoarthritic knee cartilage. *Osteoarthritis Cartilage*. 16(5): 615-623.

- Bayliss, M. T. and Ali, S. Y., 1978. Age-related changes in the composition and structure of human articular-cartilage proteoglycans. *Biochem J.* 176(3): 683-693.
- Bayliss, M. T., Howat, S., Davidson, C. and Dudhia, J., 2000. The organization of aggrecan in human articular cartilage. Evidence for age-related changes in the rate of aggregation of newly synthesized molecules. *J Biol Chem.* 275(9): 6321-6327.
- Bayliss, M. T., Osborne, D., Woodhouse, S. and Davidson, C., 1999. Sulfation of chondroitin sulfate in human articular cartilage. The effect of age, topographical position, and zone of cartilage on tissue composition. *J Biol Chem.* 274(22): 15892-15900.
- Below, S., Arnoczky, S. P., Dodds, J., Kooima, C. and Walter, N., 2002. The split-line pattern of the distal femur: A consideration in the orientation of autologous cartilage grafts. *Arthroscopy.* 18(6): 613-617.
- Benninghoff, A., 1925. Form und bau der Gelenkknorpel in ihren Beziehungen Zur Funktion. *Zweiter Teil: der Aufbau des Gelenkknorpels in seinen Beziehungen zur Funktion.* 2: 783-862.
- Binnig, G., Quate, C. F. and Gerber, C., 1986. Atomic Force Microscope. *Physical Review Letters.* 56(9): 930-933.
- Bitton, R., 2009. The economic burden of osteoarthritis. *Am J Manag Care.* 15(8 Suppl): S230-235.
- Bock, H. C., Michaeli, P., Bode, C., Schultz, W., Kresse, H., Herken, R. and Miosge, N., 2001. The small proteoglycans decorin and biglycan in human articular cartilage of late-stage osteoarthritis. *Osteoarthritis Cartilage.* 9(7): 654-663.
- Bonassar, L. J., Frank, E. H., Murray, J. C., Paguio, C. G., Moore, V. L., Lark, M. W., Sandy, J. D., Wu, J. J., Eyre, D. R. and Grodzinsky, A. J., 1995. Changes in cartilage composition and physical properties due to stromelysin degradation. *Arthritis Rheum.* 38(2): 173-183.
- Bonnevie, E. D., Baro, V. J., Wang, L. and Burris, D. L., 2012. Fluid load support during localized indentation of cartilage with a spherical probe. *J Biomech.* 45(6): 1036-1041.

- Bramono, D. S., Richmond, J. C., Weitzel, P. P., Kaplan, D. L. and Altman, G. H., 2004. Matrix metalloproteinases and their clinical applications in orthopaedics. *Clin Orthop Relat Res*(428): 272-285.
- Broom, N. D. and Poole, C. A., 1983. Articular cartilage collagen and proteoglycans. Their functional interdependency. *Arthritis Rheum.* 26(9): 1111-1119.
- Brown, G. M., Huckerby, T. N., Bayliss, M. T. and Nieduszynski, I. A., 1998. Human aggrecan keratan sulfate undergoes structural changes during adolescent development. *J Biol Chem.* 273(41): 26408-26414.
- Brown, J. C., Sasaki, T., Gohring, W., Yamada, Y. and Timpl, R., 1997. The C-terminal domain V of perlecan promotes beta1 integrin-mediated cell adhesion, binds heparin, nidogen and fibulin-2 and can be modified by glycosaminoglycans. *Eur J Biochem.* 250(1): 39-46.
- Bruns, R. R., Press, W., Engvall, E., Timpl, R. and Gross, J., 1986. Type VI collagen in extracellular, 100-nm periodic filaments and fibrils: identification by immunoelectron microscopy. *J Cell Biol.* 103(2): 393-404.
- Buckwalter, J. A. and Martin, J. A., 2006. Osteoarthritis. *Adv Drug Deliv Rev.* 58(2): 150-167.
- Buckwalter, J. A., Roughley, P. J. and Rosenberg, L. C., 1994. Age-related changes in cartilage proteoglycans: quantitative electron microscopic studies. *Microsc Res Tech.* 28(5): 398-408.
- Burkhardt, D., Michel, B. A., Baici, A., Kissling, R. and Theiler, R., 1995. Comparison of chondroitin sulphate composition of femoral head articular cartilage from patients with femoral neck fractures and osteoarthritis and controls. *Rheumatol Int.* 14(6): 235-241.
- Cao, L., Youn, I., Guilak, F. and Setton, L. A., 2006. Compressive properties of mouse articular cartilage determined in a novel micro-indentation test method and biphasic finite element model. *J Biomech Eng.* 128(5): 766-771.
- Carrillo, F., Gupta, S., Balooch, M., Marshall, S. J., Marshall, G. W., Pruitt, L. and Puttlitz, C. M., 2005. Nanoindentation of polydimethylsiloxane elastomers: Effect of crosslinking, work of adhesion, and fluid environment on elastic modulus. *Journal of Materials Research.* 20(10): 2820-2830.

- Caterson, B., Flannery, C. R., Hughes, C. E. and Little, C. B., 2000. Mechanisms involved in cartilage proteoglycan catabolism. *Matrix Biol.* 19(4): 333-344.
- Caterson, B., Mahmoodian, F., Sorrell, J. M., Hardingham, T. E., Bayliss, M. T., Carney, S. L., Ratcliffe, A. and Muir, H., 1990. Modulation of native chondroitin sulphate structure in tissue development and in disease. *J Cell Sci.* 97 (Pt 3): 411-417.
- Cawston, T. E. and Young, D. A., 2010. Proteinases involved in matrix turnover during cartilage and bone breakdown. *Cell Tissue Res.* 339(1): 221-235.
- Chahine, N. O., Wang, C. C., Hung, C. T. and Ateshian, G. A., 2004. Anisotropic strain-dependent material properties of bovine articular cartilage in the transitional range from tension to compression. *J Biomech.* 37(8): 1251-1261.
- Chang, J., Nakajima, H. and Poole, C. A., 1997. Structural colocalisation of type VI collagen and fibronectin in agarose cultured chondrocytes and isolated chondrons extracted from adult canine tibial cartilage. *J Anat.* 190 (Pt 4): 523-532.
- Chen, S. S., Falcovitz, Y. H., Schneiderman, R., Maroudas, A. and Sah, R. L., 2001. Depth-dependent compressive properties of normal aged human femoral head articular cartilage: relationship to fixed charge density. *Osteoarthritis Cartilage.* 9(6): 561-569.
- Choi, J. B., Youn, I., Cao, L., Leddy, H. A., Gilchrist, C. L., Setton, L. A. and Guilak, F., 2007. Zonal changes in the three-dimensional morphology of the chondron under compression: the relationship among cellular, pericellular, and extracellular deformation in articular cartilage. *J Biomech.* 40(12): 2596-2603.
- Chuang, C. Y., Lord, M. S., Melrose, J., Rees, M. D., Knox, S. M., Freeman, C., Iozzo, R. V. and Whitelock, J. M., 2010. Heparan sulfate-dependent signaling of fibroblast growth factor 18 by chondrocyte-derived perlecan. *Biochemistry.* 49(26): 5524-5532.
- Cohen, M., Klein, E., Geiger, B. and Addadi, L., 2003. Organization and adhesive properties of the hyaluronan pericellular coat of chondrocytes and epithelial cells. *Biophys J.* 85(3): 1996-2005.

- Coles, J. M., Blum, J. J., Jay, G. D., Darling, E. M., Guilak, F. and Zauscher, S., 2008. In situ friction measurement on murine cartilage by atomic force microscopy. *J Biomech.* 41(3): 541-548.
- Collins, D. H. and McElligott, T. F., 1960. Sulphate ($^{35}\text{SO}_4$) uptake by chondrocytes in relation to histological changes in osteoarthritic human articular cartilage. *Ann Rheum Dis.* 19: 318-330.
- Costa, K. D., 2003. Single-cell elastography: probing for disease with the atomic force microscope. *Dis Markers.* 19(2-3): 139-154.
- Costa, K. D. and Yin, F. C., 1999. Analysis of indentation: implications for measuring mechanical properties with atomic force microscopy. *J Biomech Eng.* 121(5): 462-471.
- Costell, M., Gustafsson, E., Aszodi, A., Morgelin, M., Bloch, W., Hunziker, E., Addicks, K., Timpl, R. and Fassler, R., 1999. Perlecan maintains the integrity of cartilage and some basement membranes. *J Cell Biol.* 147(5): 1109-1122.
- Cs-Szabo, G., Melching, L. I., Roughley, P. J. and Glant, T. T., 1997. Changes in messenger RNA and protein levels of proteoglycans and link protein in human osteoarthritic cartilage samples. *Arthritis Rheum.* 40(6): 1037-1045.
- Cs-Szabo, G., Roughley, P. J., Plaas, A. H. and Glant, T. T., 1995. Large and small proteoglycans of osteoarthritic and rheumatoid articular cartilage. *Arthritis Rheum.* 38(5): 660-668.
- Darling, E. M., Topel, M., Zauscher, S., Vail, T. P. and Guilak, F., 2008. Viscoelastic properties of human mesenchymally-derived stem cells and primary osteoblasts, chondrocytes, and adipocytes. *J Biomech.* 41(2): 454-464.
- Darling, E. M., Wilusz, R. E., Bolognesi, M. P., Zauscher, S. and Guilak, F., 2010. Spatial mapping of the biomechanical properties of the pericellular matrix of articular cartilage measured in situ via atomic force microscopy. *Biophys J.* 98(12): 2848-2856.
- Darling, E. M., Zauscher, S. and Guilak, F., 2006. Viscoelastic properties of zonal articular chondrocytes measured by atomic force microscopy. *Osteoarthritis Cartilage.* 14(6): 571-579.

- David, G., Bai, X. M., Van der Schueren, B., Cassiman, J. J. and Van den Berghe, H., 1992. Developmental changes in heparan sulfate expression: in situ detection with mAbs. *J Cell Biol.* 119(4): 961-975.
- Dean, D., Han, L., Grodzinsky, A. J. and Ortiz, C., 2006. Compressive nanomechanics of opposing aggrecan macromolecules. *J Biomech.* 39(14): 2555-2565.
- Desrochers, J., Amrein, M. A. and Matyas, J. R., 2010. Structural and functional changes of the articular surface in a post-traumatic model of early osteoarthritis measured by atomic force microscopy. *J Biomech.*
- Desrochers, J., Amrein, M. W. and Matyas, J. R., 2012. Viscoelasticity of the articular cartilage surface in early osteoarthritis. *Osteoarthritis Cartilage.* 20(5): 413-421.
- Di Benedetto, F., Biasco, A., Pisignano, D. and Cingolani, R., 2005. Patterning polyacrylamide hydrogels by soft lithography. *Nanotechnology.* 16(5): S165-S170.
- Diekman, B. O., Christoforou, N., Willard, V. P., Sun, H., Sanchez-Adams, J., Leong, K. W. and Guilak, F., 2012. Cartilage tissue engineering using differentiated and purified induced pluripotent stem cells. *Proc Natl Acad Sci U S A.* 109(47): 19172-19177.
- Dimitriadis, E. K., Horkay, F., Maresca, J., Kachar, B. and Chadwick, R. S., 2002. Determination of elastic moduli of thin layers of soft material using the atomic force microscope. *Biophys J.* 82(5): 2798-2810.
- DiSilvestro, M. R. and Suh, J. K., 2002. Biphasic poroviscoelastic characteristics of proteoglycan-depleted articular cartilage: simulation of degeneration. *Ann Biomed Eng.* 30(6): 792-800.
- Dodge, G. R. and Poole, A. R., 1989. Immunohistochemical detection and immunochemical analysis of type II collagen degradation in human normal, rheumatoid, and osteoarthritic articular cartilages and in explants of bovine articular cartilage cultured with interleukin 1. *J Clin Invest.* 83(2): 647-661.
- Doerge, K. J., Sasaki, M., Kimura, T. and Yamada, Y., 1991. Complete coding sequence and deduced primary structure of the human cartilage large aggregating proteoglycan, aggrecan. Human-specific repeats, and additional alternatively spliced forms. *J Biol Chem.* 266(2): 894-902.

- Dudhia, J., 2005. Aggrecan, aging and assembly in articular cartilage. *Cell Mol Life Sci.* 62(19-20): 2241-2256.
- Durigova, M., Troeberg, L., Nagase, H., Roughley, P. J. and Mort, J. S., 2011. Involvement of ADAMTS5 and hyaluronidase in aggrecan degradation and release from OSM-stimulated cartilage. *Eur Cell Mater.* 21: 31-45.
- Durr, J., Lammi, P., Goodman, S. L., Aigner, T. and von der Mark, K., 1996. Identification and immunolocalization of laminin in cartilage. *Exp Cell Res.* 222(1): 225-233.
- Eisenberg, S. R. and Grodzinsky, A. J., 1985. Swelling of articular cartilage and other connective tissues: electromechanochemical forces. *J Orthop Res.* 3(2): 148-159.
- Elkin, B. S., Azeloglu, E. U., Costa, K. D. and Morrison, B., 3rd, 2007. Mechanical heterogeneity of the rat hippocampus measured by atomic force microscope indentation. *J Neurotrauma.* 24(5): 812-822.
- Elsaid, K. A., Fleming, B. C., Oksendahl, H. L., Machan, J. T., Fadale, P. D., Hulstyn, M. J., Shalvoy, R. and Jay, G. D., 2008. Decreased lubricin concentrations and markers of joint inflammation in the synovial fluid of patients with anterior cruciate ligament injury. *Arthritis Rheum.* 58(6): 1707-1715.
- Elsaid, K. A., Jay, G. D. and Chichester, C. O., 2003. Detection of collagen type II and proteoglycans in the synovial fluids of patients diagnosed with non-infectious knee joint synovitis indicates early damage to the articular cartilage matrix. *Osteoarthritis Cartilage.* 11(9): 673-680.
- Engelmayr, G. C., Jr. and Sacks, M. S., 2008. Prediction of extracellular matrix stiffness in engineered heart valve tissues based on nonwoven scaffolds. *Biomech Model Mechanobiol.* 7(4): 309-321.
- Engler, A., Bacakova, L., Newman, C., Hategan, A., Griffin, M. and Discher, D., 2004. Substrate compliance versus ligand density in cell on gel responses. *Biophys J.* 86(1 Pt 1): 617-628.
- Engler, A. J., Sen, S., Sweeney, H. L. and Discher, D. E., 2006. Matrix elasticity directs stem cell lineage specification. *Cell.* 126(4): 677-689.
- Ernst, S., Langer, R., Cooney, C. L. and Sasisekharan, R., 1995. Enzymatic degradation of glycosaminoglycans. *Crit Rev Biochem Mol Biol.* 30(5): 387-444.

- Fermor, B., Christensen, S. E., Youn, I., Cernanec, J. M., Davies, C. M. and Weinberg, J. B., 2007. Oxygen, nitric oxide and articular cartilage. *Eur Cell Mater.* 13: 56-65; discussion 65.
- Flahiff, C. M., Kraus, V. B., Huebner, J. L. and Setton, L. A., 2004. Cartilage mechanics in the guinea pig model of osteoarthritis studied with an osmotic loading method. *Osteoarthritis Cartilage.* 12(5): 383-388.
- Flahiff, C. M., Narmoneva, D. A., Huebner, J. L., Kraus, V. B., Guilak, F. and Setton, L. A., 2002. Osmotic loading to determine the intrinsic material properties of guinea pig knee cartilage. *J Biomech.* 35(9): 1285-1290.
- Flannery, C. R., Lark, M. W. and Sandy, J. D., 1992. Identification of a stromelysin cleavage site within the interglobular domain of human aggrecan. Evidence for proteolysis at this site in vivo in human articular cartilage. *J Biol Chem.* 267(2): 1008-1014.
- Fraser, J. R., Laurent, T. C. and Laurent, U. B., 1997. Hyaluronan: its nature, distribution, functions and turnover. *J Intern Med.* 242(1): 27-33.
- Fraser, S. A., Crawford, A., Frazer, A., Dickinson, S., Hollander, A. P., Brook, I. M. and Hatton, P. V., 2006. Localization of type VI collagen in tissue-engineered cartilage on polymer scaffolds. *Tissue Eng.* 12(3): 569-577.
- French, M. M., Smith, S. E., Akanbi, K., Sanford, T., Hecht, J., Farach-Carson, M. C. and Carson, D. D., 1999. Expression of the heparan sulfate proteoglycan, perlecan, during mouse embryogenesis and perlecan chondrogenic activity in vitro. *J Cell Biol.* 145(5): 1103-1115.
- Fukui, N., Ikeda, Y., Ohnuki, T., Tanaka, N., Hikita, A., Mitomi, H., Mori, T., Juji, T., Katsuragawa, Y., Yamamoto, S., Sawabe, M., Yamane, S., Suzuki, R., Sandell, L. J. and Ochi, T., 2008. Regional differences in chondrocyte metabolism in osteoarthritis: a detailed analysis by laser capture microdissection. *Arthritis Rheum.* 58(1): 154-163.
- Funderburgh, J. L., 2000. Keratan sulfate: structure, biosynthesis, and function. *Glycobiology.* 10(10): 951-958.

- Gad, M., Itoh, A. and Ikai, A., 1997. Mapping cell wall polysaccharides of living microbial cells using atomic force microscopy. *Cell Biol Int.* 21(11): 697-706.
- Gadher, S. J., Eyre, D. R., Duance, V. C., Wotton, S. F., Heck, L. W., Schmid, T. M. and Woolley, D. E., 1988. Susceptibility of cartilage collagens type II, IX, X, and XI to human synovial collagenase and neutrophil elastase. *Eur J Biochem.* 175(1): 1-7.
- Gandhi, N. S. and Mancera, R. L., 2008. The structure of glycosaminoglycans and their interactions with proteins. *Chem Biol Drug Des.* 72(6): 455-482.
- Gendron, C., Kashiwagi, M., Lim, N. H., Enghild, J. J., Thogersen, I. B., Hughes, C., Caterson, B. and Nagase, H., 2007. Proteolytic activities of human ADAMTS-5: comparative studies with ADAMTS-4. *J Biol Chem.* 282(25): 18294-18306.
- Gibson, G. J., Verner, J. J., Nelson, F. R. and Lin, D. L., 2001. Degradation of the cartilage collagen matrix associated with changes in chondrocytes in osteoarthritis. Assessment by loss of background fluorescence and immunodetection of matrix components. *J Orthop Res.* 19(1): 33-42.
- Glasson, S. S., Askew, R., Sheppard, B., Carito, B., Blanchet, T., Ma, H. L., Flannery, C. R., Peluso, D., Kanki, K., Yang, Z., Majumdar, M. K. and Morris, E. A., 2005. Deletion of active ADAMTS5 prevents cartilage degradation in a murine model of osteoarthritis. *Nature.* 434(7033): 644-648.
- Goldring, S. R., 2008. The role of bone in osteoarthritis pathogenesis. *Rheum Dis Clin North Am.* 34(3): 561-571.
- Grodzinsky, A. J., Levenston, M. E., Jin, M. and Frank, E. H., 2000. Cartilage tissue remodeling in response to mechanical forces. *Annu Rev Biomed Eng.* 2: 691-713.
- Guilak, F., 2011. Biomechanical factors in osteoarthritis. *Best Pract Res Clin Rheumatol.* 25(6): 815-823.
- Guilak, F., Alexopoulos, L. G., Haider, M. A., Ting-Beall, H. P. and Setton, L. A., 2005. Zonal uniformity in mechanical properties of the chondrocyte pericellular matrix: micropipette aspiration of canine chondrons isolated by cartilage homogenization. *Ann Biomed Eng.* 33(10): 1312-1318.

- Guilak, F., Alexopoulos, L. G., Upton, M. L., Youn, I., Choi, J. B., Cao, L., Setton, L. A. and Haider, M. A., 2006. The pericellular matrix as a transducer of biomechanical and biochemical signals in articular cartilage. *Ann N Y Acad Sci.* 1068: 498-512.
- Guilak, F., Jones, W. R., Ting-Beall, H. P. and Lee, G. M., 1999. The deformation behavior and mechanical properties of chondrocytes in articular cartilage. *Osteoarthritis Cartilage.* 7(1): 59-70.
- Guilak, F. and Mow, V. C., 2000. The mechanical environment of the chondrocyte: a biphasic finite element model of cell-matrix interactions in articular cartilage. *J Biomech.* 33(12): 1663-1673.
- Guilak, F., Ratcliffe, A. and Mow, V. C., 1995. Chondrocyte deformation and local tissue strain in articular cartilage: a confocal microscopy study. *J Orthop Res.* 13(3): 410-421.
- Guilak, F., Sah, R. L. and Setton, L. A., 1997. Physical Regulation of Cartilage Metabolism. *Basic Orthopaedic Biomechanics.* V. C. Mow and W. C. Hayes. Philadelphia, Lippincott-Raven Publishers: 179-207.
- Guo, S. and Akhremitchev, B. B., 2006. Packing density and structural heterogeneity of insulin amyloid fibrils measured by AFM nanoindentation. *Biomacromolecules.* 7(5): 1630-1636.
- Gustafsson, E., Aszodi, A., Ortega, N., Hunziker, E. B., Denker, H. W., Werb, Z. and Fassler, R., 2003. Role of collagen type II and perlecan in skeletal development. *Ann N Y Acad Sci.* 995: 140-150.
- Haga, H., Sasaki, S., Kawabata, K., Ito, E., Ushiki, T. and Sambongi, T., 2000. Elasticity mapping of living fibroblasts by AFM and immunofluorescence observation of the cytoskeleton. *Ultramicroscopy.* 82(1-4): 253-258.
- Hagiwara, H., Schroter-Kermani, C. and Merker, H. J., 1993. Localization of collagen type VI in articular cartilage of young and adult mice. *Cell Tissue Res.* 272(1): 155-160.
- Hall, M. L., Krawczak, D. A., Simha, N. K. and Lewis, J. L., 2009. Effect of dermatan sulfate on the indentation and tensile properties of articular cartilage. *Osteoarthritis Cartilage.* 17(5): 655-661.

- Hambach, L., Neureiter, D., Zeiler, G., Kirchner, T. and Aigner, T., 1998. Severe disturbance of the distribution and expression of type VI collagen chains in osteoarthritic articular cartilage. *Arthritis Rheum.* 41(6): 986-996.
- Han, L., Frank, E. H., Greene, J. J., Lee, H. Y., Hung, H. H., Grodzinsky, A. J. and Ortiz, C., 2011. Time-dependent nanomechanics of cartilage. *Biophys J.* 100(7): 1846-1854.
- Harding, J. W. and Sneddon, I. N., 1945. The elastic stresses produced by the indentation of the plane surface of a semi-infinite elastic solid by a rigid punch. *Mathematical Proceedings of the Cambridge Philosophical Society.* 41: 16-26.
- Hayashi, K., Madri, J. A. and Yurchenco, P. D., 1992. Endothelial cells interact with the core protein of basement membrane perlecan through beta 1 and beta 3 integrins: an adhesion modulated by glycosaminoglycan. *J Cell Biol.* 119(4): 945-959.
- Hedbom, E. and Heinegard, D., 1989. Interaction of a 59-kDa connective tissue matrix protein with collagen I and collagen II. *J Biol Chem.* 264(12): 6898-6905.
- Hedbom, E. and Heinegard, D., 1993. Binding of fibromodulin and decorin to separate sites on fibrillar collagens. *J Biol Chem.* 268(36): 27307-27312.
- Hedlund, H., Hedbom, E., Heinegard, D., Mengarelli-Widholm, S., Reinholt, F. P. and Svensson, O., 1999. Association of the aggrecan keratan sulfate-rich region with collagen in bovine articular cartilage. *J Biol Chem.* 274(9): 5777-5781.
- Heinegard, D., 2009. Proteoglycans and more--from molecules to biology. *Int J Exp Pathol.* 90(6): 575-586.
- Hennerbichler, A., Rosenberger, R., Arora, R. and Hennerbichler, D., 2008. Biochemical, biomechanical and histological properties of osteoarthritic porcine knee cartilage: implications for osteochondral transplantation. *Arch Orthop Trauma Surg.* 128(1): 61-70.
- Hing, W. A., Sherwin, A. F. and Poole, C. A., 2002. The influence of the pericellular microenvironment on the chondrocyte response to osmotic challenge. *Osteoarthritis Cartilage.* 10(4): 297-307.

- Hofmann, U. G., Rotsch, C., Parak, W. J. and Radmacher, M., 1997. Investigating the cytoskeleton of chicken cardiocytes with the atomic force microscope. *J Struct Biol.* 119(2): 84-91.
- Hollander, A. P., Pidoux, I., Reiner, A., Rorabeck, C., Bourne, R. and Poole, A. R., 1995. Damage to type II collagen in aging and osteoarthritis starts at the articular surface, originates around chondrocytes, and extends into the cartilage with progressive degeneration. *J Clin Invest.* 96(6): 2859-2869.
- Hopf, M., Gohring, W., Kohfeldt, E., Yamada, Y. and Timpl, R., 1999. Recombinant domain IV of perlecan binds to nidogens, laminin-nidogen complex, fibronectin, fibulin-2 and heparin. *Eur J Biochem.* 259(3): 917-925.
- Hopf, M., Gohring, W., Mann, K. and Timpl, R., 2001. Mapping of binding sites for nidogens, fibulin-2, fibronectin and heparin to different IG modules of perlecan. *J Mol Biol.* 311(3): 529-541.
- Horikawa, O., Nakajima, H., Kikuchi, T., Ichimura, S., Yamada, H., Fujikawa, K. and Toyama, Y., 2004. Distribution of type VI collagen in chondrocyte microenvironment: study of chondrons isolated from human normal and degenerative articular cartilage and cultured chondrocytes. *J Orthop Sci.* 9(1): 29-36.
- Hu, K., Radhakrishnan, P., Patel, R. V. and Mao, J. J., 2001. Regional structural and viscoelastic properties of fibrocartilage upon dynamic nanoindentation of the articular condyle. *J Struct Biol.* 136(1): 46-52.
- Huang, C. Y., Stankiewicz, A., Ateshian, G. A. and Mow, V. C., 2005. Anisotropy, inhomogeneity, and tension-compression nonlinearity of human glenohumeral cartilage in finite deformation. *J Biomech.* 38(4): 799-809.
- Hughes, L. C., Archer, C. W. and ap Gwynn, I., 2005. The ultrastructure of mouse articular cartilage: collagen orientation and implications for tissue functionality. A polarised light and scanning electron microscope study and review. *Eur Cell Mater.* 9: 68-84.
- Hunziker, E. B., Michel, M. and Studer, D., 1997. Ultrastructure of adult human articular cartilage matrix after cryotechnical processing. *Microsc Res Tech.* 37(4): 271-284.

- Hunziker, E. B., Quinn, T. M. and Hauselmann, H. J., 2002. Quantitative structural organization of normal adult human articular cartilage. *Osteoarthritis Cartilage*. 10(7): 564-572.
- Hutter, J. L. and Bechhoefer, J., 1993. Calibration of Atomic-Force Microscope Tips. *Review of Scientific Instruments*. 64(7): 1868-1873.
- Hwang, W. S., Li, B., Jin, L. H., Ngo, K., Schachar, N. S. and Hughes, G. N., 1992. Collagen fibril structure of normal, aging, and osteoarthritic cartilage. *J Pathol*. 167(4): 425-433.
- Iozzo, R. V., 1998. Matrix proteoglycans: from molecular design to cellular function. *Annu Rev Biochem*. 67: 609-652.
- Ishiguro, N., Ito, T., Oguchi, T., Kojima, T., Iwata, H., Ionescu, M. and Poole, A. R., 2001. Relationships of matrix metalloproteinases and their inhibitors to cartilage proteoglycan and collagen turnover and inflammation as revealed by analyses of synovial fluids from patients with rheumatoid arthritis. *Arthritis Rheum*. 44(11): 2503-2511.
- Janoff, A., Feinstein, G., Malemud, C. J. and Elias, J. M., 1976. Degradation of cartilage proteoglycan by human leukocyte granule neutral proteases--a model of joint injury. I. Penetration of enzyme into rabbit articular cartilage and release of ³⁵SO₄-labeled material from the tissue. *J Clin Invest*. 57(3): 615-624.
- Jeffery, A. K., Blunn, G. W., Archer, C. W. and Bentley, G., 1991. Three-dimensional collagen architecture in bovine articular cartilage. *J Bone Joint Surg Br*. 73(5): 795-801.
- Julkunen, P., Wilson, W., Jurvelin, J. S. and Korhonen, R. K., 2009. Composition of the pericellular matrix modulates the deformation behaviour of chondrocytes in articular cartilage under static loading. *Med Biol Eng Comput*. 47(12): 1281-1290.
- Junqueira, L. C., Bignolas, G. and Brentani, R. R., 1979. Picrosirius staining plus polarization microscopy, a specific method for collagen detection in tissue sections. *Histochem J*. 11(4): 447-455.
- Junqueira, L. C. and Montes, G. S., 1983. Biology of collagen-proteoglycan interaction. *Arch Histol Jpn*. 46(5): 589-629.

- Jurvelin, J. S., Buschmann, M. D. and Hunziker, E. B., 1997. Optical and mechanical determination of Poisson's ratio of adult bovine humeral articular cartilage. *J Biomech.* 30(3): 235-241.
- Jurvelin, J. S., Buschmann, M. D. and Hunziker, E. B., 2003. Mechanical anisotropy of the human knee articular cartilage in compression. *Proc Inst Mech Eng H.* 217(3): 215-219.
- Kavanagh, E. and Ashhurst, D. E., 1999. Development and aging of the articular cartilage of the rabbit knee joint: Distribution of biglycan, decorin, and matrilin-1. *J Histochem Cytochem.* 47(12): 1603-1616.
- Kawabata, K., Moore, A. R. and Willoughby, D. A., 1996. Impaired activity of protease inhibitors towards neutrophil elastase bound to human articular cartilage. *Ann Rheum Dis.* 55(4): 248-252.
- Kempson, G. E., Muir, H., Pollard, C. and Tuke, M., 1973. The tensile properties of the cartilage of human femoral condyles related to the content of collagen and glycosaminoglycans. *Biochim Biophys Acta.* 297(2): 456-472.
- Kielty, C. M., Lees, M., Shuttleworth, C. A. and Woolley, D., 1993. Catabolism of intact type VI collagen microfibrils: susceptibility to degradation by serine proteinases. *Biochem Biophys Res Commun.* 191(3): 1230-1236.
- Kielty, C. M., Whittaker, S. P., Grant, M. E. and Shuttleworth, C. A., 1992. Type VI collagen microfibrils: evidence for a structural association with hyaluronan. *J Cell Biol.* 118(4): 979-990.
- Kim, E., Guilak, F. and Haider, M. A., 2008. The dynamic mechanical environment of the chondrocyte: a biphasic finite element model of cell-matrix interactions under cyclic compressive loading. *J Biomech Eng.* 130(6): 061009.
- Kim, E., Guilak, F. and Haider, M. A., 2010. An axisymmetric boundary element model for determination of articular cartilage pericellular matrix properties in situ via inverse analysis of chondron deformation. *J Biomech Eng.* 132(3): 031011.
- Kirn-Safran, C., Farach-Carson, M. C. and Carson, D. D., 2009. Multifunctionality of extracellular and cell surface heparan sulfate proteoglycans. *Cell Mol Life Sci.* 66(21): 3421-3434.

- Kleemann, R. U., Kroker, D., Cedraro, A., Tuischer, J. and Duda, G. N., 2005. Altered cartilage mechanics and histology in knee osteoarthritis: relation to clinical assessment (ICRS Grade). *Osteoarthritis Cartilage*. 13(11): 958-963.
- Knight, M. M., Lee, D. A. and Bader, D. L., 1998. The influence of elaborated pericellular matrix on the deformation of isolated articular chondrocytes cultured in agarose. *Biochim Biophys Acta*. 1405(1-3): 67-77.
- Knight, M. M., Ross, J. M., Sherwin, A. F., Lee, D. A., Bader, D. L. and Poole, C. A., 2001. Chondrocyte deformation within mechanically and enzymatically extracted chondrons compressed in agarose. *Biochim Biophys Acta*. 1526(2): 141-146.
- Knox, S., Merry, C., Stringer, S., Melrose, J. and Whitelock, J., 2002. Not all perlecan are created equal: interactions with fibroblast growth factor (FGF) 2 and FGF receptors. *J Biol Chem*. 277(17): 14657-14665.
- Knudson, C. B., 1993. Hyaluronan receptor-directed assembly of chondrocyte pericellular matrix. *J Cell Biol*. 120(3): 825-834.
- Knudson, C. B., 2003. Hyaluronan and CD44: strategic players for cell-matrix interactions during chondrogenesis and matrix assembly. *Birth Defects Res C Embryo Today*. 69(2): 174-196.
- Knudson, C. B. and Knudson, W., 2001. Cartilage proteoglycans. *Semin Cell Dev Biol*. 12(2): 69-78.
- Knudson, W., Aguiar, D. J., Hua, Q. and Knudson, C. B., 1996. CD44-anchored hyaluronan-rich pericellular matrices: an ultrastructural and biochemical analysis. *Exp Cell Res*. 228(2): 216-228.
- Korhonen, R. K. and Herzog, W., 2008. Depth-dependent analysis of the role of collagen fibrils, fixed charges and fluid in the pericellular matrix of articular cartilage on chondrocyte mechanics. *J Biomech*. 41(2): 480-485.
- Korhonen, R. K., Julkunen, P., Rieppo, J., Lappalainen, R., Konttinen, Y. T. and Jurvelin, J. S., 2006. Collagen network of articular cartilage modulates fluid flow and mechanical stresses in chondrocyte. *Biomech Model Mechanobiol*. 5(2-3): 150-159.
- Korhonen, R. K., Laasanen, M. S., Toyras, J., Lappalainen, R., Helminen, H. J. and Jurvelin, J. S., 2003. Fibril reinforced poroelastic model predicts specifically

mechanical behavior of normal, proteoglycan depleted and collagen degraded articular cartilage. *J Biomech.* 36(9): 1373-1379.

Krishnan, P., Hocking, A. M., Scholtz, J. M., Pace, C. N., Holik, K. K. and McQuillan, D. J., 1999. Distinct secondary structures of the leucine-rich repeat proteoglycans decorin and biglycan. Glycosylation-dependent conformational stability. *J Biol Chem.* 274(16): 10945-10950.

Kvist, A. J., Johnson, A. E., Morgelin, M., Gustafsson, E., Bengtsson, E., Lindblom, K., Aszodi, A., Fassler, R., Sasaki, T., Timpl, R. and Aspberg, A., 2006. Chondroitin sulfate perlecan enhances collagen fibril formation. Implications for perlecan chondrodysplasias. *J Biol Chem.* 281(44): 33127-33139.

Kvist, A. J., Nystrom, A., Hultenby, K., Sasaki, T., Talts, J. F. and Aspberg, A., 2008. The major basement membrane components localize to the chondrocyte pericellular matrix--a cartilage basement membrane equivalent? *Matrix Biol.* 27(1): 22-33.

Laasanen, M. S., Toyras, J., Korhonen, R. K., Rieppo, J., Saarakkala, S., Nieminen, M. T., Hirvonen, J. and Jurvelin, J. S., 2003. Biomechanical properties of knee articular cartilage. *Biorheology.* 40(1-3): 133-140.

Lai, W. M., Hou, J. S. and Mow, V. C., 1991. A triphasic theory for the swelling and deformation behaviors of articular cartilage. *J Biomech Eng.* 113(3): 245-258.

Lai, W. M., Sun, D. D., Ateshian, G. A., Guo, X. E. and Mow, V. C., 2002. Electrical signals for chondrocytes in cartilage. *Biorheology.* 39(1-2): 39-45.

Lang, A., Horler, D. and Baici, A., 2000. The relative importance of cysteine peptidases in osteoarthritis. *J Rheumatol.* 27(8): 1970-1979.

Lark, M. W., Bayne, E. K., Flanagan, J., Harper, C. F., Hoerrner, L. A., Hutchinson, N. I., Singer, II, Donatelli, S. A., Weidner, J. R., Williams, H. R., Mumford, R. A. and Lohmander, L. S., 1997. Aggrecan degradation in human cartilage. Evidence for both matrix metalloproteinase and aggrecanase activity in normal, osteoarthritic, and rheumatoid joints. *J Clin Invest.* 100(1): 93-106.

Last, J. A., Liliensiek, S. J., Nealey, P. F. and Murphy, C. J., 2009. Determining the mechanical properties of human corneal basement membranes with atomic force microscopy. *J Struct Biol.* 167(1): 19-24.

- Le, N. A. and Fleming, B. C., 2008. Measuring fixed charge density of goat articular cartilage using indentation methods and biochemical analysis. *J Biomech.* 41(3): 715-720.
- Lee, D. A. and Bader, D. L., 1995. The development and characterization of an in vitro system to study strain-induced cell deformation in isolated chondrocytes. *In Vitro Cell Dev Biol Anim.* 31(11): 828-835.
- Lee, G. M., Johnstone, B., Jacobson, K. and Caterson, B., 1993. The dynamic structure of the pericellular matrix on living cells. *J Cell Biol.* 123(6 Pt 2): 1899-1907.
- Lee, G. M., Paul, T. A., Slabaugh, M. and Kelley, S. S., 2000. The incidence of enlarged chondrons in normal and osteoarthritic human cartilage and their relative matrix density. *Osteoarthritis Cartilage.* 8(1): 44-52.
- Leipzig, N. D. and Athanasiou, K. A., 2005. Unconfined creep compression of chondrocytes. *J Biomech.* 38(1): 77-85.
- LeRoux, M. A., Arokoski, J., Vail, T. P., Guilak, F., Hyttinen, M. M., Kiviranta, I. and Setton, L. A., 2000. Simultaneous changes in the mechanical properties, quantitative collagen organization, and proteoglycan concentration of articular cartilage following canine meniscectomy. *J Orthop Res.* 18(3): 383-392.
- Lewis, N. T., Hussain, M. A. and Mao, J. J., 2008. Investigation of nano-mechanical properties of annulus fibrosus using atomic force microscopy. *Micron.* 39(7): 1008-1019.
- Li, L. P., Buschmann, M. D. and Shirazi-Adl, A., 2003. Strain-rate dependent stiffness of articular cartilage in unconfined compression. *J Biomech Eng.* 125(2): 161-168.
- Little, C. B., Hughes, C. E., Curtis, C. L., Janusz, M. J., Bohne, R., Wang-Weigand, S., Taiwo, Y. O., Mitchell, P. G., Otterness, I. G., Flannery, C. R. and Caterson, B., 2002. Matrix metalloproteinases are involved in C-terminal and interglobular domain processing of cartilage aggrecan in late stage cartilage degradation. *Matrix Biol.* 21(3): 271-288.
- Loparic, M., Wirz, D., Daniels, A. U., Raiteri, R., Vanlandingham, M. R., Guex, G., Martin, I., Aebi, U. and Stolz, M., 2010. Micro- and nanomechanical analysis of articular cartilage by indentation-type atomic force microscopy: validation with a gel-microfiber composite. *Biophys J.* 98(11): 2731-2740.

- Ludwig, T., Kirmse, R., Poole, K. and Schwarz, U. S., 2008. Probing cellular microenvironments and tissue remodeling by atomic force microscopy. *Pflugers Arch.* 456(1): 29-49.
- Lyyra, T., Arokoski, J. P., Oksala, N., Vihko, A., Hyttinen, M., Jurvelin, J. S. and Kiviranta, I., 1999. Experimental validation of arthroscopic cartilage stiffness measurement using enzymatically degraded cartilage samples. *Phys Med Biol.* 44(2): 525-535.
- Magnussen, R. A., Guilak, F. and Vail, T. P., 2005. Cartilage degeneration in post-collapse cases of osteonecrosis of the human femoral head: altered mechanical properties in tension, compression, and shear. *J Orthop Res.* 23(3): 576-583.
- Maleski, M. P. and Knudson, C. B., 1996. Matrix accumulation and retention in embryonic cartilage and in vitro chondrogenesis. *Connect Tissue Res.* 34(1): 75-86.
- Maroudas, A., Bayliss, M. T., Uchitel-Kaushansky, N., Schneiderman, R. and Gilav, E., 1998. Aggrecan turnover in human articular cartilage: use of aspartic acid racemization as a marker of molecular age. *Arch Biochem Biophys.* 350(1): 61-71.
- Maroudas, A., Bayliss, M. T. and Venn, M. F., 1980. Further studies on the composition of human femoral head cartilage. *Ann Rheum Dis.* 39(5): 514-523.
- Maroudas, A. and Venn, M., 1977. Chemical composition and swelling of normal and osteoarthrotic femoral head cartilage. II. Swelling. *Ann Rheum Dis.* 36(5): 399-406.
- Martel-Pelletier, J., Boileau, C., Pelletier, J. P. and Roughley, P. J., 2008. Cartilage in normal and osteoarthritis conditions. *Best Pract Res Clin Rheumatol.* 22(2): 351-384.
- Martin, I., Obradovic, B., Freed, L. E. and Vunjak-Novakovic, G., 1999. Method for quantitative analysis of glycosaminoglycan distribution in cultured natural and engineered cartilage. *Ann Biomed Eng.* 27(5): 656-662.
- Martin, J. A., Miller, B. A., Scherb, M. B., Lembke, L. A. and Buckwalter, J. A., 2002. Co-localization of insulin-like growth factor binding protein 3 and fibronectin in human articular cartilage. *Osteoarthritis Cartilage.* 10(7): 556-563.
- Matsuo, E. S., Orkisz, M., Sun, S. T., Li, Y. and Tanaka, T., 1994. Origin of Structural Inhomogeneities in Polymer Gels. *Macromolecules.* 27(23): 6791-6796.

- McDevitt, C. A., 1973. Biochemistry of articular cartilage. Nature of proteoglycans and collagen of articular cartilage and their role in ageing and in osteoarthritis. *Ann Rheum Dis.* 32(4): 364-378.
- McDevitt, C. A., Marcelino, J. and Tucker, L., 1991. Interaction of intact type VI collagen with hyaluronan. *FEBS Lett.* 294(3): 167-170.
- McDevitt, C. A. and Muir, H., 1976. Biochemical changes in the cartilage of the knee in experimental and natural osteoarthritis in the dog. *J Bone Joint Surg Br.* 58(1): 94-101.
- McLeod, M. A., Wilusz, R. E. and Guilak, F., 2013. Depth-dependent anisotropy of the micromechanical properties of the extracellular and pericellular matrices of articular cartilage evaluated via atomic force microscopy. *J Biomech.* 46(3): 586-592.
- Meachim, G., Denham, D., Emery, I. H. and Wilkinson, P. H., 1974. Collagen alignments and artificial splits at the surface of human articular cartilage. *J Anat.* 118(Pt 1): 101-118.
- Melching, L. I., Fisher, W. D., Lee, E. R., Mort, J. S. and Roughley, P. J., 2006. The cleavage of biglycan by aggrecanases. *Osteoarthritis Cartilage.* 14(11): 1147-1154.
- Melrose, J., Fuller, E. S., Roughley, P. J., Smith, M. M., Kerr, B., Hughes, C. E., Caterson, B. and Little, C. B., 2008a. Fragmentation of decorin, biglycan, lumican and keratocan is elevated in degenerate human meniscus, knee and hip articular cartilages compared with age-matched macroscopically normal and control tissues. *Arthritis Res Ther.* 10(4): R79.
- Melrose, J., Hayes, A. J., Whitelock, J. M. and Little, C. B., 2008b. Perlecan, the "jack of all trades" proteoglycan of cartilaginous weight-bearing connective tissues. *Bioessays.* 30(5): 457-469.
- Melrose, J., Roughley, P., Knox, S., Smith, S., Lord, M. and Whitelock, J., 2006. The structure, location, and function of perlecan, a prominent pericellular proteoglycan of fetal, postnatal, and mature hyaline cartilages. *J Biol Chem.* 281(48): 36905-36914.

- Melrose, J., Smith, S., Cake, M., Read, R. and Whitelock, J., 2005. Perlecan displays variable spatial and temporal immunolocalisation patterns in the articular and growth plate cartilages of the ovine stifle joint. *Histochem Cell Biol.* 123(6): 561-571.
- Menninger, H., Burkhardt, H., Roske, W., Ehlebracht, W., Hering, B., Gurr, E., Mohr, W. and Mierau, H. D., 1981. Lysosomal elastase: effect on mechanical and biochemical properties of normal cartilage, inhibition by polysulfonated glycosaminoglycan, and binding to chondrocytes. *Rheumatol Int.* 1(2): 73-81.
- Michalek, A. J. and Iatridis, J. C., 2007. A numerical study to determine pericellular matrix modulus and evaluate its effects on the micromechanical environment of chondrocytes. *J Biomech.* 40(6): 1405-1409.
- Mio, K. and Stern, R., 2002. Inhibitors of the hyaluronidases. *Matrix Biol.* 21(1): 31-37.
- Mizrahi, J., Maroudas, A., Lanir, Y., Ziv, I. and Webber, T. J., 1986. The "instantaneous" deformation of cartilage: effects of collagen fiber orientation and osmotic stress. *Biorheology.* 23(4): 311-330.
- Mok, M. T., Ilic, M. Z., Handley, C. J. and Robinson, H. C., 1992. Cleavage of proteoglycan aggregate by leucocyte elastase. *Arch Biochem Biophys.* 292(2): 442-447.
- Momohara, S., Kashiwazaki, S., Inoue, K., Saito, S. and Nakagawa, T., 1997. Elastase from polymorphonuclear leukocyte in articular cartilage and synovial fluids of patients with rheumatoid arthritis. *Clin Rheumatol.* 16(2): 133-140.
- Monfort, J., Tardif, G., Reboul, P., Mineau, F., Roughley, P., Pelletier, J. P. and Martel-Pelletier, J., 2006. Degradation of small leucine-rich repeat proteoglycans by matrix metalloprotease-13: identification of a new biglycan cleavage site. *Arthritis Res Ther.* 8(1): R26.
- Moreno Flores, S. and Toca-Herrera, J. L., 2009. The new future of scanning probe microscopy: Combining atomic force microscopy with other surface-sensitive techniques, optical microscopy and fluorescence techniques. *Nanoscale.* 1(1): 40-49.

- Morgelin, M., Paulsson, M., Hardingham, T. E., Heinegard, D. and Engel, J., 1988. Cartilage proteoglycans. Assembly with hyaluronate and link protein as studied by electron microscopy. *Biochem J.* 253(1): 175-185.
- Mourao, P. A., 1988. Distribution of chondroitin 4-sulfate and chondroitin 6-sulfate in human articular and growth cartilage. *Arthritis Rheum.* 31(8): 1028-1033.
- Mow, V. C., Ateshian, G. A., Lai, W. M. and Gu, W. Y., 1998. Effects of fixed charges on the stress-relaxation behavior of hydrated soft tissues in a confined compression problem. *International Journal of Solids and Structures.* 35(34-35): 4945-4962.
- Mow, V. C., Bachrach, N. M., Setton, L. A. and Guilak, F., 1994. Stress, Strain, Pressure, and Flow Fields in Articular Cartilage and Chondrocytes. *Cell Mechanics and Cellular Engineering.* V. C. Mow, F. Guilak, R. Tran-Son-Tay and R. M. Hochmuth. New York, Springer-Verlag: 345-379.
- Mow, V. C. and Guo, X. E., 2002. Mechano-electrochemical properties of articular cartilage: their inhomogeneities and anisotropies. *Annu Rev Biomed Eng.* 4: 175-209.
- Mow, V. C., Kuei, S. C., Lai, W. M. and Armstrong, C. G., 1980. Biphasic creep and stress relaxation of articular cartilage in compression? Theory and experiments. *J Biomech Eng.* 102(1): 73-84.
- Mow, V. C., Ratcliffe, A. and Poole, A. R., 1992. Cartilage and diarthrodial joints as paradigms for hierarchical materials and structures. *Biomaterials.* 13(2): 67-97.
- Muir, H., Bullough, P. and Maroudas, A., 1970. The distribution of collagen in human articular cartilage with some of its physiological implications. *J Bone Joint Surg Br.* 52(3): 554-563.
- Murray, D. H., Bush, P. G., Brenkel, I. J. and Hall, A. C., 2010. Abnormal human chondrocyte morphology is related to increased levels of cell-associated IL-1beta and disruption to pericellular collagen type VI. *J Orthop Res.* 28(11): 1507-1514.
- Nagase, H. and Kashiwagi, M., 2003. Aggrecanases and cartilage matrix degradation. *Arthritis Res Ther.* 5(2): 94-103.
- Nakada, H. I. and Wolfe, J. B., 1961. Studies on the enzyme chondroitinase: product structure and ion effects. *Arch Biochem Biophys.* 94: 244-251.

- Nguyen, B. V., Wang, Q. G., Kuiper, N. J., El Haj, A. J., Thomas, C. R. and Zhang, Z., 2010. Biomechanical properties of single chondrocytes and chondrons determined by micromanipulation and finite-element modelling. *J R Soc Interface*.
- Nicodemus, G. D. and Bryant, S. J., 2008. The role of hydrogel structure and dynamic loading on chondrocyte gene expression and matrix formation. *J Biomech*. 41(7): 1528-1536.
- Obeid, E. M., Adams, M. A. and Newman, J. H., 1994. Mechanical properties of articular cartilage in knees with unicompartmental osteoarthritis. *J Bone Joint Surg Br*. 76(2): 315-319.
- Obrink, B., Laurent, T. C. and Carlsson, B., 1975. The binding of chondroitin sulphate to collagen. *FEBS Lett*. 56(1): 166-169.
- Oegema, T. R., Jr., Laidlaw, J., Hascall, V. C. and Dziewiatkowski, D. D., 1975. The effect of proteoglycans on the formation of fibrils from collagen solutions. *Arch Biochem Biophys*. 170(2): 698-709.
- Ohya, T. and Kaneko, Y., 1970. Novel hyaluronidase from streptomyces. *Biochim Biophys Acta*. 198(3): 607-609.
- Owen, C. A. and Campbell, E. J., 1999. The cell biology of leukocyte-mediated proteolysis. *J Leukoc Biol*. 65(2): 137-150.
- Park, S., Costa, K. D., Ateshian, G. A. and Hong, K. S., 2009. Mechanical properties of bovine articular cartilage under microscale indentation loading from atomic force microscopy. *Proc Inst Mech Eng [H]*. 223(3): 339-347.
- Paulsson, M., Morgelin, M., Wiedemann, H., Beardmore-Gray, M., Dunham, D., Hardingham, T., Heinegard, D., Timpl, R. and Engel, J., 1987. Extended and globular protein domains in cartilage proteoglycans. *Biochem J*. 245(3): 763-772.
- Pelham, R. J., Jr. and Wang, Y., 1997. Cell locomotion and focal adhesions are regulated by substrate flexibility. *Proc Natl Acad Sci U S A*. 94(25): 13661-13665.
- Peyton, S. R. and Putnam, A. J., 2005. Extracellular matrix rigidity governs smooth muscle cell motility in a biphasic fashion. *J Cell Physiol*. 204(1): 198-209.

- Plaas, A., Osborn, B., Yoshihara, Y., Bai, Y., Bloom, T., Nelson, F., Mikecz, K. and Sandy, J. D., 2007. Aggrecanolytic in human osteoarthritis: confocal localization and biochemical characterization of ADAMTS5-hyaluronan complexes in articular cartilages. *Osteoarthritis Cartilage*. 15(7): 719-734.
- Polur, I., Lee, P. L., Servais, J. M., Xu, L. and Li, Y., 2010. Role of HTRA1, a serine protease, in the progression of articular cartilage degeneration. *Histol Histopathol*. 25(5): 599-608.
- Poole, A. R., Guilak, F. and Abramson, S. A., 2007. Etiopathogenesis of Osteoarthritis. *Osteoarthritis: Diagnosis and Medical/Surgical Management*. R. W. Moskowitz, R. D. Altman, M. C. Hochberg, J. A. Buckwalter and V. M. Goldberg. Philadelphia, PA, Lippincott, Williams & Wilkins: 27-49.
- Poole, A. R., Pidoux, I., Reiner, A. and Rosenberg, L., 1982. An immunoelectron microscope study of the organization of proteoglycan monomer, link protein, and collagen in the matrix of articular cartilage. *J Cell Biol*. 93(3): 921-937.
- Poole, A. R., Rosenberg, L. C., Reiner, A., Ionescu, M., Bogoch, E. and Roughley, P. J., 1996. Contents and distributions of the proteoglycans decorin and biglycan in normal and osteoarthritic human articular cartilage. *J Orthop Res*. 14(5): 681-689.
- Poole, C. A., 1997. Articular cartilage chondrons: form, function and failure. *J Anat*. 191(Pt 1): 1-13.
- Poole, C. A., Ayad, S. and Gilbert, R. T., 1992. Chondrons from articular cartilage. V. Immunohistochemical evaluation of type VI collagen organisation in isolated chondrons by light, confocal and electron microscopy. *J Cell Sci*. 103 (Pt 4): 1101-1110.
- Poole, C. A., Ayad, S. and Schofield, J. R., 1988. Chondrons from articular cartilage: I. Immunolocalization of type VI collagen in the pericellular capsule of isolated canine tibial chondrons. *J Cell Sci*. 90 (Pt 4): 635-643.
- Poole, C. A., Flint, M. H. and Beaumont, B. W., 1984. Morphological and functional interrelationships of articular cartilage matrices. *J Anat*. 138 (Pt 1): 113-138.
- Poole, C. A., Flint, M. H. and Beaumont, B. W., 1985. Morphology of the pericellular capsule in articular cartilage revealed by hyaluronidase digestion. *J Ultrastruct Res*. 91(1): 13-23.

- Poole, C. A., Flint, M. H. and Beaumont, B. W., 1987. Chondrons in cartilage: ultrastructural analysis of the pericellular microenvironment in adult human articular cartilages. *J Orthop Res.* 5(4): 509-522.
- Poole, C. A., Gilbert, R. T., Herbage, D. and Hartmann, D. J., 1997. Immunolocalization of type IX collagen in normal and spontaneously osteoarthritic canine tibial cartilage and isolated chondrons. *Osteoarthritis Cartilage.* 5(3): 191-204.
- Poole, C. A., Glant, T. T. and Schofield, J. R., 1991a. Chondrons from articular cartilage. (IV). Immunolocalization of proteoglycan epitopes in isolated canine tibial chondrons. *J Histochem Cytochem.* 39(9): 1175-1187.
- Poole, C. A., Matsuoka, A. and Schofield, J. R., 1991b. Chondrons from articular cartilage. III. Morphologic changes in the cellular microenvironment of chondrons isolated from osteoarthritic cartilage. *Arthritis Rheum.* 34(1): 22-35.
- Price, F. M., Levick, J. R. and Mason, R. M., 1996. Glycosaminoglycan concentration in synovium and other tissues of rabbit knee in relation to synovial hydraulic resistance. *J Physiol.* 495 (Pt 3): 803-820.
- Pritzker, K. P., Gay, S., Jimenez, S. A., Ostergaard, K., Pelletier, J. P., Revell, P. A., Salter, D. and van den Berg, W. B., 2006. Osteoarthritis cartilage histopathology: grading and staging. *Osteoarthritis Cartilage.* 14(1): 13-29.
- Pullig, O., Weseloh, G. and Swoboda, B., 1999. Expression of type VI collagen in normal and osteoarthritic human cartilage. *Osteoarthritis Cartilage.* 7(2): 191-202.
- Quinn, T. M., Hunziker, E. B. and Hauselmann, H. J., 2005. Variation of cell and matrix morphologies in articular cartilage among locations in the adult human knee. *Osteoarthritis Cartilage.* 13(8): 672-678.
- Radhakrishnan, P., Lewis, N. T. and Mao, J. J., 2004. Zone-specific micromechanical properties of the extracellular matrices of growth plate cartilage. *Ann Biomed Eng.* 32(2): 284-291.
- Radmacher, M., Fritz, M. and Hansma, P. K., 1995. Imaging soft samples with the atomic force microscope: gelatin in water and propanol. *Biophys J.* 69(1): 264-270.

- Radmacher, M., Tillmann, R. W., Fritz, M. and Gaub, H. E., 1992. From molecules to cells: imaging soft samples with the atomic force microscope. *Science*. 257(5078): 1900-1905.
- Rieppo, J., Hyttinen, M. M., Halmesmaki, E., Ruotsalainen, H., Vasara, A., Kiviranta, I., Jurvelin, J. S. and Helminen, H. J., 2009. Changes in spatial collagen content and collagen network architecture in porcine articular cartilage during growth and maturation. *Osteoarthritis Cartilage*. 17(4): 448-455.
- Rilla, K., Tiihonen, R., Kultti, A., Tammi, M. and Tammi, R., 2008. Pericellular hyaluronan coat visualized in live cells with a fluorescent probe is scaffolded by plasma membrane protrusions. *J Histochem Cytochem*. 56(10): 901-910.
- Rizkalla, G., Reiner, A., Bogoch, E. and Poole, A. R., 1992. Studies of the articular cartilage proteoglycan aggrecan in health and osteoarthritis. Evidence for molecular heterogeneity and extensive molecular changes in disease. *J Clin Invest*. 90(6): 2268-2277.
- Rosenberg, L., Johnson, B. and Schubert, M., 1965. Proteinpolysaccharides from human articular and costal cartilage. *J Clin Invest*. 44(10): 1647-1656.
- Rossi, M., Morita, H., Sormunen, R., Airene, S., Kreivi, M., Wang, L., Fukai, N., Olsen, B. R., Tryggvason, K. and Soininen, R., 2003. Heparan sulfate chains of perlecan are indispensable in the lens capsule but not in the kidney. *EMBO J*. 22(2): 236-245.
- Rotsch, C., Braet, F., Wisse, E. and Radmacher, M., 1997. AFM imaging and elasticity measurements on living rat liver macrophages. *Cell Biol Int*. 21(11): 685-696.
- Roughley, P. J., 2001. Articular cartilage and changes in arthritis: noncollagenous proteins and proteoglycans in the extracellular matrix of cartilage. *Arthritis Res*. 3(6): 342-347.
- Roughley, P. J., 2006. The structure and function of cartilage proteoglycans. *Eur Cell Mater*. 12: 92-101.
- Roughley, P. J., Barnett, J., Zuo, F. and Mort, J. S., 2003. Variations in aggrecan structure modulate its susceptibility to aggrecanases. *Biochem J*. 375(Pt 1): 183-189.

- Roughley, P. J., White, R. J., Magny, M. C., Liu, J., Pearce, R. H. and Mort, J. S., 1993. Non-proteoglycan forms of biglycan increase with age in human articular cartilage. *Biochem J.* 295 (Pt 2): 421-426.
- Samosky, J. T., Burstein, D., Eric Grimson, W., Howe, R., Martin, S. and Gray, M. L., 2005. Spatially-localized correlation of dGEMRIC-measured GAG distribution and mechanical stiffness in the human tibial plateau. *J Orthop Res.* 23(1): 93-101.
- Sandell, L. J., 2007. Anabolic factors in degenerative joint disease. *Curr Drug Targets.* 8(2): 359-365.
- Sandell, L. J. and Aigner, T., 2001. Articular cartilage and changes in arthritis. An introduction: cell biology of osteoarthritis. *Arthritis Res.* 3(2): 107-113.
- Sandy, J. D., Neame, P. J., Boynton, R. E. and Flannery, C. R., 1991. Catabolism of aggrecan in cartilage explants. Identification of a major cleavage site within the interglobular domain. *J Biol Chem.* 266(14): 8683-8685.
- Sandy, J. D., O'Neill, J. R. and Ratzlaff, L. C., 1989. Acquisition of hyaluronate-binding affinity in vivo by newly synthesized cartilage proteoglycans. *Biochem J.* 258(3): 875-880.
- Sato, M., Suzuki, K., Ueki, Y. and Ohashi, T., 2007. Microelastic mapping of living endothelial cells exposed to shear stress in relation to three-dimensional distribution of actin filaments. *Acta Biomater.* 3(3): 311-319.
- Schinagl, R. M., Gurskis, D., Chen, A. C. and Sah, R. L., 1997. Depth-dependent confined compression modulus of full-thickness bovine articular cartilage. *J Orthop Res.* 15(4): 499-506.
- Schmidt, M. B., Mow, V. C., Chun, L. E. and Eyre, D. R., 1990. Effects of proteoglycan extraction on the tensile behavior of articular cartilage. *J Orthop Res.* 8(3): 353-363.
- Scott, J. E., 1988. Proteoglycan-fibrillar collagen interactions. *Biochem J.* 252(2): 313-323.
- Scott, J. E. and Stockwell, R. A., 2006. Cartilage elasticity resides in shape module decoran and aggrecan sumps of damping fluid: implications in osteoarthrosis. *J Physiol.* 574(Pt 3): 643-650.

- Sen, S. and Kumar, S., 2009. Combining mechanical and optical approaches to dissect cellular mechanobiology. *J Biomech.*
- Setton, L. A., Elliott, D. M. and Mow, V. C., 1999. Altered mechanics of cartilage with osteoarthritis: human osteoarthritis and an experimental model of joint degeneration. *Osteoarthritis Cartilage.* 7(1): 2-14.
- Shieh, A. C. and Athanasiou, K. A., 2006. Biomechanics of single zonal chondrocytes. *J Biomech.* 39(9): 1595-1602.
- Silver, F. H., Bradica, G. and Tria, A., 2004. Do changes in the mechanical properties of articular cartilage promote catabolic destruction of cartilage and osteoarthritis? *Matrix Biol.* 23(7): 467-476.
- Smith, S. M., West, L. A., Govindraj, P., Zhang, X., Ornitz, D. M. and Hassell, J. R., 2007. Heparan and chondroitin sulfate on growth plate perlecan mediate binding and delivery of FGF-2 to FGF receptors. *Matrix Biol.* 26(3): 175-184.
- Snyder, P. W., Johannes, M. S., Vogen, B. N., Clark, R. L. and Toone, E. J., 2007. Biocatalytic microcontact printing. *J Org Chem.* 72(19): 7459-7461.
- Soder, S., Hambach, L., Lissner, R., Kirchner, T. and Aigner, T., 2002. Ultrastructural localization of type VI collagen in normal adult and osteoarthritic human articular cartilage. *Osteoarthritis Cartilage.* 10(6): 464-470.
- Solau-Gervais, E., Zerimech, F., Lemaire, R., Fontaine, C., Huet, G. and Flipo, R. M., 2007. Cysteine and serine proteases of synovial tissue in rheumatoid arthritis and osteoarthritis. *Scand J Rheumatol.* 36(5): 373-377.
- Song, R. H., Tortorella, M. D., Malfait, A. M., Alston, J. T., Yang, Z., Arner, E. C. and Griggs, D. W., 2007. Aggrecan degradation in human articular cartilage explants is mediated by both ADAMTS-4 and ADAMTS-5. *Arthritis Rheum.* 56(2): 575-585.
- Specks, U., Mayer, U., Nischt, R., Spissinger, T., Mann, K., Timpl, R., Engel, J. and Chu, M. L., 1992. Structure of recombinant N-terminal globule of type VI collagen alpha 3 chain and its binding to heparin and hyaluronan. *EMBO J.* 11(12): 4281-4290.
- Starkey, P. M., Barrett, A. J. and Burleigh, M. C., 1977. The degradation of articular collagen by neutrophil proteinases. *Biochim Biophys Acta.* 483(2): 386-397.

- Stockwell, R. A., 1971. The interrelationship of cell density and cartilage thickness in mammalian articular cartilage. *J Anat.* 109(Pt 3): 411-421.
- Stockwell, R. A. and Scott, J. E., 1967. Distribution of acid glycosaminoglycans in human articular cartilage. *Nature.* 215(5108): 1376-1378.
- Stolz, M., Gottardi, R., Raiteri, R., Miot, S., Martin, I., Imer, R., Stauffer, U., Raducanu, A., Duggelin, M., Baschong, W., Daniels, A. U., Friederich, N. F., Aszodi, A. and Aebi, U., 2009. Early detection of aging cartilage and osteoarthritis in mice and patient samples using atomic force microscopy. *Nat Nanotechnol.* 4(3): 186-192.
- Stolz, M., Raiteri, R., Daniels, A. U., VanLandingham, M. R., Baschong, W. and Aebi, U., 2004. Dynamic elastic modulus of porcine articular cartilage determined at two different levels of tissue organization by indentation-type atomic force microscopy. *Biophys J.* 86(5): 3269-3283.
- Struglics, A. and Hansson, M., 2012. MMP proteolysis of the human extracellular matrix protein aggrecan is mainly a process of normal turnover. *Biochem J.* 446(2): 213-223.
- Sun, D. D., Guo, X. E., Likhitpanichkul, M., Lai, W. M. and Mow, V. C., 2004. The influence of the fixed negative charges on mechanical and electrical behaviors of articular cartilage under unconfined compression. *J Biomech Eng.* 126(1): 6-16.
- SundarRaj, N., Fite, D., Ledbetter, S., Chakravarti, S. and Hassell, J. R., 1995. Perlecan is a component of cartilage matrix and promotes chondrocyte attachment. *J Cell Sci.* 108 (Pt 7): 2663-2672.
- Tesche, F. and Miosge, N., 2004. Perlecan in late stages of osteoarthritis of the human knee joint. *Osteoarthritis Cartilage.* 12(11): 852-862.
- Thomopoulos, S., Williams, G. R., Gimbel, J. A., Favata, M. and Soslowsky, L. J., 2003. Variation of biomechanical, structural, and compositional properties along the tendon to bone insertion site. *J Orthop Res.* 21(3): 413-419.
- Tillet, E., Wiedemann, H., Golbik, R., Pan, T. C., Zhang, R. Z., Mann, K., Chu, M. L. and Timpl, R., 1994. Recombinant expression and structural and binding properties of alpha 1(VI) and alpha 2(VI) chains of human collagen type VI. *Eur J Biochem.* 221(1): 177-185.

- Tomkoria, S., Patel, R. V. and Mao, J. J., 2004. Heterogeneous nanomechanical properties of superficial and zonal regions of articular cartilage of the rabbit proximal radius condyle by atomic force microscopy. *Med Eng Phys.* 26(10): 815-822.
- Tortorella, M. D., Pratta, M., Liu, R. Q., Austin, J., Ross, O. H., Abbaszade, I., Burn, T. and Arner, E., 2000. Sites of aggrecan cleavage by recombinant human aggrecanase-1 (ADAMTS-4). *J Biol Chem.* 275(24): 18566-18573.
- Tracqui, P., Broisat, A., Toczek, J., Mesnier, N., Ohayon, J. and Riou, L., 2011. Mapping elasticity moduli of atherosclerotic plaque in situ via atomic force microscopy. *J Struct Biol.* 174(1): 115-123.
- Trickey, W. R., Baaijens, F. P., Laursen, T. A., Alexopoulos, L. G. and Guilak, F., 2006. Determination of the Poisson's ratio of the cell: recovery properties of chondrocytes after release from complete micropipette aspiration. *J Biomech.* 39(1): 78-87.
- Trickey, W. R., Lee, G. M. and Guilak, F., 2000. Viscoelastic properties of chondrocytes from normal and osteoarthritic human cartilage. *J Orthop Res.* 18(6): 891-898.
- Trickey, W. R., Vail, T. P. and Guilak, F., 2004. The role of the cytoskeleton in the viscoelastic properties of human articular chondrocytes. *J Orthop Res.* 22(1): 131-139.
- Vanden Berg-Foels, W. S., Scipioni, L., Huynh, C. and Wen, X., 2012. Helium ion microscopy for high-resolution visualization of the articular cartilage collagen network. *J Microsc.* 246(2): 168-176.
- Venn, M. and Maroudas, A., 1977. Chemical composition and swelling of normal and osteoarthrotic femoral head cartilage. I. Chemical composition. *Ann Rheum Dis.* 36(2): 121-129.
- Venn, M. F., 1978. Variation of chemical composition with age in human femoral head cartilage. *Ann Rheum Dis.* 37(2): 168-174.
- Verma, P. and Dalal, K., 2011. ADAMTS-4 and ADAMTS-5: key enzymes in osteoarthritis. *J Cell Biochem.* 112(12): 3507-3514.

- Verzijl, N., DeGroot, J., Thorpe, S. R., Bank, R. A., Shaw, J. N., Lyons, T. J., Bijlsma, J. W., Lafeber, F. P., Baynes, J. W. and TeKoppele, J. M., 2000. Effect of collagen turnover on the accumulation of advanced glycation end products. *J Biol Chem.* 275(50): 39027-39031.
- Villanueva, I., Weigel, C. A. and Bryant, S. J., 2009. Cell-matrix interactions and dynamic mechanical loading influence chondrocyte gene expression and bioactivity in PEG-RGD hydrogels. *Acta Biomater.* 5(8): 2832-2846.
- Vincent, T., Hermansson, M., Bolton, M., Wait, R. and Saklatvala, J., 2002. Basic FGF mediates an immediate response of articular cartilage to mechanical injury. *Proc Natl Acad Sci U S A.* 99(12): 8259-8264.
- Vincent, T. L., Hermansson, M. A., Hansen, U. N., Amis, A. A. and Saklatvala, J., 2004. Basic fibroblast growth factor mediates transduction of mechanical signals when articular cartilage is loaded. *Arthritis Rheum.* 50(2): 526-533.
- Vincent, T. L., McLean, C. J., Full, L. E., Peston, D. and Saklatvala, J., 2007. FGF-2 is bound to perlecan in the pericellular matrix of articular cartilage, where it acts as a chondrocyte mechanotransducer. *Osteoarthritis Cartilage.* 15(7): 752-763.
- Vogel, K. G., 1994. Glycosaminoglycans and Proteoglycans. *Extracellular Matrix Assembly and Structure.* P. D. Yurchenco, D. E. Birk and R. P. Mecham. New York, Academic Press: 243 -279.
- Wang, C. C., Chahine, N. O., Hung, C. T. and Ateshian, G. A., 2003. Optical determination of anisotropic material properties of bovine articular cartilage in compression. *J Biomech.* 36(3): 339-353.
- Wang, C. C., Deng, J. M., Ateshian, G. A. and Hung, C. T., 2002a. An automated approach for direct measurement of two-dimensional strain distributions within articular cartilage under unconfined compression. *J Biomech Eng.* 124(5): 557-567.
- Wang, C. C., Guo, X. E., Sun, D., Mow, V. C., Ateshian, G. A. and Hung, C. T., 2002b. The functional environment of chondrocytes within cartilage subjected to compressive loading: a theoretical and experimental approach. *Biorheology.* 39(1-2): 11-25.
- Wang, Q. G., El Haj, A. J. and Kuiper, N. J., 2008. Glycosaminoglycans in the pericellular matrix of chondrons and chondrocytes. *J Anat.* 213(3): 266-273.

- Whitelock, J. M., Melrose, J. and Iozzo, R. V., 2008. Diverse cell signaling events modulated by perlecan. *Biochemistry*. 47(43): 11174-11183.
- Whitelock, J. M., Murdoch, A. D., Iozzo, R. V. and Underwood, P. A., 1996. The degradation of human endothelial cell-derived perlecan and release of bound basic fibroblast growth factor by stromelysin, collagenase, plasmin, and heparanases. *J Biol Chem*. 271(17): 10079-10086.
- Wiberg, C., Hedbom, E., Khairullina, A., Lamande, S. R., Oldberg, A., Timpl, R., Morgelin, M. and Heinegard, D., 2001. Biglycan and decorin bind close to the n-terminal region of the collagen VI triple helix. *J Biol Chem*. 276(22): 18947-18952.
- Wiberg, C., Heinegard, D., Wenglen, C., Timpl, R. and Morgelin, M., 2002. Biglycan organizes collagen VI into hexagonal-like networks resembling tissue structures. *J Biol Chem*. 277(51): 49120-49126.
- Wiberg, C., Klatt, A. R., Wagener, R., Paulsson, M., Bateman, J. F., Heinegard, D. and Morgelin, M., 2003. Complexes of matrilin-1 and biglycan or decorin connect collagen VI microfibrils to both collagen II and aggrecan. *J Biol Chem*. 278(39): 37698-37704.
- Williams, G. M., Chan, E. F., Temple-Wong, M. M., Bae, W. C., Masuda, K., Bugbee, W. D. and Sah, R. L., 2010. Shape, loading, and motion in the bioengineering design, fabrication, and testing of personalized synovial joints. *J Biomech*. 43(1): 156-165.
- Wilusz, R. E., Defrate, L. E. and Guilak, F., 2012. Immunofluorescence-guided atomic force microscopy to measure the micromechanical properties of the pericellular matrix of porcine articular cartilage. *J R Soc Interface*. 9(76): 2997-3007.
- Winter, G. M., Poole, C. A., Ilic, M. Z., Ross, J. M., Robinson, H. C. and Handley, C. J., 1998. Identification of distinct metabolic pools of aggrecan and their relationship to type VI collagen in the chondrons of mature bovine articular cartilage explants. *Connect Tissue Res*. 37(3-4): 277-293.
- Witsch-Prehm, P., Miehle, R. and Kresse, H., 1992. Presence of small proteoglycan fragments in normal and arthritic human cartilage. *Arthritis Rheum*. 35(9): 1042-1052.

- Wong, B. L. and Sah, R. L., 2010. Mechanical asymmetry during articulation of tibial and femoral cartilages: local and overall compressive and shear deformation and properties. *J Biomech.* 43(9): 1689-1695.
- Wu, J. Z. and Herzog, W., 2002. Elastic anisotropy of articular cartilage is associated with the microstructures of collagen fibers and chondrocytes. *J Biomech.* 35(7): 931-942.
- Yamagata, T., Saito, H., Habuchi, O. and Suzuki, S., 1968. Purification and properties of bacterial chondroitinases and chondrosulfatases. *J Biol Chem.* 243(7): 1523-1535.
- Yin, J. H., Xia, Y. and Ramakrishnan, N., 2011. Depth-dependent Anisotropy of Proteoglycan in Articular Cartilage by Fourier Transform Infrared Imaging. *Vib Spectrosc.* 57(2): 338-341.
- Youn, I., Choi, J. B., Cao, L., Setton, L. A. and Guilak, F., 2006. Zonal variations in the three-dimensional morphology of the chondron measured in situ using confocal microscopy. *Osteoarthritis Cartilage.* 14(9): 889-897.
- Zhen, E. Y., Brittain, I. J., Laska, D. A., Mitchell, P. G., Sumer, E. U., Karsdal, M. A. and Duffin, K. L., 2008. Characterization of metalloprotease cleavage products of human articular cartilage. *Arthritis Rheum.* 58(8): 2420-2431.
- Zhu, W., Mow, V. C., Koob, T. J. and Eyre, D. R., 1993. Viscoelastic shear properties of articular cartilage and the effects of glycosidase treatments. *J Orthop Res.* 11(6): 771-781.

Biography

Rebecca Elizabeth Wilusz was born on February 26, 1985, in Durham, North Carolina, and was raised in East Windsor, New Jersey. Rebecca earned a Bachelor of Science in Engineering *summa cum laude* from Duke University in 2007 with a dual major in biomedical and mechanical engineering and a minor in history. She earned Graduation with Distinction in Biomedical Engineering, the Howard G. Clark Biomedical Research Award, and induction into Tau Beta Pi, Pi Tau Sigma, Phi Alpha Theta, and Phi Eta Sigma honor societies. As a graduate student, Rebecca was a National Science Foundation Graduate Student Research Fellow (2007 – 2010), a Duke University James B. Duke Fellow (2007 – 2011), and a Duke University Pratt-Gardner Fellow (2007 – 2008). She was named Department of Biomedical Engineering Most Outstanding Teaching Assistant in May 2008. In addition, Rebecca served as co-chair of the Graduate & Professional Student Council Basketball Committee, Graduate Basketball Head Usher, and a graduate assistant for Duke University Athletics in Intercollegiate Athletic Facilities and Game Operations.

Peer – Reviewed Publications

McLeod, M.A., **Wilusz, R.E.**, Guilak, F. Depth-Dependent Anisotropy of the Micromechanical Properties of the Extracellular and Pericellular Matrices of Articular Cartilage Evaluated via Atomic Force Microscopy. *Journal of Biomechanics*, 46(3):586-592, 2013.

Sanchez-Adams, J., **Wilusz, R.E.**, Guilak, F. Atomic Force Microscopy Reveals Regional Variations in the Micromechanical Properties of the Pericellular and Extracellular Matrices of the Meniscus. *Journal of Orthopaedic Research, in press*.

Wilusz, R.E., DeFrate, L.E., Guilak, F. A Biomechanical Role for Perlecan in the Articular Cartilage Pericellular Matrix. *Matrix Biology*, 31(6):320-7, 2012.

Wilusz, R.E., DeFrate, L.E. Guilak, F. Immunofluorescence-Guided Atomic Force Microscopy to Measure the Micromechanical Properties of the Pericellular Matrix of Porcine Articular Cartilage, *Journal of the Royal Society Interface*, 9(76): 2997-3007, 2012.

Riera, K.M., Rothfus, N.E., **Wilusz, R.E.**, Weinberg, J.B., Guilak, F., McNulty, A.L. Interleukin-1 and Tumor Necrosis Factor-alpha Decrease Cell Proliferation and Repair in Meniscal Microwounding and Tissue Repair Model Systems. *Arthritis Research & Therapy*, 13(6):R187-207, 2011.

Darling, E.M.*, **Wilusz, R.E.***, Bolognesi, M.P., Zauscher, S., Guilak, F. Spatial Mapping of the Biomechanical Properties of the Pericellular Matrix of Articular Cartilage Measured *in situ* via Atomic Force Microscopy. *Biophysical Journal*, 98(12):2848-56, 2010. (*E.M. Darling and R.E. Wilusz contributed equally to this work)

McNulty, A.L., Estes, B.T., **Wilusz, R.E.**, Guilak, F. Dynamic Loading Enhances Integrative Meniscal Repair in the Presence of Interleukin-1. *Osteoarthritis and Cartilage*, 18(6):830-8, 2010.

Wilusz, R.E., Weinberg, J.B., Guilak, F., McNulty, A.L. Inhibition of Integrative Repair of the Meniscus Following Acute Exposure to Interleukin-1 *in vitro*. *Journal of Orthopaedic Research*, 26(4):504-12, 2008.

Conference Presentations

Podium Presentation, 2012 Orthopaedic Research Society Annual Meeting, San Francisco, CA. **Wilusz, R.E.**, DeFrate, L.E., Guilak, F. Co-Localization of Type VI Collagen and Perlecan to Lower Modulus Regions of the Pericellular Matrix of Porcine Articular Cartilage.

Podium Presentation, 2011 Orthopaedic Research Society Annual Meeting, Long Beach, CA. **Wilusz, R.E.**, Zauscher, S., Guilak, F. Elastic Mapping of Osteoarthritic Changes in the Micromechanical Properties of the Pericellular Matrix in Human Articular Cartilage.

Podium Presentation, 2010 Musculoskeletal Biology and Bioengineering Gordon Research Conference, Andover, NH. **Wilusz, R.E.**, Darling, E.M., Bolognesi, M.P., Zauscher, S., Guilak, F. Spatial Mapping of the Biomechanical Properties of the Pericellular Matrix of Articular Cartilage Measured *in situ* via Atomic Force Microscopy.

Podium Presentation, 2009 Orthopaedic Research Society Annual Meeting, Las Vegas, NV. Darling, E.M., **Wilusz, R.E.**, Bolognesi, M.P., Zauscher, S., Guilak, F. Biomechanical Properties of Articular Cartilage Pericellular Matrix Measured *in situ* via Atomic Force Microscopy.

Poster, 2013 Orthopaedic Research Society Annual Meeting, San Antonio, TX. **Wilusz, R.E.**, Guilak, F. The Mechanical Properties of the Chondrocyte Pericellular Matrix Exhibit High Resistance to Enzymatic Digestion of Glycosaminoglycans.

Poster, 2012 Orthopaedic Research Society Annual Meeting, San Francisco, CA. McLeod, M.A., **Wilusz, R.E.**, Guilak, F. Depth-Dependent Anisotropy of the Micromechanical Properties of Porcine Articular Cartilage Measured via Atomic Force Microscopy.

Poster, 2009 American Society of Mechanical Engineers Summer Bioengineering Conference, Squaw Valley, CA. **Wilusz, R.E.**, Darling, E.M., Bolognesi, M., Zauscher, S., Guilak, F. The Inhomogeneous Mechanical Properties of the Pericellular Matrix of Articular Cartilage Measured *in situ* by Atomic Force Microscopy.

Poster, 2007 Orthopaedic Research Society Annual Meeting, San Diego, CA. **Wilusz, R.E.**, McNulty, A.L., Weinberg, J.B., Guilak, F. Inhibition of Integrative Repair of the Meniscus Following Acute Exposure to Interleukin-1 *in vitro*.